Dissecting the intricacies of sterol dysregulation in Huntington's disease

Thesis submitted for the degree of
Doctor of Philosophy
at the University of Leicester

by

Mariana De Fátima Silva Santos

Department of Neuroscience Psychology and Behaviour

University of Leicester

April 2016

Abstract

Dissecting the intricacies of sterol dysregulation in Huntington's disease.

Mariana De Fátima Silva Santos

Background: Huntington's disease (HD) is a devastating neurodegenerative condition, caused by an expanded polyglutamine tract in the Huntingtin (Htt) protein. HD is manifested by personality changes, movement disorders and/or dementia. Prior evidence exists for sterol dysregulation in HD models, observed both in neurons and astrocytes. In the brain the cholesterol is produced *in situ*, as the blood brain barrier prevents the cholesterol metabolized in the periphery to be used by the brain cells. The consensus stablished supports the idea that neurons synthesize the cholesterol needed in the soma, but rely on the cholesterol delivered by astrocytes in the form of apolipoproteins at synapses. A key player studied to be responsible to communicate the cholesterol status of neurons to astrocytes is the 24S-hydroxycholesterol (24S-OHC) also knows as the cerebrosterol (the brain oxysterol).

Aim: Prior results from the lab showed cholesterol accumulation in primary striatal neurons infected with lentiviral expression vectors encoding a mutant Htt fragment (Htt171-82Q) compared to cells expressing a wild-type Htt fragment (Htt171-18Q). Following on these results and the previous published work from different laboratories, the aim of this thesis was to investigate the sterol status of HD striatal neurons in order to better understand this process and the consequences for the neurons and astrocytes' health in the context of HD.

Methods: Filipin staining, cholesterol oxidase assay, isotope-dilution gas chromatography-mass spectrometry, NeuN positive staining cell count – neuronal cell death assay, Mitosox assay, Fluo-4 AM imaging, extracellular multi-electrode array recordings, immunocytochemistry and real-time quantitative PCR.

Results: I observed sterol accumulation in primary striatal neurons expressing mutant Htt, which one release into the medium significantly increased levels of 24S-OHC. The cerebrosterol is toxic to striatal neurons and the mechanism elucidated was by inducing increased superoxide levels in the mitochondria. Besides the toxicity effect, 24S-OHC was observed to sensitize N-Methyl-D-aspartate (NMDA) receptor function, measured by increased calcium influx in the presence of NMDA and increased amplitude and frequency of firing in the presence of glutamate, modulating NMDA receptor activity. In addition, the studies collected support that 24S-OHC induces sterol dysregulation in astrocytes by downregulating SREBP2 target genes and the purposed mechanism is by blocking the transcription factor's migration into the nucleus, in this way promotes inhibition of cholesterol and its precursors synthesis. In parallel 24S-OHC up-regulates LXR target genes aiming to increase cholesterol efflux.

Conclusion: The results part of this thesis conveyed with others' published work and brought novelty into the field. Like others I observed sterol accumulation at the plasma membrane and in lysosomes and stablished a link with the sterol dyshomeostasis observed in my model with HD hallmarks – mitochondrial stress and excitotoxicity, caused by the increased of 24S-OHC efflux. In addition, I was also able to link the sterol dysregulation in neurons with astrocyte's cholesterol dyshomeostasis, as evidenced by a different group.

This thesis provides new insights into the potential aetiopathogenic mechanisms of HD and reconcile some apparently disparate previous findings regarding sterol disposition in this disorder.

Acknowledgements

In this section I will acknowledge the people who helped and supported me through out my PhD and made a positive contribution to this thesis.

The first person to acknowledge is Professor Flaviano Giorgini, who introduced me to Professor Ruth Luthi-Carter, who became my supervisor and gave me the great opportunity to work with her and develop this story.

Over the past 4 years, the guidance, the support and all the knowledge I received from Professor Ruth helped me to elaborate the project that I present here; therefore, Ruth, thank you so much.

My thesis committee were also important over these years. The yearly discussions conveyed different perspectives on this thesis. Many thanks to Professor Flaviano Giorgini and Professor John Challiss.

Thank you to Dr. Alberto Capurro who helped me with the multi-electrode array experiments, and Dr. Volko Straub for the advice and support for the calcium imaging experiments.

Being in a foreign country makes a person experience new challenges and being far from family, the main safety net, obliges one to find a new social community to belong to and feel safe. My family in Leicester made me feel safe and loved.

Over 7 years in Leicester I had time to make many friends. Even though some of them left before I concluded the PhD they are still with me. I want to thank Ana, Melissa, Lidia, Vincenzo, Ines, Clara, Paola, Simona, Sara, Max, Alessandro, Alfredo, David Lam, David Michod, Victoria, Mariaelena, Tania, Diana, Virginia, Mafalda, Marta, Sandra, Vitor, Jesvin, Ghazi, James, Ian, João, Carlo and others who crossed my path and somehow helped my time in Leicester to be remembered with a smile.

Also important was my experience before the PhD in the laboratory of Dr. Miguel Martins. During that period, he taught me two of the most important

things in science, how to properly design experiments choosing the right controls and critically understand the results without jumping to conclusions! Moreover he trained me to think about the protocols, and to understand and trouble shoot when something was not working. His presence at my side at the bench was invaluable for my development as a scientist and to successfully complete my PhD. Obrigada Miguel.

At last I want to thank the support of my mum, dad and brother.

A special thank you to a special friend who helped, support, advised and to whom I listened. His advice helped me to keep control in difficult moments. Thank you ☺

I would like also to thank Professors Miho Terunuma and Leslie Jones, my internal and external advisers, respectively with whom I had a very satisfactory VIVA, which turned out to be a great discussion about my PhD work. Also they were incredible in helping me to put together the last version of the thesis, therefore Thank you so much!

“I know I was born and I know that I’ll die, the in between is mine” Eddie Vedder.

List of Contents

List of Figures

List of Tables

List of Abbreviations

24S-OHC	24S-hydroxycholesterol - Cerebrosterol
3-NP	3-Nitropropionic acid
7α-OHC	7α-Hydroxycholesterol
ABCA1	ATP-binding cassette transporter (member 1)
ABCG1	ATP-binding cassette sub-family G member 1
ABCG4	ATP-Binding Cassette, Sub-Family G, Member 4
ACAT	Sterol O-acyltransferase
ACAT2	Acetoacetyl-CoA Thiolase
acetyl-CoA	Acetyl Coenzyme A
AD	Alzheimer's disease
AMPA	α-amino-3-hydroxy-5-methyl-4-isoxazolepropionic acid
Apo	Apolipoproteins
APP	Amyloid Precursor Protein
Aβ	beta-plated amyloid plaque
BBB	Blood Brain Barrier
BCA	Bicinchoninic Acid
BDNF	Brain-Derived Neurotrophic Factor
BSA	Bovine Serum Albumin
$CaCl_2$	Calcium Cloride
CAG	Cytosine-Adenine-Guanine
CBP	CREB-binding protein
cDNA	Complementary DNA
CHOP	C/EBP homologous protein

CIP4	Cdc42-interating protein
CNS	Central Nervous System
CO2	Carbon dioxide
CRF	Central Research Facility
CSF	Cerebrospinal fluid
Ct	threshold cycle
CTFB	Complete Transcription Factor Binding assay buffer
CYP7A	Cholesterol 7α-monooxygenase
CYP27	Putative cytochrome p450 cyp27 subfamily protein
CYP46A1	Cholesterol 24-hydroxylase
Da	Daltons
DARPP-32	Dopamine- and cAMP-regulated phosphoprotein
DHCR7	7-Dehydrocholesterol Reductase
DIV	Days in vitro
DMSO	Dimethyl sulfoxide
DNA	Deoxyribonucleic acid
dNTPs	Deoxynucleotide
dsDNA	Double strand DNA
DTT	Dithiothreitol
E	Embryonic day
EBSS	Earle's Balanced Salt Solution
EDTA	Ethylenediaminetetraacetic acid
ER	Endoplasmic Reticulum
FDFT1	Farnesyl-Diphosphate Farnesyltransferase 1

FPP	Farnesyl Pyrophosphate
GFAP	Glial fibrillary acidic protein
Glut4	Glucose transporter type 4
gp78	Glycoprotein 78
H2O2	Hydrogen Peroxide
HBSS	Hanks' Balanced Salt Solution
HD	Huntington’s disease
HEAT	Huntingtin, Elongation factor 3, regulatory A subunit of protein phosphatase 2A, and lipid kinase Tor
HMG-CoA	3-Hydroxyl-3-Methylglutaryl Coenzyme A
HMGCR	HMG-CoA reductase
HMGCS1	3-Hydroxy-3-Methylglutaryl-CoA Synthase 1
HRP	Horseradish Peroxidase
Htt	Huntingtin
IDMS	Isotope dilution mass spectrometry
iGluRs	ionotropic Glutamate Receptors
Insig	Insulin induced gene 1
KCl	Potassium clorride
KO/ -/-	Knockout
LDLr	Low density lipoprotein receptor
LOAD	Late onset Alzheimer’s Disease
LSOs	lysosomal storage organelles
LXRs	Liver X receptors
Ly	Lysosome

MBP	Myelin Basic Protein
MEA	Multi electrode array
MK-801	Dizocilpine
mRNA	Messenger Ribonucleic acid
MTT	3-[4,5-dimethylthiazol-2-yl]-2,5 diphenyl tetrazolium bromide
NaCl	Sodium Cloride
NaHCO3	Sodium Bicarbonate
NES	Nuclear Export Signal
Neu-N	Neuronal Nuclei
NMDA	N-methyl-D-aspartate
NMDARs	NMDA receptors
NPC	Niemann-Pick disease type C
NRSF	Neuro-Restrictive Silencer Factor
ns	Non-Significance
OHC	Hydroxycholesterol
P	Post-natal day
PD	Parkinson’s disease
PFA	Paraformaldehyde
PGC1α	Peroxisome proliferator-activated receptor gamma coactivator 1-alpha
PGK	Phosphoglycerate Kinase 1 Promoter
PM	Plasma membrane
PMSF	Phenylmethanesulfonyl fluoride
polyQ	Polyglutamine

PSD 95	Post Synaptic Density protein 95
qRT-PCR	Real-Time Quantitative Polymerase Chain Reaction
REST	Repressor Element-1 Silencing Transcription factor
RIPA	Radioimmunoprecipitation assay
ROI	Regions Of Interest
ROS	Reactive Oxygen Species
rpm	Rotations Per Minute
RT	Room Temperature
S1P	Site 1 proteases
S2P	Site 2 proteases
Scap	SREBP cleavage activating protein
SDS	Sodium dodecyl sulfate
SEM	Standard Error of the Mean
SH3GL3	Endophilin A3
SLOS	Smith-Lemli-Optiz syndrome
SRE	Sterol Regulatory Element
SREBP2	Sterol Regulatory Element-Binding Protein 2
SREBPs	Sterol Regulatory Element Binding Proteins
TG	Thapsigargin
TM	Tunicamycin
Trc8	Translocation in renal carcinoma, chromosome 8 gene
TRE	Tetracyclin-response element regulated promoter
tTA1	Tetracycline-controlled transactivator
UPS	Ubiquitin Proteasome System

X Times

1. Introduction

1.1. Huntington's disease

1.1.1. Genetic and clinical features

Huntington's disease (HD) is an autosomal dominantly inherited disorder, occurring at a prevalence of 5 to 12 in every 100,000 people in United Kingdom (Evans et al., 2013; Wexler et al., 2016).

Huntington's disease is caused by a CAG trinucleotide repeat expansion in the *Huntingtin (Htt)* gene. The expanded repeats are translated into an abnormally long polyglutamine (polyQ) tract localized in the N-terminal domain of the Huntingtin protein (Htt) (Walker, 2007). A stretch of less than 35Q in the Htt protein is considered normal, and HD is fully penetrant when the Htt contains a polyQ of more than 40. When the length of this stretch is 36-39 polyQ, HD may or may not manifest (i.e. alleles show reduced penetrance). More than 60 polyQ repeats usually causes juvenile-onset HD (onset ≤20 years of age), as shown in Figure 1.1. Long CAG repeats are instable and can expand, especially during spermatogenesis (Walker, 2007).

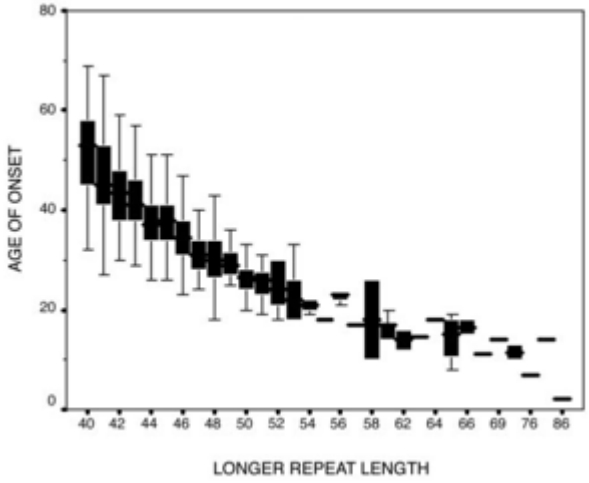

Figure 1.1: **Correlation of age of onset with polyglutamine repeats.** The longer the polyglutamine length, the earlier the age of onset. There is high variability in the age of onset, when repeats are fewer than 50. The curvilinear relationship between the two variables shows that polyglutamine chains longer than 60 typically cause an age of onset around 20 years or less (juvenile-onset HD). Figure from Wexler et al., 2004.

The longer the polyQ stretch, the earlier the first disease symptoms appear. The clinical syndrome is manifested as progressive personality changes, movement disorders, impaired cognition, memory loss, and sleep disturbances (Gagnon et al., 2008). The average course of the disease usually lasts between 10 to 20 years from the onset of the first symptoms (Landles and Bates, 2004). Disease symptoms progress until constant patient care and surveillance is needed (Leegwater-Kim and Cha, 2004). The first HD symptoms typically comprise personality changes (e.g. difficulty with multitasking, irritability) accompanied by depression and/or the appearance of involuntary movements and/or poor coordination (Biglan et al., 2009; Duff et al., 2010). In the middle stages of the disease, the movement disorder characterized by involuntary twitching and writhing movements of the face, trunk and extremities, known as “chorea”, worsens and is accompanied with progressive brain atrophy (Figure 1.2) (Ross and Tabrizi, 2011). In the latter stages of the disease chorea becomes very severe, patients have difficulty in swallowing and choke often. A common feature described at this stage is changes in metabolism accompanied by weight loss, which may be due in part to pathophysiologic changes in the hypothalamus (Politis et al., 2008; van der Burg et al., 2009).

Dementia is understood as a progressive decline in cognitive abilities leading to social impairment. In HD, patients show a profile characterized by attention deficits, difficulty in problem solving, impaired planning and cognitive deficit. The cognitive impairments, which can occur at any stage, can prevent a patient from carrying out their usual routine. Moreover, evidence exists for progressive memory loss in HD patients being more emphasized at the late stages of the disease (Peavy et al., 2010).

Significant brain atrophy is observed in HD, with the most affected area being the striatum, especially the caudate and putamen. It is believed that the HD pathology is related to the vulnerability of GABAergic medium-sized spiny neurons (Mitchell et al., 1999). Other affected brain areas in HD are the layers III, V, and VI, in the cortex together with the hippocampus, thalamus, globus pallidus, subthalamic nucleus, substantia nigra and white matter (Vonsattel, 2008; Walker, 2007; Zheng and Diamond, 2012).

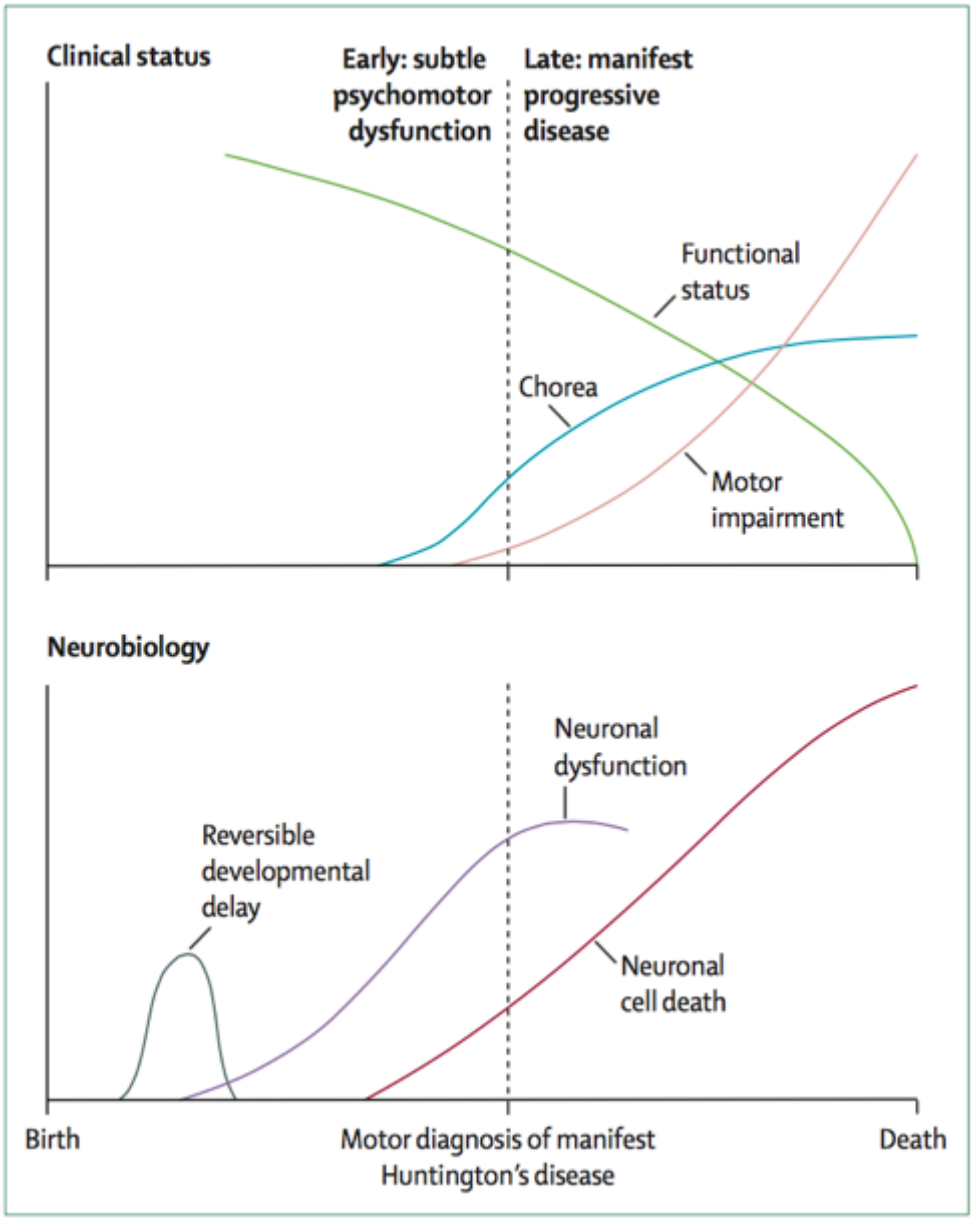

Figure 1.2: **Progression of Huntington's disease: clinical status and neuropathological changes over a patient's lifespan.** The first signs of changes in functional status and neuronal dysfunction typically begin years before a motor diagnosis is given. Neuronal cell death occurs in parallel to chorea and motor impairment. Both neuronal degeneration and motor impairment worsen until death. Figure from "Huntington's disease: from molecular to pathogenesis to clinical treatment" (Ross and Tabrizi, 2011).

The "*Interesting Transcript 15*" (*IT15*) gene, which contains 67 exons and locates in the chromosome 4p16.3, translates into the Htt protein, which one is composed of 3144 amino acids (considering 23 glutamines in the variable polyQ domain (≥36 glutamines mutant Htt) and 11 prolines in the adjacent

variable polyproline domain) with a molecular weight of 347855 Daltons (Da). Huntingtin is ubiquitously expressed in humans and rodents, with higher levels in the central nervous system (CNS) and testes (DiFiglia et al., 1995; Ferrante et al., 1997; Fusco et al., 1999; Trottier et al., 1995).

1.1.2. Structural features of the Huntingtin protein

Despite the fact that Htt was identified more than 20 years ago, its cellular roles are still somewhat unclear. Huntingtin has been observed to be distributed in various cellular compartments including the plasma membrane, endoplasmic reticulum, microtubules, mitochondria and clathrin-coated vesicles (DiFiglia et al., 1995; Gutekunst et al., 1998; Sharp et al., 1995). Htt protein can also be detected in the nucleus where the mutant form can accumulate particularly (Kegel et al., 2002; Tao and Tartakoff, 2001; Wheeler et al., 2000).

The multiple sites for Htt's localization reflects the multitude of roles and protein-protein interactions described for this protein. So far more than 300 proteins are known to interact with Htt including proteins involved in transcription, cellular trafficking, signalling and metabolism (Harjes and Wanker, 2003). Some proteins have a differential affinity for the mutant form; examples of this are: Calmodulin (Bao et al., 1996), CREB-binding protein (CBP) (Chai et al., 2001; Steffan et al., 2000), Cdc42-interating protein (CIP4) (Holbert et al., 2003), endophilin A3 (SH3GL3) (Sittler et al., 1998), and paired amphipathic helix protein Sin3a (Steffan et al., 2000), among others, which implies dysregulation of gene expression, alteration of cellular trafficking and endocytosis, and impairment of neurotransmission. Furthermore, Htt has been shown to interact with specific lipids membranes (Kegel et al., 2005; Suopanki et al., 2006; Gao et al., 2016).

The functional domains identified in Htt include a proline-rich domain next to the polyglutamine tract (Figure 1.3) (Steffan et al., 2004). It also contains three series of HEAT (Huntingtin, Elongation factor 3, regulatory A subunit of protein phosphatase 2A, and lipid kinase TOR) repeats which are usually involved in protein-protein interactions and observed in proteins with role in intracellular trafficking and chromosomal segregation (Andrade and Bork, 1995; Neuwald and Hirano, 2000; Takano and Gusella, 2002) (Figure 1.3). The

identification of a Nuclear Export Signal (NES) in the C-terminal region of the protein indicates that Htt can shuttle between the nucleus and the cytoplasm, which is consistent with a proposed role for Htt as part of a nuclear-cytoplasmic shuttling protein complex, as Htt can mediate the transport of specific transcription factors such as CBP into the nucleus (Xia et al., 2003) (Figure 1.3).

The N-terminus of Htt contains numerous sites that can be target of post translational modifications (PTMs), which ones are important regulators of Htt stability, localization and function, and affect its aggregation, accumulation and toxicity (Arndt et al., 2015). The PTMs studied in the N-terminus of Htt were ubiquitination and SUMOylation (Kalchman et al., 1996; Steffan et al., 2004) (Figure 1.3 see red and blue circles), acetylation (Jeong et al., 2009) and phosphorylation (Aiken et al., 2009; Thompson et al., 2009). Also Htt is believed to be palmitoylated (DiFiglia et al., 1995; Huang et al., 2004).

Different studies have reported that Htt phosphorylation, at serines 13 and 16 is associated with reduced levels of mutant Htt toxicity as has been observed to regulate mutant Htt aggregation (Mishra et al., 2012; Arndt et al., 2015).

Ubiquitination and SUMOylation compete for the same lysines - 6,9 and 15, however have opposing roles on Htt related toxicity. While SUMOylation has been implicated in Htt toxicity, as confers stability to the exon 1 fragments reducing aggregation (Steffan et al., 2004), ubiquitination tags the proteins for degradation by the ubiquitin proteasome system reducing in this way the toxicity of mutant Htt (Jana et al., 2005). Likewise in primary striatal and cortical neurons and in a transgenic *C. elegans* model of HD, it was observed that acetylation increases clearance of Htt through autophagy, specifically when the modification occurs at lysine 444, reversing the toxic effects of mutant huntingtin (Jeong et al., 2009).

Other cellular processing events can generate Htt fragments containing the N-terminal region with the polyQ stretch. Huntingtin can be proteolysed by calpain (aminoacids 469 and 536, see Figure 1.3 blue arrows), and there is evidence that such cleavage occurs preferentially in the mutant form. Besides calpain, Htt is proteolysed by caspases, cathepsins and the metalloproteinase

MMP10 (Saudou and Humbert, 2016) as indicated in Figure 1.3 (green and orange arrows). These sites are present in both wild type and mutant Htt, and *in vitro* both are good candidates for proteolysis. However in human post-mortem brain tissues a specific increase was observed in the activity of these proteases in HD brains compared to controls (Wellington et al., 2002). Nevertheless, the known sites of proteolysis do not fully explain the origin of the N-terminal fragments found in HD postmortem brains. Sathasivam and colleagues discovered that the pathogenic exon 1 Htt fragments result from aberrant splicing (Sathasivam et al., 2013). By taking advantage of a series of knock-in HD mouse lines: HdhQ20, Q50, Q80, Q100, Q150, zQ175 and mice expressing Htt human: YAC128 and BACHD, they demonstrated that aberrant splicing of mutant Htt occurs and generates a short polyadenylated mRNA that is translated into an exon 1 protein, which is highly pathogenic (Sathasivam et al., 2013).

The increased generation and accumulation of Htt fragments facilitates their assembly into toxic aggregates, which can be found in the cytoplasm and nucleus (Rubinsztein and Carmichael, 2003; Saudou and Humbert, 2016). Htt aggregates and amyloid inclusion bodies are cleared by the ubiquitin proteasome system (UPS) and through autophagy (more detail in section 1.1.4).

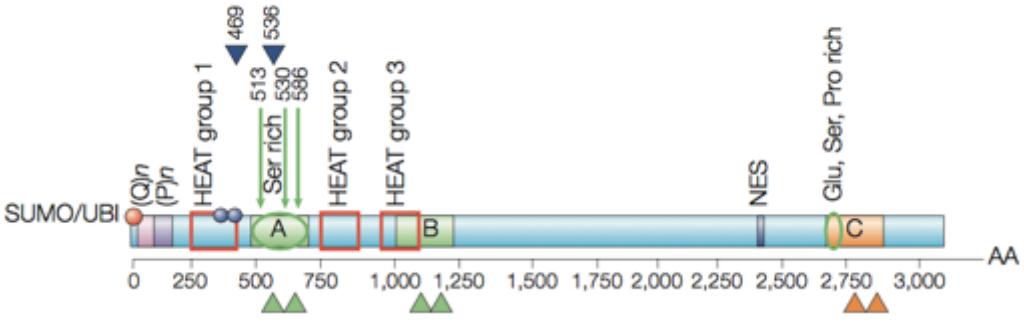

Figure 1.3: **Schematic representation of the Huntingtin protein: known functional domains and other regions of interest.** The N-terminal of Huntingtin protein is rich in functional domains. The glutamine repeat tract is present in the first amino acids that constitute the protein Q(n) (pink rectangle), which is followed by the polyproline sequence, P(n) (purple rectangle). HEAT repeats are represented by red squares indicating the three main clusters. The blue arrowheads indicate the calpain cleavage sites, and the green and orange arrows and arrowheads indicate other regions of proteolysis. A, B and C identify brain-region-selective cleavage domains: B region is cleaved preferentially in cerebral cortex, C in the striatum, and A in both brain structures. The red and purple circles indicate the sites of other post-translational modifications: ubiquitination (UBI) and/or sumoylation (SUMO) (red), and phosphorylation at serine 421 and serine 434 (purple). The C-terminal region of Huntingtin contains the nuclear export signal (NES). The glutamic acid (Glu), serine (Ser) and rich regions are indicated (serine rich regions encircled in green). Figure from Cattaneo et al., 2005.

1.1.3. Huntingtin functions

There has been intense research aimed at understanding a potential role of context and function of the Htt protein in the specificity and severity of the pathogenicity of HD (Saudou and Humbert, 2016). Htt is ubiquitous both at the tissue and subcellular levels. It interacts with many partners and has long been considered having no clearly defined cellular function only based on different studies performed over the years Htt roles have been progressively clarified with a multitude of cellular roles been attributed to Htt.

Some of the functions that have been described for wild-type Htt at the molecular level include vesicular trafficking, endocytosis, vesicle recycling, endosomal trafficking and autophagy regulation (Saudou and Humbert, 2016). Huntingtin develops these roles either directly or through interaction with specific partners like Huntingtin interacting protein 1 (HIP1), dynein and dynamin 1, in special. More specifically Htt orchestrates the transport of synaptic precursor vesicles (Zala et al., 2013), autophagosomes (Wong and Holzbaur, 2014), endosomes and lysosomes (Caviston et al., 2011; Liot et al., 2013) BDNF containing vesicles (Gauthier et al., 2004), amyloid precursor protein-positive vesicles (Colin et al., 2008; Her and Goldstein, 2008) and GABA receptor-containing vesicles (Twelvetrees et al., 2010). Huntingtin interacts with HIP1 to facilitate clathrin-mediated endocytosis by supporting membrane invagination and the assembly of clathrin coating, and binds to

dynamin 1 to facilitate membrane fission in endocytosis (Engqvist-Goldstein et al., 2001; Legendre-Guillemin et al., 2002; Waelter et al., 2001; El-Daher et al., 2015; Kaltenbach et al., 2007; Moreira Sousa et al., 2013). Moreover, Htt complex with dynein/dynactin/HAP1 regulates retrograde transport of autophagosomes along axons (Wong and Holzbaur, 2014). The identification of a p62-interaction domain in Htt provides clues to the mechanism by which Htt regulates cargo recognition and autophagy induction, further supporting a role of Htt in selective autophagy (Rui et al., 2015).Wild-type Htt holds prosurvival properties as highlighted in several studies showing that expression of wild-type Htt in cell lines and primary cultures of neurons protects cell death induced by different stimuli, including mutant Htt itself, while depletion makes striatal neurons susceptible to apoptotic stimuli (Leavitt et al., 2006; Rigamonti et al., 2000; Zhang et al., 2003; Ho et al., 2001)

The role of Htt as a transcriptional regulator is based on its structure, interactors and through repeated transcriptional dysregulation observed in postmortem human HD brains (Saudou and Humbert, 2016). The polyQ tract motif in Htt is found in transcription factors and serves to mediate the binding between transcriptional factors and transcriptional regulators (Saudou and Humbert, 2016). Wild-type Htt binds several transcription factors including CBP (Steffan et al., 2000), the specific protein-1 (SP-1) (Dunah et al., 2002), the nuclear factor-kB (NF-kB) (Takano and Gusella, 2002) and the tumour suppressor protein 53 (p53) (Steffan et al., 2000), the Repressor Element-1 Silencing Transcription Factor (REST) / Neuron-Restrictive Silencing Factor (NRSF). Huntingtin prevents the recruitment of REST/NRSF to target gene promoters, and by doing so promotes the transcription of brain-derived neurotrophic factor (BDNF) (Ross, 2004; Zuccato et al., 2001; De Fabiani et al., 2010) .

Huntingtin is also involved in another very important neuronal function, synaptic plasticity, by interacting with the SH3 domain of Post Synaptic Density protein 95 (PSD95) (Duyao et al., 1993). Moreover, Htt is also implicated in the regulation of calcium mobilisation (Lim et al., 2008). At last studies with Huntingtin knockout (KO) mice fail to survive beyond embryonic day 8.5, demonstrating the importance of Htt for embryogenesis (Nasir et al., 1995).

1.1.4. Pathogenesis of HD

HD is a complex disease triggered by multiple events, including the proteolysis and aggregation of mutant Htt (for Htt structure refer to section 1.1.2) that lead to a myriad of cellular dysfunctions, such as the impairment of the ubiquitin proteasome system, mitochondrial dysfunction and excitotoxicity. Moreover, recent research implicates both the polyQ protein and the expanded RNA in causing toxicity leading to neurodegeneration in HD, highlighting the possibility for the transport of the toxic protein and RNA in extracellular vesicles and in this way spreading the pathology through other cells (Zhang et al., 2016).

Huntingtin cleavage

N-terminal fragments containing the polyQ tract aggregate and incite more neuronal toxicity than full-length mutant Htt. Such fact was highlighted by several studies which all concluded that caspase-dependent proteolytic cleavage of mutant Htt might be one of the pathological pathways that leads to degeneration of striatal neurons in HD (Goldberg et al., 1996; Graham et al., 2006; Wellington et al., 2002). Therefore a therapeutic strategy has been to inhibit cleavage (Graham et al., 2006) and to modify the Htt protein – taking advantage of antisense oligonucleotides to induce skipping of exon 12 in Htt, where cleavage sites are localized, inhibiting the formation of mutant Htt, therefore reducing toxicity (Evers et al., 2014).

The importance of mutant Htt cleavage for the pathology is highlighted by successful studies where the actions of the cleavage-mediated proteins were inhibited. The use of a peptide that compete for caspase-6 activity and inhibits the proteolysis of Htt was shown to protect cells from mutant Htt related toxicity and continuous administration of the peptide protected pre-symptomatic BACHD form motor deficits and behavioural abnormalities and resulted in partial recovery of motor performance in the same model at advanced disease state (Aharony et al., 2015). Taking advantage of the same HD rat model was observed that treatment for 12 months with olesoxime, a mitochondria-targeting compound, reduced levels of mutant Htt fragments due to suppression of calpain-mediated cleavage and ameliorated BACHD cognitive and psychiatric phenotypes (Clemens et al., 2015).

Huntingtin aggregation

Aggregation is a dynamic process (Bates, 2003; Hands and Wyttenbach, 2010) and is another hallmark of Huntington's pathology. The expanded polyQ repeat in mutant Htt causes the misfolding of the abnormal protein and the formation of mutant Htt aggregates in neuronal nuclei and neuropils in HD patients brains (DiFiglia et al., 1997; Gutekunst et al., 1999). Evidences point that the aggregates are formed by the cleaved N-terminal portion of the mutant Htt, based on specific antibodies staining and by the use of HD mice models expressing N-terminal mutant Htt, which ones form abundant aggregates in their neuronal nuclei and processes (Davies et al., 1997; Schilling et al., 1999).

The degree of toxicity conferred by the mutant Htt aggregates is still debated, studies report that mutant Htt aggregates are both harmful and beneficial, as demonstrated by studies showing that dying cells do not contain aggregates and these are important for the extent cells' lifespan (Arrasate et al., 2004). Perhaps the toxicity exerted by the aggregates depends on the disease stage, interaction with other proteins and organelles and the degree of cellular functions, consequently disturbed. Wild type Htt has been found entangled in the aggregates (Rajan et al., 2001) and this observation may explains why wild type cannot buffer Htt mutant toxic's effects. The hypothesis that rose is that aggregates retain the pathogenic Htt, being instead protective.

Mutant Huntingtin impairs ubiquitin-proteasome system

The ubiquitin-proteasome system (UPS) consists in targeting proteins to degradation by adding ubiquitin in specific lysine residues, and this clearance system is dysregulated in HD (Bence et al., 2001; DiFiglia et al., 1997; Holmberg et al., 2004). Aggregated and misfolded Htt is itself target of UPS. However due to the long polyQ the degradation is not efficient and Htt with long glutamine stretch blocks the catalytic core of this clearance system, impeding the degradation of other substrates (Imarisio et al., 2008).

Besides the UPS, cells count on autophagy to eliminate the unwanted cellular residues. Huntingtin aggregates are also cleared by autophagy (Ravikumar et al., 2004; Sarkar and Rubinsztein, 2008).

Activation of autophagy by overexpression of key autophagic components or by rapamycin treatment increases removal of Htt and reduces aggregates formation (Jia et al., 2007; Ravikumar et al., 2004).

Mitochondrial dysfunction

Mitochondrial dysfunction in HD results in impaired energy production, reduction of membrane potential, inability to buffer intracellular calcium, and can ultimately trigger apoptosis (Browne et al., 1997; Panov et al., 2002). Mutant Htt may have a detrimental effect on mitochondria by interacting with the outer membrane (Orr et al., 2008; Panov et al., 2002). Moreover mutant Htt inhibits the Peroxisome proliferator-activated receptor gamma coactivator 1-alpha (PGC-1α) transcription, impairing mitochondrial biogenesis (Cui et al., 2006). Mitochondria are the power source of the cells, generating energy, and reactive oxygen species (ROS) are the residues produced. In non-pathologic conditions, the cell is able to eliminate ROS, however in HD an increase in ROS is observed, which causes lipid peroxidation and DNA damage (Bogdanov et al., 2001; Perez-Severiano et al., 2000; Polidori et al., 1999).

Excitotoxicity

Excitotoxicity in the striatum occurs when excessive glutamatergic signaling and disrupted intracellular calcium levels lead to mitochondrial energy failure and cell death. Excitotoxicity is another pathological pathway triggering the neurodegeneration of striatal neurons (Cicchetti et al., 2011). Striatal neurons are 95% projection neurons (GABAergic) and 5% interneurons (GABAergic, cholinergic) (Rikani et al., 2014). GABAergic projection neurons are selectively affected in HD (Vonsattel and DiFiglia, 1998). Studies have shown that cells expressing GluN1/GluN2B, the predominant NMDA receptor (NMDAR) subunits in GABAergic projection-medium size spiny neurons (MSN), together with mutant Htt, are particularly sensitive to excitotoxicity (Zeron et al., 2001). Moreover, data from HD mouse models demonstrated an altered NMDAR function in corticostriatal synapses, and NMDAR mediated toxicity was potentiated in striatal neurons (Fan and Raymond, 2007). Furthermore, there is evidence that Htt and PSD-95 interact directly and form a complex together with

NMDAR, which favors excitotoxicity in HD (Sun et al., 2001). These are some of the many proposed mechanisms by which NMDAR sensitivity and excitotoxicity is increased in HD (Dong et al., 2009) and is accepted that in HD, changes in glutamate release, uptake and postsynaptic signaling converge to promote the excitotoxicity of MSN (Sepers and Raymond, 2014). Increased glutamate release occurs at early stages of HD, followed by the loss of glutamatergic terminals in fully symptomatic HD, indicating a disconnection of the cortex and striatum (Raymond et al., 2011). At corticostriatal synapses, glutamate is removed from the extracellular space by astrocytes that express glutamate transporters (GLT), however has been consistently observed reduced mRNA and protein levels of GLT-1 in symptomatic rodent models of HD (Miller et al., 2012; Estrada-Sanchez and Rebec, 2012; Faideau et al., 2010) and reduced expression in post-mortem HD brain despite the increased number of astrocytes. These observations link to the astrocytes deficient uptake of excess glutamate at the corticostriatal synapses, promoting excitotoxicity, such is highlighted by studies with restricted expression of mutant Htt to astrocytes alone is sufficient to reduce GLT-1 expression, reduce glutamate uptake and cause dysfunction (Bradford et al., 2009; Faideau et al., 2010).

1.2. Sterol biosynthesis and its known regulatory mechanisms

Cholesterol is an essential component of eukaryotic membranes and sterol biosynthesis (synthesis of cholesterol itself and precursors) is believed to be an evolutionary acquisition that allowed the development of eukaryotic life (de Duve, 2007). Cholesterol is a major component of membrane lipids and regulates plasma membrane organization, rigidity (Miao et al., 2002), and selective permeability (Haines, 2001), thereby having a strong influence on intercellular signalling (Maxfield and Tabas, 2005). Cholesterol levels need to be regulated within a very narrow range, as small changes in cholesterol content induce consequential changes in overall membrane composition and membrane-associated signalling.

Mammals acquire sterols from both dietary intake and via *de novo* synthesis of cholesterol (Espenshade and Hughes, 2007; Maxfield and van Meer, 2010). It has been observed that a healthy adult human may typically

ingest 0.3 g and synthesize a relatively larger 1 g of cholesterol per day. Besides the amount of cholesterol ingested, only roughly half of dietary cholesterol is absorbed (Ostlund et al., 1999). Therefore, *de novo* synthesis is clearly the major source of whole body cholesterol. Of this, liver accounts for approximately 20%-25% of cholesterol production (van der Wulp et al., 2013). In the liver occurs the catabolism of cholesterol leading to the formation of oxysterols which ones are obtained by the introduction of a hydroxyl group in the cholesterol by action of specific monooxygenase, mainly those belonging to the cytochrome P-450 family, leading ultimately to the formation of bile acids (Crosignani et al., 2011).

Almost all cells can undertake *de novo* cholesterol synthesis from acetyl coenzyme A (acetyl-CoA) (Bloch, 1987). In the first step of this process, two molecules of acetyl-CoA are condensed by the cytoplasmic enzyme acetoacetyl-CoA thiolase (encoded by the *ACAT2* gene) to form acetoacetyl-CoA. Acetoacetyl-CoA and a third molecule of acetyl-CoA are converted to 3-hydroxyl-3-methylglutaryl coenzyme A (HMG-CoA) by HMG-CoA synthase, in the cytoplasm. HMG-CoA is then converted to mevalonate by HMG-CoA reductase (HMGCR), which is anchored by its N-terminal domain into the membrane of the endoplasmic reticulum (ER). Mevalonate undergoes two successive phosphorylations (catalyzed by mevalonate kinase, and phosphomevalonate kinase), to form isopentenyl-5-pyrophosphate in cytosol, which is in equilibrium with its isomer, dimethylallyl pyrophosphate. One molecule of each isomer is then converted to geranyl pyrophosphate to which an additional isopentenyl-5-pyrophosphate is added to form farnesyl pyrophosphate (FPP), an important precursor for protein prenylation (Zhang and Casey, 1996), and heme A, dolichol and ubiquinone synthesis. Finally, squalene synthase catalyzes the head-to-tail condensation of two molecules of FPP, yielding squalene. Like HMGCR, squalene synthase is tightly associated with the ER. Squalene then undergoes a two-step cyclization to yield the first sterol product, lanosterol. Through a series of 19 additional reactions, lanosterol is trimmed to cholesterol (Figure 1.4). Cholesterol is converted into 7α-hydroxycholesterol (7α-OHC) by cholesterol 7α-monooxygenase (CYP7A) in the liver, or into 27-OHC by Putative cytochrome p450 cyp27 subfamily protein

(CYP27) in extra-hepatic cells, and this derivative can undergo further hydroxylation at the 7α position by an oxysterol 7α-hydroxylase (CYP7B) distinct from CYP7A in when reaches the liver (Crosignani et al., 2011). These oxysterols accounts for more than 95% of total bile acid synthesis per day (De Fabiani et al., 2010; Javitt, 2002).

The order and mechanisms of these subsequent reactions is debated, with two alternative pathways often referred to as the Kandutsch-Russel pathway, via lathosterol, being the cholesterol immediate precursor 7-dehydrocholesterol (Katja et al., 2009) and the Bloch pathway, via desmosterol (Bloch, 1965; Tabernero et al., 1993). A number of human malformation syndromes are related with disruption of the enzymatic activities involved in these late steps of cholesterol biosynthesis (Phillipi et al., 2008).

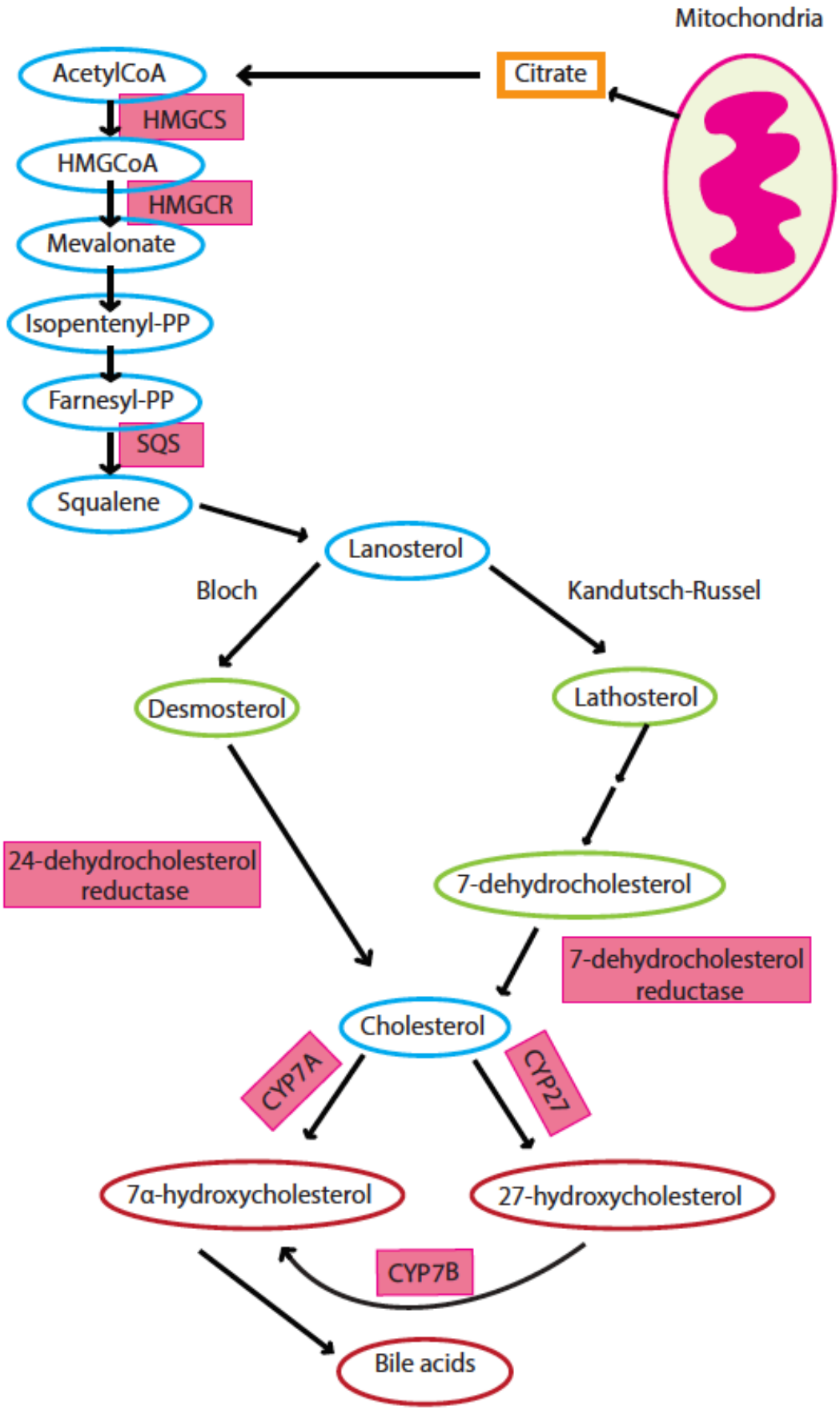
Mitochondria
AcetylCoA
Citrate
HMGCS
HMGCoA
HMGCR
Mevalonate
Isopentenyl-PP
Farnesyl-PP
SQS
Squalene
Lanosterol
Bloch
Kandutsch-Russel
Desmosterol
Lathosterol
24-dehydrocholesterol reductase
7-dehydrocholesterol
7-dehydrocholesterol reductase
Cholesterol
CYP7A
CYP27
7α-hydroxycholesterol
27-hydroxycholesterol
CYP7B
Bile acids

Figure 1.4: **Cellular sterol biosynthesis.** Citrate from the mitochondria is converted into acetyl-CoA in the cytosol and this step initiates the cholesterol biosynthetic pathway. The rate-limiting step involves the synthesis of mevalonate by HMG-CoA reductase (HMGCR). After the synthesis of lanosterol, the pathway diverges and cholesterol can be synthesised from the precursors desmosterol or lathosterol. The immediate cholesterol precursor through the Kandutsch-Russel pathway is 7-dehydrocholesterol. In vivo conversion of cholesterol into bile acids occurs following different pathways and begins by the introduction of one hydroxyl group at different positions of cholesterol: C7α, C27. In the liver 27-hydroxycholesterol can undergo further hydroxylation at the 7α position being converted into 7 α-hydroxycholesterol. These intermediates enriched the bile acids (figure adapted from Leoni and Caccia, 2015, for information on detailed pathway follow figure and text from Introduction section 1.2.

The genes encoding cholesterol biosynthetic enzymes are under the coordinated control of transcription factors known as sterol regulatory element binding proteins (SREBPs). Two genes encode three isoforms of SREBPs. SREBP-2, encoded by one gene, is believed to be specialized to transcribe cholesterol biosynthesis (and some other cholesterol homeostasis-related) genes (Horton et al., 2002). While the *SREBP-1* gene produces two isoforms, SREBP-1a, which regulates genes involved in both cholesterol and fatty acid synthesis and SREBP-1c, which demonstrates stronger regulation of fatty acid biosynthesis genes. Once synthesized, SREBPs localize in the endoplasmic reticulum (ER) in an inactive form. Their C-terminal region binds to the SREBP cleavage activating protein (Scap), which one serves as a sensor for cellular cholesterol levels and coordinates SREBPs localization and activation, either in the nucleus when the cell is in need of cholesterol (Rawson, 2003) or in the ER when sterol levels are high, keeping the complex SREBP-Scap- Insulin induced gene 1 (INSIG) intact (Peng et al., 1997; Rawson, 2003).

The intracellular levels of sterols are meticulously controlled. When cells are depleted of sterols (Figure 1.5 A), signals direct the transcription of genes for production and sterol cellular import, such as *HMGCR* and *Low density lipoprotein receptor (LdLr).* Such genes are under the control of SREBP-2. Under these conditions (Figure 1.5 A), cholesterol no longer occupies its binding site on Scap and the Scap-SREBP complex is released from INSIG to be transported to the Golgi apparatus. In the Golgi, SREBP undergoes two sequential proteolytic cleavages, by the Site 1 (S1P) and Site 2 (S2P)

proteases, to release its N-terminal DNA-binding domain, which is then transported to the nucleus (SREBP N-terminus) (Rawson, 2003). Concomitant dimerization and nuclear transport of the SREBP constitute conversion to its active form. In the nucleus the active SREBP2 recognises sterol regulatory element (SRE) sequences, where the transcription factor binds to and increases the transcription rate of genes involved in sterol synthesis (ex. *HMGCR*) and uptake (ex. *LDLR*) (Espenshade and Hughes, 2007).

Although cleavage by SP1 and SP2 is typically seen as the major regulatory step in SREBP activation, evidence for additional regulatory control by phosphorylation (Kotzka et al., 2012) and acetylation (Ponugoti et al., 2010; Walker et al., 2010) has been reported.

When sterol levels increase (Figure 1.5 B), SREBPs are inhibited (retained in the ER) and in parallel Liver X receptors (LXRs), a family of transcription factors activated by oxysterols, initiate the transcription of genes responsible for sterol transport out of the cell (Espenshade, 2006). Scap alters its conformation; loop1 of the Scap protein binds cholesterol and allosterically regulates the conformation of loop 6, allowing the complex to bind to INSIG, retaining it in the ER (Figure 1.5 B). INSIG also contains a sterol-binding domain that regulates its interaction with Scap by sensing the presence of oxysterols (Radhakrishnan et al., 2007). Moreover, INSIG promotes HMGCR degradation when sterol levels are high (Goldstein, DeBose-Boyd et al. 2006) (Figure 1.5 B).

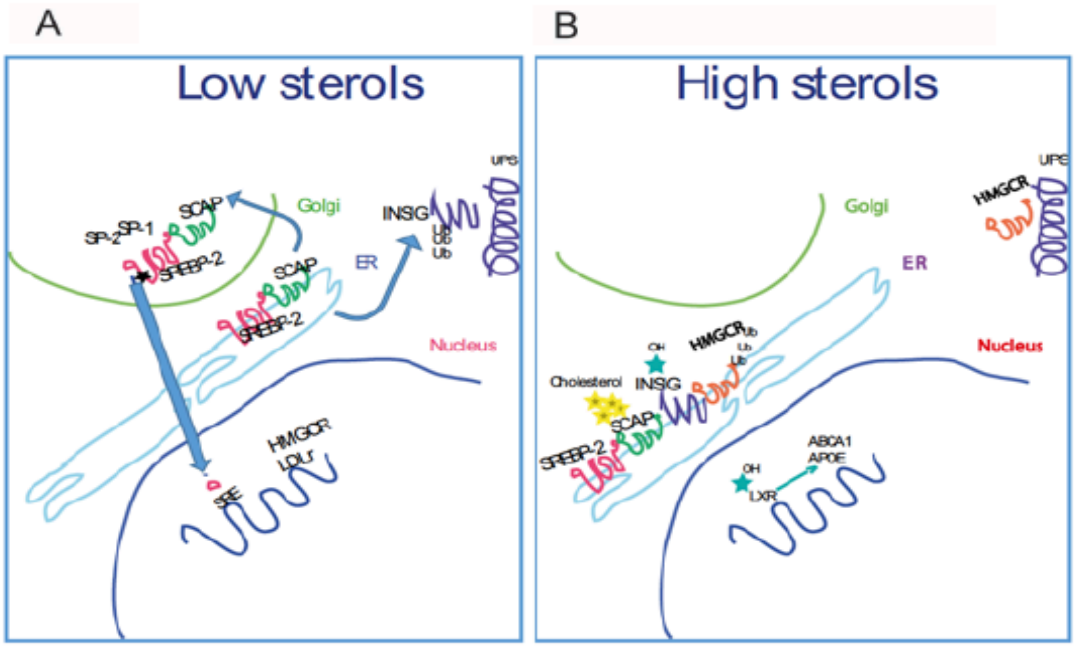

Figure 1.5: **Cellular regulation of sterols. A-** Under low cholesterol conditions the cell acts in order to elevate its levels of cholesterol. A key player in the process is SREBP-2, a protein that reside in the ER and is bound to SCAP. In a situation of low sterols, the complex SREBP-2/SCAP is independent from INSIG, which one is ubiquitinated and degraded by the proteasome system (UPS), allowing the complex to migrate from the ER to the Golgi. In the Golgi, SREBP-2 suffers two sequential cleavages by SP-1 and SP-2 resulting in a fragment which consists in the N-terminal of SREBP-2. This fragment migrates into the nucleus where recognizes sterol regulatory element (SRE) in the promoter of genes as examples: HMGCR and LDLr, which transcription promotes the synthesis of cholesterol and uptake, respectively. **B-** Under high sterol conditions the cell acts to stop cholesterol synthesis and uptake and promotes cholesterol efflux. SCAP senses cholesterol which alters its conformation gaining affinity for INSIG, which senses oxysterols and is retained in the ER. Therefore, SREBP-2/SCAP/INSIG form a complex held in the ER, and SREBP-2 target genes are not transcribed. INSIG in the ER promotes HMGCR ubiquitination, being degraded by the UPS. In the nucleus oxysterols are LXR agonists promoting the transcription of genes such as (example) ABCA1 and APOE, leading to cholesterol efflux and transport out of the cells.

HMGCR is the rate-limiting enzyme in the cholesterol biosynthetic pathway, (Jasinska et al., 2007) and is subject to tight regulation. When in sterol-replete conditions, INSIGs mediate the association between HMGCR and membrane-bound ubiquitin ligases (glycoprotein 78). The ligase ubiquitinates HMGCR, which one becomes a target for degradation by the 26S proteasome.

The cholesterol biosynthesis intermediate lanosterol can also promote HMGCR degradation (Song et al., 2005). Diminished ATP levels can inhibit the activity of HMGCR by triggering its phosphorylation by AMP dependent protein kinase, presumably to balance cholesterol synthesis with other cellular energetic demands (Sato et al., 1993).

1.3. Cholesterol dynamics in the brain

The importance of cholesterol for the nervous system was recognized by Couerbe in 1834, when he referred to cholesterol as the principal element in nervous system (Bickel, 1996). Unlike other organs, the brain satisfies its sterol needs almost entirely via *de novo* synthesis *in situ* (Dietschy, 2009).

Sterols are essential for neuronal development and survival, with cholesterol being particularly important for the functions of axons and synapses (Koudinov and Koudinova, 2001). Cholesterol is also the precursor for neurosteroids and an integral component of neuritic transport vesicles (Pfrieger, 2003 a; 2003 b). Oxysterols also serve important roles in transcellular communication in the brain (Bjorkhem, 2006; Gill et al., 2008; Miyoshi et al., 2014; Radhakrishnan et al., 2007). Brain cholesterol synthesis and disposition is likewise maintained under tight metabolic control, albeit with some unique features.

1.3.1. Brain cholesterol homeostasis and distribution

The central nervous system (brain and spinal cord, CNS) is separated from the cholesterol exchange orchestrated by the liver by the blood brain barrier. Therefore, the CNS must synthesize its own cholesterol (Chobanian et al., 1962; Turley et al., 1996). The brain's relative cholesterol content is almost 10 times higher (15-20 mg/g) than in the body as a whole (approx. 2.2 mg/g), representing about 25% of the total body cholesterol (Dietschy and Turley, 2004). The importance of cholesterol for neuronal electrical conductivity is undoubtedly a major reason for these high concentrations. Cholesterol in myelin surrounding axons confers high conductance and low resistance, allowing fast and efficient forward neuronal conduction of action potentials (Saher et al.,

2011). The central myelining cells, oligodendrocytes, contain the majority of brain cholesterol (more than 70%) (Muse et al., 2001) with the remaining pools distributed among astrocytes (glia 20%) and neuronal cell membranes (10%) (Dietschy and Turley, 2004).

Whereas the timing of the myelination process varies considerably among mammalian species, the developmental rates of cholesterol synthesis nonetheless reflect the extensive need for cholesterol in this process. In mouse, hamster and human, myelination occurs during the first period of postnatal life (Dietschy and Turley, 2004). Messenger RNA (mRNA) levels for HMGCR, which encodes the rate-limiting enzyme of sterol biosynthesis, rapidly increase in mouse brain five days before birth, consistent with the rapid generation of axonal and dendritic processes and the proliferation of oligodendrocytes (Hanaka et al., 2000). Cholesterol synthesis and its incorporation into myelin, peaks between 2 and 3 weeks of age, while the incorporation of other lipids appear to proceed more continuously (Ando et al., 2003; Quan et al., 2003). The decrease in brain cholesterol synthesis is paralleled by an increased expression of CYP46A1, a p450 family enzyme that hydroxylates cholesterol to form 24S-hydroxycholesterol (24S-OHC). The significance of this enzyme will be discussed below.

In contrast to the high cholesterol synthesis seen during postnatal brain development, radionuclide incorporation studies suggest that total cholesterol synthesis is very low in the adult CNS when compared to other tissues (Pfrieger, 2003 a; 2003 b). Whereas the rate of incorporation during myelination peaks at 0.26 mg/day in the developing mouse brain, cholesterol incorporates in the adult brain at a much slower rate of 0.012 mg/day (Quan et al., 2003). Interestingly, this rate of incorporation is estimated to be around 3 times lower than the rate of cholesterol synthesis (0.035 mg/day) suggesting that a small portion of brain cholesterol is constantly renewed and excess cholesterol is excreted to the systemic circulation (Quan et al., 2003). In adults, the rate of cholesterol incorporation into the main pool, the mature myelin sheath, is measured as negligible (Ando et al., 2003). As the myelin pool is stable, the remaining cholesterol production is thought to reflect a much more dynamic compartmentalization of sterols in neurons and astrocytes.

Both neurons and astrocytes possess the enzymatic machinery needed for cholesterol biosynthesis and are capable of synthesizing cholesterol *in vitro* (Saito et al., 1987). However, uncertainty exists whether both continue to do so during adulthood under normal conditions. *In vitro* studies of isolated neuronal and astrocytic cultures have indicated that astrocytes might be much more efficient cholesterol synthesizers (Nieweg et al., 2009; Tabernero et al., 1993). *In vitro* studies, have also suggested that astrocytes and neurons express different ratios of enzymes and/or use different biochemical pathways for the synthesis of cholesterol, causing accumulation of different sterol species or precursors in each cell type. Lanosterol seems to accumulate in neurons, due to the decreased levels of enzymes to convert it into cholesterol. Nevertheless was detected 7-dehydrocholesterol in neurons hypothesizing that these synthesise cholesterol via Kandutsch-Russel pathway (Leoni and Caccia, 2015) (Figure 1.4). In contrast, cholesterol and desmosterol predominate in astrocytes, presumably representing synthesis via the Bloch pathway (Figure 1.4) (Nieweg et al., 2009). Although the potential biological relevance of these differences remains unclear, astrocytes do excrete lipoproteins rich in desmosterol and lathosterol (thus differing from the composition of plasma lipoproteins). The view that astrocytes produce the majority of cholesterol in all brain regions is not uniformly accepted, as *in vitro* and *in vivo* observation are discordant. For example, one recent study reported that the relative mRNA expression of cholesterol synthesizing genes is higher in the hippocampus *in vivo* than in glial cells (Valdez et al., 2010). Nonetheless, the current consensus opinion seems to rest in favour the delivery of sterols from astrocytes to neurons.

1.3.2. Brain cholesterol transport

In the same way that glucose-derived lactate is ‘fed’ to neurons by astrocytes, it is generally presumed that astrocytes also bear the work of cholesterol production. An alternate but related view is that even if neurons synthesize their own cholesterol at the cell body, they rely on cholesterol from astrocytic stores to maintain synapses (Brown and Goldstein, 1986; Mauch et al., 2001; Simons and Ikonen, 2000). Other studies have shown that neurons

may be particularly reliant on cholesterol supplied from astrocytes after brain injury and cell damage (ischemia and excitotoxicity) (Aoki et al., 2003; Champagne et al., 2005; Xu et al., 2006).

The potential mechanisms coordinating the shuttling of cholesterol from astrocytes to neurons have been explored considerably in retinal ganglion cells. In this context, astrocytes were shown to excrete cholesterol via ApoE-containing lipoproteins, whose uptake into neurons was dependent on LDLR-mediated transport (Rothe and Muller, 1991). Extrusion of sterol-loaded lipoproteins from astrocytes appears to be mediated primarily by ATP binding cassette transporter 1 (ABCA1) (Bjorkhem et al., 2011; Bu, 2009; Vance et al., 2005; Wahrle et al., 2004).

Neurons also possess mechanisms to extrude cholesterol which may rely on a different transporter, ABCG4 (Chen et al., 2013). One presumed function of this export is to release sterols when they are present in excess. The enzyme CYP46A1, expressed exclusively in neurons, hydroxylates cholesterol into the main oxysterol in the brain: 24S-hydroxycholesterol (24S-OHC) the cerebrosterol (Dietschy and Turley, 2004), which is subsequently released from the neurons. 24S-OHC is believed to be more than a derivative of cholesterol, when this in excess in neurons, the body of knowledge supports 24S-OHC as a signal molecule between neurons and astrocytes (Brown and Goldstein, 1997; Whitney et al., 2002). The current consensus is that 24S-OHC informs astrocytes on the sterol status of neurons thereby serving as a feedback signal to cease sterol production and delivery. Additional possible roles of 24S-OHC will be discussed in later sections of the thesis.

1.3.3. Oxysterols

Oxyterols are the product of cholesterol oxidation. The introduction of hydroxyl group occurs enzymatically (Russell, 2003) or by reactive oxygen species (Murphy and Johnson, 2008). Oxysterols were first identified as the intermediates in bile acid and steroid hormone production. Now their importance is known to go beyond those roles.

In contrast to cholesterol, steroid side-chain oxidized cholesterol species are able to cross lipophilic membranes at higher rates, potentially with and

without the help of transporters and receptors. Cholesterol oxidation into 27-OHC and 24S-OHC may thus facilitates the cell's efflux of sterols and participate in maintaining sterol homeostasis (Bjorkhem, 2013).

The main oxysterols discussed in the literature are the bile acid intermediates: 7α-hydroxycholesterol, 27-hydroxycholesterol, 24S-hydroxycholesterol and 25S-hydroxycholesterol, and 22R-hydroxycholesterol, a steroid hormone synthesis precursor (Crosignani et al., 2011). As discussed above, synthesis of 24S-OHC occurs exclusively in neurons, and is thought to comprise a major mechanism of cholesterol elimination from the brain (Bjorkhem et al., 1997; Lutjohann et al., 1996). Besides 24S-OHC, cholesterol is converted, to a lesser extent, into 27-OHC in the brain by the cytochrome P450 Family 27 subfamily A member 1/ Sterol 27-hydroxylase (CYP27A1), and then into 7α-hydroxy-3-oxo-4-cholestonic acid (7-OH-4-C) by the enzyme CYP7B. In the liver is eliminated, as well the others oxysterols (Bjorkhem et al., 2009).

Oxysterols are now known to also fulfil signalling roles in the regulation of cholesterol homeostasis, including regulating the activities of SREBP (Brown and Goldstein, 2009; Radhakrishnan et al., 2007) and LXR (Janowski et al., 1999) transcription factors. In addition, oxysterols bind to G protein-coupled (Iguchi et al., 2010) and ionotropic receptors (Paul et al., 2013).

Current evidence also suggests that oxysterols may play roles in pathogenic processes in the brain from their involvement in modulating neuroinflammation and cell death (Gamba et al., 2015).

1.3.4. Cholesterol dyshomeostasis in neurodegenerative diseases

An imbalance in cholesterol homeostasis in the brain has been linked to neurodegenerative diseases such as Niemann-Pick disease type C (NPC), Smith-Lemli-Optiz syndrome (SLOS), Alzheimer's (AD), Parkinson's disease (PD) and Huntington's disease (HD).

NPC disease is a rare autosomal recessive neurovisceral pathology caused by loss-of-function mutations in either NPC1 or NPC2. Symptoms of NPC include delays in motor milestones, speech delay, ataxia, dystonia and

dementia, and systemic symptoms: hepatosplenomegaly (Patterson et al., 2012).

Although the functions of the NPC1 and NPC2 proteins are still not completely clear, current knowledge highlights their role in the cholesterol transport within the late endosomal-lysosomal compartment (Vanier, 2015). Therefore the consequence of mutations in NPC1 or NPC2 is a disruption of sterol disposition, leading to the accumulation of unesterified cholesterol in most organs (Chang et al., 2005). In NPC, lipids are trapped in endosomal/lysosomal vesicles during cholesterol import; therefore they do not reach the ER, consequently cholesterol is neither esterified by Sterol O-acyltransferase (ACAT) for storage nor incorporated into the plasma membrane where it is needed for proper membrane function. Moreover, the accumulation of lipids within lysosomal storage organelles interferes with normal protein and lipid trafficking (Choudhury et al., 2004; Pipalia et al., 2007).

Efforts to develop therapies to treat NPC patients have attempted to rescue lipids trapped in the endosome/lysosomes vesicles, and so far cyclodextrin has been showing some good results. Subcutaneous injections of this cholesterol-binding compound were published to slow neurodegeneration and expand the *NPC1*$^{-/-}$ mice life span (Liu et al., 2009).

SLOS is an autosomal recessive disorder caused by mutations in the gene encoding the enzyme 7-dehydrocholesterol reductase (*DHCR7)*, which is involved in the last step of the cholesterol biosynthetic pathway (Irons and Tint, 1998), resulting in high levels of 7-dehydrocholesterol (7DHC) and low levels of cholesterol.

SLOS patients exhibit pre- and post-natal growth retardation, microcephaly, intellectual disability and the external malformations (e.g. abnormally shaped facial features, cleft palate, and underdeveloped external genitalia in males (Nowaczyk and Irons, 2012; Smith et al., 1964). Whereas most SLOS research has focused on cholesterol deficiency, it is also possible that the accumulation of 7-dehydrocholesterol may be pathogenic (Vance, 2012).

The first line of therapy is to feed patients with a high fat diet in order to normalize plasma cholesterol levels (Porter and Herman, 2011), which seems

quite beneficial. However, it is difficult to understand how the ingested lipids could replace cholesterol in the brain (Dietschy and Turley, 2001).

Subtler effects of sterol dysregulation have also been implicated in AD, PD or HD. Interest in these effects has increased in recent years.

Late onset Alzheimer's Disease (LOAD) is a sporadic, age-related form of dementia (Castellani, 2010). LOAD brains show cortical and hippocampal atrophy and histological tissue modifications related to the deposition of extracellular beta-plated amyloid plaque (Aβ) and intracellular Tau protein neurofibrillary tangles (Castellani, 2010), characteristic of Alzheimer's disease in general.

The major aetiologic link between LOAD and cholesterol homeostasis is that the *APOE4* allele was shown in numerous studies to increase the risk of LOAD (Corder et al., 1993). Inheritance of one copy of *APOE4* allele increases the risk fourfold, while two copies raises the risk of disease by tenfold. One of the mechanisms by which ApoE4 facilitates AD pathogenesis may be its propensity to undergo proteolytic cleavage, resulting in loss of function, leading to impaired cholesterol transport and beta-amyloid clearance (Rohn, 2013).

Although it is generally accepted that increased brain cholesterol favours development of AD, results of clinical trials with statins (HMGCR inhibitors) in AD patients have not universally supported this idea, with some studies suggesting a beneficial effect (Jick et al., 2000), and others showing no effect (Feldman et al., 2010). Although there are still strong supporters of such compounds, recent results have also uncovered potential adverse effects of this approach to treatment, especially in the hippocampus; statins treatment decreased cholesterol levels to an extent that caused decreased synapse density and synaptic vesicle release impairment (Mailman et al., 2011).

Parkinson's disease is the second most common neurodegenerative disease after AD. Like in AD, a low number of PD cases is caused by mutation in specific genes: α-synuclein, DJ-1, Parkin, PINK1, LRRK2, whereas the majority of the cases are sporadic (Davie, 2008). PD is characterized by degeneration of dopaminergic neurons in the substantia nigra (Jankovic, 2008)

and development of Lewy Bodies in neurons, formed mainly by the aggregation of α-synuclein protein (Breydo et al., 2012).

Cholesterol dyshomeostasis in PD is debated, due to the conflicting results obtained thus far (Paul et al., 2015).

Studies have been conducted to understand whether ApoE4 alleles increase the risk to develop the disease; these proved inconclusive, however. Nevertheless, increased risk to develop PD was observed in individuals carrying both LDL receptor related protein associated protein 1 (LRPAP1) I along with APOE e4 allelic variants (Singh et al., 2014).

No differences in sphingomyelin or cholesterol content were observed in post mortem samples from patients with early motor stages and incidental PD compared to healthy subjects (Martin et al., 2014). However significantly reduced levels of polyunsaturated fatty acids were observed in raft fractions from PD patients (Bar-On et al., 2006).

Attempts have been made to better understand the effects of sterol dysregulation by reducing sterol levels in cultured neuron and animal models of synucleinopathies. Treatment with the cholesterol extracting drug methyl-β-cyclodextrin decreases the levels of α-synuclein preventing its aggregation. Moreover, treatment with statins also reduces the aggregation of α-synuclein *in vitro* and *in vivo* (Martin et al., 2014).

The optimal approach to implementing such therapies will be to determine the right concentration of statins to use in order to lower cholesterol levels and restore the AD and PD phenotypes without compromising normal synaptic activity. More importantly investigation continues to better understand the specific aspects of sterol dyshomeostasis in these neurodegenerative diseases in order to more efficiently tackle the underlying issues.

In Huntington's disease (HD) dysregulation, of cholesterol homeostasis has also elicited increased attention. Being the main aim of my studies, I will discuss this in detail.

1.4. Evidence for cholesterol dyshomeostasis in HD

During the past ten years, a number of groups have identified changes in sterol homeostasis in HD.

Among the first reports, Sipione et al. aimed to study early cellular and molecular dysfunctions caused by expanded poly(Q) Huntingtin fragments. They observed by DNA microarray analysis that mRNAs encoding for proteins involved in cholesterol biosynthesis were downregulated in their cell system (Sipione et al., 2002).

Though blood lipid parameters had been studied previously in HD patients, no significant changes being observed in cholesterol levels (Hooghwinkel et al., 1966), the investigation of brain sterol metabolism in HD has received increasing attention from 2005. The same group that observed the downregulation of mRNAs from proteins involved in the cholesterol biosynthetic pathway showed the decreased expression of HMGCR, CYP51 and DHCR7 mRNAs in R6/2 HD mouse, human HD brain (cortex and striatum) and peripheral cells. They attributed this reduction in gene expression to impairment in SREBP2 translocation into the nucleus as detected *in vitro* in HD19 cells (Q26) and HD 43 cells (Q105), and HD mouse brain tissue (Table 1) (Valenza et al., 2005).

Valenza M., et al subsequently published two papers on abnormalities in cholesterol and cholesterol precursors in HD models; one in R6/2 mice (Table 1) (Valenza, Leoni et al., 2007) and the other in YAC128 mice (Table 1) (Valenza, Carrol et al., 2007). The brains of R6/2 transgenic mice presented progressively decreased levels of lathosterol and lanosterol, and exhibited lower activity of HMGCR beginning with pre-symptomatic stages of the disease. Despite the reduction in the cholesterol biosynthesis its levels, as detected by isotope-dilution mass spectrometry, are constant. To explain this fact the authors hypothesized the existence of a possible compensatory mechanism. However, this data is somewhat contradictory to what was published in their previous paper (Table 1) (Valenza et al., 2005), which used a different sterol detection method (cholesterol oxidase assay). Finally, they measured the levels of 24S-OHC and concluded that these were not significantly affected in R6/2 mice (Valenza, Leoni et al., 2007). Findings reported by this group in YAC128 HD mice, however, showed a small but significant decrease in 24S-OHC at 10 months of age (Valenza, Carrol et al., 2007). The brains of YAC128 mice also presented a reduction in HMGCR activity at 10 months of age, which correlated

with significantly decreased levels of lathosterol, desmosterol, and 24S-OHC. The surprisingly finding of this study was the possible ability of Htt overexpression (wild type protein with 18CAG) to induce higher activity of the cholesterol biosynthetic pathway as compared with littermate controls (Table 1) (Valenza, Carrol et al., 2007).

In parallel to the above work, however, Trushina et al. demonstrated cholesterol accumulation in neurons and brains from HD72 mice and in differentiated PC12 cells, using filipin staining and thin-layer chromatography. The mechanism presented to support these observations is that mutHtt binds to Cav1 and inhibits clathrin-independent endocytosis, thereby causing accumulation of plasma membrane cholesterol within caveolae (Table 1) (Trushina et al., 2006). Trushina et al. also showed cholesterol accumulation in primary striatal neurons from HD72 HD mice (Trushina et al., 2009). Moreover they demonstrated that Tricyclic Pyrone (TP) compounds both suppress the aggregation of mutHtt and abolish cholesterol accumulation in HD72 neurons.

In another study focusing on neuronal effects, Del Toro et al. observed cholesterol accumulation in striatal cells derived from wild-type (7Q) versus mutHtt-expressing knock-in mice (111Q), as well as other HD systems, by a combination of filipin staining and biochemical methods (Table 1) (del Toro et al., 2010). In this publication the authors also considered effects of mutHtt at the plasma membrane. Like Trushina et al. previously, they showed that mutHtt increases cholesterol-rich plasma membrane subdomains (as reflected in the levels of Cav-1 and glycosphingolipid GM1). Interestingly, they go on to provide an alternate mechanism of toxicity, however, by suggesting that in HD-like conditions NMDA receptors are redistributed into cholesterol-enriched extrasynaptic domains, which are more prone to induce excitotoxicity (Fernandes and Raymond, 2009). Importantly, they observed enhancement in NMDAR-mediated excitotoxicity which was reversed by treatment with the cholesterol lowering drugs simvastatin and B-cyclodextrin (del Toro et al., 2010).

Other work by the Cattaneo group explored additional aspects of the HD-associated sterol dysregulation that occur in glial cells. Astrocytes from Htt transgenic mice with progressive increases in CAG repeats showed

downregulation of proteins involved in the cholesterol biosynthetic pathway and genes responsible for the transport of cholesterol (Valenza et al., 2010). In the same study, the authors reported that the ApoE complexes from HD mouse cerebrospinal fluid was associated with smaller lipoproteins. Moreover the authors claimed that the low cholesterol biosynthesis was caused by impaired SREBP translocation to the nucleus. Thus, they suggested that astrocytes contributed to sterol dyshomeostasis due to mutant Htt, causing astrocytes to deliver less ApoE-bound cholesterol to neurons (Table 1.1) (Valenza et al., 2010). Further studies by this group using both R6/2 mice and differentiated neural stem cells also supported this conclusion. Glial conditioned medium from wild type astrocytes was able to rescue HD-related neurite outgrowth deficits and increase the number of Bassoon/GABA or Bassoon/vGLUT2 punctata in both striatal and cortical HD neurons, respectively (Table 1.1) (Valenza et al., 2015).

An additional non-neuronal aspect of the dysregulation of sterol homeostasis in HD was highlighted by studies of Xiang Z., which showed abnormalities in oligodendrocytes. Oligodendrocytes from R6/2 mice and BACHD transgenic rats, showed postnatal defects in myelination, which they linked to the HD-related hypofunction of the transcriptional co-regulator PGC1α. These effects were linked to specific deficiencies in PGC1α-induced expression of the sterol biosynthesis genes *HMGCS1* and *HMGCR*, as well as the gene encoding myelin basic protein (Table 1.1) (Xiang et al., 2011).

Our lab entered into this research area somewhat by chance. Our first publication (Luthi-Carter et al., 2010) entered into the HD cholesterol research field by uncovering a new mechanism of action of the Sirt 2 inhibitors AK-1 and AGK-2. SIRT2 is a tubulin deacetylase and an important regulator of cell division and myelinogenesis (North and Verdin, 2007; Werner et al., 2007; Li et al., 2007), nevertheless the exact roles of SIRT2 in non-dividing cells such as neurons are still unclear. The neuroprotection achieved by AK-1 and AGK-2 in primary striatal cells carrying the mutant Htt (82Q) includes the suppression of toxic aggregates. Surprisingly, however, HD cells treated with AK-1 showed a transcriptomic profile in which the genes encoding the enzymes involved in the cholesterol biosynthetic pathway were downregulated. Following on from this

result, the lab demonstrated that the specific sterol-regulatory effect reversed the cellular accumulation of cholesterol and rescued the viability of striatal neurons (Table 1.1). Following on this discovery the team identified and tested a more blood brain barrier (BBB) permeable Sirt 2 inhibitor: AK-7 (Taylor et al., 2011), which demonstrated the same cellular and biochemical effects. Kazantsev and other members of the original team further went on to show that AK-7 demonstrated therapeutic efficacy in two HD mouse models, the R6/2 (which expresses a mutHtt fragment) and the 140 CAG Htt knock-in model (Chopra et al., 2012). Chronic treatment with AK-7 ameliorated HD phenotypes including improving motor function, extending survival and reducing brain atrophy.

From this collection of publications I must point out a duality: one set of results support a reduction of cholesterol and sterol precursors (lanosterol, lathosterol and desmosterol) in HD, and attribute this to an effect of decreased expression of genes involved in the cholesterol biosynthetic pathway (Valenza M., 2005, 2007, 2007, 2010), whereas another line of evidence shows that cholesterol accumulates and/or redistributes in HD models (Trushina et al., 2006; del Toro et al., 2010; Luthi-Carter et al., 2010). The cholesterol phenotype in HD afflicted patients and HD models might thus be very complex and dependent on disease progression and the preponderant cell type affected. Research efforts need to be pursued in order to deepen the understanding on how mutant Htt affects cholesterol synthesis and trafficking in the different brain cell subpopulations, and how these subpopulations interact.

I hope to reconcile some of these disparate findings in the present project.

HD model	Phenotype	Bibliography reference
Primary fibroblasts from HD patient Post-mortem brain tissue (striatum and cortex) R6/2 model (striatum and cortex)	HMGCR, CYP51 and 7dhcr mRNA levels decreased	Valenza, Rigamonti et al. 2005
Striatal neurons and brain (HD 72) mice	Cholesterol accumulation (Filipin staining and thin layer chromatography)	Trushina, Singh et al. 2006
R6/2 mice (striatum, cortex and hippocampus)	Decreased leves of lanosterol, lathosterol (Isotope dilution mass-spectrometry)	Valenza, Leoni et al. 2007
YAC 128	Decreased sterol (striatum) Decreased lathosterol, lanosterol and 24S-OHC (brain) HMGCR decreased activity (brain) Decreased cholesterol, lathosterol, desmosterol and 24S-OHC in plasma	Valenza, Carrol et al. 2007
YAC 128 (brain) YAC 72 (striatum and cortex) Hdh Q111/Q111 (brain)	Decreased lathosterol and cholesterol	Valenza, Leoni et al. 2010
R6/2, YAC 128, HD rat, Hdh Q111/Q111 (brain)	Decreased 24S-OHC	
R6/2 and YAC 128 astrocytes	Decreased mRNA levels HMGCR, CYP51 and 7dhcr	
YAC 128 astrocytes	Decreased ABCA1 and ApoE mRNA	
YAC 128 mice	Decreased ApoE (size)	
Striatal cells knock-in mice Q111	Cholesterol accumulation at PM and in intracellular deposits (filipin and nile red staining) Total cholesterol and triglyceride (enzymatic methods)	del Toro, Xifro et al. 2010
HD human caudate	Total cholesterol increased	
Striatal neurons (Sprague Dawley) infected Htt 171-82Q	Increased sterol levels (Cholesterol oxidase assay)	Luthi-Carter, R., Taylor D. et al. 2010
Rs/2 and BACHD oligodendrocytes	Post natal defects in myalination	Xiang, Valenza et al. 2011

Table 1.1: **Summary of Huntington's disease research, on sterol metabolism**. Different HD models were used to determine the sterol status in HD affected specimens. The different groups involved in the investigation of sterol dysregulation in HD applied different methods for sterol analyses. For more details see introduction section 1.4.

1.5. Aims of the thesis

The idea for my PhD project laid on the previous published work from the laboratory, in which they observed sterol accumulation in primary striatal neurons expressing mutant Htt.

The field of research comprehending the sterol dyshomeostasis in HD is controversial, therefore there is an urge to understand how the sterol status of the brain progresses along the disease and how it relates with the disease hallmarks. Therefore, the main motivation to pursue this project was to clarify these aspects and to convey the available knowledge from the different groups in the field.

Taking advantage of a disease model *in vitro* that recapitulates the early stages of the disease, as neuronal death and Htt aggregates do not occur at DIV 13 *in vitro,* allowed me to tackle the sterol status at an early aetiologic event in HD. In section 3.1 I proposed to investigate the sterol accumulation and intracellular compartmentalization at the plasma membrane and lysosomes. Also taking advantage of this *in vitro* model I aimed to investigate in section 3.1 the type of sterol enriched in the medium of primary striatal neurons expressing the N-terminal fragment of Htt with 82Q. Having identified 24S-OHC as a sterol enriched in the medium of HD neurons, in section 3.2, I intended to disseminate the effects of 24S-OHC for the neuronal health taking in consideration the HD hallmarks such as excitotoxicity, endoplasmic reticulum (ER) stress and increased respiratory oxidative species (superoxide), in order to understand if this aetiologic aspect observed in the model – increased 24S-OHC efflux from HD neurons, can sensitize neurons to develop the proposed HD hallmarks.

In the last section 3.3, I aimed to investigate the effects of physiologic concentrations of 24S-OHC for the sterol status and health of astrocytes *in vitro.* I hypothesised that 24S-OHC acted at the transcriptional level regulating SREBP2 and LXR target genes, altering in this way astrocytes' sterol status. Moreover, I proposed to investigate if 24S-OHC could affect astrocytes' survival and influence HDs' hallmarks investigated in section 3.2- ER stress and increased superoxide levels.

I intended that the results presented in this thesis provided a new and more cohesive view of transcellular sterol dysregulation and neurodegeneration in HD.

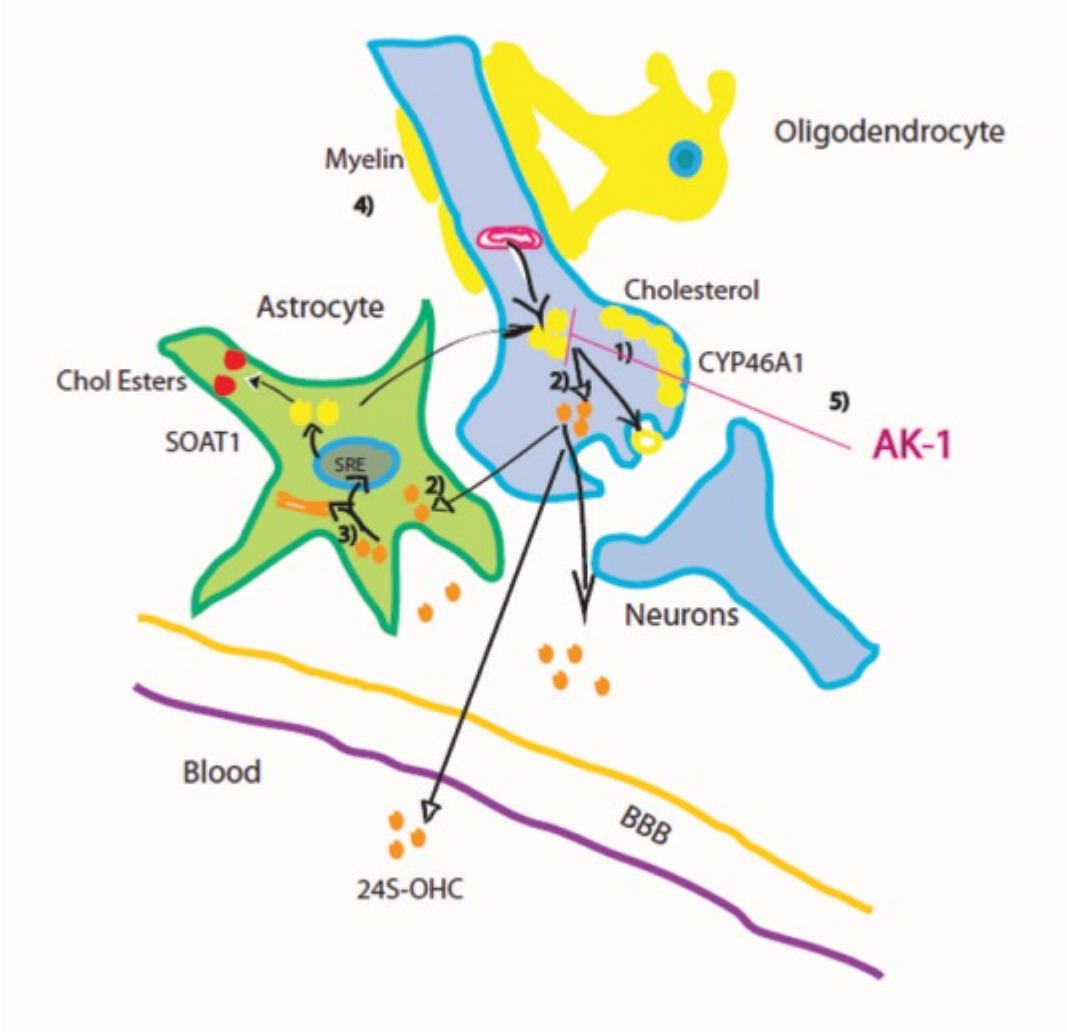

Figure 1.6: **Working model of sterol dyshomeostasis in HD.** Based on publications (Trushina et al., 2006; del Toro et al., 2010; Luthi-Carter et al., 2010). **1)** HD neurons accumulate more sterols and/or show abnormal sterol distribution compared to their wild-type counterparts. **2)** CYP46A1 in neurons converts accumulated/redistributed sterols into 24S-OHC (orange dots), which can signal to adjacent astrocytes (and possibly also oligodendrocytes). **3)** Astrocytes respond by decreasing sterol biosynthesis, which may eventually lead to a decreased level of cholesterol in neurons. **4)** Myelin synthesis is disrupted in oligodendrocytes via transcellular and/or cell-autonomous mechanisms. **5)** AK-1 and similar compounds counteract the early initial phase of sterol accumulation in neurons.

2. Material and Methods

2.1. Primary striatal neuron preparation

2.1.1. Poly-L-lysine and Poly-D-lysine coating plates

A solution of 0.1mg/mL of poly-L-lysine (Sigma - P1274) was prepared in tissue culture graded water and used to coat plastic plates, while poly-D-lysine (Sigma – P7280) at the same concentration and same preparation was used to coat glass cover slips.

The poly-L/D-lysine solution was added to the plates/cover slips, the enough volume to cover the entire wells surface. Plates were left inside the hood overnight. In the morning the poly-L/D-lysine solution was removed, and surfaces were washed 3 times with sterile water.

During the preparation of the primary neurons, the surfaces were dried inside the hood, to be ready to receive the primary cells at the end of the preparation.

2.1.2. Dissection of striatum from E16 embryos

Timed-pregnant Sprague-Dawley rat were requested from Charles River and maintained until embryonic day (E) 16 in the Central Research Facility (CRF) unit of the University of Leicester. Once reached the embryonic day 16 the female rat was euthanized by CO_2 asphyxiation, by a member of the CRF facility, who was responsible to remove the uterus and place them in cold DMX solution (Ca^{2+} - and Mg^{2+} -free phosphate buffered saline (PBS) (Invitrogen - 20012019), 0.6% glucose (Sigma), 10 mM HEPES (Calbiochem: 391338 (MW : 238.3)) and 1% Penicilin-Streptomicin (10,000 units/mL, 10,000 µg/mL, respectively, Invitrogen-15140-122).

The embryos were dissociated from the embryonic sac and decapitated under a sterile hood. Dissection was performed under the SXZ12-131 stereomicroscope (Olympus) in ice-cold dissection medium (DMX). All the dissecting tools used were sterilized in 70% ethanol and flamed.

Brains were removed from the skull and transferred to a 60mm dish on ice filled with DMX solution. Each brain was turned into ventral view, two

hemispheres were separated and ganglionic eminences removed and isolated in another 60mm dish with DMX.

After dissociation of all the brains, tissue was minced with forceps and transferred into a 50 millilitre falcon tube (Smith et al., 1964). After the tissue was settled in the bottom of the falcon, the supernatant- DMX was removed and a volume of 10 mL from a solution of 0.05% Trypsin (Life technologies - 15090046) diluted in DMX, was added to start the tissue digestion at 37^0C for 10 minutes (Phillipi et al., 2008).

In order to stop trypsin action, the digested tissues were let to settle at the bottom of tube, and solution was removed, 10 mL of culture medium (NBM) with 10% horse serum was then added and incubated for 2-3 min at room temperature (RT). Culture medium (NBM) is constituted by: Neurobasal medium (Invitrogen - 21103-049), 2% B27 (Invitrogen - 17504.044), 0.5 mM of penicillin-streptomycin, 15mM of KCl and 0.5 mM L-Glutamine (Life technologies – 25030-081). After the incubation period the supernatant was removed and 10 mL of medium with horse serum was added to initiate tissue trituration using a 5 mL pipette. After the tissue trituration, the homogenous solution was centrifuged at 1300 rpm for 8 min. At the end of the centrifugation, the supernatant was discarded and the cells were re-suspended in 10 mL of NBM. The last step before counting consisted in filtering the cells using 100 µm filter (name brand).

Before plating, cells were counted to determine the number of viable cells per millilitre. To enable live cells visualisation, trypan blue was used. Trypan blue cell count is a method based on the principle that live cells possess an intact membrane which blocks the passage of blue dyes, therefore excludes necrotic cells observed under the microscope as dark blue cell body, from a shiny and transparent viable cell (Strober, 2001). The solution for cell counts consisted in ¼ of cells, ¼ trypan blue and ½ medium, and from this volume, only 5 µL were loaded into a clean haemocytometer (Figure 2.1).

Upper and lower central grids (blue circle) were used to count the number of cells in it and the total number was determined by using the formula: (number of cells upper/ number of cell lower)/2 x dilution factor x 10^4. The factor 10^4 comes from the fact that each small square (delineated in pink- Figure 2.1) has an area of 0.04 mm^2 and the haemocytometer hold the cover slip 0.1mm off the

grid, therefore the volume of the entire middle square is (0.04 x 25) x 0.1= $0.1mm^3$= 10^{-4} cm^3=10^{-4} mL (Figure 2.1).

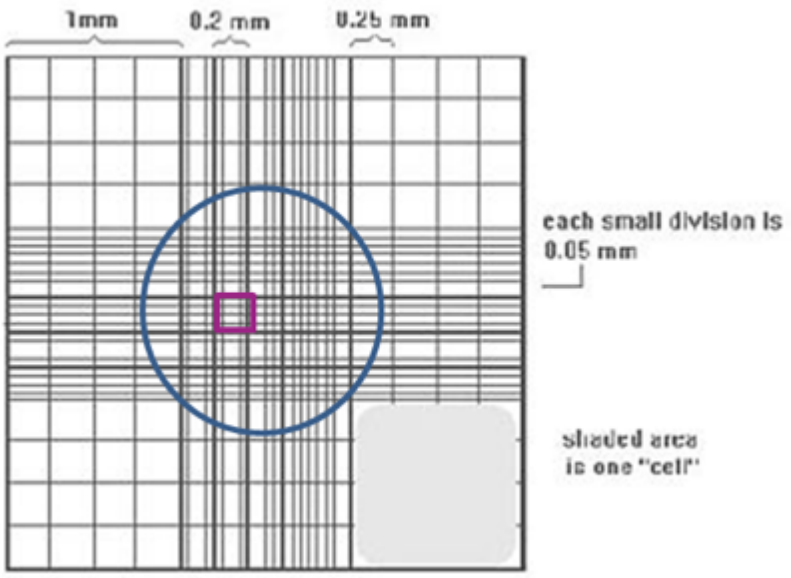

Figure 2.1: **Representation of haemocytometer grid.** The cells inside the limits of the square with more divisions, represented by a blue circle, were counted, and the formula used to determine the number of cells has in consideration the area of the pink square: 0.04 mm^2 x 25 (total number of squares in the blue circle) = 1 mm^2 the haemocytometer hold the cover slip 0.1mm off the grid, therefore: 1 mm^2 x 0.1mm = 0.1 mm^3 = 10^{-4} mL.

Striatal cells were then plated at a concentration of $5x10^5$ cells/mL, at a final volume of 3 mL in a 6 well plate, 1.2 mL in 12 well plate and 600 µL in a 24 well plate. Plates were kept at 37^0C with 5% CO_2 and half volume of media was replaced once per week (Zala et al., 2005).

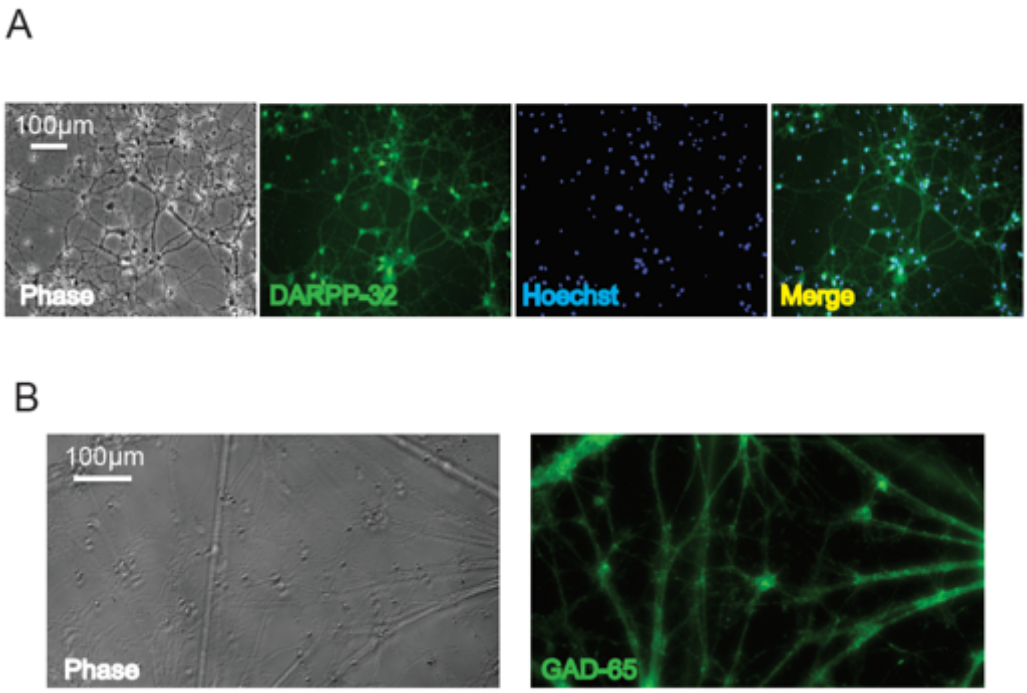

Figure 2.2: **Cultured medium spiny neurons express DARPP-32 and GAD-65. A-** The marker for medium spiny neurons: DARPP-32 and **B-** GABAergic cells: GAD-65 were used to classify the cells as medium spiny neurons (DARPP-32 positives/GAD-65 positives) (Iwabuchi et al., 2013).

2.2. Primary astrocyte preparation

As previously described for striatal neuron preparation, a pregnant Sprague Dawley was requested to Charles River to arrive in the CRF unit at E16, and was kept in that facility until the pups were born. At P1 the pups were collected and transported into an appropriate laboratory where the rest of the protocol took place.

Each pup was decapitated and the head was kept inside a glass flask filled with Earle's Balanced Salt Solution (EBSS) (Ca/Mg free) [Invitrogen 14155-048] base solution completed with 1% $MgSO_4$ (stock 3.82g/100ml) [Sigma M2643], 0.3% (W/V) BSA (fraction V) [Sigma A9418] and 0.25% (W/V) glucose (D-(+)-Glucose) [Sigma G5767]. In order to extract the brain, the first step was to cut off the skin from the direction of the neck to the middle of the eyes, and fold the tissue laterally. The skull was removed carefully not to damage the brain underneath it. Once the skull is all removed, the brain was

retrieved, the cerebellum was cut off and the cortices were isolated. Tissues were kept in cold EBSS solution. The cortices were minced into small pieces and transferred into a falcon tube. Digestion occurred in the presence of a trypsin solution (2.5mg Trypsin (Sigma T9201) in 10mL EBSS), at 37^0C for 15 min.

After the digestion, cells in a falcon tube were placed inside the hood, and $1/6^{th}$ volume of the following solution was added: 1% DNase (stock 4mg/ml in PBS, DNase I, Type IV, 15KU [Sigma D5025]), 0.12% (w/v) trypsin inhibitor (Type 1-S [Sigma T9003]), 1% $MgSO_4$ in EBSS solution, and incubated for 5 min. After incubation, supernatant was decanted off and 2.5 mL of the described solution, not diluted this time, was added to the trypsinized cells. The cells were triturated with a 5 mL pipette.

The last step consisted in adding a solution of BSA (0.4g) and a volume of 80 µL from a solution of 0.3M $MgSO_4$ in 10mL EBSS. A homogenate was centrifuged at 1000 rpm for 8 min. After discarding supernatant, the pellet was re-suspended in DMEM media containing 1% Gentamycin, 1% fungizone and 10% fetal calf serum (FCS). Cells from 3 brains were plated in 175cm^2 flask in a volume of 50 mL.

Mixed culture of astrocytes were incubated at 37^0C with 5% CO_2 for 3 days. At 3 Days *in vitro* (DIV) media was changed and at DIV 6 the mixed culture was shaken at 320 rpm over night at 37^0C, this step cleared out the unwanted cells such as microglia, oligodendrocytes and possible fibroblasts.

After shaking the medium containing unwanted cells was discarded (for astrocytes culture purity see Figure 2.3). The remaining cells attached to the flask were washed with PBS and trypsinized. DMEM medium complete with antibiotics and FCS was added to inhibit trypsin, and the cell suspension was collected and centrifuged at 1300 rpm for 8 min. Cell pellet was re-suspended in 20 mL of DMEM, complete and proceed to cell count as described in 2.1.2. Astrocytes were plated at $0.16x10^6$ cells/mL in different dishes format depending on the experimental aim. One day after plating, media was changed to DMEM with gentamycin, fungizone and G5 supplement (Invitrogen 17503-012) and astrocytes were left to differentiate in that media for 48h, after that experiments were initiated.

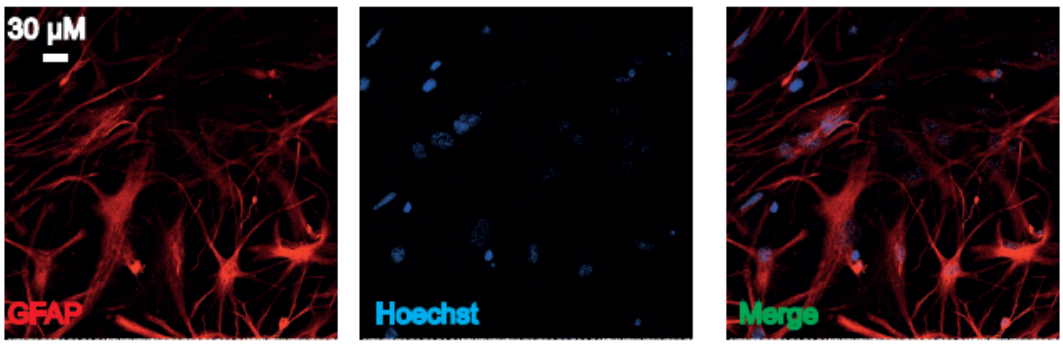

Figure 2.3: **Characterization of cultured astrocytes by immunostaining.** Glial fibrillary acidic protein (GFAP) labels astrocytes (red) and Hoechst labels nucleus (blue). The merge image shows the elevated purification of the astrocytes culture.

2.3. Primary striatal neuron infections with lentiviral expression vectors, a Huntington's disease model *in vitro*

The model used to replicate HD pathology was generated by infecting primary striatal neurons with two lentiviral vectors. The first one contains the cDNA of the first 171 amino acids of Huntingtin followed by 18 or 82 polyglutamines (nonpathologic Htt171-18Q or mutant Htt171-82Q), respectively, under the control of Tetracycline-response element regulated promoter (TRE), the plasmid is the following: SIN-TRE-Htt171-18Q/82Q-WPRE (Gagnon et al.) (Figure 2.3) The second vector encodes the tetracycline Transactivator (tTA) under the control of phosphoglycerate kinase 1 (PGK) promoter: SIN-PGK-tTA-WPRE (Regulier et al., 2002) (Figure 2.3)

The viral productions were performed in 293T cells, by laboratory of Nicole Deglon in Lausanne, with a four-plasmid system as described previously (Zala et al 2005; Deglon et al., 2000; de Almeida et al., 2001; Regulier et al., 2003). The viruses were resuspended in PBS with 1% BSA and matched for particle content to 1500 ng p24 antigen/mL for 18/82Q virus and 2400 ng p24 antigen/mL for tTA virus as measured by ELISA (RETROtek, Gentaur, Paris, France). The cell cultures were infected at DIV 2, with Htt-expressing lentiviruses at a concentration of 50 ng/mL in the culture medium together with a vector encoding the tetracycline-controlled transactivator tTA1 under the control of PGK promoter (at a concentration of 80ng p24/mL). At DIV 6, half of

the medium was replaced with freshly prepared culture medium. The transduction efficiency of primary neurons under these conditions has been shown to be ≥95% (Runne et al., 2008; Zala et al., 2005). Moreover the high transduction rate and sustained transgene expression observed by neurons infected with lentiviral vectors, allows the study of mutant Htt-induced cell toxicity and its cellular pathways (de Almeida et al., 2002; Regulier et al., 2003; Zala et al., 2004) more efficiently than through transfection methods, where the transgene expression is low and not consistent.

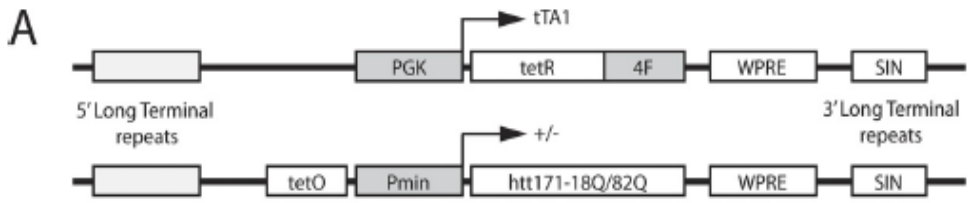

Figure 2.4: **Schematic representation of lentiviral vector system.** Lentiviral vector system used for the expression of tetracycline-regulated wild-type (18 CAG) or mutated (82 CAG) followed by the first 171 amino acids of human Huntingtin (SIN-TRE-Htt171-18Q/82Q-WPRE), added together at DIV 2 with the tTA transactivator (SIN-PGK-tTA-WPRE): tetracycline gene under control of Phosphoglyceryl kinase (PGK) promoter, which corresponds to a highly expressed housekeeping gene in neurons.

2.4. MTT assay

MTT (3-(4,5-dimethylthiazol-2-yl)-2,5-diphenyltetrazolium bromide) assay (M6494 - Life technologies) is a method that allows the determination of the number of viable cells.

The method consists in adding MTT (3-(4,5-dimethylthiazol-2-yl)-2,5-diphenyltetrazolium bromide) to cultured cells, and this compound is converted into formazan crystals by the actively respiring cells (Liu et al., 1997). The formazan crystals are dissolved in DMSO and their concentration determined by optical density at 540 nm using a Tecan absorbance reader.

MTT stock made at 12 mM, was prepared in PBS the day before of the assay, and stored at 4^0C.

On the day of the assay, MTT was added to primary cells after respective treatments were performed at a final concentration of 1.2 mM, and incubated for 4h in the incubator (37^0C). The assay was terminated by dissolving the formazan crystals with DMSO, and absorbance was read at 540 nm.

2.5. Immunostaining

Cell cultures were washed with cold PBS and fixed in 4% paraformaldehyde (Sigma P6148) for 10 min at room temperature. Cultures were subsequently washed with PBS and then incubated in a blocking and permeabilizing solution of 5%BSA + 0.1%Trition-X100 in PBS for 1h at RT. The cells were then incubated overnight at 4^0C in blocking solution containing primary antibody: GFAP (MAB3771), NeuN (MAB 377 Milipore), DARPP-32 (Chemicon AB 1656), SREBP2 (ab30682), GluN1 (NMDA subunit) (BD biosciences 556308) and GluN2B (NMDA subunit) (BD biosciences 610416). The primary cells were incubated with each antibody at a concentration of 1:400 GFAP and NeuN; DARPP-32, GluN1, GluN2B and SREBP2 at 1:200. Cells were washed after primary antibody incubation, to eliminate unspecific binding, and incubated for 1h at RT with secondary antibodies coupled with fluorophores. The secondary antibodies used were anti-mouse Alexa fluor 488 (Life technologies A21121) at 1:500; anti-mouse Alexa fluor 546 (Life technologies A21123) at 1:500 to bind to GFAP, and cells containing the primary antibody for DARPP-32 were incubated with goat anti-rabbit Alexa fluor 488 (Life technologies A11008) while cells incubated primarily with SREBP2 were incubated with goat anti-rabbit Alexa fluor 546 (Life technologies A11035). After 1h of incubation with secondary antibody diluted in blocking and permeabilizing solution, cells were washed with PBS.

When cells were immunostained for NMDA receptor isoforms GluN1 and GluN2B as well as with SREBP2 and DARPP-32, a further staining followed: Hoechst was applied at 0.0001 mg/mL for 30min at RT to label the nucleus.

Primary neurons on coverslips stained with GluN1 and GluN2B antibodies were mounted in mowiol and let them to dry overnight. Images were accessed using Leica SP5 CLSM confocal microscope, with a magnification of 60x.

Primary neurons labelled with NeuN, DARPP-32 and GFAP, and astrocytes incubated with SREBP2 were grown on 24 well plates. For both experiments, the images were taken using Nikon inverted microscope (Nikon eclipse Ti) with a magnification of 20x.

2.5.1. Fluorescence microscopy

NeuN cell counts and NeuN integrated density: For the purpose of the analyses, all the images were taken with the same exposure. The analyses were performed in the following way: 1) open NeuN image and make a copy; 2) Select the copy image, adjust threshold and analyse particles, send to regions of interest (ROI); 3) Select the original image and add particles from ROI, measure integrated density (the product of area with mean grey value, being the last one the sum of the grey values of all pixels in the selection divided by the number of pixels). The number of particles corresponded to the number of NeuN positive counts. These procedures were performed in the same way for all the images for Htt171-18Q versus Htt171-82) and for NMDA and 24S-hydroxycholesterol treatment neurotoxicity experiments. In an experiment, 18 wells per condition were analysed (N=1, n=18) to validate the HD model, and to determine the toxicity of NMDA and 24S-OHC, 3 wells were used per condition, and the experiments were performed 3 times (N=3, n=9). Where manual scans were performed, the same sequence were always followed: taking a picture on the top, bottom, left, right and centre of each well. On image J, only the ROI from 10 to infinite size (microns) were considered in counting.

SREBP2: For the purpose of the analyses, all the images were taken with the same exposure. The analysed were performed in the following way: for each images there were two channels, Hoechst and SREBP2. To determine the intensity of SREBP2 in the nucleus, the analyses started by opening the Hoechst channel, adjusting the threshold and analysing particles (nucleus), send the regions of interest: nucleus to ROI. Select the SREBP2 image and add particles from ROI, measure integrated density. I performed the same sequence for all the images in both conditions (DMSO versus 24S-hydroxycholesterol treated cells). Two independent experiments were performed for each condition 18 wells per condition were analysed (N=2, n=39).

2.6. Filipin staining

Filipin is a known antifungal, naturally extracted from the bacteria *Streptomyces filipinensis* (Gottlieb et al., 1958). When filipin binds to unesterified sterols fluoresces under ultraviolet transillumination (Schroeder et al., 1971). This property has made filipin a histochemical marker for free cholesterol in numerous diseases (del Toro et al., 2010; Harzer and Kustermann-Kuhn, 2001; te Vruchte et al., 2004; Trushina et al., 2006).

Striatal neurons plated in 24 well plates ($5x10^5$/mL) were fixed in 4% PFA for 10 min at RT, 11 days after transfection with Huntingtin expression vectors (Htt171-18Q/82Q). In order to quench the paraformaldehyde, cells were incubated with 1.5mg glycine/mL PBS for 10min at RT. Cells were rinsed with 1XPBS and incubated protected from light with 500 µL of 5 µg/mL filipin (Sigma, F9765) in PBS for 2h at RT. Cells were washed again with 1X PBS, coverslips were mounted in mowiol, let dry protected from light. Cells were observed under the confocal microscope: Leica SP5 CLSM, using a UV filter set (340-380 nm excitation, 40 nm dichroic, 430-nm long pass filter). Images were taken with a 60x magnification, zoom factor 2.5 1024x1024 pixels.

2.7. Live cell stains

Primary neurons were cultured in a 24 well plate format on coverslips, and on the day to be fixed, cells were incubated with 5 µg/mL of the plasma membrane marker (C10046- Molecular probes) and 75 nM of the lysosome marker (L7528- Molecular probes). Upon adding the reagents into the cultured medium, cells were left inside the incubator for 1h. After that time, dye was removed and cells were washed with 1X PBS and fixed with 4% PFA for 10 min at RT. Followed by filipin staining and confocal analyses.

Plasma membrane deep red excitation/emission: 649/666 nm, and Lysotracker red DND-99 excitation/emission: 577/590 nm. Images were taken with a 60x magnification, zoom factor 2.5 1024x1024 pixels.

2.7.1. U-18666A treatment

The amphipathic steroid 3-β-[2-(diethylamino)ethoxy]androst-5-en-17-one, named as U-18666A by the company Upjohn, has been widely used in lipid research (Cenedella, 2009). Due to its structure as an amphipatic cationic amine can interact with several proteins and cause several effects in the cell. Was discovered that U-18666A blocks cholesterol synthesis by inhibiting the enzyme oxidosqualene cyclase (Sexton et al., 1983). Moreover the same compound inhibits the escape of cholesterol from late endosomes and lysosomes (Liscum and Faust, 1989). Interestingly, this effect caused by U-18666A mimics what happens in Niemann-Pick disease type C, being therefore a recurrent used compound, to mimic the intracellular disease phenotype (Mohammadi et al., 2001).

I treated primary striatal neurons with U-18666A to cause increased sterol accumulation in lysosomes, acting as positive control for the filipin staining with lysosomal marker.

Striatal cells plated in 24 well plates were treated with 1.25 μM of U-18666A dissolved in culture medium for 48h prior to cells fixation.

2.7.2. Confocal microscopy

Filipin: For the purpose of the analyses, all the images were taken with the same exposure. The analyses were performed in the following way: open filipin image and make a copy. Select the copy image, adjust threshold and analyse particles, send to regions of interest (ROI). Select the original image and add particles from ROI, measure integrated density. I performed the same sequence for all the images in both conditions (Htt171-18Q versus Htt171-82Q). I performed 3 independent experiments; the number of wells analysed per experiment were 4 in each condition (N=3, n= 12).

Plasma membrane: For the purpose of the analyses, all the images were taken with the same exposure. The analyses were performed in the following way: for each image there were two channels, plasma membrane and filipin. To determine the intensity of filipin in the plasma membrane, the analysis started by opening the plasma membrane channel, adjusting the threshold and

analysing particles (plasma membrane structures), sending the regions of interest (plasma membrane structures) to ROI. Then I selected the filipin image and added particles from ROI, and measured integrated density. I performed the same for all the images in both conditions (Htt-171 18Q versus Htt-171 82Q). I performed 3 independent experiments; the number of wells analysed per experiment were 4 in each condition (N=3, n= 12).

Lysosome: For the purpose of the analyses, all the images were taken with the same exposure. The analyses were performed in the following way: for each image there were two channels, Lysotracker and filipin. To determine the intensity of filipin in the lysosome positive structures, the analyses started by opening the lysosome channel, adjusting the threshold and analysing particles (lysosome positive structures), sending the regions of interest (lysosome) to ROI. Then I selected the filipin image and added particles from ROI, and measured integrated density. I performed the same for all the images in both conditions (Htt-171 18Q versus Htt-171 82Q). I performed 3 independent experiments, the number of wells analysed per experiment were 4, in each condition (N=3, n= 12).

2.8. NMDA treatment

Cells cultured in 24 well plates were exposed to different NMDA concentrations (1, 10, 50, 100, 200, 500 and 1000 µM) at DIV 13. I treated the cells with NMDA in Locke's solution (154 mM NaCl, 5.6 mM KCl, 2.3 mM $CaCl_2$, 25 mM $NaHCO_3$, 10 mM HEPES, 20 mM glucose and 10 µM glycine, solution pH 7.3). The cells were incubated for 20 min in the incubator (Xifro et al., 2008). The Locke's solution and NMDA was replaced for conditioned medium (half medium from the cells, removed in the beginning of the experiment and half fresh medium) at the end of the experiment time (20 min). 24h after NMDA treatment, cell viability was accessed by NeuN staining and cell count using the Nikon inverted microscope (Nikon eclipse Ti) with a magnification of 20x.

Experiments containing MK-801, NMDA receptor antagonist, this compound was added 30 min before (in the medium) to NMDA addition, and maintained during NMDA treatment.

2.9. Cholesterol Assay

2.9.1. Cell harvesting

In order to perform this assay the first step was to prepare the cellular lysate.

Neuronal cells cultured in a 12-well plate were harvested on ice. The medium, in which they were cultured in, was either collected into an Eppendorf tube and stored at -80^{0}C for future analyses (Isotope dilution mass spectrometry analyses) or disposed off. Cells were washed with 1X PBS to remove any traces of culture medium, and harvested in 150 µL of 1X Reaction Buffer, diluted in deionized water from 5X Reaction Buffer (0.5 M potassium phosphate, pH 7.4, 0.25 M NaCl, 25 mM cholic acid, 0.5% Triton® X-100 - Invitrogen A12216). Cells were scraped from the wells, collected into an eppendorf on ice and sonicated. The lysates were centrifuged at 13,000 rpm for 15min at 37 ^{0}C and the supernatant was collect. Samples were stored in the -80^{0}C or proceeded to cholesterol assay and BCA assay.

2.9.2. BCA assay

Protein concentration was determined using the colorimetric assay BCA assay from Pierce (Thermo Scientific: 23227). A standard curve was conducted with 8 samples of known concentration (2, 1, 0.75, 0.5, 0.25, 0.125, 0.025 and 0 µg/µL) using the BSA diluted in 1X Reaction buffer (5X reaction buffer: 0.5 M potassium phosphate, pH 7.4, 0.25 M NaCl, 25 mM cholic acid, 0.5% Triton® X-100 - Invitrogen A12216). 5 µL of each sample or standard was pipetted into a multiwall transparent plate (Sterilin), and 100 µL of BCA assay reagents were added. Incubation of the plate took place for 30 min at 37^{0}C, after which the absorbance was read in a Tecan machine at 562nm.

2.9.3. Cholesterol Oxidase Assay

The amplex red cholesterol kit (Invitrogen A12216) is based on the simple fluorimetric chemical reaction that allows the sensitive quantification of cholesterol. The assay is based on an enzyme-coupled reaction that detects both free cholesterol and cholesteryl esters. Cholesteryl esters are hydrolyzed

by cholesterol esterase into cholesterol, which is then oxidized by cholesterol oxidase and the final products are hydrogen peroxide (H_2O_2) and the corresponding ketone product. The H_2O_2 is then detected using 10-acetyl-3,7-dihydroxyphenoxazine (Amplex® Red reagent). In the presence of horseradish peroxidase (HRP), Amplex® Red reagent reacts with H_2O_2 with a 1:1 stoichiometry to produce highly fluorescent resorufin (absorption and fluorescence emission maxima of approximately 571 nm and 585 nm, respectively) (Zhou et al., 1997).

In order to perform this assay I setup a standard curve with 8 samples (0, 2, 4, 10, 20, 50, 75 and 100 µg/mL of cholesterol) each of them were pipetted (a volume of 25 µL) in triplicate into a 96 well plate (Corning 3340). The samples in 1X Reaction buffer (5X reaction buffer: 0.5 M potassium phosphate, pH 7.4, 0.25 M NaCl, 25 mM cholic acid, 0.5% Triton® X-100), were pipetted the volume of 12.5 µL in triplicate, and in order to dilute them was added a volume of 12.5 µL of 1X Reaction buffer. On top of the diluted samples and the standards, the same volume (25 µL) of working solution was added (Amplex red reagent, HRP, cholesterol oxidase, cholesterol esterase in 1X Reaction buffer). The plate was incubated for 30 min at 37^0C, the Tecan machine was used to measure the fluorescence at an excitation of 560nm and emission at 590nm.

2.10. RNA analysis

2.10.1. RNA extraction

The principle of RNA extraction using Trizol (Sigma T9424) and chloroform is based on the fact that RNA is separated from DNA in the presence of chloroform in an acidic environment. Trizol recreates that environment once is a mono-phasic solution of phenol and guanidine isothiocyanate. Moreover Trizol enables RNA integrity while promotes cell lysis. Trizol enables the separation of DNA, proteins and RNA. After centrifugation, RNA remains in the aqueous phase (upper) while DNA and proteins are restricted in the organic phase and interface. The RNA, in the aqueous phase is isolated, by precipitation with isopropanol.

Detailed protocol for 24 well plates: Was added a volume of 500 µL Trizol reagent to each sample and let act for 5 min at Room Temperature (RT). After that a volume of 100 µL of chloroform was added, the lids of the Eppendorf tubes were closed to proceed to the mix of the samples by vigorous shake of the samples by hand for 15 seconds. Incubation took place at RT for 3 min. Samples were centrifuged at 12,000 g for 15 min at 4^0C. In order to harvest upper (aqueous) phase, which one contains RNA, into a new Eppendorf tube, the tube was inverted 45^0, after harvest RNA, was added 250 µL of isopropanol. This step was followed by incubation for 10 min at RT to let RNA precipitate. The samples were, then centrifuged at 12,000 g for 10 min at 4^0C and proceed to the careful removal of supernatant; at this stage RNA is a gel-like pellet, which can be aspirated in the process. RNA pellet was washed 2 times by adding 500 µL of 80% ethanol followed by centrifugation at 7,500 g for 5 min at 4^0C. Once RNA was washed, samples dried out for 5 min, after that the pellet was resuspended in 50 µL RNAase-free water and samples were incubated for 5 min at 60^0C to help RNA solubilisation. Store RNA at -80^0C.

2.10.2. Reverse transcription and qRT-PCR

The concentration of the RNA extracted from the primary striatal cells and astrocytes was measured in the Thermo Scientific NanoDrop. Absorbance measurements made in any spectrophotometer includes the absorbance of all molecules in the sample. Nucleotides absorb at 260 nm while protein and phenol at 280 nm. RNA samples are considered pure if the 260/280 ratio is approximately 2.0. The trizol reagent is a phenolic solution and absorbs in the UV at 230 nm and around 270 nm. Moreover EDTA, carbohydrates and guanidine isothiocyanate are some of the molecules that absorb at 230 nm and can increase the 260/230 ratio, and compromise the RNA purity (expected at 2.0 – 2.2).

Only samples with good quality of RNA were considered for reverse transcriptase and real-time quantitative PCR (qRT-PCR) analyses.

RNA samples were normalized to the same concentration and converted to complementary DNA (cDNA) using the Reverse Transcriptase (MultiScribe™), a recombinant enzyme isolated from moloney murine leukemia

virus (rMoMuLV). This polymerase uses RNA as template and in the presence of primers and dNTPs has the capacity to synthesize single stranded complementary DNA (4368814 Applied Biosystems).

The mix was then composed by 10 µL of RNA extracted, 2 µL buffer (2X), 2 µL Random primers, 0.8 µL dNTPS and 1 µL MultiScribe enzyme. The optimal cycles for the reaction are the following:

	Step 1	Step 2	Step 3	Step 4
Temperature (^{0}C)	25	37	85	4
Time	10 min	120 min	5 min	infinitum

The thermal cycler used for the reaction is Light Cycler 480 Roche.

A concentration of 5 ng of cDNA was used to perform real-time quantitative polymerase chain reaction (qRT-PCR). The qRT-PCR method used was SYBR green (SYBR green PCR Master Mix from Applied biosystems, catalog number 4309155), the master mix contains SYBR green I dye, Amplitaq gold DNA polymerase, dNTPs with dUTP and a passive reference, all diluted in an optimized buffer.

SYBR green I dye is an asymmetrical molecule that belongs to the polymethine group. Is a synthetic dye that binds preferentially double stranded DNA, the complex dye and DNA absorbs light with λ_{max}= 497 and emits green light: λ_{max}= 520, being this light captured by the PCR machine in real time, which allows to determine the amount of double stranded DNA in the sample. The data collect is represented in a numeric value: Ct, which means threshold cycle. The Ct is the intersection between an amplification curve and a horizontal line that separates in the amplification curve at which cycle of the reaction the amplicon started to be synthesized (Figure 2.5). The lower the Ct more template there is in the sample.

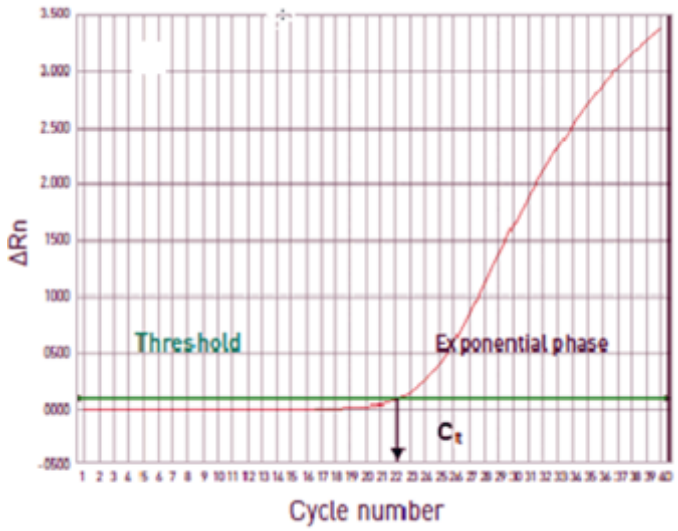

Figure 2.5: **Schematic representation of a qRT-PCR reaction.** Ct is the value resultant from the intersection of the threshold line, which one is positioned at the point when the amplification curve turns vertical, with the amplification curve.

Amplitaq gold DNA polymerase is a recombinant thermostable DNA polymerase isolated from *Thermus aquaticus,* this enzyme requires heat activation (95^0C) (Faloona et al, 1990; Chou et al 1992), well above the temperature for optimal annealing (60^0C). Considering the requirements of the enzyme used, the amplicon reactions occurred in a defined sequence: polymerase is activated, binds template (cDNA), temperature decreases and primers anneal at specific position on the template, and polymerase starts to synthesise. This process results in specific PCR products.

A passive reference is included in the mix, corresponds to a reference dye that does not act during the PCR reactions, is useful as internal reference, to which SYBR green can be normalized to during data analysis.

The primers used to amplify the desired sequence in the cDNA, were designed by me, and ordered from Sigma. Each pair of primers (forward and reverse) was used at 200 nM in the reaction mix. The primers efficiency was determined using 10 fold dilutions of cDNA corresponding to input RNA amounts of 100, 10, 1, 0.1 and 0.01 ng/μL. The Ct values, resultant from the qRT-PCR reaction from each pair of primers, were plotted versus the $\log_{10}$ of cDNA concentrations. The slope, resultant from the line that unites the points

on the graph, was calculated and used in account to determine the amplification efficiency (E): $E= 10^{(-1/slope)}$ (Table 2.1).

The pairs of primers used in this thesis had efficiencies close to 2.0, and one single melting curve.

Primer efficiency was taken in consideration in data analyse.

Gene name		Sequence	Efficiency
HMGCR	Primer F	GGTGCATCGCCATCCTGTA	1.99
	Primer R	GCTGACGCAGGTTCTGGAA	
LDLr	Primer F	CAGCTCTGTGTGAACCTGGA	1.76
	Primer R	TTCTTCAGGTTGGGGATCAG	
ABCA1	Primer F	GGTTTGGGGAGGAAATTGAT	1.8
	Primer R	AACCATCCACAGCAACCTTC	
ABCG4	Primer F	ACATCTTGGCAGGGTACAGG	1.87
	Primer R	ACCATCATGGCCTCTAGCAC	
APOE	Primer F	GTTTCGGAAGGAGCTGACTG	1.74
	Primer R	TGTGTGACTTGGGAGCTCTG	
CYP46A1	Primer F	GAAGGTCATGCTGGAGGGTA	1.8
	Primer R	TGAGAATCTGCGTGAGGATG	
HMGCS1	Primer F	AGCCTTTGGGGATGTGAAAT	1.69
	Primer R	TGTGCCAGAACAGAAGCAAG	
FDFT1	Primer F	AGCAGGAGTCAAGCCCTACA	1.84
	Primer R	CCAAAGGGTGACAGTGAGGT	
ABCG1	Primer F	GAGAAGGATGAAGGCAGACG	1.7
	Primer R	ACAGGAGGGTTGTTGACCAG	
SREBP1C	Primer F	CATCCGCTTCTTACAGCACA	2.2
	Primer R	TCATGCCCTCCATAGACACA	
Glut4	Primer F	GCTTCTGTTGCCCTTCTGTC	1.5
	Primer R	TGGACGCTCTCTTTCCAACT	
CHOP	Primer F	TATCTCATCCCCAGGAAACG	2
	Primer R	AGGTGCTTGTGACCTCTGCT	
BiP	Primer F	CCTGTTGCTGGACTCTGTGA	1.7
	Primer R	GGAATAGGTGGTCCCCAAGT	
bAct	Primer F	AGCCATGTACGTAGCCATCC	1.89
	Primer R	TCTCAGCTGTGGTGGTGAAG	

Table 2.1: **Primer sequences and efficiencies.** The table list the genes names, which RNA 's were measured in this thesis, and the respective sequence and efficiency.

The qRT-PCR reaction mix consisted of: 5 ng cDNA, 1X SYBR green PCR Master Mix and 200 nM Forward Primer and 200 nM Reverse Primer.

The cycle programme run was the following:

Temperature (C)	50	95	95	60	72
Time	2 min	10 min	15 sec	1 min	10 min

40 cycles

The plate setup was usually a 384 well format, where for each condition a minimum of 3 biological replicates together with 3 technical replicates were run.

The selected method to analyse the results was the Pfaffl method (Figure 2.6). The Pfaffl method is a relative quantification analysis that takes in consideration the steady-state mRNA levels of a gene of interest and compares it to the mRNA levels of an internal control (housekeeping gene) in order to normalize for variation in RNA input. The expression ratio also corrects for differences in amplification efficiencies for different primer pairs. The mathematical model is the following:

$$\text{Ratio} = \frac{(\text{E target})^{\text{dCt target (mean control - mean sample)}}}{(\text{E reference})^{\text{dCt reference (mean control - mean sample)}}}$$

Figure 2.6: **Pfaffl mathematical model for calculation of relative expression from qRT-PCR assay results.** The mRNA levels of the gene of interest (target) are determined relatively to a housekeeping gene (reference). The primers efficiency is elevated to the difference of Ct values between control and test samples. Calculating the ratio, or the fold change of mRNA expression of the target gene relatively to the housekeeping gene (reference).

	Average Cts	
	Htt-171 18Q	Htt-171 82Q
HMGCR	22.4	22.6
HMGCS1	17.9	18.1
LDLr	25.4	25.7
FDFT1	22.2	22.96
ABCA1	26.2	26.4
ABCG4	25.4	25.5
ApoE	21.6	21.6
CYP46A1	26.1	26.3
Actin	20	

Table 2.2: **qRT-PCR results for genes involved on cholesterol metabolism in primary striatal neurons.** The Cts from all the genes analysed, do not vary between the two conditions: Htt-171 18Q versus Htt-171 82Q.

0 μM 24S-OHC	0.5 μM 24S-OHC	1 μM 24S-OHC	2 μM 24S-OHC	4 μM 24S-OHC	
18.88	18.34	18.87	18.79	18.69	Actin
23.52	22.58	23.04	23.04	22.85	BiP
28.59	27.54	28.30	28.29	28.03	CHOP

8 μM 24S-OHC	10 μM 24S-OHC	20 μM 24S-OHC	
17.60	18.45	19.14	Actin
22.98	23.70	24.31	BiP
28.01	28.96	29.98	CHOP

TM	TG	
17.64	19.51	Actin
21.19	20.07	BiP
26.20	24.59	CHOP

Table 2.3: **qRT-PCR results for genes involved on endoplasmic reticulum stress in primary striatal neurons.** The Cts from the genes analysed (BiP and CHOP) are lower in table C compared to A and B. Treating cells with tunicamycin (TM) and thapsigargin (TG) induces BiP and CHOP overexpression. The same is not so evident between 24S-OHC concentrations in table A and B.

0 µM 24S-OHC	0.5 µM 24S-OHC	1 µM 24S-OHC	2 µM 24S-OHC	0 .5µM TO901317	Time	Gene
17.52	16.79	17.57	16.98	17.93	2h	Actin
16.76	17.31	17.14	17.04	17.17	4h	
16.14	16.42	17.31	17.21	17.30	12h	
16.82	17.68	17.41	16.97	16.88	24h	
24.83	24.76	25.69	24.74	25.00	2h	HMGCR
24.86	27.86	28.57	27.93	25.28	4h	
23.76	25.58	27.95	27.60	24.68	12h	
24.75	27.02	28.22	27.33	25.10	24h	
21.88	21.39	22.09	21.75	22.55	2h	HMGCS1
21.69	23.06	23.73	23.50	22.39	4h	
20.51	22.59	24.64	24.60	22.60	12h	
21.99	23.53	25.42	25.52	24.19	24h	
26.09	25.85	26.35	26.34	26.79	2h	FDFT1
25.91	27.31	27.96	28.10	26.69	4h	
24.71	26.17	27.93	28.15	26.78	12h	
25.60	27.12	27.61	27.01	26.56	24h	
25.10	25.12	25.61	24.60	25.06	2h	LDLr
24.91	28.21	28.57	28.31	25.11	4h	
23.93	25.48	27.42	27.80	25.20	12h	
25.55	27.79	28.10	28.02	25.20	24h	
25.92	25.34	25.79	24.82	24.35	2h	ABCA1
25.93	25.02	24.79	24.76	22.12	4h	
26.49	24.06	24.55	24.39	22.80	12h	
26.48	24.51	23.97	22.73	21.63	24h	
30.53	31.46	31.23	30.60	29.96	2h	ABCG1
29.77	29.58	29.32	27.10	26.32	4h	
30.61	26.15	26.59	26.76	27.03	12h	
33.12	29.48	29.02	27.39	26.46	24h	
22.65	22.72	23.17	22.84	22.58	2h	SREBP1C
21.93	23.67	24.53	21.05	20.75	4h	
23.51	21.51	20.90	22.72	21.69	12h	
23.31	20.83	20.37	19.66	19.98	24h	
29.54	30.16	29.34	29.26	30.41	2h	Glut4
30.51	30.95	30.72	29.14	29.90	4h	
30.35	30.79	30.39	31.26	31.78	12h	
32.67	32.07	32.38	32.05	30.19	24h	
22.59	21.88	22.50	21.89	22.49	2h	ApoE
22.24	22.98	23.31	22.35	21.73	4h	
21.35	21.72	23.30	23.55	22.34	12h	
23.14	23.73	23.85	22.71	21.57	24h	

Table 2.4: **qRT-PCR results for genes involved on cholesterol metabolism in astrocytes.** Table presents the average Cts from different time points from different concentrations of 24S-OHC and one concentration of TO-901317. For more detail see Figure 3.3.1.

2.11. Isotope Dilution Mass Spectrometry (IDMS)

Isotope dilution mass spectrometry allowed the quantification of 24S-hydroxycholesterol (24S-OHC) in the striatal cells and cultured medium.

This technique relies on the isotope composition and the mass of each compound. Thus the sample, in our case 24S-OHC, with known mass and isotope composition was blended with a Spike. The Spike is an isotopically enriched compound with known mass, isotope composition, and will be an internal reference, once the amount of it used to blend with our sample is known, and will be used to calculate isotope ratio.

The mixture of sample and Spike is ionized and the electrons in the molecules gain charge. Acceleration is induced causing the electrons to travel in an electric field. There the molecules are separated in function of mass-to-charge ratio. Electrons are deflected by a magnetic field and hit a detection material that acquires the data. The amount of sample is then calculated considering the values acquired by the detection machine, which counted spike molecules, and sample molecules, plus is known the amount of Spike in the initial mixture, so the amount of sample is determined by the ratio:

$$\frac{\text{Amount Initial Sample (24S-OHC)}}{\text{Amount Initial Spike}} = \frac{\text{Amount Sample (24S-OHC) detected}}{\text{Amount Spike detected}}$$

2.12. SDS Page

Cells plated on 6 well Nunc plates were carefully washed with 4^0C cold PBS and lysed with 150 µL of RIPA buffer complete (150mM NaCl, 1% Triton X-100, 0.5% sodium deoxycholate, 0.1% SDS and 50mM Tris pH 8.0), 1% phosphatase inhibitor cocktail 2 (P5726 Sigma) and 3 (P0044 Sigma), 10% Phenylmethanesulfonyl fluoride (PMSF, dissolved at 200 mM in isopropanol, P7626 Sigma) and 1% of protease inhibitor cocktail (P8340 Sigma).

RIPA was let to act for 5 min and after that cells were harvest from the well with a scraper, and content transfer to an Eppendorf tube on ice. In order to get a cell lysate, samples in Eppendorf tubes were let on ice for 30 min and

vortexed every 10 min. After that time were centrifuged for 15 min at 12,000 rpm at 4^0C. After centrifugation supernatant was collected into a new Eppendorf tube and protein content was determined by BCA assay (Material and Methods section 2.7.2).

Lysates were mixed with 4X sample buffer (40% Glycerol, 240mM Tris-Cl pH 6.8, 8% SDS, 0.1% bromophenol blue and water) and the mixture was incubated for 5 min at 99^0C, before loading in a SDS-page gel. The protein amount loaded was between 20-30 µg, and the gel percentage was dependent on the molecular weight of the protein target, therefore for HMGCR (97 kDa) 7.5%, for histone H1 (runs at 30 kDa) 12.5%, and the same, 12.5%, was used to detect tubulin.

In order to separate the proteins by molecular size in the acrylamide SDS page gels, I used the BioRad mini system. Proteins run at 150V for 1h-1h30 with 1X SDS-running buffer (Table 2.6) 5 µL pre-stained broad range molecular weight marker (BioRad, 161-0373) served as a molecular weight standard.

2.13. Western Blotting

Following SDS-Page, proteins were transfer onto a nitrocellulose membrane (Nitrocellulose Hybond ECL GZRPN2003D Fischer Scientific) for 1.5h at 100V in 1X transfer buffer (Table 2.6), in a BioRad system. Subsequently nitrocellulose membrane was stained with Ponceau red, to check whether the proteins have been transferred to the membrane correctly. Next step consisted in distain the membrane with distilled water to remove any traces of Ponceau red, and block with 5% BSA (5g of BSA in 100 mL of 1X TBS (10X: 30.25g Trizma base, 90g NaCl, distilled water to 1L, pH 8.1) +0.1% Tween 20). After 1h blocking at RT, primary antibodies were incubated o/n at 4^oC (more antibodies details in Figure 2.6) in blocking solution.

Catalog number	Company	Antibody name	Concentration	Raised	Incubation time
ab174830	abcam	HMGCR	1/500	rabbit	over night
05-457	Milipore	anti Histone 1	1/500	mouse	over night
T5168	Sigma	α-Tubulin	1/1000	mouse	1h RT
926-32211	LiCor	IRDye® 800CW Goat polyclonal anti-Rabbit IgG (H+L)	1/10,000	Goat	1h RT
925-68072	LiCor	IRDye® 680RD Donkey anti-Mouse IgG (H + L)	1/10,000	Goat	1h RT

Table 2.5: Primary and secondary antibody details.

Next day, primary antibodies were collected and membranes washed in 1XTBS-Tween, 3 times for 10 min. After washes blots were incubated with secondary antibodies as specified in Figure 2.6, covered in aluminium foil. Before scan the blots. Membranes were washed with TBS-Tween: 1X 5 min, 1X 15 min, 2X 10 min. Bands were detected and quantified with LI-COR Odyssey Infrared Imager (LI-COR Biosciences).

2.14. Mitosox superoxide indicator

Mitosox red reagent (Life Technologies – M36008) is a cell permeant dye, specifically targeted to mitochondria in live cells. Mitosox oxides in the presence of superoxide, and emits fluorescence at wavelength of 600 nm.

Primary striatal cells and astrocytes differentiated were treated for 24h with 2 μM of 24S-OHC and for 12h with 10 mM of 3-NP.

Mitosox was loaded to live cells, after the specified time of incubation with the respective drug, in HBSS/ Ca/Mg at 5 μM. The incubation took place in the incubator during 10 min. After incubation time, cells were washed 3 times with HBSS/ Ca/Mg and images taken with Nikon inverted microscope (Nikon eclipse Ti) with a magnification of 20x.

For the purpose of the analyses, all the images were taken with the same exposure. The analysis was performed in the following way: open Mitosox image and make a copy. Select the copy image, adjust threshold and analyse particles, send to regions of interest (ROI). Select the original image and add particles from ROI, measure integrated density. Were performed 2 independent experiments, for each one of them 8 biological replicates were used for DMSO and 2 μM 24S-OHC and 4 biological replicates were considered for 3-NP (N=2, n=16 / n=8), for the experiment with primary striatal neurons. In astrocytes treated with increasing concentrations of 24S-OHC, only one experiment was performed with 4 technical replicates (N=1, n=4).

2.15. SREBP2 Transcription Factor Assay

The SREBP2 transcription factor assay kit (Cayman chemical – 10007819) is a sensitive method to detect the specific transcription factor: SREBP2 contained in nuclear extracts. The assay is based on the premise that SREBP2 contained in nuclear extracts isolated from cells, recognizes the sterol responsive element and binds to it. Further on, SREBP2 bound to dsDNA is recognised by a primary antibody, which one was raised against a secondary antibody conjugated with HRP that provides a sensitive readout at 450 nm.

To perform this experiment, astrocytes were plated on 10 cm dishes, 2 days after being in G5 supplement. While under treatment with DMSO, 24S-OHC, U-18666A, tunicamycin (TM) and thapsigargin (TG), the medium was without fetal bovine serum and correspondent compounds were added: 2 μM of 24S-OHC for 12h, 0.5 μg/mL U-18666A for 48h, 0.5 μg/mL TM and 100 nM TG for 24h.

At the end of the treatments astrocytes were harvested on ice and preceded to fractionation protocol to isolate nuclear extracts.

Astrocytes growing on a 10 cm dish were scraped on PBS, and pellet collected after centrifugation at 5,000 g for 5 min. Pellet was lysed in 100 μL cytoplasm extraction buffer (10 mM HEPES pH 7.9, 1mM EDTA, 60 mM KCl, 0.075% Igepal plus proteases and phosphatase inhibitors) passing pellet through a 200 μL pipette. Lyse continued at 4^0C for 45 min, terminating with centrifugation at 5.000 g for 5 min to generate cytoplasm. Another centrifugation at 12,000 g for 10 min took place, to yield final cytoplasm extract. The final pellet containing the nucleus was lysed in nuclear extraction buffer (20 mM Tris-HCL, 1.5 mM $MgCl_2$, 420 mM NaCl, 25% glycerol, 0.2 mM EDTA, 0.5% Igepal, proteases and phosphatase inhibitors). Five molar was added to the resuspended nuclear pellet in extraction buffer, and incubation lasted for 45 min at 4^0C. The last centrifugation, at 12,000 g for 10 min, yielded nuclear extract (Zhao and Brinton, 2003).

Prior to use samples for SREBP2 transcription factor assay, nuclear isolation was confirmed by western blot. Histone H1 was the nuclear marker chosen, and α-Tubulin the cytoplasm (Figure 2.7).

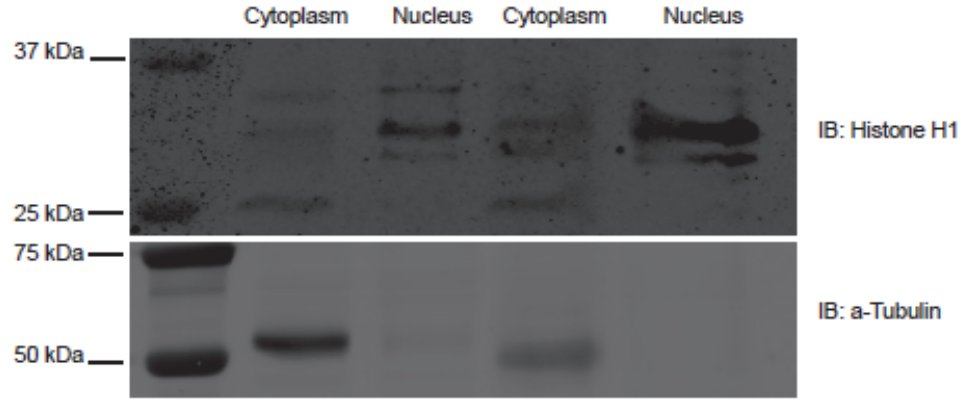

Figure 2.7: **Subcellular fractionation of astrocytes.** Astrocytes were lysed and cytoplasm and nuclear fraction used for western blot analyses. Respective cellular fractions were identified with specific antibodies, cytoplasm with α-Tubulin (50 kDa) and nucleus with Histone-H1 (31 kDa). Posteriorly nuclear fraction was used in the SREBP2 transcription factor assay kit.

Nuclear extractions from the different treated samples were normalised, after protein concentration was determined by BCA assay (Material and Methods section 2.9.2). Nuclear extracts were loaded in the 96 well assay plate at 10 µL volume (approximately 10 µg protein).

The assay was performed as indicated in the assay protocol (Cayman - 10007819):

Prepare complete transcription factor binding assay buffer (CTFB): 73 µL ultrapure water, 25 µL 4X transcription factor binding assay buffer, 1 µL reagent A and 1 µL 300 mM DTT (volumes required per well).

Add 90 µL CTFB per well (80 µL if adding competitor dsDNA, 100 µL to blank and non-specific binding wells).

Add 10 µL of competitor dsDNA to appropriate wells.

Add 10 µL of positive control (from kit) to appropriate wells: positive control and competitor sdDNA).

Add 10 µL study samples (astrocytes treated) to appropriate wells.

Incubate over night at 4^0C.

Wash wells 5 times with 200 µL 1X wash buffer.

Add 100 µL of diluted SREBP2 antibody per well, except blank.

Incubate one hour at room temperature.

Wash wells 5 times with 200 µL 1X wash buffer.

Add 100 µL of diluted secondary antibody per well, except blank.

Incubate one hour at room temperature.

Wash wells 5 times with 200 µL 1X wash buffer.

Add 100 µL developing solution per well.

Incubate 20 min with gentle agitation.

Add 100 µL of stop solution per well.

Measure absorbance at 450 nm.

The samples' OD at 450 nm is approximately 0.4, the negative controls provided by the kit (blank, competitor dsDNA and non-specific binding) OD at 450 nm is around 0.05, while the positive control provided in the kit OD at 450 nm 1.8.

2.16. Calcium Imaging

Calcium imaging was performed on DIV 13 striatal neurons growing in 30 mm culture dish. Calcium imaging consists of loading the cells with the membrane-permeable calcium indicator Fluo-4 AM (Life technologies F-142012; Ex 494/ Em 506), which exhibits an increase in fluorescence upon binding of calcium (Ca^{2+}).

At DIV 13 primary striatal neurons were incubated in 2 µM Fluo-4 AM in HBSS without calcium and magnesium (Life technologies 14170-112) for 30 min at 37^0C to load the neurons with the dye. After dye-loading, cells were washed 3 times with HBSS solution (material and methods section 2.6).

After washing, neurons were either incubated for 5 minutes with Locke's solution (control) or 10 µM 24S-hydroxycholesterol in Locke's solution.

A patch pipette (resistance: 5-6 MΩ) was filled with 10 µM NMDA and connected to a custom-build picospritzer for focal application of NMDA. The NMDA-loaded pipette was positioned, consistently, approximately 80 µm over the neurons in the center of the dish.

The cultures were imaged with a Nikon TE2000 inverted microscope at 20x magnification using a QIClick ccd camera (QImaging) and a custom-build LED light source with appropriate filters (Semrock: excitation: FF01-475/35; emission: FF01-530/43; dichroic: FF499-DiO1). Image acquisition was

performed using the Micromanager (v. 1.4.22) software package that controlled both the camera and light source.

Series of 120 or 200 frames were collected at intervals of 500 ms, and a puff of NMDA (50 ms, 10 psi) was applied at frame 40 (20 s after start of the image acquisition).

The image series were analysed using Fiji-ImageJ. Data was analysed as $\Delta F/F_0$. For this purpose, images prior to NMDA application (images 1 to 40) were averaged (F_0) and subtracted from all images in a series. The resulting ΔF series was divided by F_0.

ROIs were manually defined for all Fluo4-loaded neurons, which responded after NMDA application (40^{th} frame). For each ROI, $\Delta F/F_0$ was measured for all images in a series. The average $\Delta F/F_0$ values for all responsive cells were averaged and plotted.

Two independent experiments using different cultures were performed. Each experiment contained both control and 24S-hydroxycholesterol-treated dishes, and all dishes were stimulated with NMDA (10 μM). In each experiment 4 dishes were used per condition (control and 24S-hydroxycholesterol-treated).

2.17. Multi Electrode Arrays

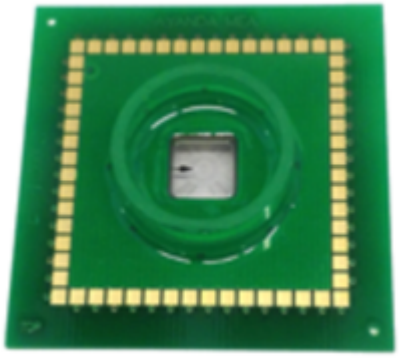

Figure 2.8: **Multi electrode arrays.** One well multi electrode array, composed by 59 active electrodes, allowed the extracellular recording of primary striatal neurons (DIV 19) cultured with glutamatergic inputs (cortex and thalamus).

Commercial MEAs (MEA60-200-30-Pt) with planar platinum substrate electrodes (QWANE, Lausanne, Switzerland) were used for ex vivo extracellular recordings. Substrate electrodes had a diameter of 30 µm (Figure 2.8) and were organized in an 8 x 8 square grid with 200-µm spacing, being in total 59 active contacts and a reference. Electrophysiological recordings were performed at 37^0C and 5% carbon dioxide, inside a low-humidity incubator comprising an electronic-friendly environment (SANYO MCO-17AIC). MEA electrodes had an impedance of 800-1100 kΩ at 1kHz. The electronic amplifier (Multi Channel Systems MEA1060-Up) had a gain of x1200, with a bandwidth filter 1-3000 Hz with large input-impedance (10^{11} Ω in parallel to 10 pF).

Before plating the neurons in the MEAs, they had to be washed with autoclaved water, sterilized with 70% ethanol for 15 min inside the hood, and coated with 0.1M boric buffer with 0.1 mg/mL poly-L-lysine over night. On the plating day, the poly-L-lysine solution was removed; the MEAs were washed with autoclaved water 3X and coated with laminin - 0.02mg/mL for 30 min at 37 ^{0}C. Laminin was removed and 100 µL of striatal neurons with thalamic and cortical inputs at 1.3X10^6 cells were placed on the middle square (Figure 2.7). MEAs were placed in the incubator for 30 minutes to let the neurons attach. Once the neurons were attached, which was visualized under the microscope, the MEAs was filled with 1 mL of neurobasal medium with supplements.

MEA Data Acquisition and Analysis. After 5 minutes of accommodation time after the mounting of each MEA inside the recording setup, spontaneous electrical activity from the cultured neurons was detected, amplified, and recorded at each of the 59 substrate extracellular electrodes simultaneously for 15 min at 25 kHz per channel. Recorded traces often consisted of single unit activity, directly related to the firing of action potentials by a neuron in the proximity of each electrode. MC_Rack software (Multi Channel Systems) was used to acquire and store the data files (2.7 Gb mcd files), which were processed off-line, channel by channel. Raw voltage wave-forms were digitally filtered between 0.3 and 4.0 kHz. The occurrence of an action potential, at a given electrode was identified by a peak-detection algorithm, based on the crossing of an adaptive threshold (Gambazzi et al., 2010). The occurrence and

duration of population bursts (episodes of synchronized activation along network (Gambazzi et al., 2010) were identified and detected as described in (van Pelt et al., 2004), by post processing the spike-time histograms.

MEA plating and treatment with 2 μM of 24S-hydroxycholesterol was performed by myself while MEA recording/analysis were carried out by Dr. Alberto Capurro.

2.18. Pharmacological treatments

To study the effect of different compounds on primary striatal neurons and astrocytes, the concentrations and treatment times were varied.

For primary striatal cells treatments, half of the culture media, in each well, was replaced with the same volume containing double concentration of the test compound. In astrocytes treatment, differentiation media (containing G5) was removed, and replaced with media without serum containing the test compound in the desired concentration.

The test compounds were the following:

AK-7 (ChemBridge, San Diego, CA, USA): 5 mM aliquots prepared in molecular biology grade dimethyl sulfoxide (DMSO) were stored at -20^{0}C. AK-7 was loaded in cells' medium to a final concentration of 10 μM and treatment lasted for 24h.

U-18666A (Cayman chemicals – 10009085): Stock solution of 2.5 mg/mL prepared in DMSO, was stored at -20^{0}C. AK-7 was loaded in cells' medium to a final concentration of 1 μM and treatment lasted for 48h.

24S-hydroxycholesterol (24S-OHC) (Enzo lifesciences – BML-GR230-0001): 2.5 mM aliquots prepared in DMSO were stored at -20^{0}C. Experiments in culture media, 24S-OHC was loaded as discussed above. In Locke's solution, 24S-OHC was added to the desired final concentration in Locke's solution to be added to each well. 24S-OHC concentrations ranged from 0.25 μM to 4 μM, and the treatments times, from 2 to 24h.

TO-901317 (Sigma – T2320): Stock solution of 2 mM prepared in DMSO, was stored at -20^{0}C. The LXR agonist: TO-901317 was loaded in astrocytes

medium to a final concentration of 0.5 µM and treatment lasted for 2, 4, 12 and 24h.

3-Nitropropionic acid (3-NP) (Sigma – N5636): was prepared fresh before each experiment. Working solution was prepared by weighting 15 mg of 3-NP (sored in fridge) and dissolving in 500 µL ethanol, making the final concentration of 250 mM. 3-NP was loaded in cells to a final concentration of 10 mM (Liot et al., 2009).

Thapsigargin (TG) and tunicamycin (TM) (Sigma – T9033 and T7765, reapectivly): TG and TM are the most commonly used compounds to induce endoplasmic reticulum stress in culture cells (Breckenridge et al., 2003).

Stock solutions prepared in DMSO (TG) and ethanol (TM) were used at final concentration of 0.1 µM (Fradejas et al., 2010) and 0.5 µg/mL (Benavides et al., 2005) in astrocytes. In striatal neurons, tunicamycin was used at 3 µg/mL (Chen et al., 2007) and thapsigargin at 0.1 µM (Galehdar et al., 2010) for 24h.

2.19. Statistical analyses

All experiments were performed with a minimum of 3 biological replicates (considering each well of a plate a biological replicate) n=3 a minimum of 2 independent experiments N=2. The exception was the MEA recordings, was only possible to record from one well MEA, due to the difficulty, I have found, of growing striatal neurons in the MEAs. And the experiment to measure superoxide production in astrocytes treated with 24S-OHC (using Mitosox), due to lack of time to perform repetitions. The represented values corresponded to the average of the data analysed, considering all the experiments performed. The error bars were calculated from Standard error of the mean (SEM = (Standard deviation / (number biological replicates^(1/2))). The respective statistical analyse used are indicated in each figure in the results chapters and considers: $p<0.05$ (*), $p<0.01$ (**), $p<0.001$ (***) and $p<0.0001$ (****). The statistical test employed was chosen based on PRISM suggestions, for the most accurate dependent on the experimental design and aim.

3. Results

3.1. Cholesterol accumulation in an *in vitro* model of Huntington's disease

Introduction. Cholesterol is an essential component of eukaryotic membranes and sterol biosynthesis is believed to be an evolutionary acquisition that allowed the development of eukaryotic life (de Duve, 2007; Numa and Tanable, 1984). Cholesterol is a major component of membrane lipids, regulates plasma membrane organization, rigidity (Miao et al., 2002), and selective permeability (Haines, 2001), thereby having a strong influence on intercellular signalling (Maxfield and Tabas, 2005). Cholesterol levels need to be regulated within a very narrow range, as small changes in cholesterol content induce consequent changes in overall membrane composition and membrane-associated signalling.

Neurons have a unique oxysterol-generating activity to keep sterol intracellular levels balanced. The enzyme responsible for hydroxylasing cholesterol to 24S-OHC is CYP46A1, a specific isoform of P450, which is expressed exclusively in neurons (Lund et al., 1999). 24S-OHC is more polar and water-soluble than its precursor and is able to traverse the plasma membrane. This mechanism is postulated to prevent accumulate neuronal cholesterol, both by direct sterol efflux and by its signalling activities (Pfrieger, 2003 a; Pfrieger and Ungerer, 2011). In addition to permeating brain cells, 24-OHC can cross the BBB and to be released into the bloodstream. Given that 24S-OHC is a metabolite unique to neurons (Bretillon et al., 2000), it has been proposed as a biomarker for neurodegeneration. Circulating 24S-OHC is thought to be eliminated by the liver (Abildayeva et al., 2006).

There is an insufficient understanding of cholesterol metabolism in the brain, and therefore its role in neurodegenerative diseases.

Huntington's disease (HD) is a progressive, fatal, autosomal dominant disorder manifested by uncontrolled movements, depression, cognitive decline and dementia (Walker, 2007; Gagnon et al., 2008). Huntington's disease is caused by a glutamine expansion in the N-terminal portion of the Htt protein. In the brain Htt is highly expressed in neurons and has been consistently reported

that medium spiny neurons are more prominently affected in HD leading to striatal neurodegeneration primarily, with other brain structures such the cortex being affected at alter stages of the pathology (Reiner et al., 1988).

Several studies suggest that mutant Htt is cleaved by proteases and that the toxic N-terminal fragment containing the PolyQ is translocated into the nucleus where it forms inclusions, consequently altering different cellular pathways. Moreover, it has also been reported that mutant Htt interacts aberrantly with proteins in the cytoplasm leading to cellular dysregulation. Several models were inspired by the effects observed with the N-terminal fragment containing the PolyQ resultant from the cleavage of mutant Htt, originating R6/1, R6/2 and N-171-82Q mice model, as an alternative to *in vivo* models was developed an *in vitro* model of HD by infecting E16 rat striatal neurons with a lentiviral vector encoding the first 171 amino acids of mutant (82Q) Htt. The high transduction rate and sustained transgene expression obtained with lentiviral vectors offer a new opportunity to analyze mutant Htt-induced cell death with cytological, molecular, and biochemical methods.

Taking advantage of the described *in vitro* model, Luthi-Carter's group investigated the neuroprotective actions of putative SIRT2 inhibitors AK-1, AGK2 and AK-7 (Luthi-Carter et al., 2010; Taylor et al., 2011). Surprisingly, HD cells treated with AK-1 show a transcriptomic profile in which the enzymes involved in the cholesterol biosynthetic pathway are downregulated, consequently less cholesterol is produced in these striatal neurons which otherwise show sterol accumulation. Both AK-1 and AGK-2 reduce the nuclear trafficking of SREBP-2, and by doing so inhibit the transcription of target genes, which proteins are in the cholesterol biosynthetic pathway, conferring neuroprotection to HD cells (Luthi-Carter; Taylor et al. 2010).

The main aim of this chapter is to elucidate the sterol status of HD primary striatal cells, and to identify the sterol species that are enriched in these cells.

3.1.1. *In vitro* model of Huntington's disease

The HD *in vitro* model used in this thesis consisted of primary striatal neurons isolated from E16 Sprague Dawley rats (see Material and Methods section 2.1), and infected with lentiviral vectors encoding the first 171 amino acids of human Htt containing 18 or 82 polyglutamine repeats (wild-type and mutant Htt, respectively: Htt171-18Q/82Q) under the control of a tetracycline-regulatable promoter (tetO). The Htt-expressing lentiviruses were applied together with a vector encoding the tetracycline-controlled transactivator (tTA1) under the control of PGK promoter (which confers high expression in neurons). In the absence of tetracycline, tTA binds the TRE sequence in the tetO promoter, activating transcription of the downstream gene, in this case Htt171-18Q/ 82Q.

It has been shown previously that Htt171-82Q expressing primary neurons generated by this procedure shows progressive neuropathology including the appearance of intracellular Htt inclusions and decreased numbers of neuronal nuclear antigen (NeuN) positive cells by 2-3 weeks post infection of medium spiny neurons (Rudinskiy et al., 2009). Here I intend to characterize the *in vitro* model taking advantage of the same methodology previously used – NeuN positive cell count and integrated density measurement (Figure 3.1.3) as well as performing another cell death assay- MTT assay (Figure 3.1.1).

As previously shown the cholesterol status is altered after 11 days in this *in vitro* model (Luthi-Carter et al., 2010), therefore for consistency purposes, the experiments presented in this thesis were performed at the same time point. The characterization of the *in vitro* model was then undertaken at this time point- DIV 13/ 11 days post infection.

The MTT assay consists of living cells' converting MTT (3-[4,5-dimethylthiazol-2-yl]-2,5 diphenyl tetrazolium bromide) into formazan crystals (van Meerloo et al., 2011). NeuN (neuronal nuclei) is neuronal marker encoded by the Fox-3 gene product, and its decreased expression in this HD model was shown previously by immunocytochemistry (Rudinskiy et al., 2009).

MTT assay analyses showed no differences in cell survival, between control primary striatal neurons versus cells expressing mutant Htt for 2 weeks in culture (Figure 3.1.1).

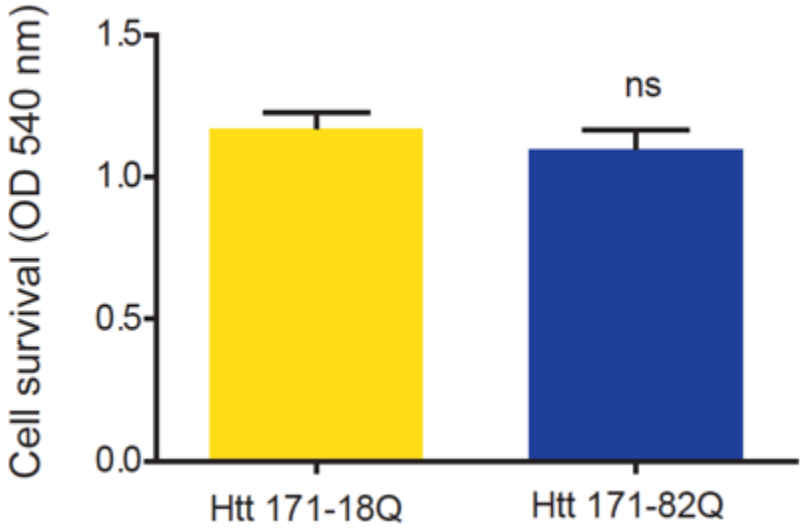

Figure 3.1.1: **Validation of HD model *in vitro* using MTT assay.** At 13 days in culture (DIV 13), primary neurons expressing mutant Htt (Htt 171-82Q), did not present differences in cell survival when compared to control cells (Htt 171-18Q). The graph represents the mean of the cell survival measured by MTT assay (OD 540 nm), standard bars = SEM.
Striatal cultures plated on 24 well plates were seeded at the same density (5x10^5 cells/ mL) and maintained in the same conditions, the only difference was the virus infection: Htt 171-18Q versus Htt 171-82Q. Two independent experiments were considered per condition and 10 wells were analysed (N=2, n=20). The statistical test used was unpaired t-test with Welch's correction, and non-significance (ns) was the result ($p>0.05$).

From the data obtained by the MTT assay, I observed that 11 days after transduction mutant Htt does not cause decrease in cell viability compared to control neurons.

I then sought to assess neurodegeneration of the model as previously performed, by immunocytochemistry (Rudinskiy et al., 2009).

Primary striatal neurons were stained with NeuN after 2 weeks in culture (Figure 3.1.2 A) and two different analyses were taken into consideration: NeuN integrated density (Figure 3.1.2 B), and NeuN cell counts (Figure 3.1.2 C) (see Material and Methods section 2.5). NeuN integrated density measurement allowed me to quantify the degree of NeuN (Fox-3) expression as an indicator of neuronal viability and NeuN cell counts aimed to quantify the number of mature neurons alive (Rudinskiy et al., 2009).

Primary striatal neurons expressing mutant Htt presented significantly decreased ($p<0.0001$) NeuN integrated density when compared to Htt171-18Q (Figure 3.1.2 A and B). However, the numbers of NeuN counts were similar between the two conditions (Figure 3.1.2 C).

Also important for characterising the model was to assess the presence of astrocytes in the cultures. Fixed cultures were stained with Glial fibrillary acidic protein (GFAP) a specific astrocytic marker. This showed that astrocytes are localized in the proximity of neurons in culture (Figure 3.1.2 A). The precise quantification of astrocytes is difficult due to their structure and GFAP staining, but they comprised a minority of cells (e.g. <20%).

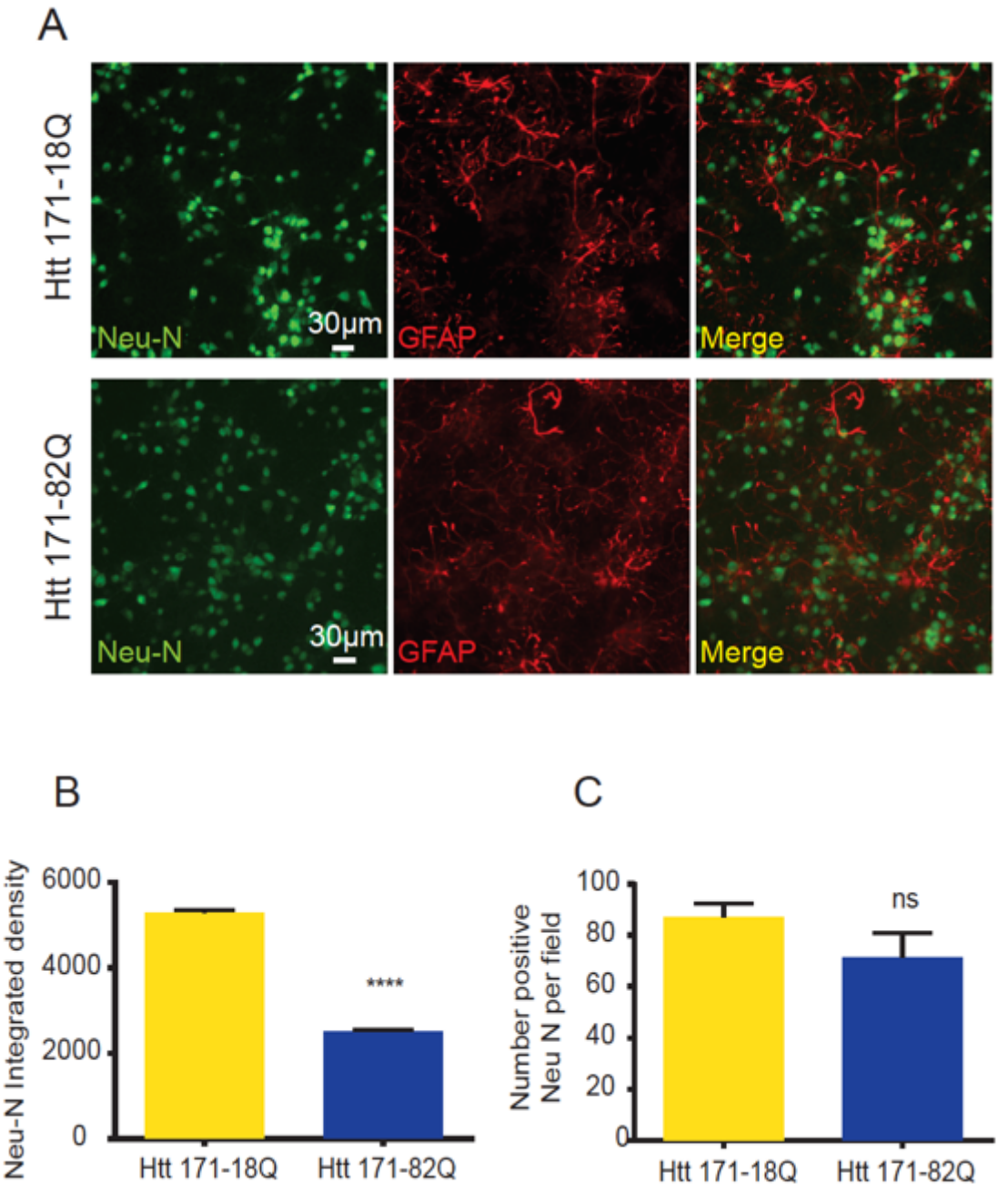
A
Htt 171-18Q
Htt 171-82Q
Neu-N
30µm
GFAP
Merge
B
Neu-N Integrated density
6000
4000
2000
0
****
Htt 171-18Q
Htt 171-82Q
C
Number positive Neu N per field
100
80
60
40
20
0
ns
Htt 171-18Q
Htt 171-82Q

Figure 3.1.2: **Validation of HD model *in vitro* by NeuN staining. A-** At 13 days in culture (DIV 13), primary neurons were fixed and stained with NeuN and GFAP. NeuN intensity was higher in neurons expressing Htt 171-18Q compared to Htt 171-82Q (NeuN panels-green). The presence of astrocytes in the culture was evidenced by the GFAP staining (GFAP panels-red). Merge images showed astrocytes surrounding neurons (Merge panels). Images taken with Nikon TIRF microscope with 20x objective, scale bar: 30 µm. **B-** The integrated density of NeuN is significantly decreased in striatal neurons expressing the mutant form of Htt (Htt 171-82Q), compared to wild type. **C-** NeuN cell counts were considered per field, and the analyses showed similar number of NeuN positive structures between conditions (Htt 171-18Q versus Htt 171-82Q). Neuronal cultures plated on 24 well plates were seeded at the same density (5x10^5 cells/ mL) and maintained in the same conditions; the only difference was the virus infection: Htt 171-18Q versus Htt 171-82Q. Two independent experiments were considered per condition and 10 wells were analysed (N=2, n=20). The statistical test used was Mann Whitney U test (Htt 171-18Q passed normality test, however Htt 171-82Q did not, therefore used a non-parametric test), $p<0.0001$ (****), ns (non-significance), standard bars = SEM.

The assessment of neurodegeneration occurred at 2 weeks after neuronal plating and at this stage a significant decrease in NeuN expression was observed, measured by integrated density (Figure 3.1.2 B) but no significant cell death was evaluated by NeuN positive nuclei counts (Figure 3.1.2 C). I can conclude by the observed in Figure 3.1.2 that at this stage neurons are at the beginning of the neurodegenerative process, which corresponds to what was previously shown for the model validation, in the process of neurodegeneration caused by mutant Htt *in vitro*, NeuN expression decreases before neuronal death occurs (Regulier et al., 2003). This provided an important baseline measure for the sterol analyses, to confirm that no overt cell death had occurred at the time of sampling.

3.1.2. Sterol accumulation in the HD model evidenced by cholesterol oxidase assay and filipin staining.

It has been previously demonstrated that primary striatal neurons expressing mutant Htt (Htt171-82Q) showed increased sterol levels (Luthi-Carter et al., 2010). I aimed to show sterol accumulation in our HD model using the cholesterol oxidase assay (Luthi-Carter et al., 2010; Taylor et al., 2011), in order to replicate previous findings, and through another epifluorescence approach, filipin staining (Trushina et al., 2006b; del Toro et al., 2010).

Cholesterol accumulation in the HD model was demonstrated by using the Amplex red cholesterol oxidase assay, which is based on an enzyme-coupled reaction that detects cholesterol and cholesteryl esters. Cholesteryl esters in the sample are first converted into cholesterol through *in vitro* hydrolysis by cholesterol esterase. Then cholesterol is oxidised and the final products are hydrogen peroxide (H_2O_2) and the corresponding ketone product. Amplex red detects the H_2O_2 and in the presence of horseradish peroxidase, occurs a 1:1 stoichiometric reaction to produce highly fluorescent resorufin (see Material and Methods 2.9.3).

Cholesterol oxidase assay analyses showed significantly increased ($p=0.01$) sterol levels in Htt171-82Q cells, compared to wild type striatal cells, validating the previously published work (Figure 3.1.3).

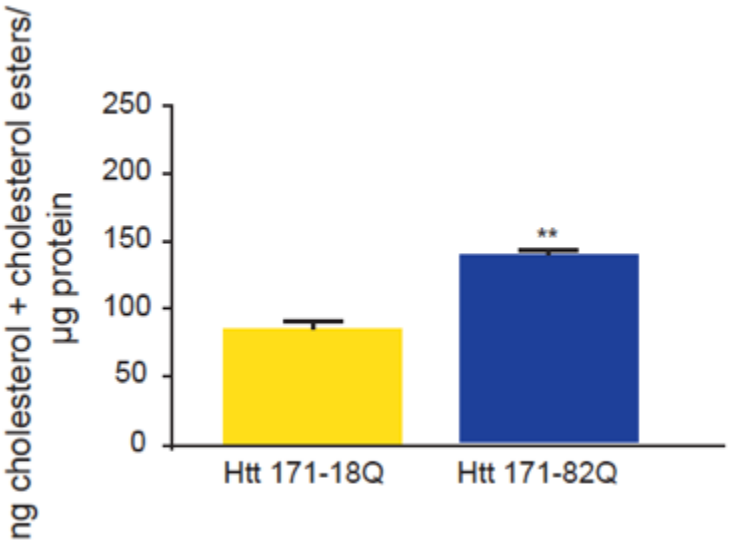

Figure 3.1.3: **Increased sterol content in Htt 171-82Q expressing primary striatal neurons.** Primary striatal neurons (DIV 13) were lysed and sterols levels assessed by cholesterol oxidase assay. The graph represents the mean of the total sterols, normalised to protein content from two independent experiments, error bars = SEM. Total sterol quantification showed a significantly higher sterol content in mutant Htt-exposed neurons (Htt 171-82Q) comparing to their wild type Htt-exposed counterparts (Htt 171-18Q). Two independent experiments were considered per condition and 10 wells were analysed (N=2, n=20). The statistical test used was unpaired t test with Welch's correction, p=0.01 (**).

In order to better understand the characteristics of sterol accumulation in the model, I also stained primary striatal neurons (2 weeks in culture) with filipin, a small molecule that specifically binds unesterified cholesterol and measured the integrated density by confocal microscopy (Figure 3.1.4 A and B).

Htt-171-82Q-exposed striatal cultures showed a higher intensity of filipin fluorescence (Figure 3.1.4 A). This observation is corroborated by the analysis done to the confocal images (Figure 3.1.4 B): mutant Htt cells presented a significant increase ($p<0.001$) in filipin integrated density compared to control cells.

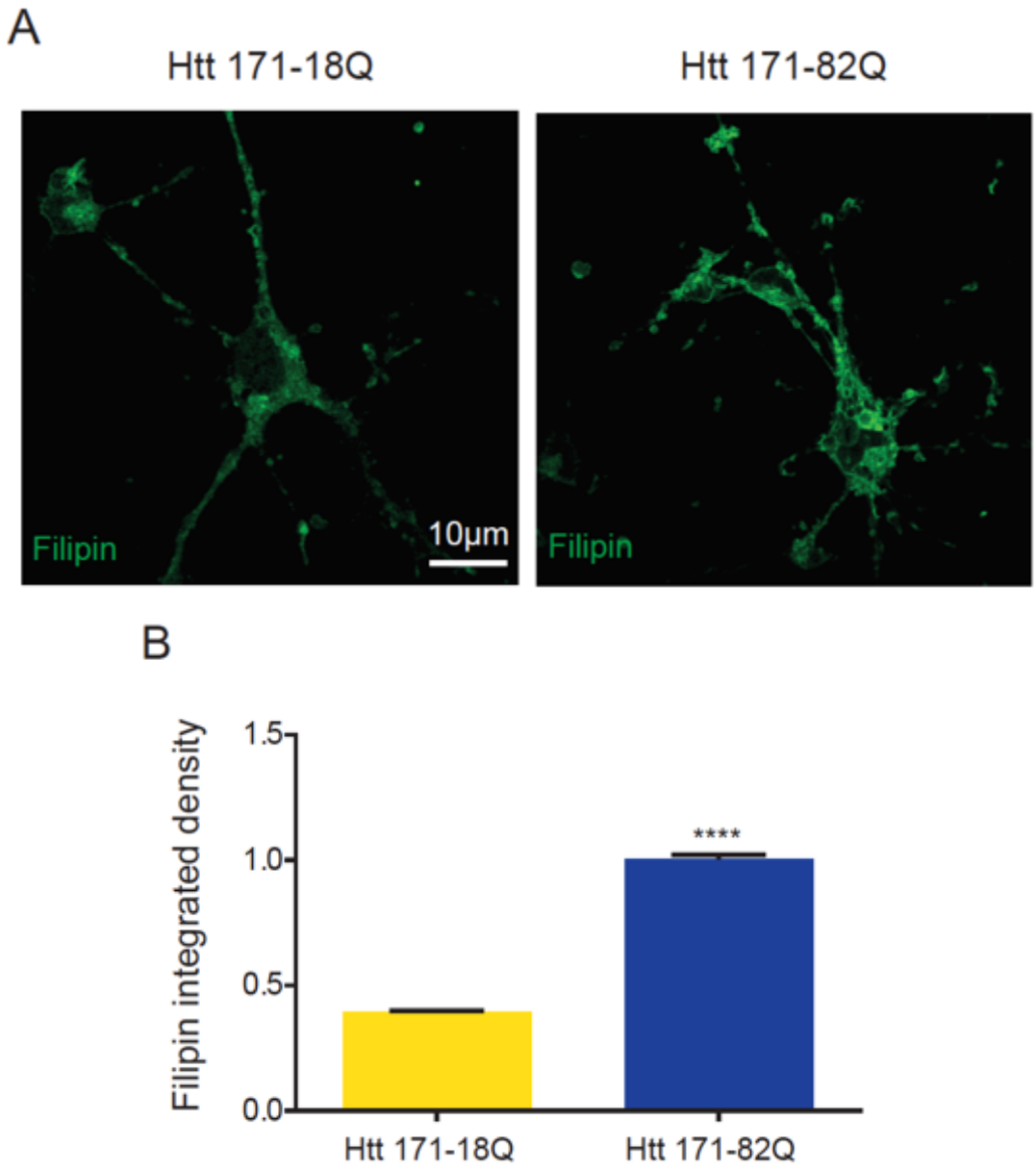

Figure 3.1.4: **Unesterified sterol accumulation in Htt 171-82Q (mutant Htt) primary striatal neurons. A-** Images representative of primary striatal neurons stained with filipin (DIV 13). Htt 171-82Q primary neurons showed higher intensity of filipin compared to Htt 171-18Q cells. Confocal images taken with Leica microscope at 60x magnification, scale bar: 10 µm. **B-** Quantification of filipin staining, resulted in significantly increased integrated density of filipin in primary striatal neurons expressing Htt 171-82Q. Graph represents the mean of 3 independent experiments (N=3, n=9 - cover slips). The statistical test used was Mann Whitney U test (Htt 171-18Q passed normality test, however Htt 171-82Q did not, therefore used a non-parametric test), $p<0.0001$ (****), error bars = SEM.

Both cholesterol oxidase assay (Figure 3.1.3) and filipin staining (Figure 3.1.4) results validate our lab previous findings of sterol accumulation. The novelty is that some of this extra cholesterol exists in an unesterified form (as determined by filipin staining).

3.1.3. Cholesterol accumulation in the HD model occurs in the plasma membrane and in lysosomes.

In order to understand the site of sterol accumulation in the HD model, I have co-stained striatal neurons with filipin and either a plasma membrane (Figure 3.1.5 A and B) (Cell MaskTM deep red plasma membrane stain) or lysosome marker (Figure 3.1.6) (Lysotracker red DND-99, high selectivity for acidic organelles).

Figure 3.1.5 A shows primary striatal cells expressing Htt 171-18Q (top panels) and Htt 171-82Q (bottom panels) stained with filipin after loading with plasma membrane marker. It is noticeable in Figure 3.1.5 A that the large percentage of the unesterified sterol in the cells is in the plasma membranes (merge panel in both conditions). Moreover the plasma membrane dye is stronger in Htt 171-82Q as observed in Figure 3.1.5 A, middle panel. As the plasma membrane dye has affinity for lipids and due to the higher quantity of cholesterol in the plasma membrane of Htt 171-82Q, the co-localization between plasma membrane marker and filipin stands out in this condition.

Primary striatal neurons expressing Htt171-82Q presented double of the integrated density of filipin staining overlapping, compared to control, with the plasma membrane labeling (Figure 3.1.5 B).

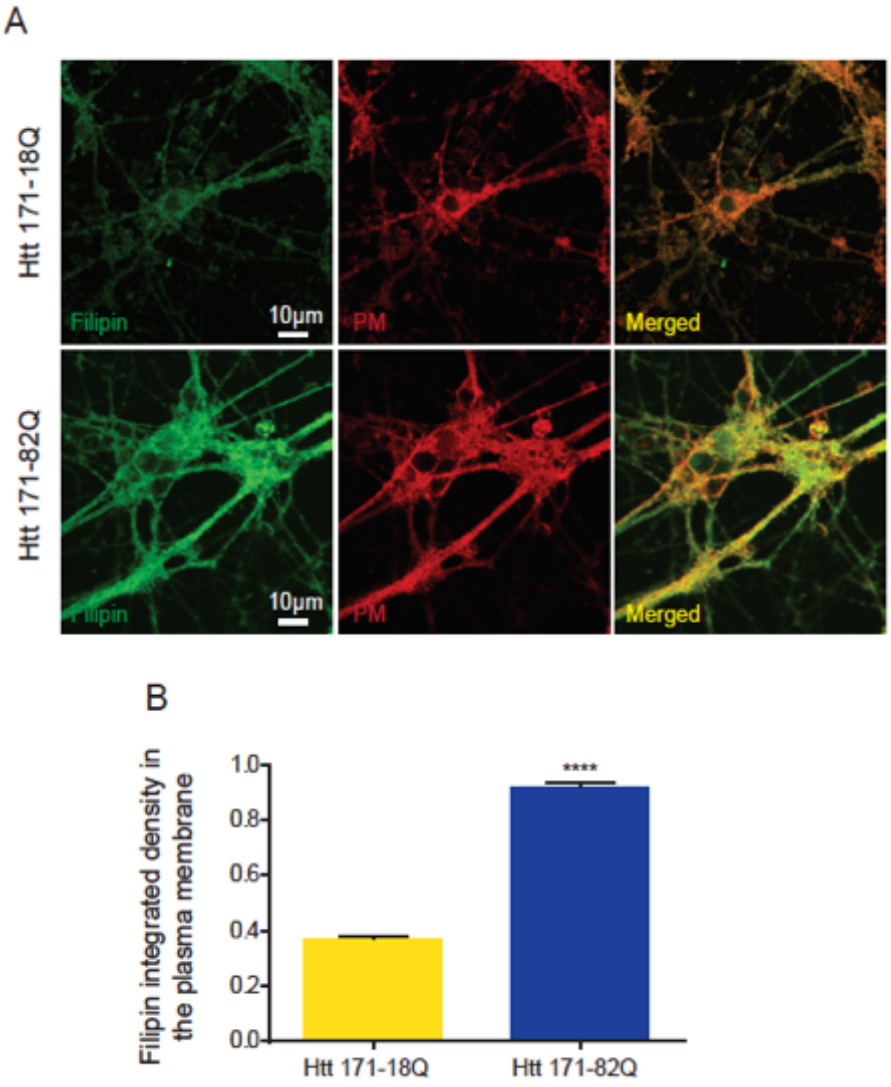

Figure 3.1.5: **Unesterified sterol accumulation in Htt 171-82Q expressing primary striatal neurons occurs in the plasma membrane. A-** Images representative of primary striatal neurons co-stained with filipin and plasma membrane marker (Cell MaskTM deep red plasma membrane stain) (DIV 13), showed that filipin intensity is higher in primary neurons expressing mutant Htt (Htt 171-82Q) (Filipin panel). Plasma membrane marker (PM) images showed neurons from both conditions retaining positively the dye. Merge images showed that in both conditions occurs co-localization of filipin staining with plasma membrane dye, indicating that unesterified cholesterol is component of plasma membranes. Confocal images taken with Leica microscope at 60x magnification, scale bar: 10 µm. **B-** Quantification of filipin integrated density in the plasma membrane, showed that Htt 171-82Q neurons exhibit more than the double of filipin in plasma membrane positive structures compared to control cells. Graph represents the mean of 3 independent experiments (N=3, n=9 - cover slips). The statistical test used was Mann Whitney U test (samples did not pass normality test, therefore used a non-parametric test), $p<0.0001$ (****), error bars = SEM.

The results obtained in Figure 3.1.5 show increased unesterifed sterols (filipin labeling) in plasma membrane of cells expressing mutant Htt (Htt 171-82Q).

However, there are some filipin-positive vesicular structures that do not co-stain with the plasma membrane marker in Htt171-82Q samples. Staining with the lysosomal marker Lysotracker red DND-99 revealed these to be lysosomes.

Lysosomal counts (Figure 3.1.6) demonstrated that striatal cells expressing mutant Htt contain more lysosomal vesicles than the wild type cells.

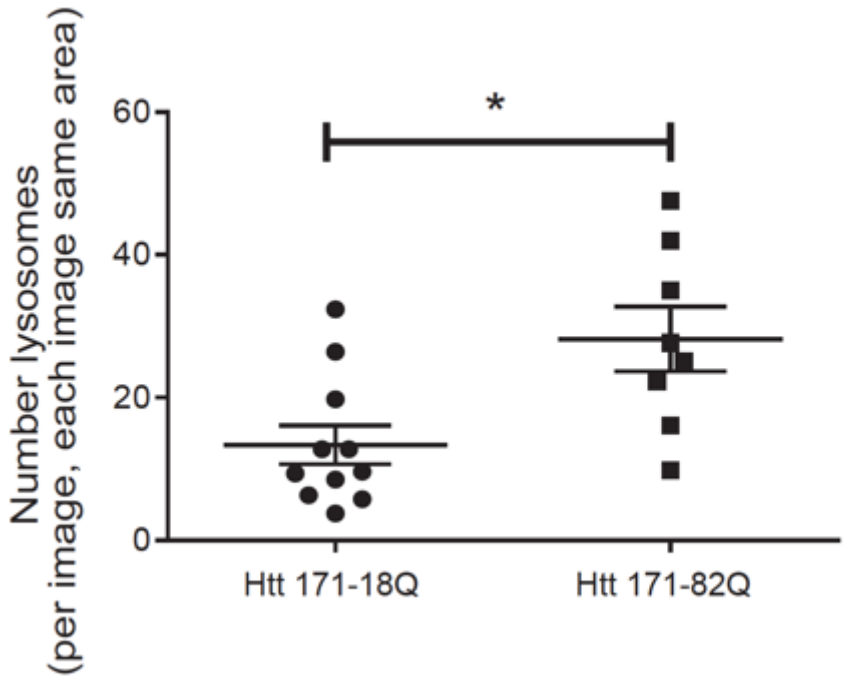

Figure 3.1.6: **Htt 171-82Q expressing cells exhibit an increased number of lysosomal vesicles compared to Htt 171-18Q expressing cells**. Striatal neurons (DIV 13) were fixed and loaded with Lysotracker red DND-99. Lysosome structures counts showed that neurons carrying mutant Htt (Htt 171-82Q) exhibited significantly, p= 0.016 (*), higher numbers of lysosomes compared to control cells. Graph represents the lysosomes counted per image analysed (Htt 171-18Q = 11 and Htt 171-82Q = 8 images) from 3 independent experiments. The statistical test used was unpaired t-tests with Welch's correction, two–tailed, error bars = SEM.

LDL receptors at the plasma membrane receive the cholesteryl ester enriched lipoporteins. These are transferred to lysosomes which ones promote the hydrolyses of cholesteryl esters to be distributed to other organelles (Brasaemle and Attie, 1990). Relocation of cholesterol from lysosomes is protein mediated as highlighted by mutation in NPC1 or NPC2 causing the neurodegenerative disease Niemann-Pick disease type C (Vanier, 2015).

Due to the importance in intracellular cholesterol distribution played by lysosomes, I sought to investigate whether in my HD model cholesterol was accumulating in those organelles.

Striatal cells from both conditions (Htt 171-18Q/82Q) were co-stained with filipin and the lysosomal marker- Lysotracker (Ly). A positive control was added to this experiment, striatal cells treated with U-18666A compound, which mimics Niemann-Pick disease type C (Cenedella, 2009) as inhibits the escape of cholesterol from late endosomes and lysosomes, accumulating sterols in lysosomal vesicles (Liscum and Faust, 1989).

Striatal neurons expressing mutant Htt and treated with U-18666A exhibited increased filipin staining compared to control neurons (Figure 3.1.7 A-filipin painel). Lysosomal marker (Ly) labelled structures in all the conditions (Figure 3.1.7 A Ly panels). Merge panel and zoom images presented the co-localization of lysosomal vesicles with filipin in mutant Htt cells and U-18666A treated neurons. However wild type neurons showed less obvious co-localization between sterols and vesicles (Figure 3.1.7 A merge). I quantified the intensity of filipin staining overlapping with Lysotracker ds red DND-99 in both control and disease cells (Htt 171-18Q/82Q), as well as U-18666A treated cells (see Material and Methods section 2.7). The analyses showed that HD neurons contained higher levels of filipin labeling in lysosomal vesicles compared to control cells. Similar values were acquired from the analysis to U-18666A treated cells compared with Htt 171-82Q neurons (Figure 3.1.7 B), however non-statistically significant when compared to wild type neurons (due to SEM bar).

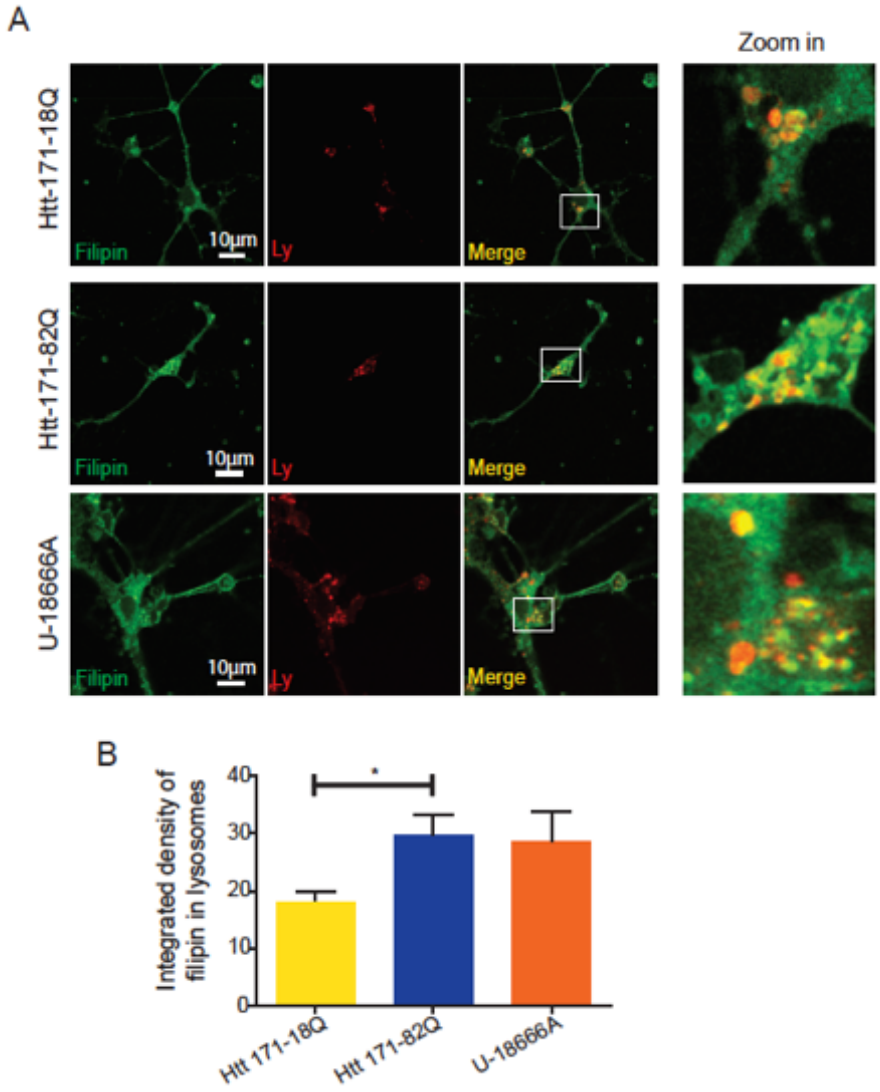

Figure 3.1.7: **Unesterified sterol accumulated in Htt 171-82 expressing neurons co-localises with lysosomes.** Primary neurons expressing Htt 171-18Q, Htt 171-82Q and treated with 1.25 µM of U-18666A for 48h were fixed at DIV 13. **A-** Representative confocal images showed increased filipin staining in mutant Htt expressing neurons, and in U-18666A treated primary cells, compared to control (Htt 171-18Q) (filipin panel). Lysosome dye (Lysotracker red DND-99) showed labelled structures in all the conditions (panel Ly), however cells expressing mut Htt (Htt 171-82Q) presented filipin engulfed in lysosome positive structures (merge-zoom panel) as showed in U-18666A. The same was not observed in Htt 171-18Q. Confocal images taken with Leica microscope at 60x magnification, scale bar: 10 µm. **B-** Quantification of integrated density of filipin in lysosomes showed that Htt 171-18Q presented significantly, p=0.027 (*) less filipin in lysosomal vesicles compared to HD cells. Htt 171-82Q exhibited similar values compared to U-18666A**.** Graph represents the average of 3 independent experiments (N=3, n=12). The statistical test used was ANOVA followed by Tukey's multiple comparison test, error bars = SEM.

These results showed that lysosomes in striatal neurons expressing Htt171-82Q have a higher intensity of filipin staining than control neurons.

Overall, the filipin staining results clarify that the sterol(s) accumulating in the HD model are at least partly in unesterified form; moreover, they localise to the plasma membrane and lysosomal vesicles.

3.1.4. Cholesterol accumulation in the HD model is not attributable to changes in expression of cholesterol synthesis or transport genes.

Previous work in the Luthi-Carter lab using microarray gene expression analysis suggests that cholesterol accumulation in Htt171-82Q cells is not due to gene expression dysregulation (i.e. neither increased expression of cholesterol synthesis nor decreased transcription of transport genes) (Luthi-Carter et al., 2010)). In order to re-examine this question and extend the analysis to specific mechanisms of sterol transport, I assessed the expression of the RNAs encoding several key sterol regulatory genes *(HMGCR, LDLr, ABCA1, ABCG4 and APOE*) by real-time quantitative PCR.

Real-time quantitative PCR (qRT-PCR) analyses showed no significant changes between control and disease conditions in the mRNAs measured: HMGCR, LDLr, ABCA1, ABCG4 and ApoE (Figure 3.1.8).

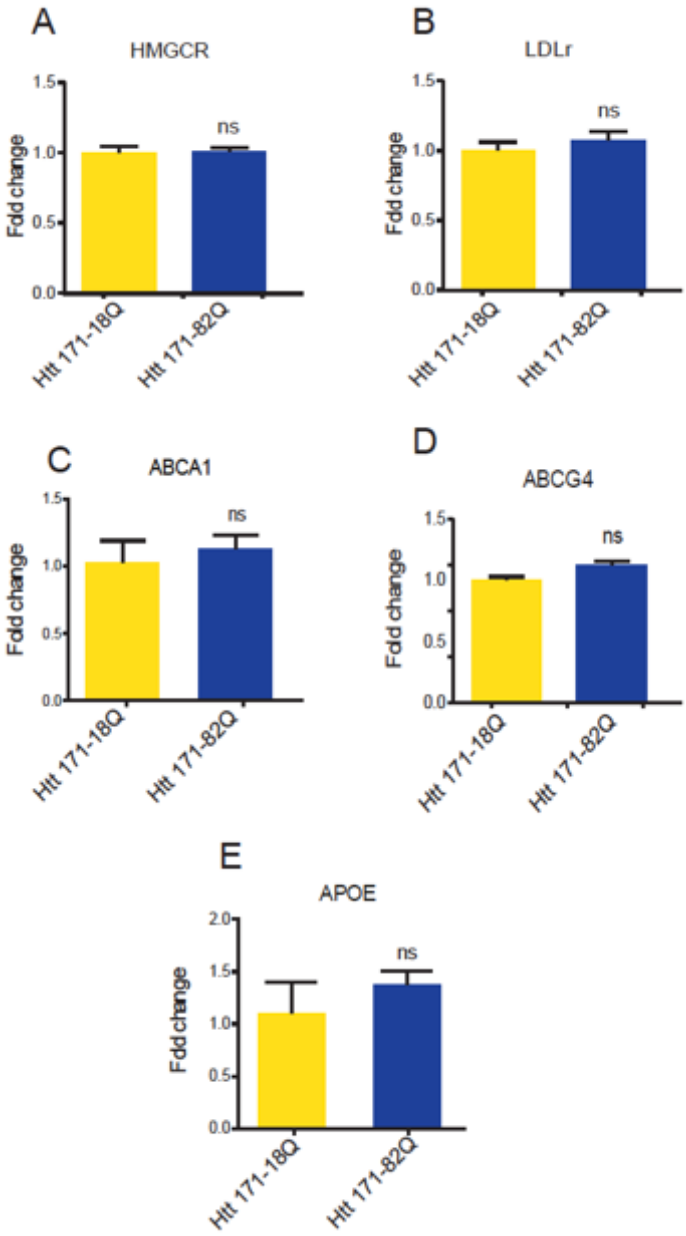

Figure 3.1.8: **Sterol accumulation in Htt 171-82Q expressing primary striatal neurons is not attributable to changes in the expression of genes responsible for cholesterol synthesis or transport.** No differences were observed in expression of mRNAs encoding proteins involved in the cholesterol biosynthesis (HMGCR, LDLr) or transport (ABCA1, ABCG4, ApoE) between Htt 171-82Q and Htt 171-18Q expressing cells. Results are presented as the fold change mean +/- SEM of three independent experiments with three biological replicates each (N=3, n=9). Statistical analysis performed was unpaired t-tests with Welch's correction, were non-significance (ns) was observed ($p>0.05$).

These results are consistent with previous microarray results from our laboratory (Luthi-Carter et al., 2010).

Since sterol biosynthesis is also regulated at the protein level through the rate-limiting enzyme HMGCR, I also examined levels of this protein in our HD system. No difference is detected between HD and control conditions, as observed in Figure 3.1.9 A and B.

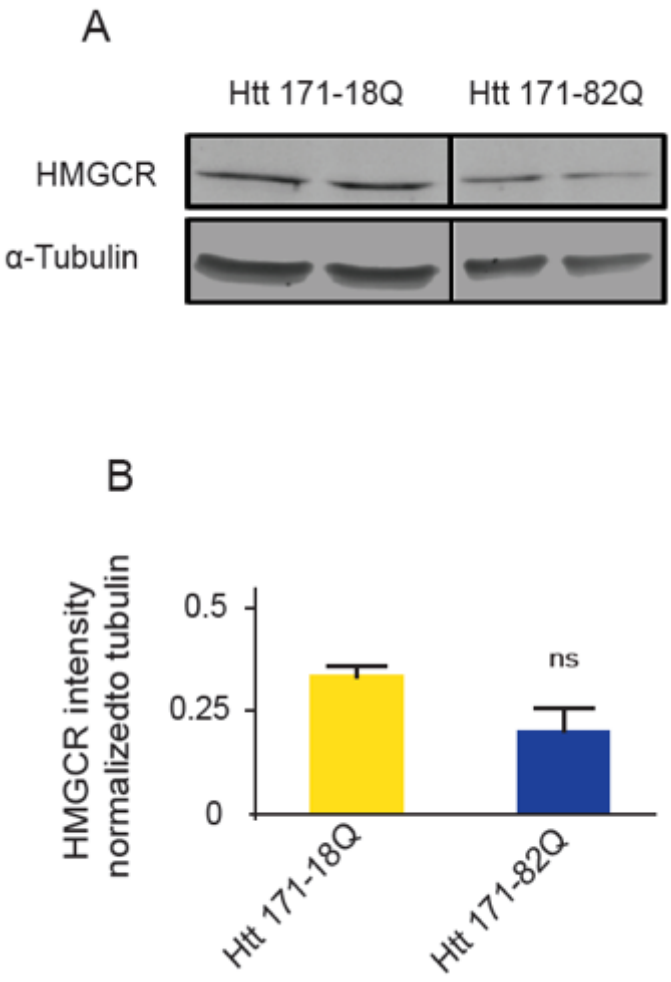

Figure 3.1.9: **Sterol accumulation in Htt 171-82Q expressing primary striatal neurons is not attributable to an increase in HMGCR protein expression. A-** Striatal neurons at DIV 13 were lysed and used for western blotting analyses with the indicated antibodies (HMGCR and loading control: α-tubulin). No differences were observed between the two conditions. **B-** Quantification of HMGCR intensity normalised to α-tubulin, resulted in non-significant (ns) differences in HMGCR protein expression between control (Htt 171-18Q) and mutant Htt (Htt 171-82Q) expressing neurons. Protein lysates from two independent experiments (N=2, n=4) was used to perform statistical analyses using unpaired t-test with Welch's correction, error bars = SEM.

The trend is for HMGCR to decrease, rather than increase. Therefore, the accumulation of sterols observed by the cholesterol oxidase assay (Figure 3.1.1) and filipin staining (Figure 3.1.2 A and B) is not a consequence of cholesterol gene expression dysregulation, or increased protein levels of HMGCR.

3.1.5. AK-7, a putative Sirt2 inhibitor, inhibits sterol accumulation.

It has been demonstrated that AGK2 a potent SIRT2 inhibitor rescued the number of dopaminergic neurons due to a α-synuclein mediated toxicity in a Parkinson's disease (PD) model, by inclusion enlargement (Outeiro et al., 2007). Given the evidence that Sirtuin 2 inhibition ameliorates the phenotype in models of PD, our lab asked whether a similar effect could be achieved in models of HD. It was observed that AGK2 and AK-1 rescued striatal neurons expressing Htt171-82Q and reduced the number of inclusions (Luthi-Carter et al., 2010). Surprisingly these compounds decreased the sterol levels exhibited by HD primary striatal neurons via inhibition of SREBP2 nuclear translocation (Luthi-Carter et al., 2010).

A blood brain barrier permeable SIRT2 inhibitor, AK-7 has been identified and tested, by the Luthi-Carter lab, as a compound, which successfully reduces cholesterol in HD neuronal models by inhibiting SREBP2 nuclear trafficking and therefore diminishing the expression of sterol biosynthesis genes (Taylor et al., 2011).

In order to reconfirm the sterol-modulating effect of AK-7 on my hands, I tested 10 μM of AK-7 for 24 h, and assessed sterol status by cholesterol oxidase assay. This analysis showed that AK-7 significantly reduces total sterols in our *in vitro* striatal neuron HD model (Figure 3.1.10), confirming the previous observations.

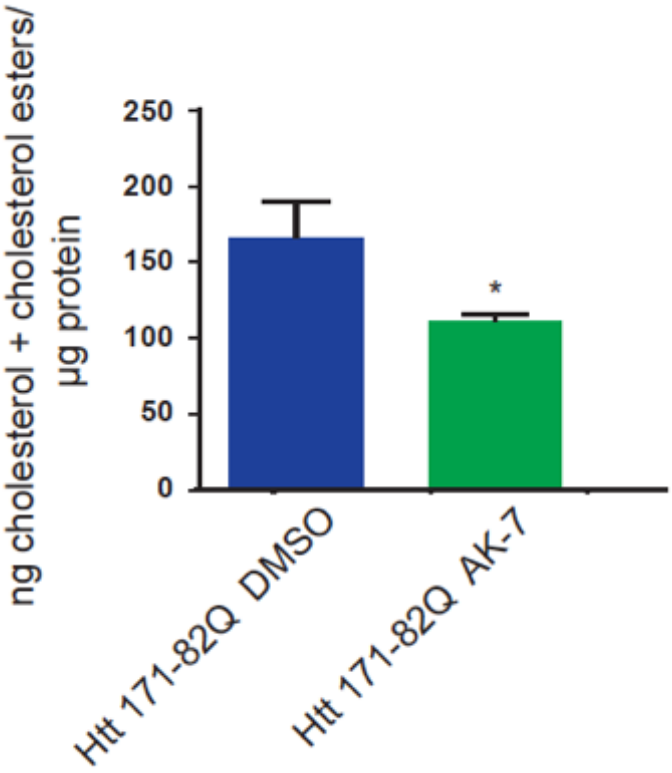

Figure 3.1.10: **AK-7 decreased sterol in Htt 171-82Q expressing primary striatal neurons.** Primary striatum neurons infected with Htt 171-82Q treated with DMSO (control) or 10 µM AK-7 for 24h, were lysed (DIV 13) and sterol status assessed by cholesterol oxidase assay. Total sterol quantification showed a significantly (p=0.01) decrease in sterol content in mutant Htt-exposed neurons (Htt171-82Q) treated with AK-7 for 24 h, comparing to the non-treated control cells (Htt171-82Q DMSO). Data from 2 independent experiments (N=2, n=12) was used to perform statistical analyses using unpaired t-tests with Welch's correction, p=0.01 (*), error bars = SEM.

3.1.6. HD model cells release higher amounts of 24S-hydroxycholesterol (24S-OHC) into the medium.

Taking into account the results that sterols accumulate in the HD *in vitro* model used in this thesis, showed by the cholesterol oxidase assay (Figure 3.1.3) and filipin staining (Figure 3.1.4), I sought to determine which specific sterol species the HD neurons accumulate. One sensitive and highly reproducible method for such analyses is isotope dilution mass spectrometry (Marullo et al., 2012), which was thus employed. These experiments were undertaken in collaboration with the laboratory of Dr. Valerio Leoni (Fondazione I.R.C.C.S. Instituto Neurologico Carlo Besta).

My primary objective was to elucidate the sterol species (24S-hydroxycholesterol, lanosterol, lathosterol, desmosterol and cholesterol) accumulating in striatal neurons expressing mutant Htt (Table 3.1.1 A). However, I also evaluated whether sterols were released into the culture medium. Therefore the culture media where striatal neurons were cultured in was also analysed implementing the same technique (Table 3.1.1 B).

The results obtained in striatal neurons (normalized to protein content), showed significant decrease in lanosterol ($p=0.0027$), lathosterol ($p=0.0021$), desmosterol ($p<0.0001$) and cholesterol ($p=0.0049$) in Htt 171-82Q cells compared to Htt 171-18Q (Table 3.1.1A). Regarding 24S-OHC, no significant differences were detected ($p=0.5091$) (Table 3.1.1 A). In the culture media however, 24S-OHC was detected as significantly increased ($p=0.0064$) in Htt 171-82Q cells compared to control neurons (Table 3.1.1 B, Figure 3.1.11). The other sterols analysed (lanosterol, lathosterol, desmosterol and cholesterol) showed no differences in the medium between the two conditions (Table 3.1.1 B).

A

	Striatal neurons (ng/mg protein)		
	Htt 171-18Q	Htt 171-82Q	p value (student T-test)
24S-OHC	11.00	11.54	0.5091
Lanosterol	460.86	321.64	0.0027
Lathosterol	533.81	386.98	0.0021
Desmosterol	1044.45	796.44	<0.0001
Cholesterol	4445.78	967.65	0.0049

B

	Medium (ng/mL)		
	Htt 171-18Q	Htt 171-82Q	p value (student T-test)
24S-OHC	4.80	5.95	0.0064
Lanosterol	1.20	1.16	0.6946
Lathosterol	6.54	7.02	0.2363
Desmosterol	36.78	38.87	0.6675
Cholesterol	561.92	596.84	0.1269

Table 3.1.1: **Isotope dilution mass spectrometry sterol profile from HD model neurons.** **A-** Primary striatal cells (DIV 13) were lysed and sterol content measured by isotope-dilution mass spectrometry. The profile of sterols quantified (lanosterol, lathosterol, desmosterol and cholesterol) showed a decrease in the neurons expressing mutant Htt (Htt 171-82Q). 24S-Hydroxycholesterol (24S-OHC) showed no differences between the two conditions. Statistical analyses showed in the table. **B-** Culture medium was collected and analysed by isotope-dilution mass spectrometry. Neurons exposed to Htt171-82Q released more cerebrosterol (24S-OHC) into the medium, compared to H171-18Q cells. No differences were encountered regarding the other sterols studied (lanosterol, lathosterol, desmosterol and cholesterol). Results from one experiment, samples from 4 different wells (4 technical replicates), (N=1, n=4), sent for analyses in the laboratory of Dr, Valerio Leoni (Fondazione I.R.C.C.S. Instituto Neurologico Carlo Besta). The statistical test performed was unpaired t-test with Welch's correction, significance and p values in the tables.

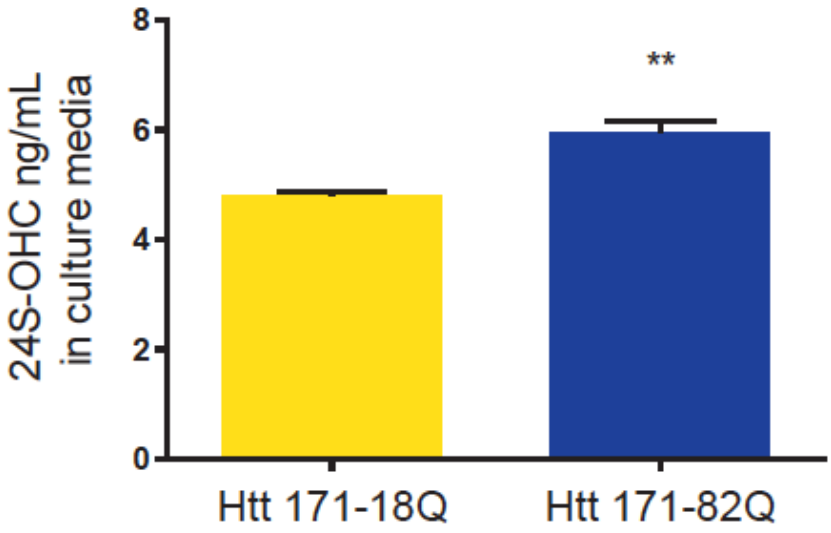

Figure 3.1.11: **Striatal neurons expressing mutant Htt (Htt 171-82Q) fragments release higher amounts of 24S-hydroxycholesterol (24S-OHC) into the medium.** Graph representative of the 24S-OHC measured in the culture media (DIV 13) by isotope-dilution mass spectrometry. Neurons exposed to Htt171-82Q released more cerebrosterol (24S-OHC) into the medium, compared to H171-18Q. Significance determined by unpaired t-test with Welch's correction, where p=0.0064 (**), error bars = SEM.

Isotope dilution mass spectrometry analyses of the cell content exhibited accumulation of the sterols analysed (lanosterol, lathosterol, desmosterol and cholesterol) by control neurons (Htt 171-18Q), counteracting the previous observations from the cholesterol oxidase assay (Figure 3.1.3) and filipin staining (Figure 3.1.4). The cell pellet showed no significant differences for 24S-OHC values, however. The results from the culture medium displayed a significant increase of 24S-OHC detected in the medium of mutant Htt striatal cells (Table 3.1.1 B and Figure 1.1.11).

CYP46A1 is the enzyme responsible for the conversion of cholesterol into 24S-OHC in neurons. In order to test whether expression of mutant Htt increased 24S-OHC via an increase in *CYP46A1* gene expression, I measured the mRNA of CYP46A1 in control versus HD model striatal neurons.

qRT-PCR analyses of CYP46A1 mRNA levels detected no difference between wild type and mutant Htt expressing neurons (Htt 171-18Q versus Htt 171-82Q) (Figure 3.1.12).

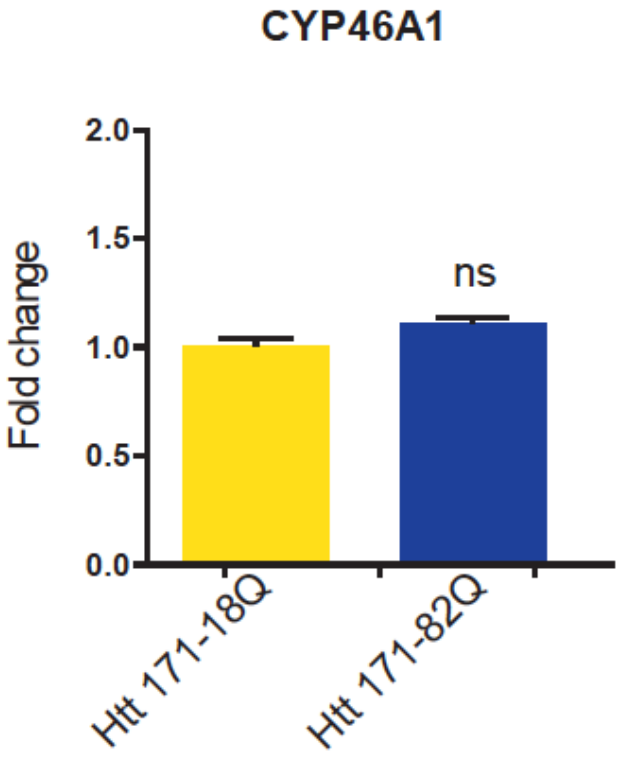

Figure 3.1.12: **CYP46A1 mRNA is not upregulated by expression of Htt 171-82Q.** CYP46A1 mRNA values, from neurons at DIV 13, were similar in both conditions (Htt 171-18Q versus Htt 171-82Q). Statistical analysis performed was unpaired t- tests with Welch's correction; the result was non-significant (ns). Data from 3 experiments, each one with 3 technical replicates (N=3, n=9), error bars = SEM.

Therefore, counter to the hypothesis that increased 24S-OHC detected in the medium (Table 3.1.1B and Figure 1.1.11) was caused by *CYP46A1* over expression, no differences in mRNA levels were observed.

I conclude that mutant Htt does not dysregulate *CYP46A1* gene expression therefore increased 24S-OHC levels observed in the medium (Figure 3.1.11) are not a reflexion of *CYP46A1* overexpression.

3.1.7. Discussion

Taking advantage of the characterized *in vitro* model (Zala et al., 2005) I observed significantly increased sterol in Htt 171-82Q expressing primary striatal neurons when compared to control, Htt 171-18Q by cholesterol oxidase assay (Figure 3.1.3) and filipin staining (Figure 3.1.4). Taking in consideration these results, the data originated by IDMS was somewhat surprising, all the sterols analysed in the cells lysate, except for 24S-OHC were significantly decreased in HD striatal neurons. Has been described that *in vitro* neurons accumulate about 40% of lanosterol and astrocytes accumulate cholesterol, moreover the cholesterol synthesis pathway taking place in these cells differs. Neurons contain mainly precursors of the Kandutsch-Russel pathway including 7-dehydrocholesterol and lathosterol, while astrocytes contained precursors of the Bloch-pathway namely desmosterol (Figure 1.4) (Nieweg et al., 2009). Considering this knowledge and the percentage of astrocytes in the cultures being about 20% I found difficult to comprehend the high values of desmosterols determined by IDMS (Table 3.1.1). Moreover there is a dependent relation with the cholesterol synthesis and efflux (Lund et al., 2003), therefore how can Htt 171-18Q neurons accumulate those levels of cholesterol and Htt 171-82Q neurons being the ones releasing significantly increased 24S-OHC? Due to the lack of understanding of the IDMS results there is the urge to repeat these experiments. Perhaps the samples preparation was not the recommended (Marullo et al., 2012), as samples should have been prepared by lipid fraction isolated with solvent extraction (hexane/isopropanol 3:2, v/v) as described by (Valenza et al., 2005) instead of the protein lysate method as described previously by Del Toro (del Toro et al., 2010). Nevertheless, in order to quantify the protein content for normalization purposes I opted for the second method.

The methods used to quantify cholesterol by filipin and cholesterol oxidase assay have limitations as both detect sterols with the 3'OH group free, which is common to many sterols (Marullo et al., 2012).

Therefore for a better understanding on the sterol status in HD, it is needed to repeat the IDMS considering both methods of samples preparation and broad list of sterols to identify and quantify.

For the proper statistical analysis of filipin staining in neurons (Figure 3.1.4) and in the plasma membrane (Figure 3.1.5), I opted for a non-parametric test as for both experiments the data regarding Htt 171-82Q did not pass the normality test. This fact is maybe justified by a model limitation, which I am not aware of as for the model characterization I only took into consideration the neuronal viability, while I should also have considered the expression of wild-type and mutant Htt.

Staining with the lysosomal marker revealed lysosomal structures in neurons in culture. Assessment of the number of lysosome structures per image resulted in a significant higher number counted in the neurons expressing Htt171-82Q (Figure 3.1.6). The increased prevalence of endosomal/lysosomal structures has also been observed to be a characteristic of HD neurons by other groups in other systems (Kegel et al., 2000; Ravikumar and Rubinsztein, 2004; Qi and Zhang, 2014).

In concordance with previous results from our lab and counteracting others who performed DNA microarrays analysis applying striatal cells expressing different N-terminal 548 amino-acid Htt fragments with 26, 67, 105 or 118 glutamines under the control of a doxycycline-regulated promoter (Sipione et al., 2002), I observed that the increased sterol in Htt171-82Q expressing neurons is not paralleled by transcriptional dysregulation of genes involved in the cholesterol synthesis or transport (Figure 3.1.8) or due to increased translation of HMGCR (Figure 3.1.9). Nevertheless would be interesting to repeat HMGCR experiments and to perform few more western blot analyses to the genes analysed by the real time qPCR.

As the increased sterol observed in the HD model, may be detrimental and contribute to disease, the existence of a compound that penetrates the blood brain barrier and effectively decreases total sterols is promising for therapeutics. Similarly to what was previously published (Taylor et al., 2011), I observed that AK-7 decreases cholesterol in primary striatal neurons expressing mutant Htt (82Q) (Figure 3.1.10). AK-7 is a sirtuin inhibitor, and the proposed mechanisms is that retaining SREBP2 in the ER downregulates its target genes (Taylor et al., 2011).

The enzyme responsible for oxidizing cholesterol to 24S-OHC is CYP46A1, exclusively expressed by neurons (Lund et al., 1999). I investigated whether mutant Htt dysregulated *CYP46A1* expression causing its overexpression which could explain the increase of 24S-OHC release. Counter to the hypothesis, no differences in CYP46A1 mRNA levels were observed between primary neurons expressing wt and mutant Htt. This suggests that mutant Htt does not enhance the expression of *CYP46A1.* Considering the result from the Isotope dilution mass spectrometry, I have to rule out the possibility that increased levels of cholesterol, CYP46A1 subtract is the explanation for the increased levels of 24S-OHC released by Htt 171-82Q neurons, as this was found decreased in the cell extract. One possible explanation is that the increased levels of 24S-OHC in the medium of Htt 171-82Q neurons due to increased CYP46A1 activity, which would be an interesting subject of future work, as attempts to regulate transcriptionally CYP46A1 resulted in the finding that from the studied compounds only oxidative stress caused a significant increase in transcriptional activity (Ohyama et al., 2006).

3.2. Assessing the effects of 24S-Hydroxycholesterol on primary striatal neurons.

Introduction: The N-methyl-D-aspartate receptor (NMDAR) belongs to the group of ionotropic glutamate receptors (iGluRs), together with AMPA and kainate receptors (Traynelis et al., 2010). NMDARs have some particularities: their activation requires release of Mg^{2+}(after depolarization), binding of the agonist glutamate and the co-agonist glycine. Once the receptor's channel is open, it is highly permeable to Ca^{2+} (Paoletti et al., 2013).

NMDARs are assembled as hetero-tetramers, most commonly composed of GluN1 subunits with GluN2, but rarely GluN3. The subunits that compose the receptor influence its biophysical and pharmacologic properties, as well as cellular interacting partners and subcellular localization. Moreover the receptor constitution is dynamic, as may vary during development, across CNS and in the occurrence of pathologies, with implications for the network function (Paoletti et al., 2013).

Presently, seven different subunits have been identified, which are encoded by 7 different genes: GluN1, GluN2 (GluN2A, GluN2B, GluN2C and GluN2D) and GluN3 (GluN3A, GluN3B) (Paoletti et al., 2013). Functional NMDARs require the assembly of the obligate GluN1 subunit, as is the one possessing the co-agonist glycine binding site with GluN2 to form glutamate binding site or a combination of GluN2 with GluN3 (Traynelis et al., 2010).

NMDARs play an important role in the regulation of excitatory synapses, being the main mediators of synaptic transmission (Paoletti et al., 2013). Abnormal NMDAR activation has been implicated in several pathophysiologies including Huntington's disease (Sepers and Raymond, 2014).

Huntington's disease affects primarily striatal medium spiny neurons (MSNs) (Vonsattel and DiFiglia, 1998) in these neurons the most expressed subunits of NMDARs are GluN1 and GluN2B (Kumar et al., 1997; Hallett et al., 2006).

It has been shown that the presence of NR2B in the NMDAR complex is sufficient to provoke excitotoxicity when the receptor is activated, independent on the cellular localization (synapses or extrasynapses) (Liu et al., 2007). This fact explains the selective sensitivity of MSNs for excitototoxic insults.

Pharmacological targeting of NMDARs as an attempt to ameliorate HD has been done without success (Sepers and Raymond, 2014). NMDARs contain in their N-terminal regulatory sites where small ligands acting as specific allosteric modulators can bind. Targeting this allosteric sites seems a beneficial approach for the discovery of new pharmacologic compounds, able to modulate NMDARs.

Nowadays, the most promising range of compounds to target NMDARs are allosteric ligands. Allosteric binding sites are less conserved than agonist binding site and channel pore, granting the possibility for subunit selectivity (Paoletti et al., 2013).

The identification of the first allosteric modulators occurred more than 20 years ago. The modulator reported was: ifenprodil, which antagonizes NMDARs (Williams, 1993). More recently the specific brain oxysterol 24S-hydroxycholesterol (24S-OHC) was found to function as positive NMDA allosteric modulator (Paul et al., 2013). 24S-OHC was shown to selectively potentiate NMDAR mediated EPSCs in rat hippocampal neurons and to enhance the ability of subthreshold stimuli to induce long-term potentiation (LTP) in hippocampal slices, moreover was able to reverse LTP deficits induced by ketamine a NMDAR channel blocker (Paul et al., 2013).

The cholesterol turnover in the brain is regulated by the oxidation of cholesterol into 24S-OHC by the enzyme CYP46A1 (Lund et al., 1999). Moreover 24S-OHC is more polar and water-soluble than its precursor and is able to traverse the plasma membrane. This mechanism is postulated to prevent accumulation in neurons (Bjorkhem et al., 1997). Nevertheless was recently described that ABCA1 actively eliminates 24S-OHC from neuronal cells (Matsuda et al., 2013). In addition to permeating brain cells, 24S-OHC can cross the blood brain barrier (BBB) and be released into the bloodstream (Bretillon et al., 2000).

In Section 3.1 I identified the sterol species enriched in the medium of Htt 171-82Q striatal neurons as 24S-OHC. Therefore the aim of this chapter is to understand the functional and physiologic effects of 24S-OHC upon primary striatal neurons.

In this thesis and in the context of an *in vitro* HD model, I aimed to explore the potential role of this molecule in HD pathogenesis. One aspect of this involved evaluating whether 24S-OHC might specifically enhance NMDAR-mediated excitotoxicity.

3.2.1. 24S-hydroxycholesterol (24S-OHC) is neurotoxic to primary striatal cells.

To determine the effect of 24S-OHC on the viability of primary striatal neurons, these cells were treated with varying concentrations of 24S-OHC (0.25, 0.5, 1, 2 and 10 μM) for 24 h. Neuronal survival was measured by NeuN positive staining cell counts, which one accounts for the specific presence of mature neurons (Kim et al., 2009; Lavezzi et al., 2013) (see Material and Methods section 2.5.1). 24S-OHC exhibited cytotoxicity in a concentration-dependent manner as can be observed in the representative images of NeuN staining (Figure 3.2.1 A) and in the graph (Figure 3.2.1 B). Even the lowest 24S-OHC concentration used (0.25 μM) caused significant cell death ($p=0.0295$). When neurons were treated with 10 μM of 24S-OHC for 24 h, cell survival was 38% of control (DMSO alone) (Figure 3.2.1 B).

A

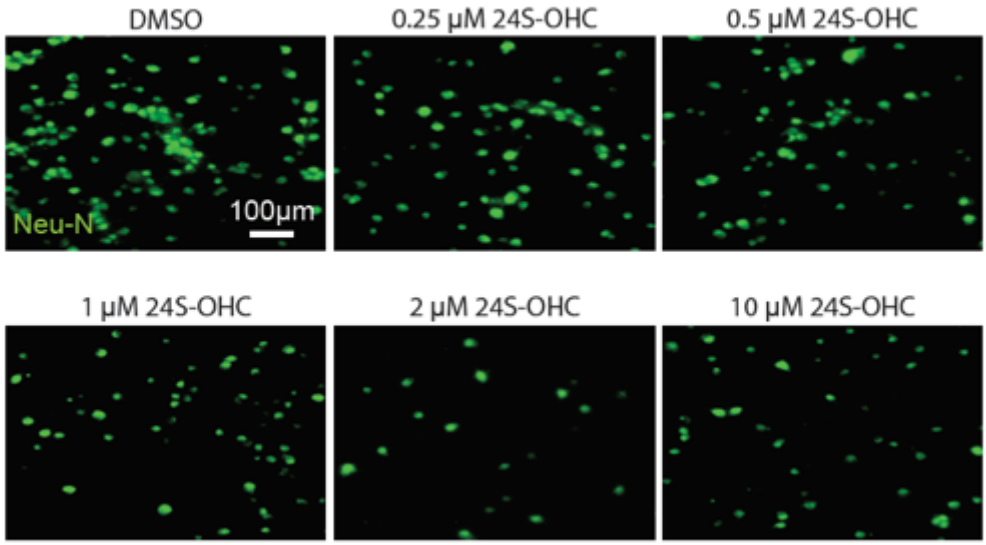
DMSO
0.25 µM 24S-OHC
0.5 µM 24S-OHC
Neu-N
100µm
1 µM 24S-OHC
2 µM 24S-OHC
10 µM 24S-OHC

B

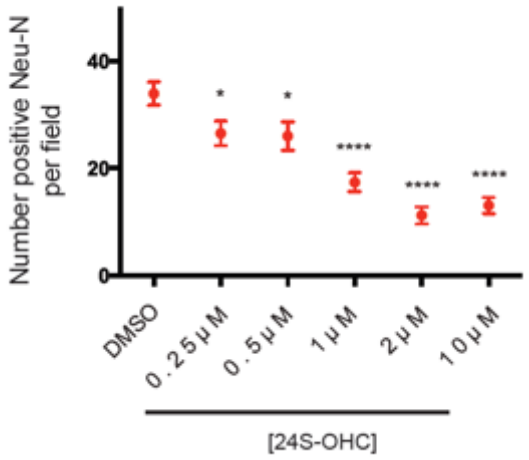
Number positive Neu-N per field
40
20
0
*
*
****
****
****
DMSO
0.25µM
0.5µM
1µM
2µM
10µM
[24S-OHC]

Figure 3.2.1: **24S-OHC is cytotoxic to primary striatal neurons.** Primary striatal neurons at DIV 13 were treated with increasing concentration of 24S-OHC (0.25, 0.5, 1, 2 and 10 μM) for 24 h. Cell survival was assessed by NeuN positive cell counts. **A-** Microscopic images of striatal neurons stained with NeuN are representative of cell loss caused by the application of increasing concentrations of 24S-OHC. **B-** 24S-OHC treatment generally resulted in proportionally greater striatal neuron loss with increasing concentrations tested. One-way ANOVA statistical test determined that the treatment between conditions was significant ($p<0.0001$), and when applied Dunnett's multiple comparison test the result showed that all the 24S-OHC concentrations tested resulted in statistical significance: 0.25 μM $p=0.0295$ (*), 0.5 μM $p=0.0410$ (*) and for 1 to 10 μM $p<0.0001$ (****). The graph represents the mean of the NeuN-positive cell counts per field +/- SEM of two independent experiments with 6 technical replicates (N=2, n=6). Images were taken using a Nikon eclipse Ti microscope at 20x magnification, scale bar: 100 μm.

3.2.2. Possible relationships of 24S-OHC and NMDA receptor related toxicities.

When looking for evidence of possible neurotoxic effects in the literature, I came across the study of (Paul et al., 2013), which identified 24S-OHC as a potent allosteric modulator of the NMDA receptor in hippocampal neurons. Therefore, I sought to investigate weather 24S-OHC can promote HD-related excitotoxicity.

One prominent and longstanding hypothesis in HD has been that excitotoxic damage via overactivation of NMDA receptors plays a role in degeneration of striatal medium spiny neurons (MSNs) (DiFiglia 1990). Thus I aimed to address whether 24S-OHC was playing the role of NMDA receptor allosteric modulator in primary striatal neurons *in vitro*, potentiating its effects. To assess these effects, I used calcium imaging, extracellular multi-electrode array electrophysiology and NeuN positive cells counts.

To study the effects on NMDA receptor I found important to control the environment, meaning the neuronal solution during the experiments, which one had to contain glucose, glycine and could not contain neither magnesium nor zinc. As neurobasal medium is constituted with magnesium and zinc I had to look for a proper solution, which I found cited in Xifro et al. denominated as Locke's solution (see Material and Methods section 2.8) (Xifro et al., 2008). Therefore I investigated the effects of 24S-OHC on neuronal survival in

conditioned environment using Locke's solution a medium that has previously reported (Xifro et al., 2008).

Primary striatal neurons at DIV 13 were treated with increasing concentrations of 24S-OHC (0.25, 0.5, 1, 2 and 10 μM) for 20 min in Locke's solution (see Material and Methods section 2.8 for details). Cell survival was assessed 24 h later by NeuN staining, which showed increased cell loss dependent on 24S-OHC concentrations (Figure 3.2.2 A). The NeuN counts from the microscope images were averaged and plotted against 24S-OHC concentrations. The graph is concordant with the images, showing that striatal neurons showed a decrease, although not significant, in number when treated with 0.5 μM of 24S-OHC (27% cell death, $p=0.997$). Under these conditions 24S-OHC exhibited significant ($p<0.0001$) cytotoxicity to striatal cells at concentrations from 1 μM, causing more than 80% cell death (Figure 3.2.2 B).

A

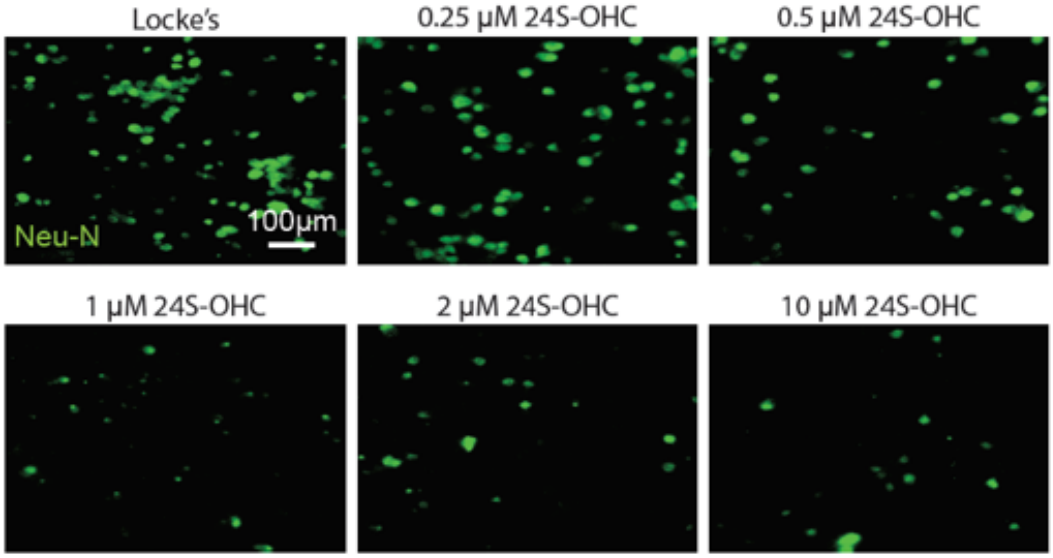
Locke's
0.25 µM 24S-OHC
0.5 µM 24S-OHC
Neu-N
100µm
1 µM 24S-OHC
2 µM 24S-OHC
10 µM 24S-OHC

B

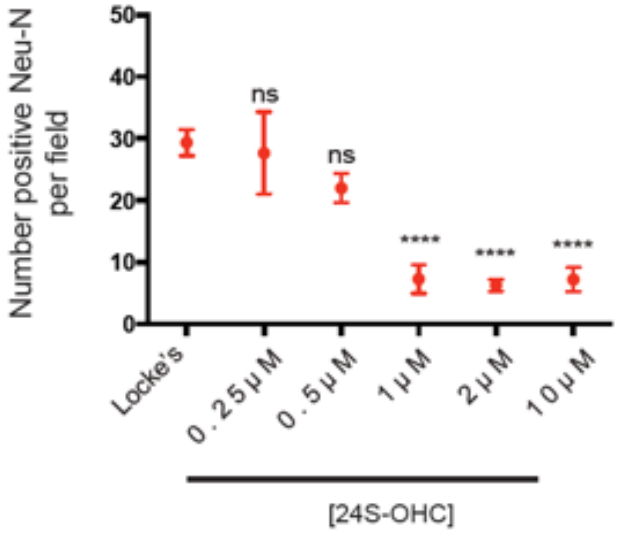
Number positive Neu-N per field
50
40
30
20
10
0
ns
ns
****
****
****
Locke's
0.25µM
0.5µM
1µM
2µM
10µM
[24S-OHC]

Figure 3.2.2: **24S-OHC is a potent neurotoxic agent in Locke's solution.** Primary striatal neurons at DIV 13 were treated with increasing concentrations of 24S-OHC (0.25, 0.5, 1, 2 and 10 µM) for 20 min in Locke's solution (see Material and Methods section 2.8 for details). Cell survival was assessed 24h later by NeuN staining. **A-** Microscopy images of striatal neurons stained with NeuN are representative of cell loss caused by the application of increasing concentration of 24S-OHC. **B-** 24S-OHC caused significant cell loss compared to control. Cell viability was assessed 24h after treatments and NeuN cell count, averaged and plotted per 24S-OHC concentrations. One-way ANOVA proved that 24S-OHC had a significant effect on cell survival ($p<0.0001$). The graph shows that primary neurons treated with 0.5 µM of 24S-OHC suffered 27% cell loss (Dunnett's multiple comparison test $p=0.0997$, not significant), increasing to 75.3% with 1 µM were $p<0.0001$ (****), 2 and 10 µM of 24S-OHC treatment corresponded to 78.7% and 75.6% of cell death respectively. The graph represents the mean NeuN count per field +/- SEM of two independent experiments with 3 technical replicates each (N=2, n=6). Images were taken using Nikon eclipse Ti microscope at 20x magnification, scale bar: 100 µm.

These results suggest that 24S-OHC is toxic to striatal neurons in culture. Concentrations from 1 µM of 24S-OHC in Locke's solution caused significant cell death (Figure 3.2.2). When applied in Locke's solution the effect observed was similar to when applied in the medium (Figure 3.2.1), which shows consistency of toxicity caused by 24S-OHC.

GluN1 and GluN2B are the two main subunit isoforms of NMDAR in medium spiny neurons *in vivo* (Kumar et al., 1997; Hallett et al., 2006) and I wanted to determine whether these subunit isoforms were expressed in primary striatal neurons *in vitro.* In order to visualise the isoforms in these neurons I stained primary striatal cells, at DIV 13 with GluN1 and GluN2B antibodies.

Representative images of immunofluorescence showed a ubiquitous distribution of GluN1 and GluN2B in primary striatal neurons (Figure 3.2.3). As negative control I incubated the fixed cultures only with secondary antibody. No background fluorescence was observed.

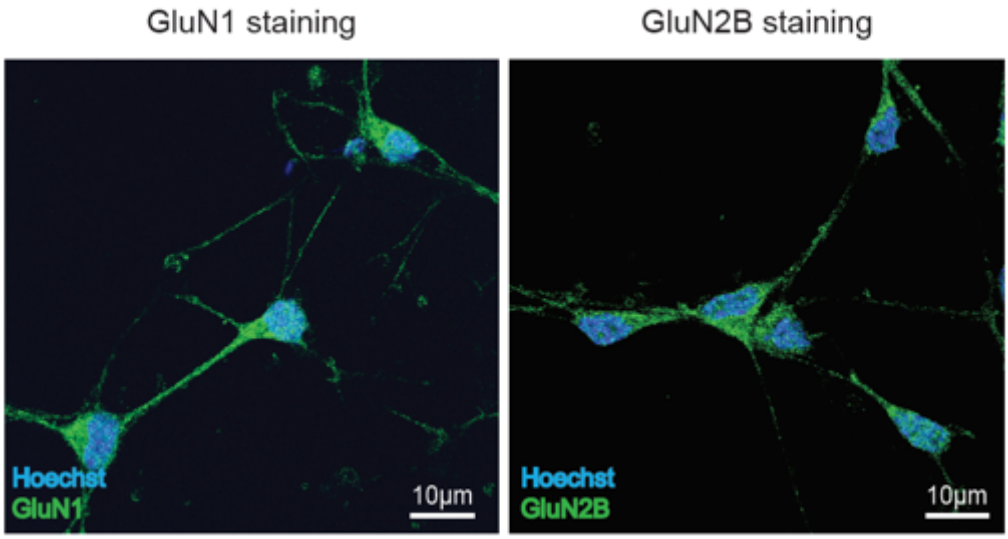

Figure 3.2.3: **Expression of NMDA receptor subunit isoforms GluN1 and GluN2B in primary striatal neurons.** Primary striatal neurons at DIV 13 were fixed and stained with GluN1 or GluN2B to evaluate the expression and localization of NMDA receptor subunit isoforms (GluN1 and GluN2B). Representative images of immunofluorescence showed a ubiquitous distribution for NMDA receptor subunits in primary striatal neurons (Alexa fluor 488-green). Hoechst labelled the nucleus. Images were taken using Leica confocal microscope at 60x magnification, scale bar: 10 µm.

The two main isoforms of NMDAR in striatal neurons are expressed at DIV 13 *in vitro.*

3.2.3. 24S-OHC effects via NMDA receptors.

In order to study the possible role of 24S-OHC as an NMDAR allosteric modulator in striatal neurons (Paul, Doherty et al. 2013) I used a calcium-imaging technique. The extracellular calcium entry in neurons occurs through NMDARs and voltage gated calcium channels (Verkhratsky, 2005), therefore I thought that the calcium influx measurement in primary striatal neurons could be a readout for the upregulation of NMDAR activity by 24S-OHC.

Primary striatal neurons at DIV 13 *in vitro* were expected to respond to NMDA application. To test this hypothesis, I imaged the culture for 200 frames

(taken at intervals of 500 ms) and at the 40th frame, 100 µM of NMDA was applied. In Figure 3.2.4 A it is possible to see that the cells in the left bottom corner, "after 100 µM NMDA" panel, increased the intensity (from 0% - blue to 100% -yellow), corresponding to higher levels of free calcium in the cell. By plotting the analysis of all images as changes in fluorescence intensity (($\Delta F/F_0$), for more details see Material and Methods section 2.16) into Z axis profile the data can be visualised as an intensity graph (Figure 3.2.4 B), which one shows a peak of intensity at the 40th frame- when NMDA was applied.

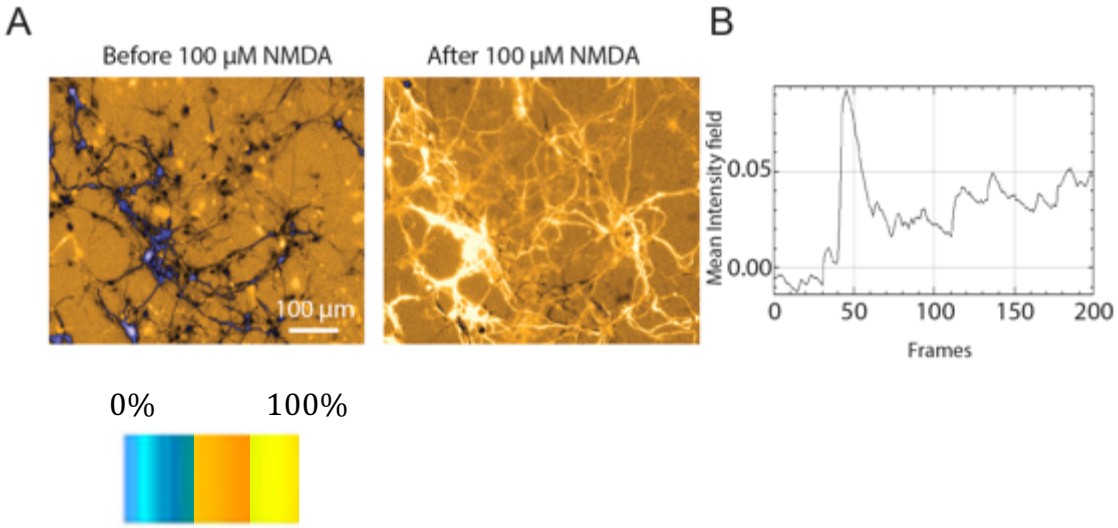

Figure 3.2.4: **Primary striatal cells respond to 100 µM NMDA application in Locke's solution.** Primary striatal neurons at DIV 13 were loaded with 2 µM Fluo-4 bathed in Locke's solution and 100 µM NMDA was applied at the 40th frame (image – $\Delta F/F_0$, composed of 200 frames). **A-** Neurons responded to NMDA application with increased fluorescence intensity, from 0% (blue pseudocolored neurons) to 100% (yellow pseudocolored neurons), panel image: after 100 µM NMDA application. **B-** The graph, representing image plot Z axis profile resulted in mean intensity per field over frame, shows increased intensity at 40th frame, when NMDA was applied. Figure representative of 3 independent experiments. Images were taken using Nikon eclipse TE 2000-U microscope at 20x magnification, scale bar: 100 µm.

MK-801 was used to confirm that the observed effect of NMDA application was indeed due to increased flux of calcium in the cells through NMDAR. Pre-treatment of primary striatal neurons with 25 µM of MK-801 (Figure 3.2.5) blocked the previously observed effect (Figure 3.2.4) of 100 µM of NMDA.

As observed in Figure 3.2.5, neurons treated with MK-801 were insensitive to NMDA application. Calcium was inhibited to enter the cell through NMDAR therefore no change in fluorescence was observed upon NMDA application. MK-801 efficiently blocked NMDAR, which consequently impeded calcium to enter the cells.

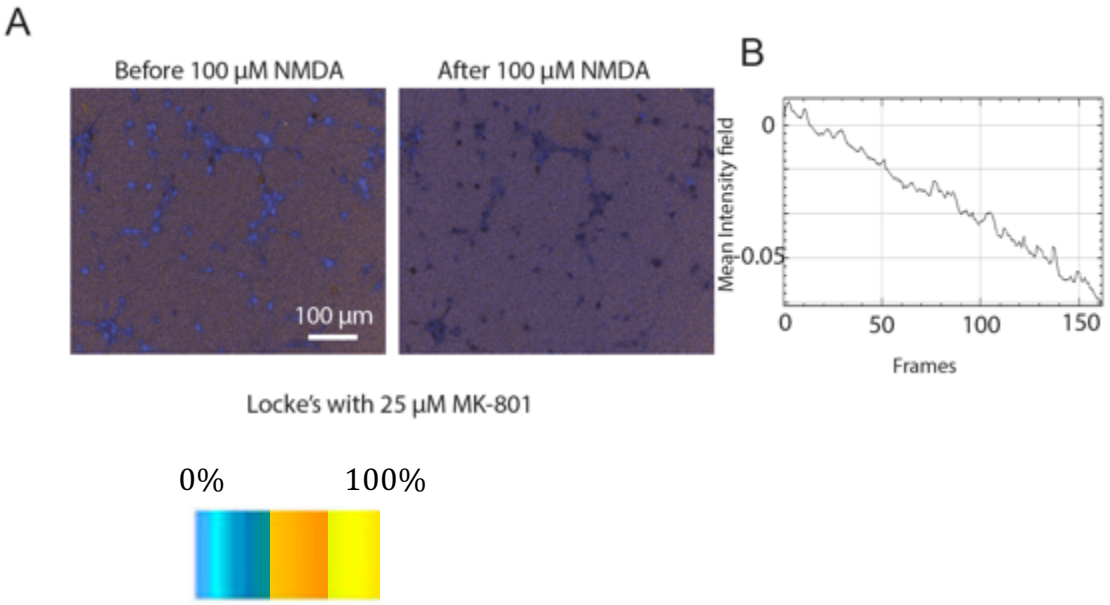

Figure 3.2.5: **Primary striatal cells do not respond to NMDA in the presence of MK-801.** Primary striatal neurons at DIV 13 were loaded with 2 µM Fluo-4, pre-treated with 25 µM of MK-801 and bathed in Locke's solution. At the 40th frame, 100 µM of NMDA was applied (image composed of 200 frames). **A-** Striatal neurons did not respond to NMDA application. Before NMDA and after 100 µM of NMDA there are no differences in intensity, as seen by the continues blue pseudocolored neurons in both panels. **B-** The graph, representing image plot Z axis profile resulted in mean intensity per field over frame, shows no increased intensity at 40th frame, when NMDA was applied. The decreased intensity observed, over frames, is due to bleaching. Figure representative of 3 independent experiments. Images were taken using Nikon eclipse TE 2000-U microscope at 20x magnification, scale bar: 100 µm.

Paul et al have previously shown that 24S-OHC is a selective positive allosteric modulator of NMDARs in rat hippocampal neurons (Paul et al., 2013). Therefore I aimed to evaluate whether 24S-OHC potentiates NMDAR effects in striatal cells, taking advantage of this calcium imaging technique.

I performed the calcium imaging experiments adapting the protocol to the conditions described in (Paul et al., 2013). That being the case I treated primary striatal neurons with 10 μM 24S-OHC and then puffed 10 μM NMDA onto the cells. Primary striatal neurons at DIV 13 were loaded with 2 μM Fluo-4 and then bathed in Locke's with 10 μM 24S-OHC (or the same volume of DMSO). Cells were pre-incubated for 5 minutes and after that time, were imaged over 120 frames, during which 10 μM of NMDA was puffed into the centre of the dish at the 40th frame, as indicated by the phase image in Figure 3.2.6 A and B.

As observed in Figure 3.2.6 A, an increase in fluorescence intensity was only observed in one neuron among the field of cells after NMDA application, with a rapid decay in intensity immediately afterwards (see accompanying time histogram). In Figure 3.2.6 B it is evident that a higher number of cells, compared to A, show an increase in fluorescence intensity after NMDA application, indicating that striatal neurons are more sensitive to NMDA application after being incubated with 10 μM of 24S-OHC as compared to Locke's and DMSO alone (3.2.6 A). Moreover after the peak of intensity at the 40th frame, the intensity does not lower to zero (3.2.6 B graph). Furthermore, neurons in other quadrants of the field continued responding to NMDA application afterwards, as observed in Figure 3.2.6 B panel "111th frame".

All the neurons that responded to NMDA application (increased fluorescence intensity of the calcium indicator dye) were analysed by averaging their intensity over time (at each recorded frame) and plotted in the graph (Figure 3.2.6 C with SEM, D and E without SEM). There is no difference in the maximum intensity (at 40th frame, when NMDA was applied) between neurons bathed with 24S-OHC compared to Locke's (Figure 3.2.6 C and D). The observable difference is the increased calcium influx in neurons bathed with 24S-OHC after 100 frames, which reaches levels of intensity close to the first peak at 40th frame (Figure 3.2.6 E curve only 10 μM 24S-OHC and 10 μM NMDA). This difference is illustrated by the observable increased fluorescence

in neurons in Figure 3.2.6 B (111th frame). While in the cultures not treated with 24S-OHC, the neurons that responded after NMDA application (40th frame) may respond a second time (113th frame), with lower intensity of calcium.

The number of neurons that responded to NMDA application, as measured by increased intracellular free calcium, were counted per field/experiment and plotted (Figure 3.2.6 F). More primary striatal neurons incubated with 10 μM of 24S-OHC responded to subsequent NMDA application compared to neurons incubated in Locke's alone (F test to compare variances resulted in p=0.0022). This indicates that cells exposed to 24S-OHC are more sensitive to application of 10 μM of NMDA in comparison to neurons incubated in Locke's alone (Figure 3.2.6 F).

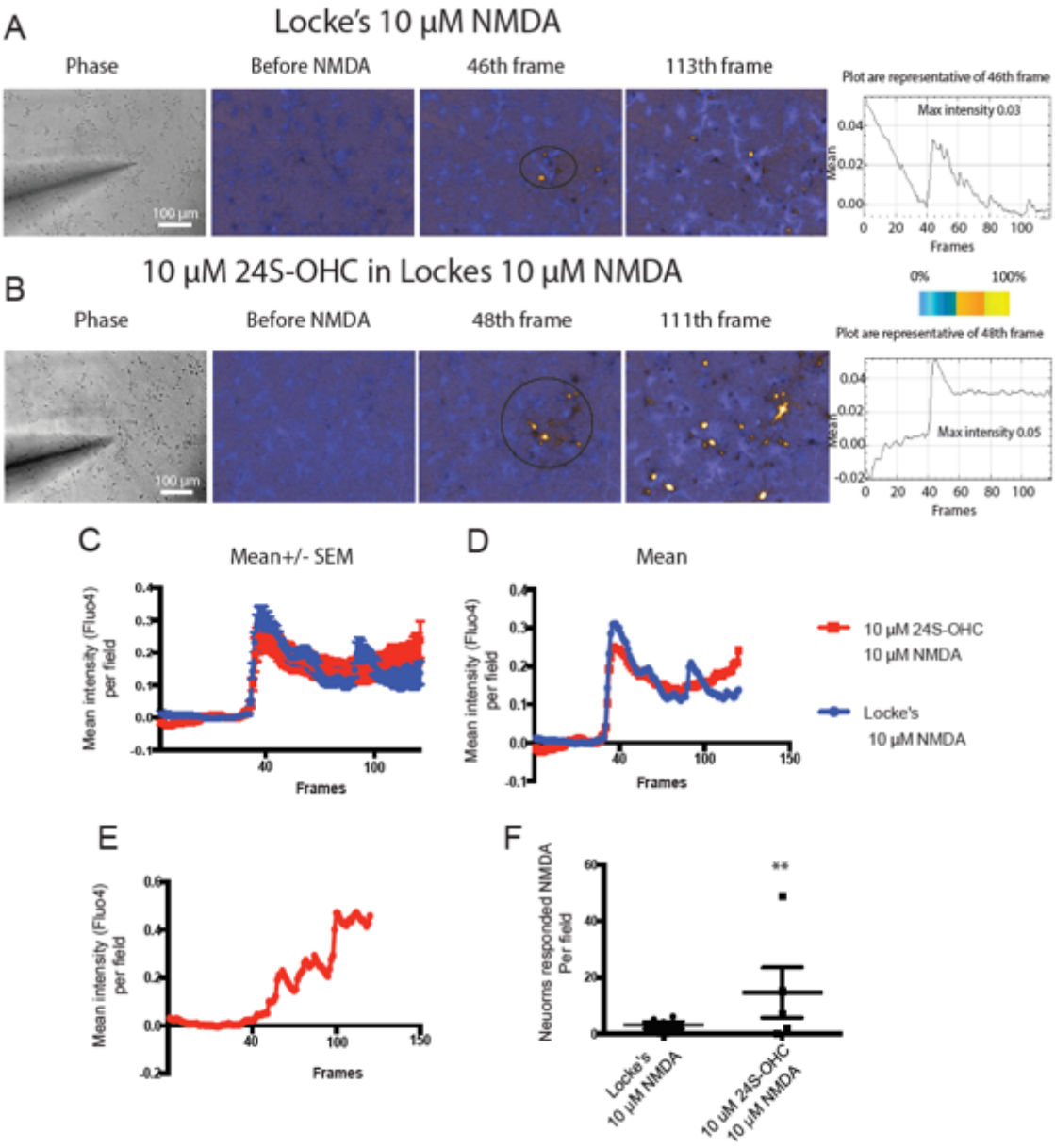
A
Locke's 10 µM NMDA
Phase
Before NMDA
46th frame
113th frame
100 µm
Plot are representative of 46th frame
Max intensity 0.03
Mean
Frames
B
10 µM 24S-OHC in Lockes 10 µM NMDA
Phase
Before NMDA
48th frame
111th frame
0%
100%
Plot are representative of 48th frame
Max intensity 0.05
C
Mean+/- SEM
Mean intensity (Fluo4) per field
Frames
D
Mean
10 µM 24S-OHC
10 µM NMDA
Locke's
10 µM NMDA
E
F
Neuorns responded NMDA Per field
**
Locke's 10 µM NMDA
10 µM 24S-OHC 10 µM NMDA

Figure 3.2.6: **Primary striatal neurons in the presence of 10 µM 24S-OHC exhibited an increased response to calcium influx after NMDA application.** Primary striatal neurons at DIV 13 were loaded with 2 µM Fluo-4 bathed in Locke's solution with DMSO or Locke's solution with 10 µM 24S-OHC. 10 µM of NMDA was applied at the 40th frame (image composed of 120 frames). **A- Control striatal neurons in Locke's:** Phase image shows patch pipette position. Before NMDA, neurons do not show calcium indicator fluorescence in the soma (0% intensity correspondent to blue pseudocolorized neurons). At the 46th frame a cell showed increased fluorescence intensity. At the 113th frame a cell close to the pipette localization showed increased intensity. The graph represents image plot Z axis profile resultant of the mean intensity per field over frame, shows increased intensity at the 40th frame when NMDA was applied, exhibiting maximum a intensity of 0.03. The intensity decreased to zero after the stimulus. **B- 24S-OHC bathed neurons:** Phase image shows the patch pipette position. Before NMDA neurons do not show calcium indicator fluorescence in the soma. At the 48th frame four cells showed increased fluorescence. At the 111th frame multiple cells throughout the field presented increased fluorescence. The graph, representing image plot Z axis profile of the mean intensity per field over frame, shows increased intensity at 40th frame, when NMDA was applied resulting in maximum intensity of 0.05. The intensity did not decrease to zero maintaining a plateau at 0.03 until the last frame: 120. **C-** The $\Delta F/F_0$ intensity of the regions of interest (neurons that increased calcium influx upon NMDA application) from the two conditions: Locke's and 10 µM 24S-OHC was determined, averaged and plotted over frames. The graph represents the mean +/- SEM of those intensities over the frame. Neurons bathed in Locke's showed two peaks of response at 40th (NMDA application) and before the 100th frame, the second with lower intensity. Striatal neurons bathed in 10 µM of 24S-OHC showed one peak of fluorescence intensity at 40th which remained elevated afterwards. **D-** Graph represents graph C without SEM bars, for easier visualization. **E-** The striatal neurons pre-incubated with 10 µM 24S-OHC, far from the pipette, responded later to NMDA application: 111th frame. The intensity continued increasing until the last frame measured: 120. **F-** The graph represents the count of neurons responding to NMDA over the 120 frames. An increased number of neurons bathed in 10 µM of 24S-OHC responded to 10 µM NMDA, compared to those bathed in Locke's (F test to compare variances resulted in p=0.0022 (**). Images and graphs representative of 2 independent experiments. Images were taken using Nikon eclipse TE 2000-U microscope at 20x magnification, scale bar: 100 µm.

I concluded that 10 µM of 24S-OHC effectively increased the sensitivity of neurons to 10 µM of NMDA.

I next took advantage of the cutting edge technique Multi Electrode Arrays (MEA) to further demonstrate the action of 24S-OHC to potentiate NMDAR actions. A mixed culture of primary striatal neurons (GABAergic) with cortical and thalamic neurons (glutamatergic), were cultured in one well MEA vessels. The purpose of the mixed culture was to better mimic the brain, and to confer glutamatergic inputs to the GABAergic cells from the striatum, such that the neuronal population would be electrophysiologically active.

In Figure 3.2.7 A is observable the sporadic population burst that occurred when the MEA was recorded for the mixed culture (DIV 19) without any treatment. Upon administration of 2 μM of 24S-OHC (Figure 3.2.7 B), the population bursts were more frequent in time (ms) and presented higher amplitude (Hz).

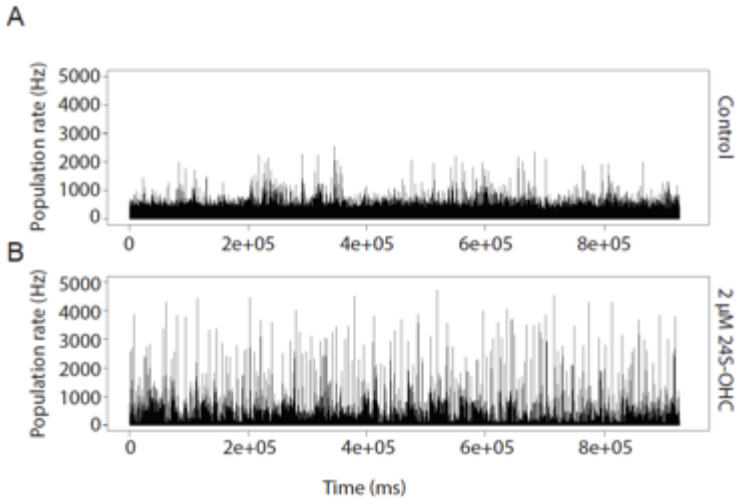

Figure 3.2.7: **24S-OHC increases the population bursts amplitude (Hz) and rate (ms) of mixed neuronal cultures. A-** Histogram shows sporadic firing from striatal neurons (DIV 19) grown with glutamatergic inputs (cortex and thalamus) with few population bursts with low amplitude (Hz). **B-** Population bursts were more frequent and presented larger amplitude (Hz) after primary striatal neurons (DIV 19) cultured with glutamatergic inputs (cortex and thalamus), were treated with 2 μM of 24S-OHC. Histogram representative from recordings of a MEA.

Therefore 24S-OHC increases the population bursts of neuronal microcircuit in a mixed neuronal culture, suggesting an excitatory effect.

In order to assess whether the spontaneous firing observed is dependent on glutamate, I treated the neurons growing on the MEA with 50 μM of AP-5 (NMDAR blocker) and 10 μM of NBQX (AMPAR blocker). Figure 3.2.8 A shows the sporadic firing exhibited by primary striatal neurons growing on MEAs with glutamatergic inputs. When the NMDA and AMPA glutamate receptors are blocked by addition to the cultures of AP-5 and NBQX (Figure 3.2.8 B), the population bursts disappear. This result indicates that the sporadic firing detected in this culture was caused by glutamate.

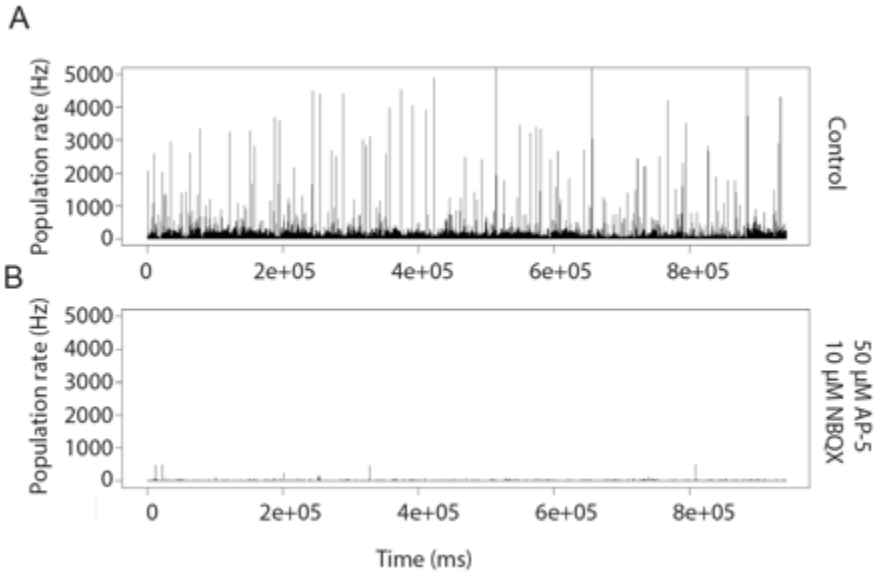

Figure 3.2.8: **The sporadic firing of neuronal cells *in vitro* is caused by glutamate. A-** Histogram shows sporadic firing from striatal neurons (DIV 19) grown with glutamatergic inputs (cortex and thalamus) with few population bursts with high amplitude (Hz). **B-** Population bursts from striatal neurons (DIV 19) grown with glutamatergic inputs, disappear upon treatment with 50 μM of AP-5 and 10 μM NBQX. Histogram representative from recordings of a MEA.

Together with the results obtained in Figure 3.2.6 I conclude that 24S-OHC potentiates NMDAR effects in primary neurons.

3.2.4. 24S-hydroxycholesterol and NMDAR-mediated toxicity.

After determining that 24S-OHC potentiates the effect of NMDAR in primary striatal neurons, I aimed to investigate if 24S-OHC exacerbates NMDA toxicity and if so whether this effect is mediated by NMDA receptors.

Before investigating the effects of 24S-OHC I first needed to establish that I could successfully implement a paradigm for assessing NMDAR toxicity. Varying concentrations of NMDA (1, 10, 50, 100, 200, 500 and 1000 μM) were applied to primary striatal neurons at DIV 13 for 20 min in Locke's solution, with Locke's solution plus DMSO serving as control, and toxicity was assessed 24h later by NeuN staining and the recording of NeuN-positive cell counts.

NMDA treatment had an effect on cell survival, decreasing cell number with increasing concentrations, as observed in the representative microscopy images (Figure 3.2.9 A). The NeuN count, averaged per field plotted against NMDA concentrations showed a concentration-dependent cell loss up to 50 μM of NMDA. Primary striatal neurons treated with 100 μM and higher concentrations presented a plateau effect with approximately 10% cell survival (the exact values for cell survival are: 100 μM - 9.78 +/- 5% control; 200 μM - 10.48 +/- 2.6% control; 500 μM - 10.05 +/- 0.22% control and 1000 μM - 10.12 +/- 0.59% control) (Figure 3.2 9 B).

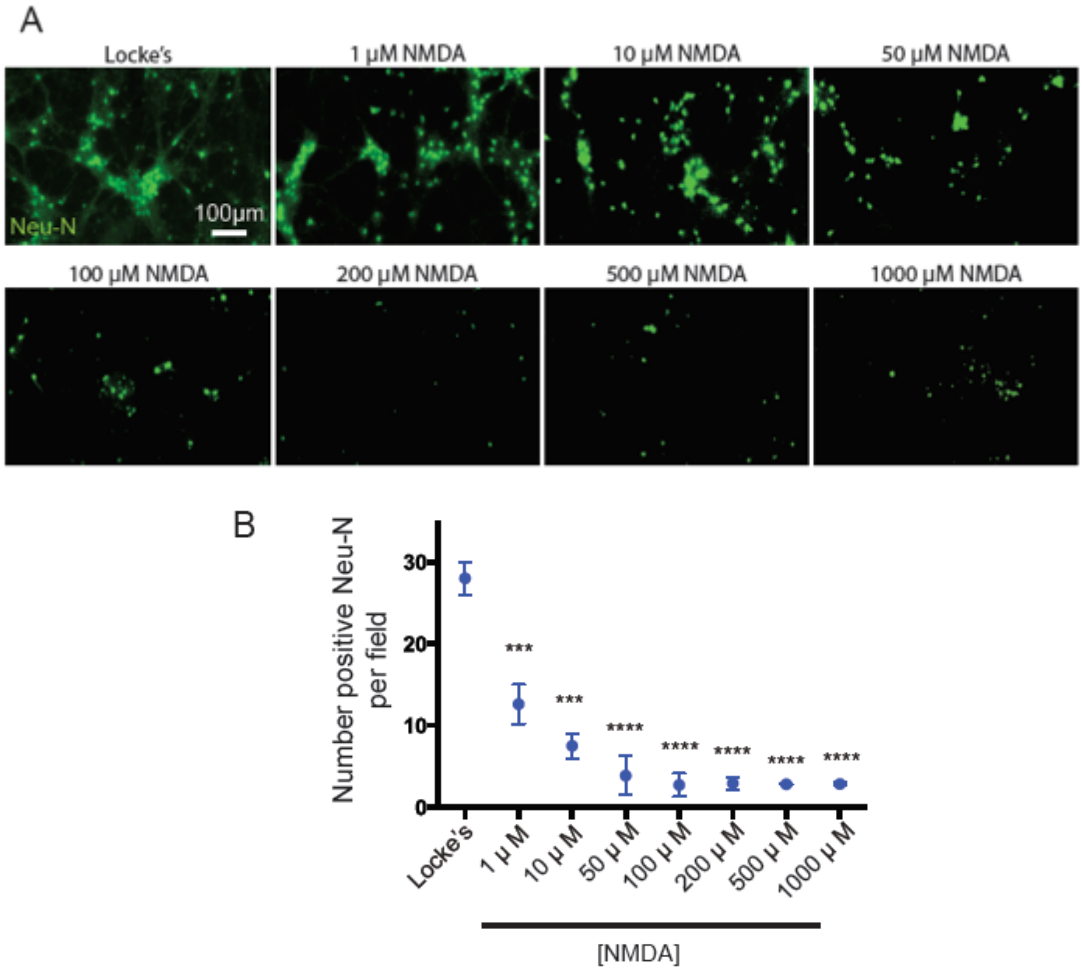

Figure 3.2.9: **Concentration-dependence of NMDA toxicity in primary striatal neurons.** Primary striatal neurons at DIV 13 were treated with varying concentrations of NMDA (1, 10, 50, 100, 200, 500 and 1000 µM) for 20 min in Locke's solution (see Material and Methods section 2.8 for details). Cell survival was assessed 24h later by NeuN staining. **A-** Microscopy images of striatal neurons stained with NeuN are representative of cell loss caused by the application of increasing concentration of NMDA. **B-** NMDA caused significant cell loss compared to control. Cell viability was assessed 24h after treatments and NeuN cell count, averaged and plotted per NMDA concentrations. One-way ANOVA statistical test showed that NMDA had a significant effect on cell survival ($p<0.0001$). The graph shows that primary neurons treated with 1 µM of NMDA 55% cell loss (Dunnett's multiple comparison test $p=0.0007$ (***), increasing to 73.2% with 10 and 86.1% with 50 µM ($p=0.0001$ (***) and $p<0.0001$ (****), respectively). Primary striatal neurons treated with 100 µM showed a significance of $p<0.0001$ (****), reached a plateau of cell death of 90.2%. Increased concentrations 200 ($p<0.0001$ (****)), 500 ($p<0.0001$ (****)) and 1000 µM ($p<0.0001$ (****)) caused the same level of toxicity (89.6%, 90% and 90%, respectively). The graph represents the mean NeuN-positive cell count per field +/- SEM of two independent experiments with 3 technical replicates each (N=2, n=6). Images were taken using Nikon eclipse Ti microscope at 20x magnification, scale bar: 100 µm.

I sought then, to verify that the cell death measured after NMDA treatment could be rescued by MK-801, a known NMDA receptor irreversible blocker.

Primary striatal neurons were pre-treated with 25 µM of MK-801 before NMDA application.

Microscopic images show that MK-801 prevented NMDA toxicity in primary striatal neurons. Primary neurons stained with NeuN showed similar cell counts after application of the different concentrations of NMDA (Figure 3.2.10 A). The mean NeuN count per field plotted against NMDA concentrations shows that MK-801 significantly rescued the noxious effect caused by NMDA on neuronal survival at all the NMDA concentrations studied except for 200 µM (Figure 3.2.10 B).

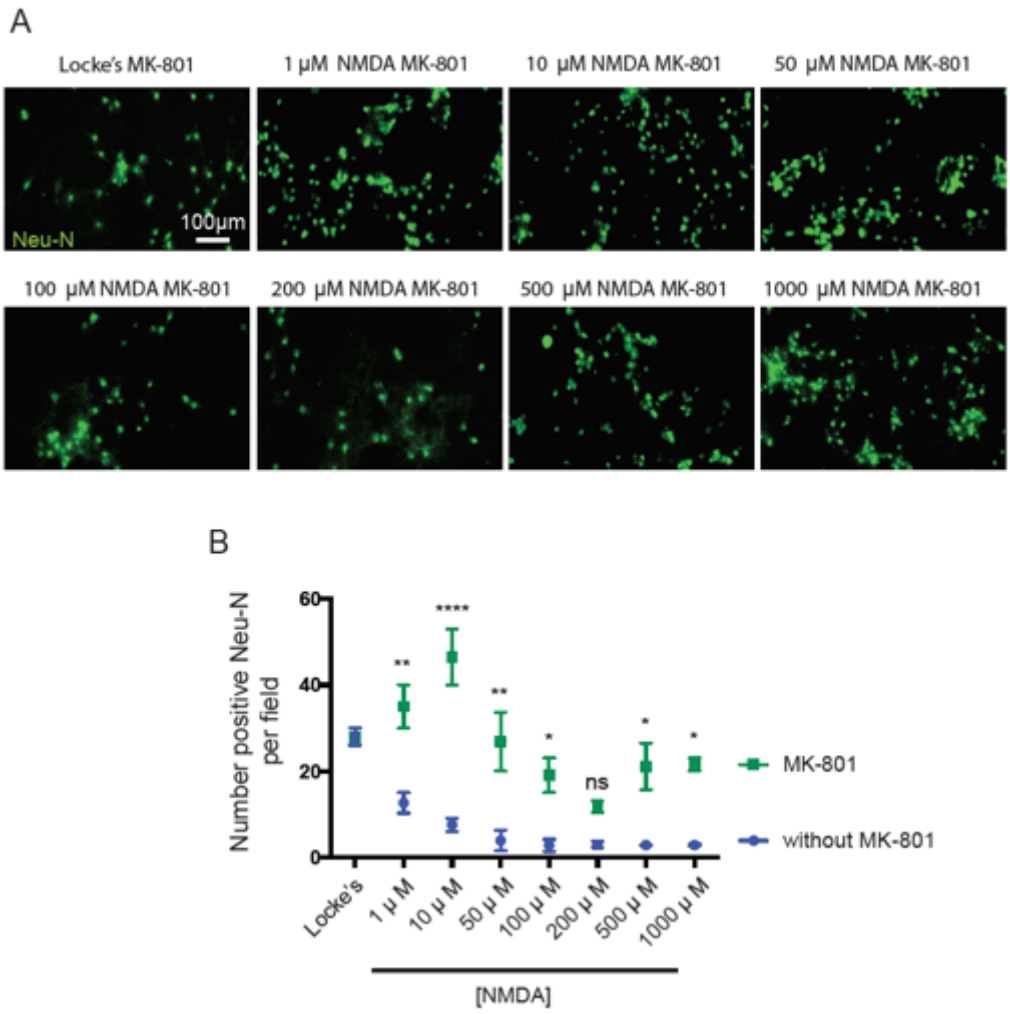

Figure 3.2.10: **MK-801 rescues NMDA toxicity in primary striatal neurons.** Primary striatal neurons at DIV 13 were treated for 30 min with 25 μM with MK-801, and treatment continued during NMDA application. Striatal neurons were treated with increasing concentrations of NMDA (1, 10, 50, 100, 200, 500 and 1000 μM) for 20 min in Locke's solution (see Material and Methods section 2.8 for details). Cell survival was assessed 24h later by NeuN staining. **A-** Microscopy images of striatal neurons stained with NeuN are representative of cell survival rescued. **B-** MK-801 had a significant effect on primary neurons treated with NMDA (Two-way ANOVA, $p=0.003$). NMDA caused toxicity, leading to significant cell death (Two-way ANOVA, $p<0.0001$) such harmful effect was rescued by pre-treatment with MK-801 (Two-way ANOVA, $p=0.0104$). Primary striatal neurons pre-treated with MK-801 with 1 and 10 μM of NMDA, presented more cells compared to control, however NMDA concentrations from 50 to 1000 μM, with neurons pre-treated with MK-801 showed protection once the cells count were similar to control, except for 200 μM, which presented half of the NeuN counts. Sidak's multiple comparison test showed significance between conditions for all NMDA concentrations except 200 μM of NMDA: (1 μM $p=0.0022$ (**), 10 μM $p<0.0001$ (****), 50 μM $p=0.0018$ (**), 100 μM $p=0.0315$ (*), 200 μM ns, 500 μM $p=0.0132$ (*) and 1000 μM $p=0.0111$ (*)). The graph represents the mean NeuN count per field +/- SEM of two independent experiments with 3 technical replicates each (N=2, n=6). Images were taken using Nikon eclipse Ti microscope at 20x magnification, scale bar: 100 μm.

In conclusion, NMDA was toxic to primary striatal neurons at DIV 13; 1 μM caused 55% cell loss and when treated with 10 and 50 μM NMDA cell death increases to 73.2% and 86.1%, respectively (Figure 3.2.9). The cell death caused by NMDA different concentrations was rescued by 25 μM MK-801 treatment (Figure 3.2.10), assuring that the cell loss observed was indeed a response to NMDA toxicity.

Having established the cell death curves for both NMDA and 24S-OHC in DIV 13 primary striatal neurons, I aimed to investigate the possible interaction between the two compounds.

3.2.5. Assessment of possible interactions of NMDA and 24S-OHC in conveying cytotoxicity

As shown previously, 24S-OHC is a potent toxic agent to primary striatal neurons (Figure 3.2.1 and 3.2.2), also I reported that 24S-OHC sensitizes neurons to calcium influx after NMDA treatment (Figure 3.2.6) and increases neurons populations bursts (Figure 3.2.7). As previous data from calcium imaging and MEAs presented arguments as 24S-OHC acts on NMDAR function, I wondered if 24S-OHC toxicity was due to NMDAR overactivation leading to excitotoxicty. Therefore I sought to test if 24S-OHC would exacerbate NMDA toxicity and if MK-801 was able to reverse the noxious effects caused by 24S-OHC alone and in combination with NMDA, demonstrating the conveying cytotoxicity and the mechanism of neuronal toxicity caused by 24S-OHC.

In order to test the hypotheses, primary striatal neurons at DIV 13 were treated with 10 μM of 24S-OHC, 10 μM of NMDA, or these two compounds in combination to assess whether 24S-OHC exacerbates NMDA effects. To test the second hypothesis, neurons were pre-treated with MK-801 before adding the test compounds. The cell survival was determined by NeuN staining and cell counts.

As observed in Figure 3.2.11 A, there is significant cell loss when neurons are treated with 10 μM NMDA or 24S-OHC separately. Similar NeuN stain is observed in panel correspondent of neurons treated with the combination of the two compounds. Primary neurons pre-treated with MK-801 and treated with 10 μM of NMDA showed similar NeuN stain compared to control. On the other hand, MK-801 combined with 10 μM of 24S-OHC resulted in NeuN positive staining similar to 10 μM of 24S-OHC treatment alone. A lower number of NeuN stain can be observed in the panel representative from neurons pre-treated with MK-801 and treated with NMDA and 24S-OHC.

The graph in Figure 3.2.11 B represents the NeuN counts from the microscope images assessed. The concentrations of NMDA and 24S-OHC used (Paul et al., 2013) reduced cell survival to 40.57 +/- 13.9% and 38.04 +/- 5.82% compared to control, respectively. Treatment with the two compounds combined reduced survival to 26.57 +/- 6.39% control. The data was analysed by one-way ANOVA, the result indicated that the treatments studied have a

significant effect ($p<0.0001$) and NMDA caused a statistically significant cell death $p=0.0416$ and 24S-OHC caused a statistically significant cell death $p=0.0203$. The two compounds combined caused a significant cell loss similar to either alone ($p=0.0237$); therefore 10 μM of 24S-OHC did not, statistically, exacerbate the toxicity caused by 10 μM of NMDA. Striatal neurons pre-treated with 25 μM of MK-801 and treated with 10 μM NMDA, showed similar NeuN counts to control. In contrast, pre-treatment with MK-801 did not protect cells against the toxic effects of 24S-OHC.

A

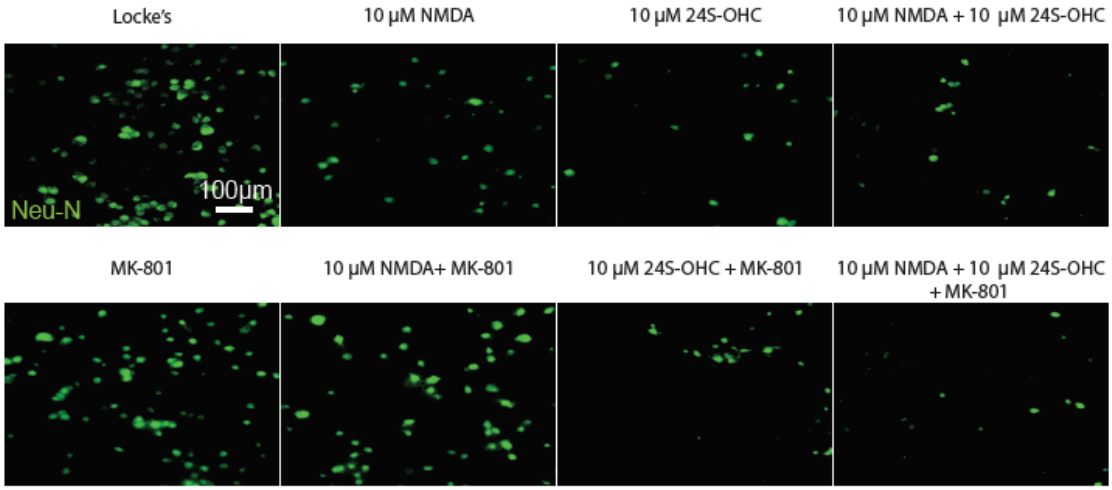
Locke's
10 µM NMDA
10 µM 24S-OHC
10 µM NMDA + 10 µM 24S-OHC
Neu-N
100µm
MK-801
10 µM NMDA+ MK-801
10 µM 24S-OHC + MK-801
10 µM NMDA + 10 µM 24S-OHC + MK-801

B

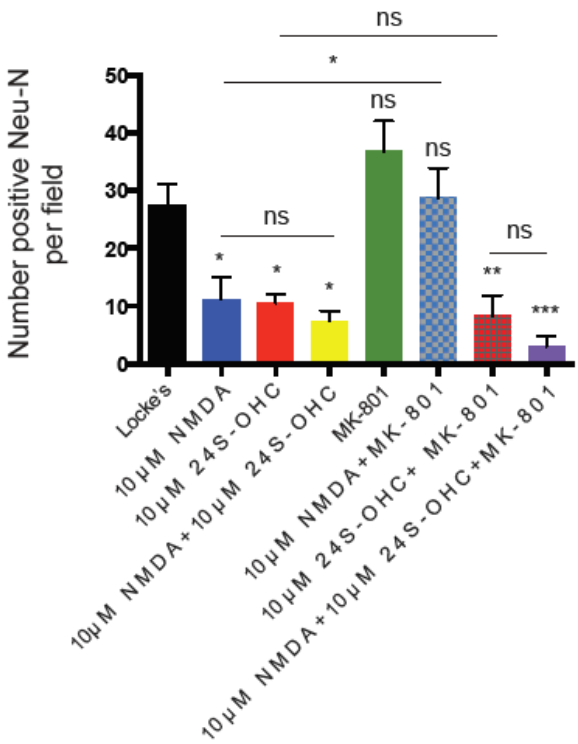
Number positive Neu-N per field
50
40
30
20
10
0
ns
*
ns
ns
ns
ns
*
*
*
**
***
Locke's
10 µM NMDA
10 µM 24S-OHC
10µM NMDA+10µM 24S-OHC
MK-801
10µM NMDA+MK-801
10µM 24S-OHC+ MK-801
10µM NMDA+10µM 24S-OHC+MK-801

Figure 3.2.11: **24S-OHC toxicity is independent on NMDAR.** Primary striatal neurons at DIV 13 were treated for 30 min with 25 µM with MK-801, and treatment continued during NMDA and 24S-OHC application. Striatal neurons were treated with 10 µM of NMDA or 10 µM of 24S-OHC or in combination with or without MK-801 pre-treatment for 20 min in Locke's solution (see Material and Methods section 2.8 for details). Cell survival was assessed 24h later by NeuN staining. **A-** Microscopic images of striatal neurons stained with NeuN are representative of cell survival averaged and plotted in the graph in B. **B-** The concentration of NMDA tested caused 40.57 +/- 13.9% and 24S-OHC 38.04 +/- 5.82% cell survival compared to control. Primary striatal neurons treated with NMDA and 24S-OHC resulted in 26.57 +/- 6.39 cell survival. One-way ANOVA was the statistical test used and resulted in significance between treatments of $p<0.0001$ and the multiple comparison test used was Tukey's, which one determined that the effect of NMDA ($p=0.0203$ (*)) alone was similar to 24S-OHC plus NMDA ($p=0.0237$ (*)). MK-801 pre-treatment was significantly protective to NMDA application ($p=0.0388$ (*)). MK-801 pre-treatment plus 24S-OHC resulted in significant of $p=0.0062$ (**) low numbers of NeuN compared to control. The combination of all the treatments: MK-801 plus NMDA and 24S-OHC resulted in average of 3 NeuN counts per filed ($p=0.0003$ (***)).
The graph represents the mean NeuN count per field +/- SEM of two independent experiments with 3 technical replicates each (N=2, n=6). Images were taken using Nikon eclipse Ti microscope at 20x magnification, scale bar: 100 µm.

These results indicate that 24S-OHC does not sensitize striatal neurons to NMDA, at the studied concentrations. Moreover the toxicity of 24S-OHC is not mediated by NMDA receptors as pre-treatment with MK-801 did not reverse the 24S-OHC's toxic effects. Even though disappointing these results were not a complete surprise as primary striatal neurons are GABAergic. Striatal neurons do not release glutamate in the culture medium, therefore, the reported toxicity caused by 24S-OHC in Figure 3.2.1 and 3.2.2 was a consequence of its actions. As reported in Paul et al., 2013 24S-OHC was observed to act as a allosteric modulator of NMDAR, therefore for this compound to modulate NMDAR needed the presence of agonist and co-agonist as observed in the referred publication, which ones were not present in the medium (Figure 3.2.1) neither in Locke's (Figure 3.2.2.)

The mechanism of 24S-OHC's toxicity to primary striatal neurons will be investigated and discussed further in the following sections.

3.2.6. 24S-hydroxycholesterol does not cause endoplasmic reticular stress.

While 24S-OHC is relevant to the neurotoxicity of striatal cells *in vivo*, increased NMDA receptor activation would not explain the death of striatal neurons *in vitro* (Figure 3.2.1), as there is no available source of synaptic glutamate. Together with the NMDAR results (Figure 3.2.11) this prompted me to also consider other possible mechanisms of 24S-OHC neurotoxicity.

Based on the prior work of Urano et al. (Urano et al., 2013), who showed that 24S-OHC induces up-regulation of GRP78/BiP through activation of unfolded protein response (UPR) pathways in SH0SY5Y and CHO cells, I sought to investigate if 24S-OHC was inducing sufficiently high levels of UPR activation / ER stress signalling to lead to neurotoxicity in striatal neurons. GRP78/BiP, a major ER chaperone protein, is a key player in UPR being overexpressed during ER stress (Bertolotti et al., 2000; Shen et al., 2002), thus serves as a marker for this process. Although the UPR is initially activated with the aim to restore ER homeostasis, a failure to do so promotes apoptosis (Oslowski and Urano, 2011) through CHOP (C/EBP homologous protein) overexpression (Ron and Habener, 1992). I thus investigated, then the hypothesis that 24S-OHC was inducing BiP overexpression through ER stress inducing using these molecular indicators.

Surprisingly, none of the genes studied responded to 24S-OHC treatment (Figure 3.2.12). BiP mRNA levels were not different between neurons treated with 24S-OHC in comparison to DMSO treated cells, while positive controls: cells treated with thapsigargin (TG) and tunicamycin (TM) resulted in more than a 4 fold change of BiP overexpression (Figure 3.2.12 A). CHOP mRNA levels showed no significant differences between cells treated with 24S-OHC in comparison to DMSO treated cells. However I observed (Figure 3.2.12 B) a non-statistically decrease in CHOP levels in response to increasing concentrations of 24S-OHC. Striatal cells treated with the positive controls TG and TM showed more than 5 fold CHOP overexpression (Figure 3.2.12 B).

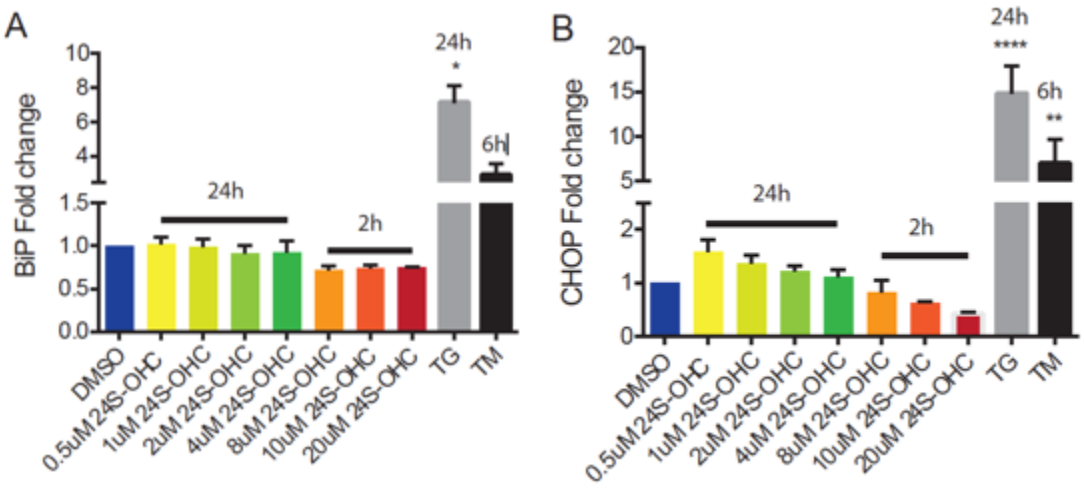

Figure 3.2.12: **24S-OHC does not cause ER stress in primary striatal neurons.** Primary striatal neurons at DIV 13 were treated with 0.5, 1, 2 and 4 μM of 24S-OHC for 24h and with 8, 10 and 20 μM of 24S-OHC for 2h. Cells treated with 1 μM TM (tunicamycin) for 6h and 100 nM of TG (thapsigargin) for 24h served as positive controls for ER stress. **A-** BiP mRNA levels were not different between neurons treated with 24S-OHC in comparison to DMSO treated cells, while positive controls resulted in more than 4 fold BiP overexpression. Statistical analyse performed was Kruskal-Wallis test followed by Dunn's multiple comparison test resulting in significance for primary cells treated with TG, p=0.0128 (*). **B-** CHOP mRNA levels presented no significant differences between cells treated with 24S-OHC in comparison to DMSO treated, even though the proportional decreasing fold change resultant from increasing concentrations of 24S-OHC. TG and TM treated neurons, presented more than 5 fold CHOP overexpression. Statistical analyse performed was Kruskal-Wallis test followed by Dunn's multiple comparison test. CHOP mRNA expression was positively increased under TG and TM treatments, where p<0.0001 (****) and p=0.0033 (**) respectively. The graphs represented the fold change mean +/- SEM from two independent experiments with 6 technical replicates each (N=2, n=12).

From Figure 3.2.12 I concluded that 24S-OHC does not induce ER stress signalling under these conditions, indicating this is unlikely to be part of the mechanism underlying the 24S-OHC toxicity that was observed in striatal cells (Figure 3.2.1).

3.2.7. 24S-hydroxycholesterol increases superoxide levels.

Lacking a mechanism to explain the neurotoxicity induced by 24S-OHC, I sought to investigate whether 24S-OHC was inducing ROS production. This hypothesis was based on previous data showing that 24S-OHC could induce ROS production (Kolsch et al., 2001; Zarrouk et al., 2015). In the referred literature they used different dyes to measure ROS, nevertheless I decided to use a different methodology and Mitosox (mitochondrial target dihydroethidium DHE) seemed an appropriate choice to measure the levels of superoxide in the mitochondria of striatal neurons treated with 24S-OHC (Kirkland et al., 2007).

Primary striatal neurons at DIV 13 were treated with 2 μM of 24S-OHC (added to culture medium) and assessed for superoxide levels after 12h and 24h of treatment. As a positive control I used neurons treated with 3-NP, a mitochondrial complex 2 inhibitor (see Material and Methods section 2.18).

Representative images of primary neurons loaded with Mitosox, showed increasing fluorescence intensity in cells treated with 2 μM of 24S-OHC from 12h to 24h. 24S-OHC treated cells presented higher fluorescence intensity compared to DMSO- control cells. Positive control showed strong fluorescence intensity, indicating increased superoxide levels (Figure 3.2.13 A).

The relative superoxide levels in each condition were determined by the measurement of the integrated density in each image, from the different conditions (see Material and Methods section 2.14). The mean intensity was plotted in graph (Figure 3.2.13 B) allowing the visualisation of the difference between conditions. The quantification of the images intensity indicated that 2 μM of 24S-OHC after 24h causes significant superoxide increase in striatal neurons compared to control. Significantly increased superoxide was also observed when comparing the positive and negative control samples (cells treated with 3-NP and DMSO, respectively).

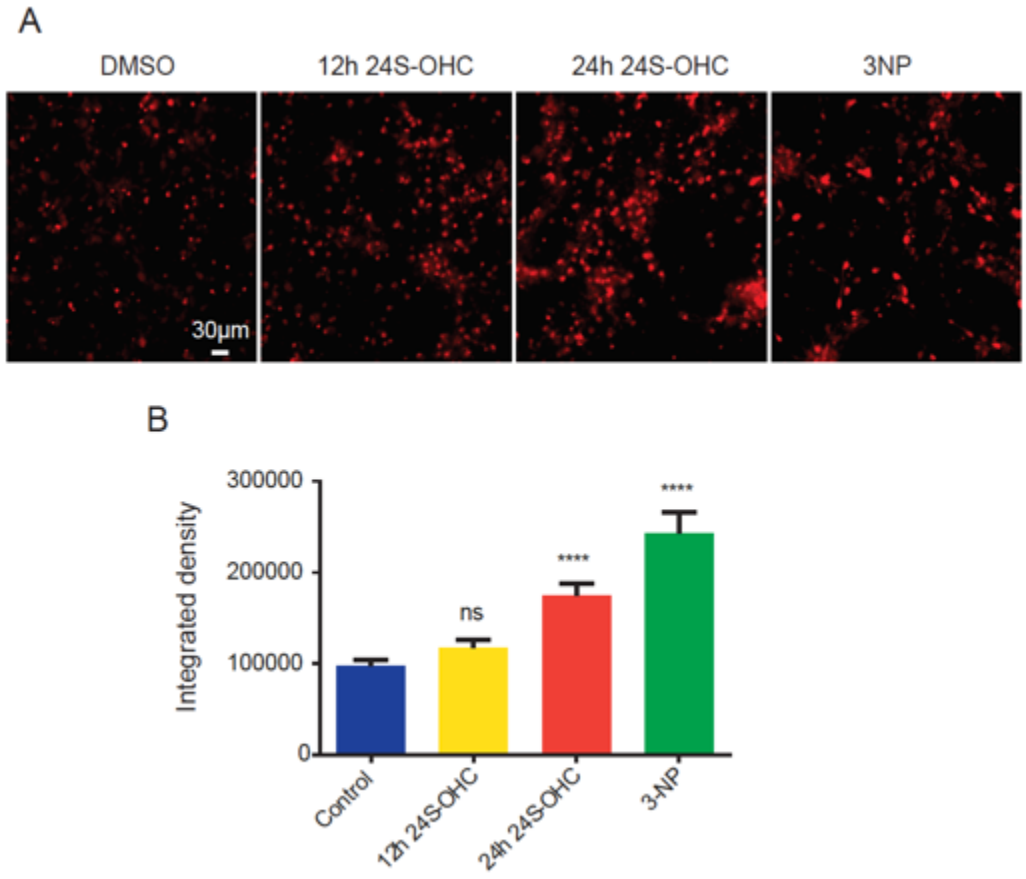

Figure 3.2.13: **24S-OHC increases superoxide levels.** Primary striatal neurons at DIV 13 were treated with 2 µM of 24S-OHC for 12 and 24h. Positive control for mitochondrial stress used was the complex 2 inhibitor: 3-NP, cells were treated with 10 mM for 12h. As a mitochondrial stress sensor read out, cells were loaded in HBSS with 5 µM mitosox red. **A-** Representative images of primary neurons loaded with mitosox, showed increasing fluorescence intensity in cells treated with 2 µM of 24S-OHC for 24h compared to 12h and even higher compared to control (DMSO). Positive control (3-NP) presented higher intensity of fluorescence, when compared to all the conditions analysed. **B-** The graph represents the mean +/- SEM of intensities from two independent experiments with 6 technical replicates each (N=2, n=12). Unpaired T-test with Welch's correction resulted in significant superoxide production after 24h of 2 µM 24S-OHC and 12h 10 mM 3-NP ($p<0.0001$ (****)). Images were taken using Nikon eclipse Ti microscope at 20x magnification, scale bar: 30 µm.

In conclusion 2 µM of 24S-OHC causes significantly increased levels of superoxide, a reactive oxygen species, after 24h. Induction of mitochondrial stress may be the mechanism leading to striatal death induced by 24S-OHC, nevertheless further investigation is needed to dissect the mechanism.

3.2.8. Discussion

In the present results section, I aimed to investigate the effects of 24S-OHC upon primary striatal neurons and most importantly to hypothesise on its role as a key player in the disease progression of HD. Therefore, I investigated 24S-OHC function on specific HD hallmarks: excitotoxicity, endoplasmic stress and generation of respiratory oxygen species.

I found that 24S-OHC is a potent cytotoxic to striatal neurons in culture (Figure 3.2.1 and 3.2.2) however its toxic effects are not through NMDAR as the cerebrosterol did not sensitize neurons to NMDA treatment (Figure 3.2.11) even though was shown to be a potent NMDAR activator. 24S-OHC potentiated NMDAR effects at the level of free intercellular calcium (Figure 3.2.6) and increased the extracellular activity of a mixed neuronal culture (Figure 3.2.7). In conclusion, 24S-OHC was proven to be a potent enhancer of NMDAR effects in this neuronal system, which is a relevant comparison to HD-affected neurons due to its expression of GluN2B (Figure 3.2.3) NMDAR isoform, which one has been described to highly sensitize neurons to excitotoxic insults (Liu et al., 2007). This result suggested that increased levels of 24S-OHC in the interstitial space of neurons expressing mutant Htt may aggravate the excitotoxic insult highlighted as a hallmark of the disease

As an attempt to relate 24S-OHC function as NMDAR activator I sought to investigate intracellular calcium stores, ER and mitochondria (Verkhratsky and Petersen, 1998) and stablish a bridge with the HD hallmarks: ER stress and mitochondrial stress. After failed to observe an effect of 24S-OHC to increase ER stress (Figure 3.2.12) I successfully measured the increased superoxide levels in primary striatal cells, after 24h treatment with 24S-OHC (Figure 3.2.13).

In order to assess the effect of 24S-OHC on striatal neurons viability I used NeuN positive cell staining. Astrocytes account for +/- 20% of the cells in the striatal cultures (Figure 3.1.2), therefore I needed an assay specific to measure neuronal viability, then I used NeuN staining. My concern on using other assays such as MTT, TUNNEL or detection of caspases cleavage would lead me to erroneous numbers as would take into account astrocytes cell death.

Regarding the concentrations of 24S-OHC chosen I would argue that these concentrations are physiologically relevant, considering that free 24S-OHC was measured in human brain homogenates has been about 30 μM (Lutjohann et al., 1996), nevertheless I would amplify the range considering the concentration detected in the IDMS of 0.015 μM (Table 3.1.1 and Figure 3.1.11). Moreover, once released, the estimated half-life of this 24S-OHC is one-half day (Bjorkhem et al., 1997), therefore the time points for the experiments were taken into consideration based on this fact.

I wanted to assure that at DIV 13 the striatal neurons culture was fully differentiated and mature therefore I performed immunocytochemistry for GluN1 and GluN2B, the two main subunit isoforms of NMDAR in medium spiny neurons *in vivo* (Kumar et al., 1997; Hallett et al., 2006) which one showed an ubiquitous pattern (Figure 3.2.3). The importance of this figure highlights that the subunits that constitute NMDAR *in vivo* are present *in vitro* and justifies this as a suitable model for looking at the interactions of 24S-OHC and NMDAR. Pre-treatment with MK-801 silenced the neurons to NMDA presence, halting the entrance of calcium (Figure 3.2.5) assuring that NMDA was the factor inducing the entrance of calcium observed in Figure 3.2.4 upon membrane depolarization, assuring me on the system functionality.

When I investigated if 24S-OHC could exacerbate NMDA toxicity, neurons were treated with 10 μM of NMDA and 10 μM of 24S-OHC in combination, which resulted in cell death values similar to the single treatments, therefore I concluded that 24S-OHC did not sensitize neurons to NMDA toxicity (Figure 3.2.11). The choice for the used concentrations was based on (Paul et al., 2013) therefore I insist that would be interesting to investigate the effect of 24S-OHC on neurons treated with concentrations of NMDA that cause less than 50% of cell death in order to see an effect due to 24S-OHC. Nevertheless, with this experiment was conclusive that the toxicity of 24S-OHC was not mediated by NMDA receptors. Although disappointing, it was not a surprising result, as the toxicity observed by 24S-OHC in primary striatal neurons (GABAergic) in Figure 3.2.1 could not be explained by the previously identified NMDA receptor mediated mechanism, as 24S-OHC acting as a positive allosteric modulator of NMDAR would only cause toxicity in the presence of a NMDAR ligand such as

glutamate, which was absent in culture medium growing primary striatal neurons (Paul et al., 2013).

The lack of evidence for NMDARs mediating the neurotoxicity of 24S-OHC in striatal cells *in vitro* (Figure 3.2.1, Figure 3.2.11) prompted to also consider other possible mechanisms of 24S-OHC neurotoxicity. In order to understand the mechanism of toxicity induced by 24S-OHC I investigated recurrent neurodegenerative stress hallmarks such as ER stress and ROS.

In contrast to the published work from Urano et al. (Urano, Ochiai et al. 2013), I was not able to observe ER stress induced by 24S-OHC in primary striatal neurons. Neurons treated with 24S-OHC did not show upregulation of ER stress markers BiP and CHOP (Figure 3.2.12).

On the other hand, the observation that 24S-OHC leads to the production of free radicals is generally consistent with previous reports using different methodologies (Kolsch et al., 2001; Noguchi et al., 2015). My results indicated that primary striatal neurons treated with 2 μM of 24S-OHC exhibited statistical significant increased superoxide levels after 24 h (Figure 3.2.13). As my approach relied on a superoxide indicator targeted to mitochondria, a mitochondrially centered effect should be considered. It is therefore interesting to consider how the effects of this sterol might be conveyed to the mitochondrial compartment, and the mechanism through which ROS accumulates under the observed conditions.

Consistent with my findings, high concentrations of 24S-OHC have also been shown to be toxic to cortical neurons previously by Yamanaka K., et al (Yamanaka et al., 2011; Yamanaka et al., 2014), who classified the observed death as having necroptotic features, but without clarifying the underlying mechanism. Further work will therefore be needed to elucidate 24S-OHC's specific molecular effects that lead to cytotoxicity.

In summary, primary striatal neurons expressing Htt 171-82Q showed sterol accumulation and increased release into the medium of 24S-OHC, before the formation of Htt toxic aggregates, therefore the sterol dyshomeostasis is an aetiologic event observed with the *in vitro* model characterized in section 3.1. Interestingly was reported in section 3.2 that 24S-OHC is a potent cytotoxic

agent to *in vitro* primary striatal neurons and is implicated in two of the characterized HD hallmarks, excitotoxicity and increased levels of superoxide in the same system. As investigated in section 3.1 a compound like AK-7 (Figure 3.1.10) would be interesting to investigate further so to decrease the release of 24S-OHC through decrease of cholesterol synthesis (Luthi-Carter et al., 2010) with the aim to stop 24S-OHC actions on HD symptoms progression.

3.3. 24S-Hydroxycholesterol effects on primary astrocytes

Introduction: Astrocytes furnish important contributions to CNS metabolism, providing neurons crucial chemical transport and metabolic support (Sofroniew and Vinters, 2010).

Although both neurons and astrocytes possess the enzymatic machinery needed for cholesterol biosynthesis and are capable of synthesizing cholesterol *in vitro* (Saito et al., 1987), uncertainty exists whether both continue to do so during adulthood under normal conditions. Therefore a consensus opinion seems to have emerged regarding the delivery of sterols from astrocytes to neurons: in the same way that glucose-derived lactate is 'fed' to neurons by astrocytes, it is expected that astrocytes also bear the work of cholesterol production (Pfrieger, 2003 b). However it is also believed that neurons might synthesize their own cholesterol at the cell body but internalize cholesterol from astrocytic stores in axons or dendrites to maintain synapses (Brown and Goldstein, 1986; Mauch et al., 2001; Simons and Ikonen, 2000). Pfrieger hypothesized that neurons rely on the cholesterol delivered in apolipoproteins (in particular ApoE), by differentiated astrocytes, to allow neurons to specialize in the transmission of action potentials (Pfrieger, 2003 b).

Neurons tightly control their levels of cholesterol, via the action of the enzyme CYP46A1 which is expressed exclusively in neurons. The enzyme converts cholesterol into 24S-OHC (cerebrosterol) (Dietschy and Turley, 2004), which is believed to signal astrocytes to report that neurons are sterol replete, thereby controlling ApoE-mediated cholesterol export (Brown and Goldstein, 1997; Whitney et al., 2002).

24S-OHC is a known Liver X Receptors (LXRs) agonist, which plays a key role on cholesterol metabolism (Joseph et al., 2002; Joseph and Tontonoz, 2003). Moreover it is thought that 24S-OHC acts as a signalling molecule between neurons and astrocytes, communicates to the astrocytes the need for lipidated cholesterol in the form of ApoE particles to be delivered to the neurons. In the astrocytes, 24S-OHC has been shown to regulate cholesterol levels via Liver X Receptors (LXRs) (Abildayeva et al., 2006). LXRs belong to the nuclear receptor superfamily, and the two isoforms LXR α and LXR β are activated by oxysterols. Specifically, 24S-OHC induces the astrocytic

transcription of LXR target genes *ApoE*, *ABCA1* and *ABCG1* (Abildayeva et al., 2006; Liang et al., 2004).

In section 3.1, I provided evidence that sterol accumulates in Htt171-82Q exposed neurons (Figure 3.1.3 and 3.1.4) and they released increased levels of 24S-OHC (Table 3.1.1). Given the previously inferred complexities of sterol regulation, both in the basal state and in HD, I next asked which were the effects caused by increased 24S-OHC released on astrocytes. In the following work I aimed to further clarify the effects exerted by 24S-OHC on astrocytes, via the two main transcriptional regulatory systems for sterol homeostasis: LXR (Eckert et al., 2007) and SREBP2 (Goldstein et al., 2006), using primary astrocytes cultured *in vitro.*

A previous study (Abildayeva et al., 2006) has shown that 24S-OHC produced in neurons increased the expression and secretion of ApoE in a dose- and time-dependent manner in astrocytes. Moreover they showed that similar results were obtained when treating astrocytes with a LXR agonist: GW683965A, suggesting that the mechanism by which ApoE gene was being expressed was LXR activity dependent. However, it should be noted that the reported studies are resultant from 24S-OHC and LXR agonist applied in medium containing 10% fetal calf serum, and the presence of lipids and lipoproteins in the serum may well have influenced the results. Therefore I felt that it was important to revisit the transcriptional regulation of ApoE, and other SREBP2 and LXR target genes via 24S-OHC under lipid-free conditions.

3.3.1. Effects of 24S-hydroxycholesterol exposure on SREBP2 target genes in astrocytes.

The first aim was to investigate the transcriptional regulatory effects of 24S-OHC on SREBP2 target genes. Genes involved in cholesterol synthesis, such as *HMGCR*, *HMGCS1* and *FDFT1*, as well as *LDLr*, involved in cholesterol uptake, were included in the mRNA measurements. Astrocytes were exposed to different concentrations of 24S-OHC (0.5, 1 and 2 μM) for a specific time period (2, 4, 12 and 24 h), after which cells were harvested for RNA extraction.

I observed that incubation with 24S-OHC resulted in downregulation of SREBP2 target genes in astrocytes (Figure 3.3.1 A, C, E and G). 24S-OHC caused significant downregulation of *HMGCR, HMGCS1* and *FDFT1* from 12 h. The 24S-OHC concentrations causing an effect were different depending on the gene: 2 μM for *HMGCR*, 1 μM for *HMGCS1* and 0.5 μM for *FDFT1*. The cerebrosterol caused a more effect on LDLr mRNA levels. *LDLr* levels were significantly decreased after 4 h treatment from 1 μM. The same was observed (with 1 and 2 μM) after 12 h and 24 h of treatment. The effect observed was attributable to SREBP2 as astrocytes treated with 0.5 μM of the LXR agonist TO-901317 caused no effect on the expression of these genes (Figure 3.3.1 B, D, F and H).

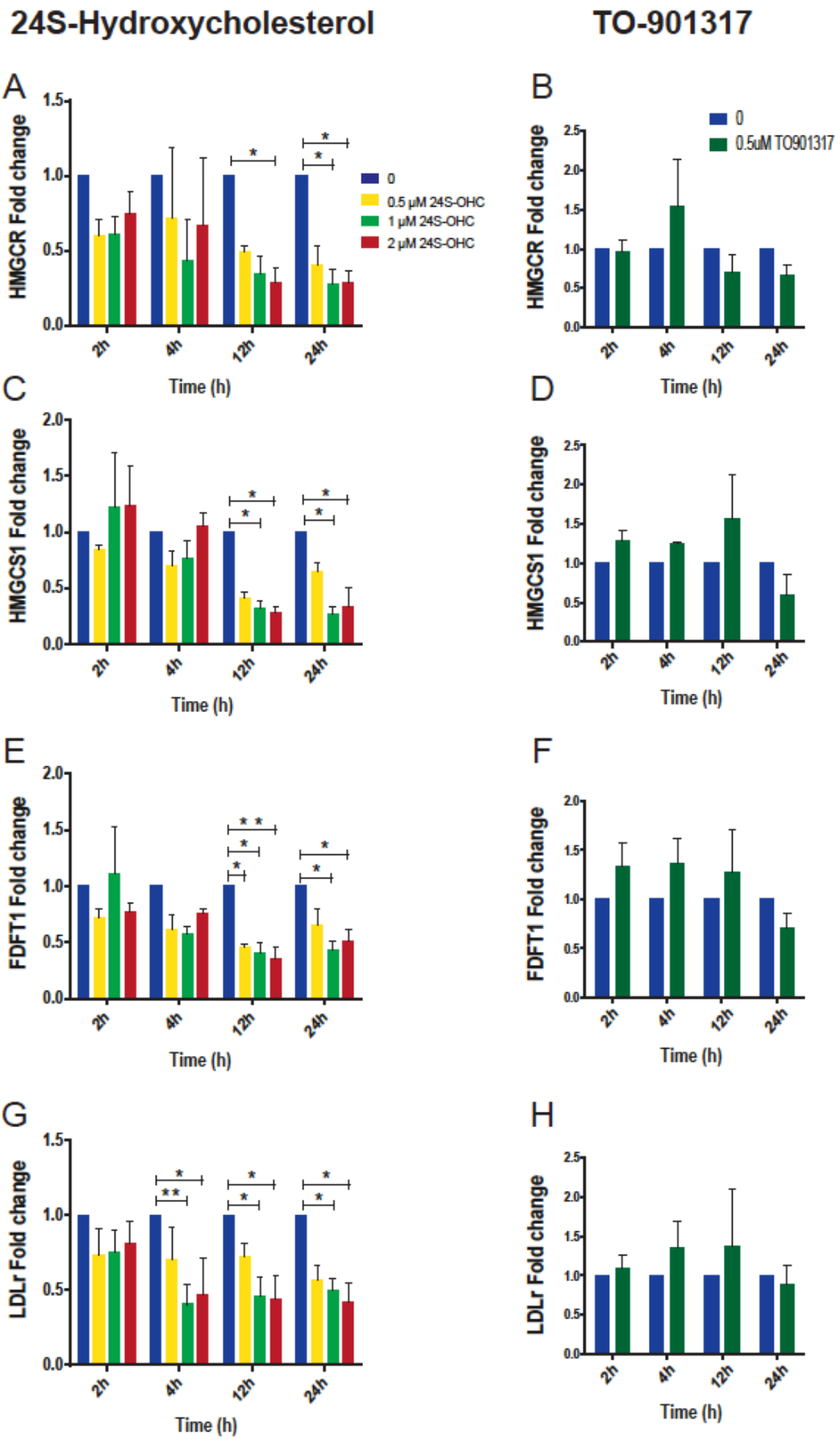
24S-Hydroxycholesterol
TO-901317
A
B
C
D
E
F
G
H
HMGCR Fold change
HMGCS1 Fold change
FDFT1 Fold change
LDLr Fold change
Time (h)
2h
4h
12h
24h
0
0.5 μM 24S-OHC
1 μM 24S-OHC
2 μM 24S-OHC
0.5uM TO901317

Figure 3.3.1: **Effects of 24S-OHC exposure on SREBP2 target gene expression in astrocytes.** Primary astrocytes were treated with increasing concentrations of 24S-OHC (0.5, 1 and 2 μM) for 2, 4, 12 and 24h. Expression levels of SREBP2 target genes: *HMGCR* (**A**), *HMGCS1* (**C**), *FDFT1* (**E**) and *LDLr* (**G**) were measured. The result was a down regulation resultant from 24S-OHC increased concentration and treatment duration. TO-901317 (LXR agonist) application did not show any effect on RNA levels from the same genes (**B, D, F** and **H**). **A-** HMGCR mRNA levels decreased significantly with 2 μM at 12h and 1 and 2 μM of 24S-OHC after 24h treatment. **B-** TO-901317 had no significant effect on HMGCR mRNA expression. **C-** *HMGCS1* downregulation was significant after 12h and 24h 24S-OHC treatment at 1 and 2 μM. **D-** TO-901317 had no significant effect on HMGCS1 mRNA expression. **E-** *FDFT1* downregulation was observed at 12h from 0.5 μM of 24S-OHC and after 24h with 1 and 2 μM of 24S-OHC. **F-** FDFT1 mRNA expression did not respond to LXR agonist: T-901317 treatment. **G-** LDLr mRNA levels decreased significantly at 1 and 2 μM of 24S-OHC from 4h of exposure. **H-** LDLr mRNA expression did not altered after TO-901317 treatment. The graphs represent the fold change mean +/- SEM from three independent experiments with 6 technical replicates each (N=3, n=18). Statistical test performed was two-way ANOVA followed by Dunnett's multiple comparison test (24S-OHC treatment) and Sidak's multiple comparison test (TO-901317). Significance is indicated as follows: $p<0.05$ (*), $p<0.01$ (**), $p<0.001$ (***) and $p<0.0001$ (****); unlabelled comparisons: no-significant.

In conclusion, as observed from the data in Figure 3.3.1, 24S-OHC treatments downregulated *LDLr* levels after 4 h incubation, and *HMGCR, HMGCS1 and FDFT1* in the timeframe of 12-24 hours, consistent with a prominent effect on SREBP2 regulation (Radhakrishnan et al., 2007a).

3.3.2. Effects of 24S-hydroxycholesterol exposure on LXR target gene expression in astrocytes.

The aim of these experiments was to investigate the transcriptional regulatory effects of 24S-OHC on LXR target genes. Astrocytes were treated with increasing concentrations of 24S-OHC (0.5, 1 and 2 μM) for a specific time period (2, 4, 12 and 24 h), were lysed and their RNA extracted for mRNA analyses for the following LXR target genes: *ABCA1, ABCG1, SREBP1c* and *Glut4* (Figure 3.3.2 A, C, E and G). 24S-OHC caused the upregulation of LXR target genes in astrocytes in a pattern similar to that observed after exposure to TO-901317 (Figure 3.3.2 B, D, F, and H).

Astrocytes incubated with 24S-OHC exhibited increased *ABCA1* expression in a time and dose-dependent manner. Significantly increased expression was reached after 24h of treatment from 1 μM (Figure 3.3.2 A). Treatment of astrocytes with 0.5 μM of the LXR agonist TO-901317 did not produce statistically significant upregulation, even though it resulted in more than a 5 fold change in mean expression (Figure 3.3.2 B). *ABCG1* expression was significantly increased upon 12 h of 24S-OHC treatment (with 2 μM), but this subsided by 24 h (Figure 3.3.2 C). The same effect was observed with the LXR agonist (Figure 3.3.2 D). Expression *of SREBP1c* demonstrated a significant increase after 12 h of 24S-OHC treatment at concentrations of 1 μM and 2 μM (Figure 3.3.2 E). TO-901317 caused significantly increased expression of *SREBP1c* after 12 h and 24 h of treatment (Figure 3.3.2 F). The effect of 24S-OHC on the regulation of *Glut4* was initiated faster and lasted for a shorter period. 24S-OHC treatments caused *Glut4* upregulation after 4 h at concentrations 0.5 and 1 μM, after which it returned to basal levels (Figure 3.3.2 G). The LXR agonist also transiently induced the expression of *Glut4* but with a longer delay (12h), returning to basal levels by 24 h (Figure 3.3.2 H).

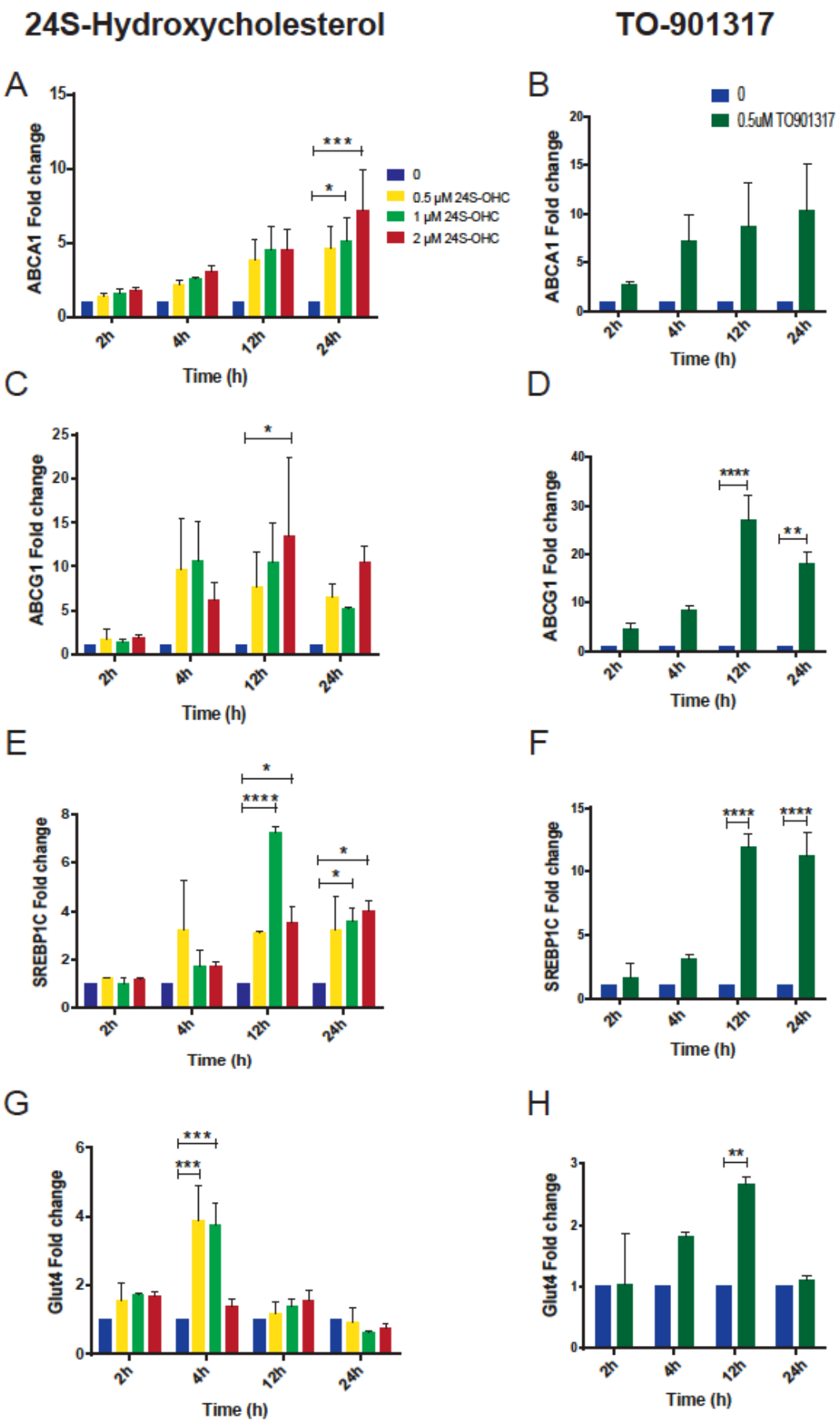
24S-Hydroxycholesterol
TO-901317
A
B
C
D
E
F
G
H
ABCA1 Fold change
ABCG1 Fold change
SREBP1C Fold change
Glut4 Fold change
Time (h)
2h
4h
12h
24h
0
0.5 μM 24S-OHC
1 μM 24S-OHC
2 μM 24S-OHC
0.5uM TO901317
*
**
***
****

Figure 3.3.2: **Effects of 24S-OHC exposure on LXR target gene expression in astrocytes.** Primary astrocytes were treated with increasing concentrations of 24S-OHC (0.5, 1 and 2 μM) for 2, 4, 12 and 24 h. Expression levels of LXR target genes: *ABCA1* (**A**), *ABCG1* (**C**), *SREBP1c* (**E**) and *Glut4* (**G**) were measured. The result was overexpression of the analysed genes, resultant from 24S-OHC increased concentration and treatment duration. TO-901317 (LXR agonist) application (0.5 μM) presented the same effect on the RNA levels of the same genes (**B, D, F** and **H**). **A-** *ABCA1* presented significant overexpression after 24h treatment with 1 (6 fold change) and 2 μM (8 fold change) of 24S-OHC. **B-** *ABCA1* overexpression in response to TO-901317 was increasing until 24h application, reaching 10 fold**. C-** *ABCG1* exhibited significant overexpression (more than 10 fold change) with 2 μM 24S-OHC after 12h treatment. However occurred a slight decrease at 24h, with all 24S-OHC concentrations. **D-** ABCG1 mRNA levels exhibited increased expression in response to LXR agonist from 12h treatment, reaching around 30 fold change and significance. However mRNA levels decreased to 20 fold change after 24h (still significant). **E-** *SREBP1c* presented significant overexpression after 12 and 24 h treatment with 1 and 2 μM 24S-OHC. However the fold change decreased from more than 6 (1 μM at 12h) to 4 at 1 μM from 12 h to 24 h 24S-OHC treatment ($p<0.0001$ (****) to $p<0.05$ (*), respectively). With 2 μM of 24S-OHC the mRNA of SREBP1c kept 4 fold until 24 h of treatment. **F-** Significant *SREBP1c* overexpression occurred after 12 h exposure with TO-901317 (more than 10 fold change) which one was maintained until 24 h of treatment. **G-** *Glut4* significant overexpression occurred after 4h exposure to 0.5 and 1 μM of 24-OHC (around 4 fold change), and decreased afterwards. **H-** Glut4 mRNA levels increased significantly only after 12h treatment TO-901317. The graphs represent the fold change mean +/- SEM from three independent experiments with 6 technical replicates each (N=3, n=18). Statistical test performed was two-way ANOVA followed by Dunnett's multiple comparison test (24S-OHC treatment) and Sidak's multiple comparison test (TO-901317). Significance is indicated as follows: $p<0.05$ (*), $p<0.01$ (**), $p<0.001$ (***) and $p<0.0001$ (****); unlabelled comparisons: no-significant.

In conclusion, the effects of 24S-OHC also appear to occur through the transcriptional upregulation of LXR target genes in astrocytes. Treatment with 0.5 μM TO-901317 caused a higher degree of induction in the studied genes compared to 24S-OHC, except for *Glut4,* where the degree of induction was similar. This indicates that TO-901317 is a more potent LXR activator than 24S-OHC. Overall, however, the fact that 24S-OHC causes overexpression of LXR target genes in cultured astrocytes in a pattern similar to the observed effects of TO-901317 (LXR agonist) indicates that 24S-OHC has a physiologically relevant activity as an endogenous LXR agonist in astrocytes *in vitro.*

3.3.3. Effects 24S-hydroxycholesterol exposure on *ApoE* gene expression in astrocytes.

ApoE has been demonstrated previously to be an LXR target gene. However when its RNA levels were measured after treatments with both 24S-OHC (Figure 3.3.3 A) and the LXR agonist TO-901317 (Figure 3.3.3 B) treatment, no differences were observed. The absence of effects on *ApoE* gene expression in astrocytes after either 24S-OHC or TO901317 exposure (Figure 3.3.3 A and B), was unexpected, and is counter to the results of (Abildayeva et al., 2006).

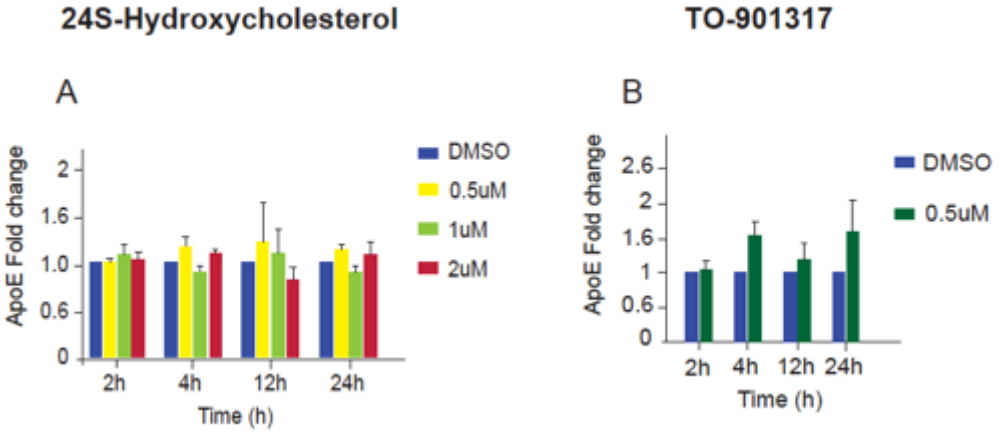

Figure 3.3.3: **Effects of 24S-OHC exposure on ApoE mRNA expression in astrocytes.** Primary astrocytes were treated with increasing concentrations of 24S-OHC (0.5, 1 and 2 μM) for 2, 4, 12 and 24 h. Expression levels of ApoE mRNA were measured. The result was no response to 24S-OHC **A**), neither to LXR agonist: TO-901317 **B**). The graphs represent the fold change mean +/- SEM from three independent experiments with 6 technical replicates each (N=3, n=18). Statistical test performed was two-way ANOVA followed by Dunnett's multiple comparison test (24S-OHC treatment) and Sidak's multiple comparison test (TO-901317).

Taking together this set of data I can conclude that 24S-OHC downregulates SREBP2 target genes and induces LXR-dependent genes in astrocytes. The regulation of *ApoE* gene expression was surprisingly not observed in astrocytes under our *in vitro* conditions, either by 24S-OHC or TO901317 exposure. This suggests that the regulation of ApoE may not be sensitive to the activation of LXRs in this paradigm.

3.3.4. The effect of 24S-hydroxycholesterol on SREBP2 nuclear translocation by immunocytochemistry.

I next sought to gain further insight into the mechanism by which 24S-OHC negatively regulates the expression of sterol biosynthesis genes in astrocytes. Cellular sterol levels are typically controlled tightly within a narrow concentration range and use SREBP2 as a master regulator of sterol synthesis. The conventional model holds that when sterol levels are replete, SREBP2 is held bound within the ER and when sterols are depleted, SREBP2 shuttles from the ER to the Golgi, undergoes sequential proteolytic cleavage releasing its N-terminal domain, and is transported into the nucleus where it functions as a transcription factor, binding to Sterol Regulatory Element (SRE) and positively regulating the expression of genes such as *HMGCR* and *LDLr* (Espenshade 2006).

As shown in figure 3.3.1, the exposure of astrocytes to 24S-OHC may also invoke these previously characterised mechanisms of SREBP2 regulation, as is supported by the downregulation of *HMGCR, HMGCS1, FDFT1* and *LDLr* (Figure 3.3.1 A, C, E and G). I aimed to further clarify the mechanism of SREBP2 target gene downregulation by 24S-OHC in astrocytes.

One of the experimental approaches by which I have examined this effect was by assessing whether 24S-OHC retains SREBP2 in the extra nuclear space (presumably representing retention in the ER) (Radhakrishnan, Ikeda et al. 2007) using immunocytochemistry.

Representative microscopy images showed that astrocytes treated with 24S-OHC showed less intensity of SREBP2 labeling (Alexa fluor 488-green) in the nucleus (Hoechst), compared to control cells (treated with DMSO) (Figure 3.3.4 A).

Further quantification supported what was observed on the representative images: astrocytes treated with 24S-OHC showed a significantly decreased intensity of SREBP2 labeling in the nucleus.

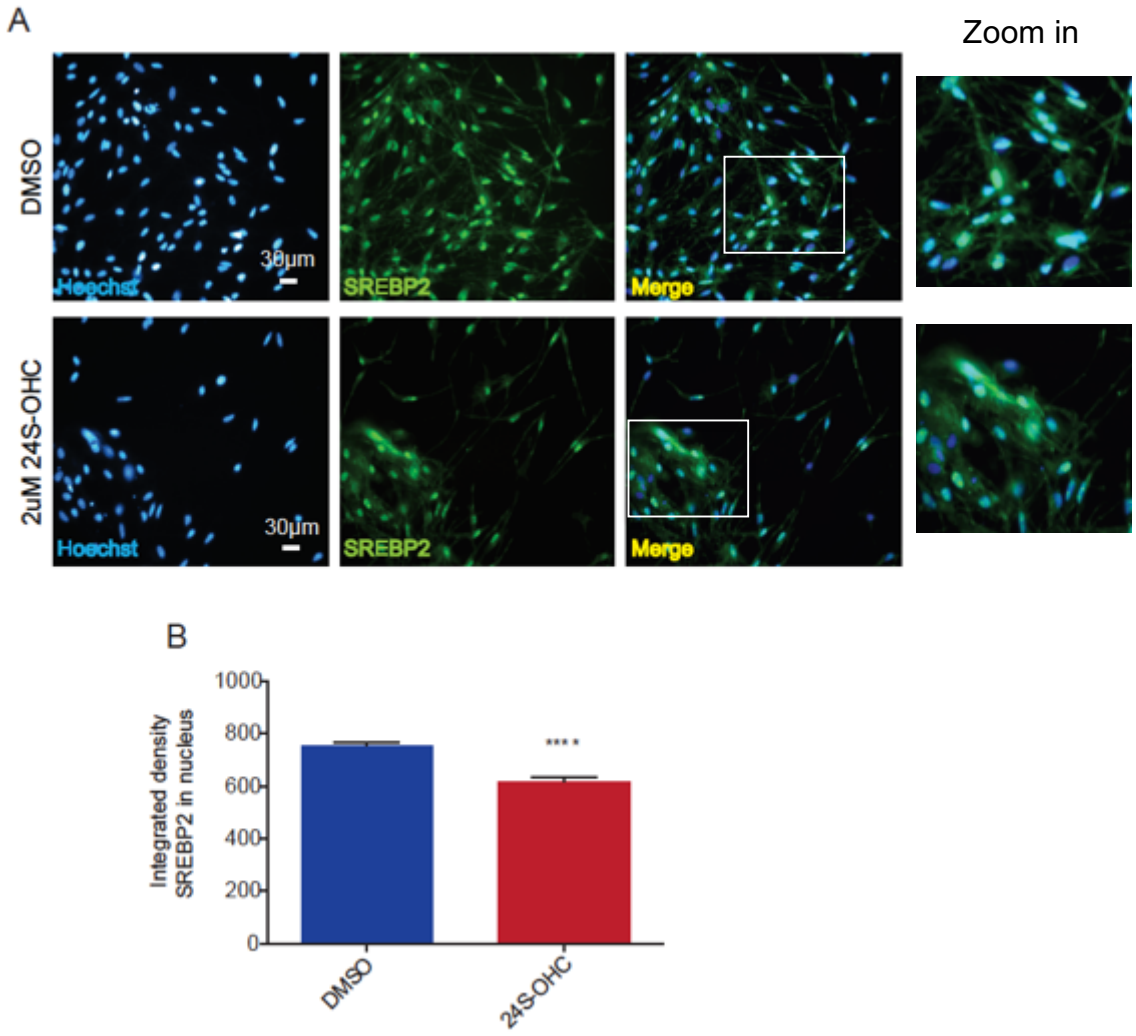

Figure 3.3.4: **24S-OHC inhibits SREBP2 nuclear localization.** Astrocytes were treated with 2 µM of 24S-OHC for 12 h. Immunocytochemical analysis showed evidence for regulation of SREBP2 nuclear localization by 24S-OHC. **A-** Representative images of primary astrocytes fixed and stained with Hoechst (Blue) and SREBP2 (Alexa fluor 488-green). Merge images showed decreased intensity of SREBP2 in the nucleus of astrocytes treated with 24S-OHC, compared to merge image from control (DMSO) scale bar: 30 µm. **B-** Graph represents mean intensity of SREBP2 in the nucleus +/- SEM. A significant decrease of $p<0.0001$(****) detected by student t-test with Welch's correction, of nuclear SREBP2 was encountered in the nucleus of astrocytes treated with 2 µM of 24S-OHC for 12h. Images were taken using Nikon eclipse Ti microscope at 20x magnification, scale bar: 30 µm.

This result demonstrates for the first time in astrocytes *in vitro*, that 24S-OHC inhibits SREBP2 nuclear migration. This result explains the observations in Figure 3.3.1 that 24S-OHC significantly downregulates SREBP2 target genes.

3.3.5. The effect of 24S-hydroxycholesterol on SREBP2 nuclear translocation – lack of validation by an SREBP2 DNA binding activity assay.

In order to further confirm that the mechanism of 24S-OHC's effects on sterol biosynthesis relied on the negative regulation of SREBP2, I employed another approach: a SREBP2 DNA binding assay (see Material and Methods section 2.15). Controls used in the assay comprised U-18666A and ER stress inducers (tunycamycin-TM and thapsigargin - TG). According to previous literature, U-18666A induces SREBP2 nuclear migration, and is therefore used as positive control; other studies also propose a mechanism in which ER stress increases SREBP2 activity, providing the rationale for using TM and TG (Rohrl et al., 2014).

To perform this experiment, astrocytes were plated on 10 cm dishes, 2 days after being in G5 supplement. During treatment (DMSO, 24S-OHC, U-18666A, TM or TG) serum-free medium was applied and the test compounds were added: 2 μM of 24S-OHC for 12 h, 1.25 μM of U-18666A for 48 h, 1 μM TM for 6 h and 100nM of TG for 24 h. At the specified times, astrocytes were lysed and the nuclear fraction isolated (Figure 2.6 in Material and Methods) as recommended in the kit (Material and Methods 2.15).

As observed in Figure 3.3.5, only TM caused the expected effect of significantly increased migration of SREBP2 to the nucleus. The other samples showed no difference when compared to control.

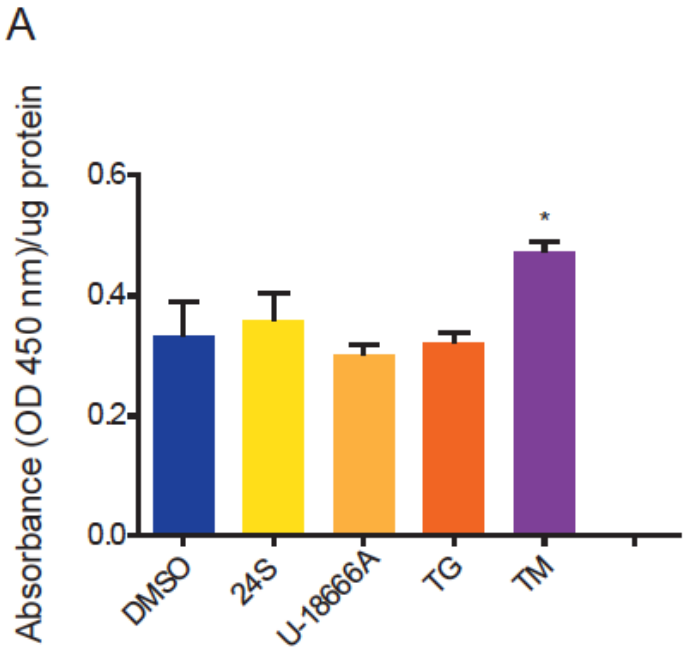

Figure 3.3.5: **No detectable change in nuclear SREBP2 binding activity after exposure to 24S-OHC.** Astrocytes were treated with 2 μM of 24S-OHC for 12 h, 1.25 μM of U-18666A for 48 h, 1 μM TM (tunicamycin) for 6 h and 100nM of TG (thapsigargin) for 24 h. No differences were observed in SREBP2 nuclear absorbance in cells treated with 24S-OHC, U-18666A, and TG. Only astrocytes treated with TM showed a significant ($p=0.0245$ (*)) increase in absorbance (more SREBP2 in the nucleus). Statistical test used was one-way ANOVA followed by Dunnett's multiple comparison test. Graph represents the average values of absorbance from 3 independent experiments.

I was expecting to detect SREBP2 in the nucleus of the positive controls (astrocytes treated with TG, TM and U-18666A), as for the test: samples treated with 24S-OHC, I was expecting significant decrease in OD compared to control (untreated-DMSO samples) as in the presence of oxysterols (24S-OHC) SREBP2 is retained in the ER and inhibited to migrate in the nucleus.

3.3.6. 24S-hydroxycholesterol causes astrocyte cell death *in vitro*.

Having regularly observed of the treated astrocytes before harvesting them, I developed the suspicion that 24S-OHC was causing cytotoxicity to astrocytes. as I believed that I was observing decreased cell numbers in the treated plates. Considering the observed 24S-OHC toxicity previously in striatal neurons (Figure 3.2.1), I wondered if 24S-OHC might also exerts a similar effect in astrocytes.

To assess the toxicity of 24S-OHC to astrocytes *in vitro*, I exposed them to increasing concentrations (0.25, 0.5, 1, 2 and 4 μM) of 24S-OHC and exposed cells for different periods of time (2, 4 12 and 24 h). MTT assay was conducted at the same time for all the samples 24h after the experiment was initiated. Astrocyte survival was assessed at these time points using the MTT assay (Figure 3.3.6 A). Figure 3.3.6 A conveys the cell death curves correspondents to all the time points analysed for the astrocytes cell death dependent on the 24S-OHC concentration used, however for a better visualisation I split the graph in the different time points studied: 2 h Figure 3.3.6 B, 4 h Figure 3.3.6 C, 12 h Figure 3.3.6 D and 24 h Figure 3.3.6 E.

The cell death curve showed that after 4 h of incubation from a concentration of 0.5 μM a decline is evident (Figure 3.3.6 C). The result of the analysis showed that 4 μM of 24S-OHC caused significant astrocyte loss after 12 h (Figure 3.3.6 D) and 24 h (Figure 3.3.6 E) of treatment ($p = 0.0238$ for 12 h and $p = 0.0485$ for 24 h), when compared to non-treated cells (DMSO) (two-away ANOVA followed by Dunnett's multiple comparison test).

Even though the statistical test only indicates significant cell death for astrocytes treated with 4 μM of 24S-OHC for 12 h and 24 h, a trend toward the same effect was observed after 4h, with ~30% cell death after exposure to 2 μM and ~50% with 4 μM.

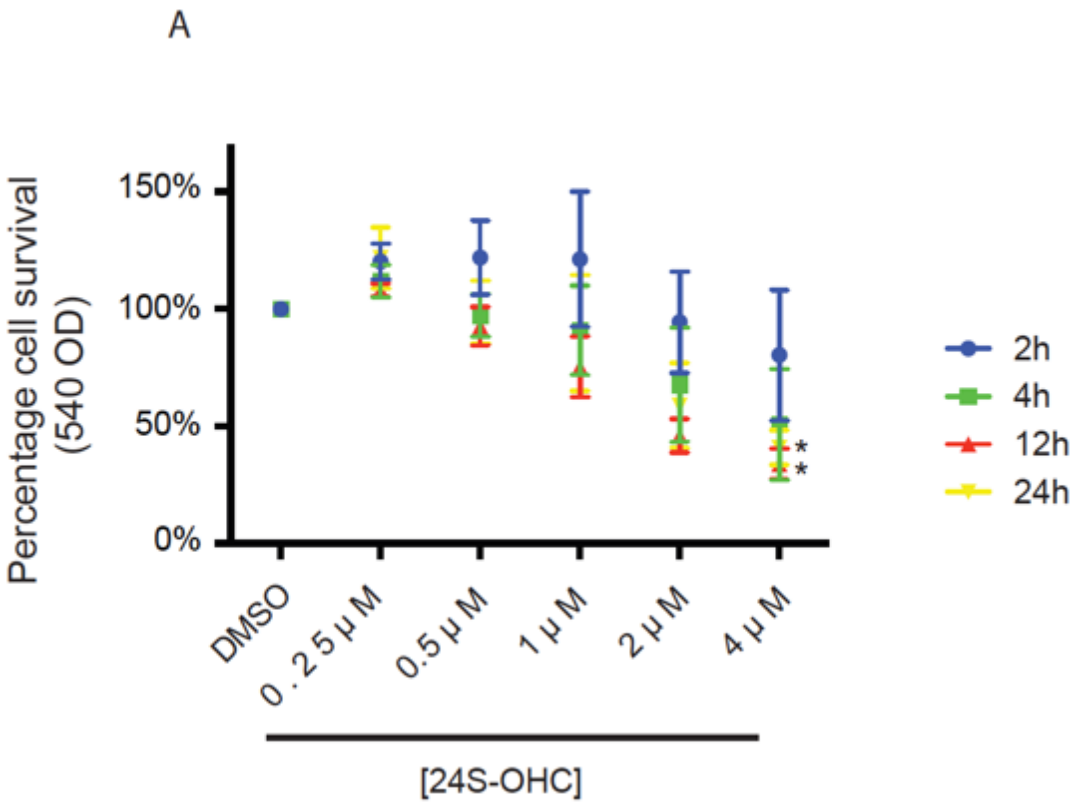
A
Percentage cell survival (540 OD)
150%
100%
50%
0%
DMSO
0.25 µM
0.5 µM
1 µM
2 µM
4 µM
[24S-OHC]
2h
4h
12h
24h
*
*

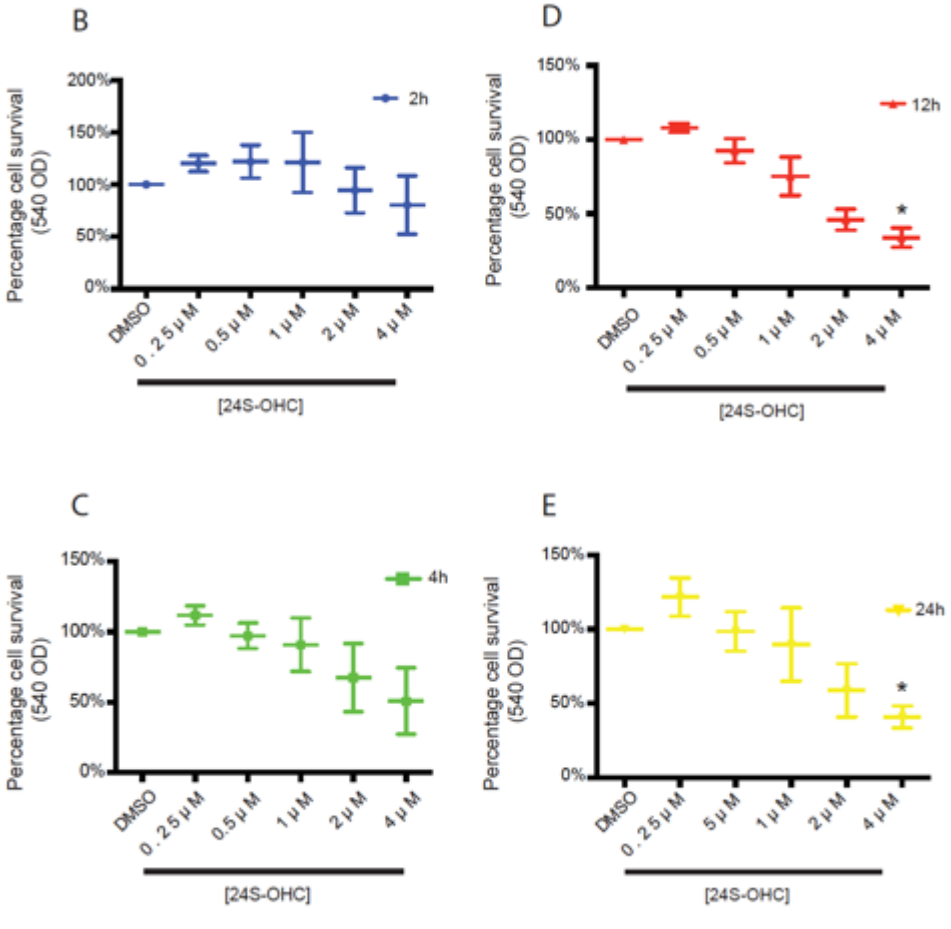
B
Percentage cell survival (540 OD)
200%
150%
100%
50%
0%
2h
DMSO
0.25 µM
0.5 µM
1 µM
2 µM
4 µM
[24S-OHC]
D
Percentage cell survival (540 OD)
150%
100%
50%
0%
12h
*
DMSO
0.25 µM
0.5 µM
1 µM
2 µM
4 µM
[24S-OHC]
C
Percentage cell survival (540 OD)
150%
100%
50%
0%
4h
DMSO
0.25 µM
0.5 µM
1 µM
2 µM
4 µM
[24S-OHC]
E
Percentage cell survival (540 OD)
150%
100%
50%
0%
24h
*
DMSO
0.25 µM
5 µM
1 µM
2 µM
4 µM
[24S-OHC]

Figure 3.3.6: **24S-OHC is cytotoxic to astrocytes. A.** Astrocytes were treated with increasing concentrations of 24S-OHC (0.25, 0.5, 1, 2 and 4 μM) for different time points (2,4 12 and 24 h). Cell survival was assessed at the end of time points (24 h) by MTT assay. The graph represents the percentage of the absorbance (OD 540nm) mean +/- SEM of two independent experiments with 12 technical replicates (N=2, n=12). Ordinary two-way ANOVA indicated that 24S-OHC concentrations cause a significant ($p<0.0001$) effect on cell survival as well as time ($p=0.016$). Two different multiple comparison tests were performed. In order to assess the effect of 24S-OHC concentrations at the same time point, Dunnett's test was preferred. After 12 h and 24 h at 4 μM of 24S-OHC treatment, occurred significant cell death when compared to DMSO ($p=0.0238$ (*) and $p=0.0485$ (*), respectively). To compare the same 24S-OHC concentration during different exposure times, Tukey's multiple comparison test was the more assertive, however resulted in non-significance. **B, C, D** and **E** represent the percentage of the absorbance (OD 540nm) mean +/- SEM after 2h, 4h, 12h and 24h of 24S-OHC treatment, respectively. Graph A was separated in B, C, D and E for better visualization.

In conclusion, astrocytes incubated with 24S-OHC exhibited cell loss in a time and concentration-dependent manner.

This result highlights for the importance of regulating the levels of 24S-OHC in the interstitial space at a low level. They also suggest that the increased level of 24S-OHC observed in our HD model might have implications for astrocyte toxicity in HD.

3.3.7. 24S-hydroxycholesterol does not induce endoplasmic reticulum stress in astrocytes.

I sought to investigate whether 24S-OHC caused UPR upregulation leading to endoplasmic reticulum (ER) stress in astrocytes, based on the same rationale that prompted my assessing a similar effect in neurons (section 3.2.6). If the hypothesis was correct, I was expecting to observe BiP and CHOP to be upregulated (Ron and Habener, 1992).

In order to test this hypothesis, astrocytes were treated with 24S-OHC (2 μM for 4 and 12 h), or the positive controls TM (tunicamycin) or TG (thapsigargin) (0.5 μg/mL and 0.1 μM for 24 h, respectively). The cells were subsequently lysed, and the RNA extracted and used for qRT-PCR analyses. The results showed that 24S-OHC does not induce UPR/ER stress in astrocytes as BiP (Figure 3.3.7 A) and CHOP (Figure 3.3.7 B) mRNA levels

were not upregulated in response to 24S-OHC treatment (Figure 3.3.7). Nonetheless, this effect was seen with the positive controls TM and TG (Figure 3.3.7), as expected.

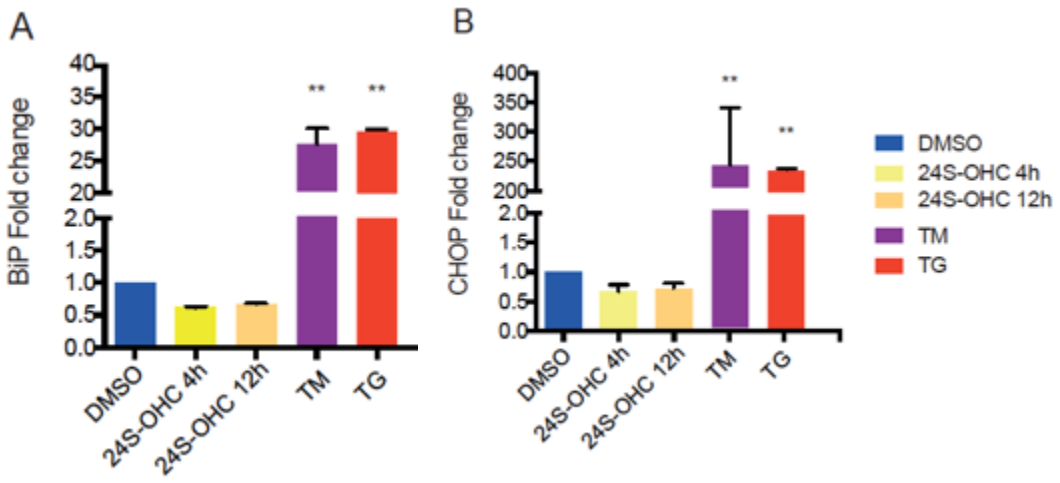

Figure 3.3.7: **24S-OHC does not induce ER stress in astrocytes.** Astrocytes were treated with 2 µM of 24S-OHC for 4 and 12 h, and positive controls used TM (tunicamycin) and TG (thapsigargin) at 0.5 µg/mL and 0.1 µM for 24 h, respectively. **A-** BiP mRNA levels were measured by qRT-PCR and no differences were observed for astrocytes treated with 24S-OHC. Positive controls: TM and TG increased BiP mRNA levels by 30 folds compared to DMSO treated astrocytes (p=0.0014 (**) and p= 0.0011 (**) respectively). **B-** CHOP mRNA levels were measured by qRT-PCR and no differences were observed for astrocytes treated with 24S-OHC. Positive controls: TM and TG increased CHOP mRNA levels by 250 folds compared to DMSO treated astrocytes (p=0.0034 (**) and p= 0.0034 (**)). Graph represents the fold change mean from two independent experiments with 6 technical replicates each (N=2, n=12) +/- SEM. Statistical test used was one-way ANOVA followed by Dunnett's multiple comparison test.

3.3.8. 24S-hydroxycholesterol increases superoxide levels in astrocytes.

Driven to find a mechanism to explain the cell death caused by 24S-OHC in astrocytes, I used the same approach as to study the mechanism of cell death induced by 24S-OHC for primary striatal neurons (Figure 3.2.10), the analysis of increased ROS accumulation using Mitosox.

Fully differentiated astrocytes were treated for 24 h with increasing concentrations of 24S-OHC (0.25, 0.5, 1 and 2 μM). The treated astrocytes exhibited increased intensity for the superoxide indicator Mitosox, in a concentration dependent manner (Figure 3.3.8 A).

The graph (Figure 3.3.8 B) shows the increase of integrated density of the Mitosox-positive particles in 24S-OHC concentration dependent manner. All the 24S-OHC concentrations studied caused statistically significant superoxide accumulation compared to the positive control – 3-NP (One-way ANOVA followed by Dunnett's multiple comparison test $p<0.01$ ***, $p<0.0001$ ****).

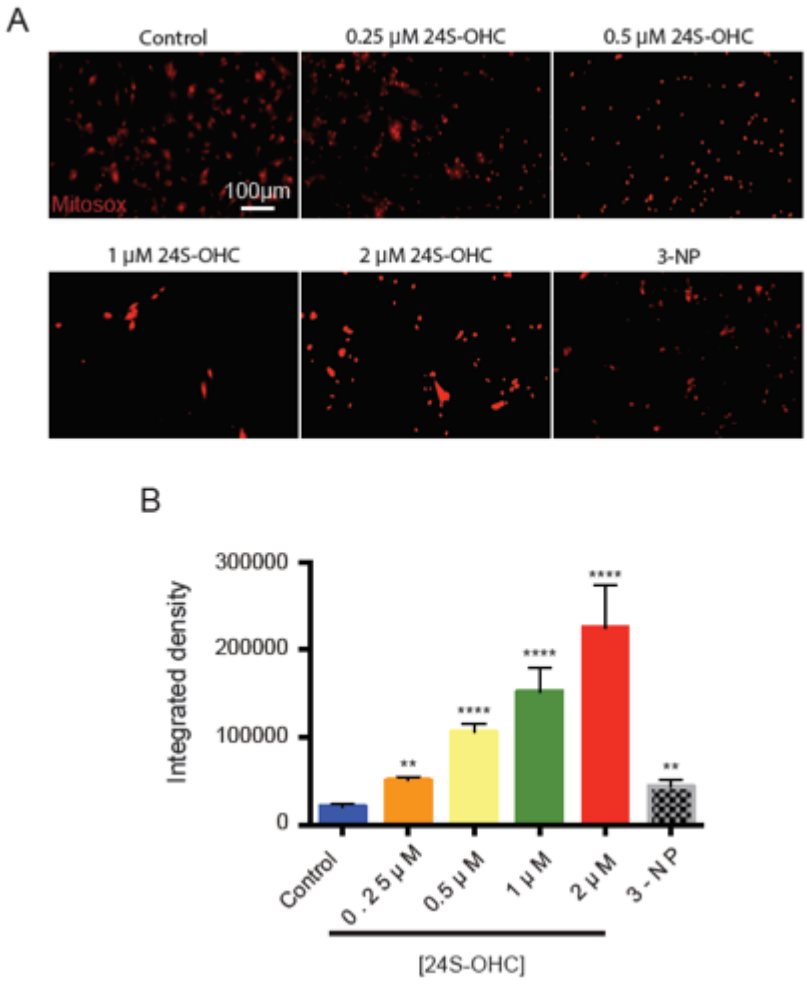

Figure 3.3.8: **24S-OHC increases superoxide levels in astrocytes.** Astrocytes upon differentiation were treated with increasing concentrations of 24S-OHC: 0.25, 0.5, 1 and 2 μM for 24 h. Positive control for mitochondrial stress used was the complex 2 inhibitor: 3-NP, used at 10 mM for 12 h. Mitosox was loaded in the cells dissolved in HBSS at 5 μM. **A-** Representative images of astrocytes loaded with mitosox, show increasing fluorescence intensity dependent on the 24S-OHC concentrations. The positive control exhibited the positive staining. **B-** The graph shows a dependency between integrated density and 24S-OHC concentrations proved by the statistical test One-Way ANOVA ($p<0.0001$). Astrocytes treated with higher concentrations exhibited increased intensity of mitosox. All the concentrations studied when compared to control caused statistical significant accumulation of superoxide in astrocytes: 0.25 μM $p=0.0075$ (**), 0.5 – 2 μM $p<0.0001$ (****) (Dunnett's multiple comparison test). Astrocytes treated with 3-NP exhibited a statistical significant increase in mitosox intensity compared to control, when a Student T-test with Welch's correction was applied ($p=0.0031$ **). The graph represents the mean +/- SEM of intensities from one experiment with 4 technical replicates (N=1, n=4). Images were taken Nikon eclipse Ti microscope at 20x magnification, scale bar: 100 μm.

Thus, a possible mechanism for the astrocytic cell death caused by 24S-OHC is increased superoxide production, which may lead to mitochondrial stress.

3.3.9. Discussion

In this chapter I addressed the effects of 24S-hydroxycholesterol (24S-OHC) on astrocytes in culture. Primarily its regulatory effects on the transcription of genes involved on sterol metabolism were explored, and consequently I studied possible toxic effects.

24S-OHC is not likely to be the only metabolite in the process of cholesterol elimination, as newer evidence supports its role as a signalling molecule that communicates between neurons and astrocytes (Wang et al., 2008). For this reason understanding in detail the signalling of this molecule in astrocytes is important for clarifying overall mechanisms of brain function.

In Results Chapter 3.3 I demonstrated the efficacy of 24S-OHC to regulate the two different transcription factors, SREBP2 and LXR. While SREBP2 upregulates genes involved in cholesterol biosynthesis and uptake, LXR was found to induce the expression of cholesterol efflux genes.

My results showed that 24S-OHC downregulates known to be SREBP2 target sterol biosynthesis genes (*HMGCR, HMGCS and FDFT1*) and transporter genes (*LDLr*) in astrocytes (Figure 3.3.1). I further showed that this effect is dissociated pharmacologically from LXR activation, as treatment with TO-901317 caused no effect (Figure 3.3.1 B, D, F and H). The actions of 24S-OHC on some of the LXR target genes studied were partially consistent with those of previous studies (Liang et al., 2004; Abildayeva et al., 2006). I showed transcriptional induction of *ABCA1* and *ABCG1* (Figure 3.3.2 A and C), consistent with a previous report (Abildayeva et al., 2006); moreover I presented that 24S-OHC caused upregulation of *SREBP1c* and *Glut4* (Figure 3.3.2 E and G). Most notably *ApoE* did not exhibit altered expression, even upon TO-901317 treatment (Figure 3.3.3 A and B).

From the results obtained I can conclude that 24S-OHC likely regulates the transcription of *ABCA1*, *ABCG1*, *SREBP1c* and *Glut4* by activating LXR, however both 24S-OHC and TO-901317 failed to cause a transcriptional change on *ApoE*.

Counteracting the importance given *in vitro* to 24S-OHC as a LXR agonist, it should be noted that studies with transgenic mice overexpressing human CYP46A1 resulted in unexpected observations. The significantly increased

levels of 24S-OHC in the brain did not alter the expression levels of LXR or SREBP2 target genes. In spite of the fact that 24S-OHC *in vitro* was shown to upregulate LXR target genes, operating as a potent LXR agonist, however *in vivo* it is not a critical activator of this nuclear receptor (Shafaati et al., 2011).

It has been shown previously that oxysterols modulate SREBP2 nuclear migration by binding to INSIG. The binding of oxysterols to INSIG invokes structural changes, causing INSIG to bind to Scap, keeping the Scap-SREP2 complex in the ER (Radhakrishnan et al., 2007). In this chapter, I showed for the first time that 24S-OHC inhibits SREBP2 nuclear migration in astrocytes (Figure 3.3.4). I succeeded in showing less intensity of SREBP2 immunostaining in the nucleus of astrocytes treated with 24S-OHC (Figure 3.3.4), whereas with a different approach using the SREBP2 DNA binding assay (Figure 3.3.5), the results were inconclusive. The lack of observed effect of 24S-OHC in the SREBP2 transcription factor assay was puzzling. Nevertheless I used my own positive controls: astrocytes treated with ER stress inducers, tunicamyin and thapsigargin (Rohrl et al., 2014), as well as U-18666A, with which increased OD was expected. However only astrocytes treated with tunicamycin showed the expected increase in absorbance, indicating the SREBP2 nuclear localization. My explanation for the lack of significance between treatments on the insufficient sensitivity of the assay for my rat samples, as the SRE in the plate and the antibody in the kit are for human samples. Even though the manufactor indicates that was fabricated to be used with human samples, predicts it to work with mammal samples. Although I used the amount of sample advised by the kit, perhaps the overall expression levels of SREBP2 maybe lower compared to the samples tested by the manufactor, therefore the SREBP2 in nucleus is not sufficient to be quantified.

Most interestingly, as previously observed in primary neurons, 24S-OHC causes toxicity to astrocytes (Figure 3.3.6) in a dose and time dependent manner. Cell loss due to 24S-OHC is not caused by ER stress (Figure 3.3.7), a mechanism more likely to be operating is the increased superoxide levels observed in astrocytes treated with 24S-OHC, which suggests mitochondrial oxidative stress (Figure 3.3.8). This effect was also observed in results chapter 3.2 with primary striatal neurons.

4. Discussion

In this thesis I uncovered some important aetiologic aspects of sterol dysregulation in an *in vitro* model of HD (Figure 3.1.1 and 3.1.2). I observed sterol accumulation in primary striatal neurons (Figure 3.1.3 and 3.1.4) which ones controlled tightly their intracellular sterols levels, by releasing increased levels of 24S-OHC into medium (Figure 3.1.11), which was then observed. While in the interstitial space 24S-OHC was hypothesised to have implications on neurons and astrocytes' health. Accordingly, I showed that increased levels of 24S-OHC were toxic to primary striatal neurons (Figure 3.2.1 and 3.2.2) and lead to increase levels of superoxide (Figure 3.2.13), anticipating a consequent mitochondrial stress event. Moreover, 24S-OHC proved to be a potent NMDAR activator inciting increased calcium influx (Figure 3.2.6) and increasing the firing pattern of a mixed neuronal culture (Figure 3.2.7), when in the presence of NMDAR agonist and co-agonist. Unfortunately, I did not succeed to demonstrate that 24S-OHC sensitized neurons to NMDA application with increased neuronal death, nevertheless I would have been more successful if I have used lower concentrations of NMDA, as the concentration used (10 μM) was causing more than 70% cell death, so a 24S-OHC effect was maybe hidden (Figure 3.2.11). Regardless I proved that 24S-OHC is a potent NMDAR modulator promoting its functions empowering to excitotoxicity and mitochondrial stress insults in striatal neurons, aggravating HD cellular symptoms. In astrocytes, 24S-OHC causes sterols dyshomeostasis by promoting sterol efflux, thought LXR genes' activation (Figure 3.3.2) and the cease of sterol biosynthesis once inhibits SREBP2 nuclear migration (Figure 3.3.4) and its target genes were found downregulated (Figure 3.3.1). These *in vitro* findings drive me to hypothesize that HD astrocytes reach a status of sterol depletion.

The field of research comprehending the sterol dyshomeostasis in HD is mainly split in two sides, findings proved that cholesterol accumulates in HD neurons (Trushina et al., 2006; del Toro et al., 2010; Luthi-Carter et al., 2010) while research from a different group suggested that sterol biosynthesis in HD neurons is impaired and this exhibited decreased levels of cholesterol

precursors (Marullo et al., 2012; Leoni and Caccia, 2015). In this thesis I conveyed the knowledge from the different groups, I observed sterol accumulation in primary striatal neurons at the plasma membrane (Figure 3.1.5) (Trushina et al., 2006) and in lysosomes (Figure 3.1.7). As previously seen by Del Toro, I linked the sterol dysregulation with increased NMDAR receptor function (del Toro et al., 2010) and finally my findings led to sterol dysregulation in astrocytes with a consequence status of sterol depletion (Valenza et al., 2015).

An interesting finding presented in this thesis was the involvement of sterol dysregulation in striatal neurons expressing Htt 171-82Q with characterized HD hallmarks, excitotoxicity and mitochondrial stress. Would be interesting in future work to understand exactly how 24S-OHC regulates these mechanisms, perhaps the finding of its binding site at plasma membrane/NMDAR would facilitate the investigation. From previous studies is known that 24S-OHC binds on an extracellular site at the plasma membrane as when applied in whole-cell pipette solution and to the cytosolic face of inside-out membrane was not effective as NMDAR modulator (Linsenbardt et al., 2014). Regarding the increased levels of superoxide after 24S-OHC treatment on striatal neurons, further investigation on the mechanism would be more elucidative as to understand how the 24S-OHC targets the mitochondria, which ROS are increased and the signalling cascade.

Since the increased sterol observed in disease conditions is detrimental, the existence of a compound that penetrates the blood brain barrier and effectively decreases total sterols is a promising step in identifying relevant therapeutics. As interesting as the observed that AK-7 decreases total sterol levels in primary striatal neurons expressing mutant Htt (Htt171-82Q) (Figure 3.1.10), would be to prove its ability to decrease 24S-OHC generation and consequent release therefore protecting neurons from the harm of excitotoxicity and mitochondrial stress. This hypothesis comes from the studied direct relation between cholesterol synthesis and 24S-OHC production (Lund et al., 2003) and as shown in Taylor et al., 2011 AK-7 efficiently retains SREBP2 in the ER promoting its target genes downregulation therefore less cholesterol

biosynthesis leading to less substrate available to produce 24S-OHC and consequently less efflux.

The finding that 24S-OHC has neurotoxic properties is not completely novel as others have reported similar observations with SH-SY5Y cells (Kolsch et al., 2001) and cortical neurons (Yamanaka et al., 2011). One previous description indicates that 24S-OHC induces neuronal cell death through necroptosis, a form of programmed necrosis (Yamanaka et al., 2011). This group reported that 24S-OHC induces cell death at concentrations higher than 10 μM in SH-SY5Y and cortical neurons, as assessed using the WST-8 assay. Considering that this assay is suitable to study induction and inhibition of cell proliferation, once is based on the extracellular reduction of WST-8 by NADPH produced in the mitochondria, may not be the most assertive method to measure neuronal cell death, once the presence of astrocytes in the cortical culture may lead to erroneous results. That is a reason why I choose to measured neuronal death taking advantage of NeuN immunostaining. Moreover they justified the lack of cell death at concentrations lower than 10 μM as an adaptive response: at “sub-lethal” concentrations 24S-OHC acts through LXR promoting transcriptional activation, initiates a signalling cascade which leads to cell death protection (Okabe et al., 2013). Nevertheless, my data supports that 24S-OHC is a toxic agent causing significant cell death to striatal neurons from the concentration of 1 μM (Figure 3.2.2). This is an important addition to the previous literature by demonstrating 24S-OHC toxicity in another neuronal subtype and at a considerably lower concentration.

24S-OHC is not likely to be only a metabolite for elimination of cholesterol, as more evidences support its role as a signalling molecule that communicates between neurons and astrocytes (Wang et al., 2008). The results presented were partially consistent with those of previous studies (Liang et al., 2004; Abildayeva et al., 2006) by showing the induction of the LXR target gene *ABCA1* (similar TO901317 administration) (Figure 3.3.2 A, B), but with a lack of effect on *ApoE* expression (Figure 3.3.3). My results also showed that 24S-OHC downregulates sterol biosynthesis genes (*HMGCR, HMGCS* and *FDFT1*), and cholesterol uptake (*LDLr*) which are also known as SREBP2 target genes,

in astrocytes (Figure 3.3.1), an effect that could be dissociated pharmacologically from LXR activation.

Drawing on data from an *in vitro* model comprised of primary rat brain cells, Abildayeva and colleagues (Abildayeva et al., 2006) have previously proposed a model in which release of 24S-OHC from neurons also induces the secretion of lipoprotein-associated cholesterol from astrocytes (Pfrieger, 2003 a). This is also consistent with the results of (Kim et al., 2007), who presented evidence that neurons release 24S-OHC to signal astrocytes to produce more ApoE-containing lipoprotein complexes. On the other hand, Abildayeva and colleagues provided an alternate perspective by showing that 24S-OHC *per se* does not induce cholesterol efflux from astrocytes, but that cholesterol efflux is nonetheless dependent on either ApoE or ApoAI.

Counteracting the importance given *in vitro* to 24S-OHC as a LXR agonist, studies with transgenic mice overexpressing human *CYP46A1*, resulted in unexpected observations, once the significantly increased levels of 24S-OHC in the brain, did not alter the transcription of LXR neither SREBP2 target genes. In spite of the fact that 24S-OHC *in vitro* was shown to upregulate LXR target genes, operating as a potent LXR agonist, *in vivo* is not a critical activator of this nuclear receptor (Shafaati et al., 2011).

More interestingly I showed for the first time in astrocytes the mechanism by which SREBP2 is retained in the cytoplasm in the presence of 24S-OHC (Figure 3.3.4), explaining the dowregulation of its target genes (Figure 3.3.1).

The cytotoxic effects of 24S-OHC not only affected neuronal survival as it also affected astrocytes'. As evidenced by the cell death curve in Figure 3.3.6, treatment of 4 μM of 24S-OHC after 12h and 24h leads to significant cell death.

The mechanism of cell death caused by 24S-OHC in astrocytes may also be caused by mitochondrial stress, once I observed increased superoxide levels in a dose depended manner, after 24 h treatment.

The working model proposed at the beginning of the thesis (Figure 1.6) lays on the hypothesis that the sterol accumulation in HD primary neurons leads to increase released of 24S-OHC into the medium. The cerebrosterol is toxic to primary striatal neurons causing cell death maybe by inducing increased

superoxide, and potentiates neuronal response to NMDAR activation, sensitising them to excitotoxicity, a mechanism known to be important in HD. Moreover, 24S-OHC downregulates SREBP2 target genes, reducing cholesterol synthesis and overexpresses LXR target genes, promoting sterol efflux in astrocytes *in vitro*. Besides altering the sterol metabolism of astrocytes, 24S-OHC also induces cell death and the mechanism tested was by inducing superoxide levels. Thus an increase in ROS and consequently mitochondrial stress maybe the cause for cell death.

Importantly, the results collected to date conveyed previous studies and shed new light on transcellular aspects of cholesterol dyshomeostasis that occur early in HD, where sterol accumulation and consequent released of 24S-OHC was observed for the first time and its effects investigated in both neurons and astrocytes.

5. Bibliography

Abildayeva, K., Jansen, P.J., Hirsch-Reinshagen, V., Bloks, V.W., Bakker, A.H., Ramaekers, F.C., de Vente, J., Groen, A.K., Wellington, C.L., Kuipers, F., et al. (2006). 24(S)-hydroxycholesterol participates in a liver X receptor-controlled pathway in astrocytes that regulates apolipoprotein E-mediated cholesterol efflux. The Journal of biological chemistry *281*, 12799-12808.

Aharony, I., Ehrnhoefer, D.E., Shruster, A., Qiu, X., Franciosi, S., Hayden, M.R., and Offen, D. (2015). A Huntingtin-based peptide inhibitor of caspase-6 provides protection from mutant Huntingtin-induced motor and behavioral deficits. Human molecular genetics *24*, 2604-2614.

Aiken, C.T., Steffan, J.S., Guerrero, C.M., Khashwji, H., Lukacsovich, T., Simmons, D., Purcell, J.M., Menhaji, K., Zhu, Y.Z., Green, K., et al. (2009). Phosphorylation of threonine 3: implications for Huntingtin aggregation and neurotoxicity. The Journal of biological chemistry *284*, 29427-29436.

Ando, S., Tanaka, Y., Toyoda, Y., and Kon, K. (2003). Turnover of myelin lipids in aging brain. Neurochemical research *28*, 5-13.

Andrade, M.A., and Bork, P. (1995). HEAT repeats in the Huntington's disease protein. Nature genetics *11*, 115-116.

Aoki, K., Uchihara, T., Sanjo, N., Nakamura, A., Ikeda, K., Tsuchiya, K., and Wakayama, Y. (2003). Increased expression of neuronal apolipoprotein E in human brain with cerebral infarction. Stroke; a journal of cerebral circulation *34*, 875-880.

Arndt, J.R., Chaibva, M., and Legleiter, J. (2015). The emerging role of the first 17 amino acids of huntingtin in Huntington's disease. Biomolecular concepts *6*, 33-46.

Arrasate, M., Mitra, S., Schweitzer, E.S., Segal, M.R., and Finkbeiner, S. (2004). Inclusion body formation reduces levels of mutant huntingtin and the risk of neuronal death. Nature *431*, 805-810.

Bao, J., Sharp, A.H., Wagster, M.V., Becher, M., Schilling, G., Ross, C.A., Dawson, V.L., and Dawson, T.M. (1996). Expansion of polyglutamine repeat in huntingtin leads to abnormal protein interactions involving calmodulin. Proceedings of the National Academy of Sciences of the United States of America *93*, 5037-5042.

Bar-On, P., Rockenstein, E., Adame, A., Ho, G., Hashimoto, M., and Masliah, E. (2006). Effects of the cholesterol-lowering compound methyl-beta-cyclodextrin in models of alpha-synucleinopathy. Journal of neurochemistry *98*, 1032-1045.

Bates, G. (2003). Huntingtin aggregation and toxicity in Huntington's disease. Lancet *361*, 1642-1644.

Benavides, A., Pastor, D., Santos, P., Tranque, P., and Calvo, S. (2005). CHOP plays a pivotal role in the astrocyte death induced by oxygen and glucose deprivation. Glia *52*, 261-275.

Bence, N.F., Sampat, R.M., and Kopito, R.R. (2001). Impairment of the ubiquitin-proteasome system by protein aggregation. Science (New York, N.Y.) *292*, 1552-1555.

Bertolotti, A., Zhang, Y., Hendershot, L.M., Harding, H.P., and Ron, D. (2000). Dynamic interaction of BiP and ER stress transducers in the unfolded-protein response. Nature cell biology *2*, 326-332.

Bickel, M.H. (1996). Brain Chemistry and the French Connection, 1791-1841: An Account of the Chemical Analyses of the Human Brain by Thouret (1791), Fourcroy (1793), Vauquelin (1811), Couerbe (1834), and Fremy (1841) (review). Bulletin of the history of medicine *70*, 717-718.

Biglan, K.M., Ross, C.A., Langbehn, D.R., Aylward, E.H., Stout, J.C., Queller, S., Carlozzi, N.E., Duff, K., Beglinger, L.J., Paulsen, J.S., et al. (2009). Motor abnormalities in premanifest persons with Huntington's disease: the PREDICT-HD study. Movement disorders : official journal of the Movement Disorder Society *24*, 1763-1772.

Bjorkhem, I. (2006). Crossing the barrier: oxysterols as cholesterol transporters and metabolic modulators in the brain. J Intern Med *260*, 493-508.

Bjorkhem, I. (2013). Five decades with oxysterols. Biochimie *95*, 448-454.

Bjorkhem, I., Cedazo-Minguez, A., Leoni, V., and Meaney, S. (2009). Oxysterols and neurodegenerative diseases. Molecular aspects of medicine *30*, 171-179.

Bjorkhem, I., Lovgren-Sandblom, A., Piehl, F., Khademi, M., Pettersson, H., Leoni, V., Olsson, T., and Diczfalusy, U. (2011). High levels of 15-oxygenated steroids in circulation of patients with multiple sclerosis: fact or fiction? J Lipid Res *52*, 170-174.

Bjorkhem, I., Lutjohann, D., Breuer, O., Sakinis, A., and Wennmalm, A. (1997). Importance of a novel oxidative mechanism for elimination of brain cholesterol. Turnover of cholesterol and 24(S)-hydroxycholesterol in rat brain as measured with 18O2 techniques in vivo and in vitro. The Journal of biological chemistry *272*, 30178-30184.

Bloch, K. (1965). The biological synthesis of cholesterol. Science (New York, N.Y.) *150*, 19-28.

Bloch, K. (1987). Summing up. Annual review of biochemistry *56*, 1-19.

Bogdanov, M.B., Andreassen, O.A., Dedeoglu, A., Ferrante, R.J., and Beal, M.F. (2001). Increased oxidative damage to DNA in a transgenic mouse model of Huntington's disease. Journal of neurochemistry *79*, 1246-1249.

Bradford, J., Shin, J.Y., Roberts, M., Wang, C.E., Li, X.J., and Li, S. (2009). Expression of mutant huntingtin in mouse brain astrocytes causes age-dependent neurological symptoms. Proceedings of the National Academy of Sciences of the United States of America *106*, 22480-22485.

Brasaemle, D.L., and Attie, A.D. (1990). Rapid intracellular transport of LDL-derived cholesterol to the plasma membrane in cultured fibroblasts. J Lipid Res *31*, 103-112.

Breckenridge, D.G., Germain, M., Mathai, J.P., Nguyen, M., and Shore, G.C. (2003). Regulation of apoptosis by endoplasmic reticulum pathways. Oncogene *22*, 8608-8618.

Bretillon, L., Lutjohann, D., Stahle, L., Widhe, T., Bindl, L., Eggertsen, G., Diczfalusy, U., and Bjorkhem, I. (2000). Plasma levels of 24S-hydroxycholesterol reflect the balance between cerebral production and hepatic metabolism and are inversely related to body surface. J Lipid Res *41*, 840-845.

Breydo, L., Wu, J.W., and Uversky, V.N. (2012). α-Synuclein misfolding and Parkinson's disease. Biochimica et Biophysica Acta (BBA) - Molecular Basis of Disease *1822*, 261-285.

Brown, M.S., and Goldstein, J.L. (1986). A receptor-mediated pathway for cholesterol homeostasis. Science (New York, N.Y.) *232*, 34-47.

Brown, M.S., and Goldstein, J.L. (1997). The SREBP pathway: regulation of cholesterol metabolism by proteolysis of a membrane-bound transcription factor. Cell *89*, 331-340.

Brown, M.S., and Goldstein, J.L. (2009). Cholesterol feedback: from Schoenheimer's bottle to Scap's MELADL. J Lipid Res *50 Suppl*, S15-27.

Browne, S.E., Bowling, A.C., MacGarvey, U., Baik, M.J., Berger, S.C., Muqit, M.M., Bird, E.D., and Beal, M.F. (1997). Oxidative damage and metabolic dysfunction in Huntington's disease: selective vulnerability of the basal ganglia. Annals of neurology *41*, 646-653.

Bu, G. (2009). Apolipoprotein E and its receptors in Alzheimer's disease: pathways, pathogenesis and therapy. Nature reviews. Neuroscience *10*, 333-344.

Castellani, R.J. (2010). Alzheimer disease. Dis Mon *56*, 484-546.

Cattaneo, E., Zuccato, C., and Tartari, M. (2005). Normal huntingtin function: an alternative approach to Huntington's disease. Nature reviews. Neuroscience *6*, 919-930.

Caviston, J.P., Zajac, A.L., Tokito, M., and Holzbaur, E.L. (2011). Huntingtin coordinates the dynein-mediated dynamic positioning of endosomes and lysosomes. Molecular biology of the cell *22*, 478-492.

Cenedella, R.J. (2009). Cholesterol synthesis inhibitor U18666A and the role of sterol metabolism and trafficking in numerous pathophysiological processes. Lipids *44*, 477-487.

Chai, Y., Wu, L., Griffin, J.D., and Paulson, H.L. (2001). The role of protein composition in specifying nuclear inclusion formation in polyglutamine disease. The Journal of biological chemistry *276*, 44889-44897.

Champagne, D., Rochford, J., and Poirier, J. (2005). Effect of apolipoprotein E deficiency on reactive sprouting in the dentate gyrus of the hippocampus following entorhinal cortex lesion: role of the astroglial response. Experimental neurology *194*, 31-42.

Chang, T.Y., Reid, P.C., Sugii, S., Ohgami, N., Cruz, J.C., and Chang, C.C. (2005). Niemann-Pick type C disease and intracellular cholesterol trafficking. The Journal of biological chemistry *280*, 20917-20920.

Chen, G., Fan, Z., Wang, X., Ma, C., Bower, K.A., Shi, X., Ke, Z.J., and Luo, J. (2007). Brain-derived neurotrophic factor suppresses tunicamycin-induced upregulation of CHOP in neurons. Journal of neuroscience research *85*, 1674-1684.

Chen, J., Zhang, X., Kusumo, H., Costa, L.G., and Guizzetti, M. (2013). Cholesterol efflux is differentially regulated in neurons and astrocytes: implications for brain cholesterol homeostasis. Biochimica et biophysica acta *1831*, 263-275.

Chobanian, A.V., Burrows, B.A., and Hollander, W. (1962). Body cholesterol metabolism in man. II. Measurement of the body cholesterol miscible pool and turnover rate. The Journal of clinical investigation *41*, 1738-1744.

Chopra, V., Quinti, L., Kim, J., Vollor, L., Narayanan, K.L., Edgerly, C., Cipicchio, P.M., Lauver, M.A., Choi, S.H., Silverman, R.B., et al. (2012). The sirtuin 2 inhibitor AK-7 is neuroprotective in Huntington's disease mouse models. Cell reports *2*, 1492-1497.

Choudhury, A., Sharma, D.K., Marks, D.L., and Pagano, R.E. (2004). Elevated endosomal cholesterol levels in Niemann-Pick cells inhibit rab4 and perturb membrane recycling. Molecular biology of the cell *15*, 4500-4511.

Cicchetti, F., Soulet, D., and Freeman, T.B. (2011). Neuronal degeneration in striatal transplants and Huntington's disease: potential mechanisms and clinical implications. Brain : a journal of neurology *134*, 641-652.

Clemens, L.E., Weber, J.J., Wlodkowski, T.T., Yu-Taeger, L., Michaud, M., Calaminus, C., Eckert, S.H., Gaca, J., Weiss, A., Magg, J.C., et al. (2015). Olesoxime suppresses calpain activation and mutant huntingtin fragmentation in the BACHD rat. Brain : a journal of neurology *138*, 3632-3653.

Colin, E., Zala, D., Liot, G., Rangone, H., Borrell-Pages, M., Li, X.J., Saudou, F., and Humbert, S. (2008). Huntingtin phosphorylation acts as a molecular switch for anterograde/retrograde transport in neurons. Embo j *27*, 2124-2134.

Corder, E.H., Saunders, A.M., Strittmatter, W.J., Schmechel, D.E., Gaskell, P.C., Small, G.W., Roses, A.D., Haines, J.L., and Pericak-Vance, M.A. (1993). Gene dose of

apolipoprotein E type 4 allele and the risk of Alzheimer's disease in late onset families. Science (New York, N.Y.) *261*, 921-923.

Crosignani, A., Zuin, M., Allocca, M., and Del Puppo, M. (2011). Oxysterols in bile acid metabolism. Clinica chimica acta; international journal of clinical chemistry *412*, 2037-2045.

Cui, L., Jeong, H., Borovecki, F., Parkhurst, C.N., Tanese, N., and Krainc, D. (2006). Transcriptional repression of PGC-1alpha by mutant huntingtin leads to mitochondrial dysfunction and neurodegeneration. Cell *127*, 59-69.

Davie, C.A. (2008). A review of Parkinson's disease. British medical bulletin *86*, 109-127.

Davies, S.W., Turmaine, M., Cozens, B.A., DiFiglia, M., Sharp, A.H., Ross, C.A., Scherzinger, E., Wanker, E.E., Mangiarini, L., and Bates, G.P. (1997). Formation of neuronal intranuclear inclusions underlies the neurological dysfunction in mice transgenic for the HD mutation. Cell *90*, 537-548.

de Almeida, L.P., Ross, C.A., Zala, D., Aebischer, P., and Deglon, N. (2002). Lentiviral-mediated delivery of mutant huntingtin in the striatum of rats induces a selective neuropathology modulated by polyglutamine repeat size, huntingtin expression levels, and protein length. The Journal of neuroscience : the official journal of the Society for Neuroscience *22*, 3473-3483.

de Duve, C. (2007). The origin of eukaryotes: a reappraisal. Nature reviews. Genetics *8*, 395-403.

De Fabiani, E., Mitro, N., Gilardi, F., and Crestani, M. (2010). Sterol-protein interactions in cholesterol and bile acid synthesis. Sub-cellular biochemistry *51*, 109-135.

del Toro, D., Xifro, X., Pol, A., Humbert, S., Saudou, F., Canals, J.M., and Alberch, J. (2010). Altered cholesterol homeostasis contributes to enhanced excitotoxicity in Huntington's disease. Journal of neurochemistry *115*, 153-167.

Dietschy, J.M. (2009). Central nervous system: cholesterol turnover, brain development and neurodegeneration. Biological chemistry *390*, 287-293.

Dietschy, J.M., and Turley, S.D. (2001). Cholesterol metabolism in the brain. Current opinion in lipidology *12*, 105-112.

Dietschy, J.M., and Turley, S.D. (2004). Thematic review series: brain Lipids. Cholesterol metabolism in the central nervous system during early development and in the mature animal. J Lipid Res *45*, 1375-1397.

DiFiglia, M., Sapp, E., Chase, K., Schwarz, C., Meloni, A., Young, C., Martin, E., Vonsattel, J.P., Carraway, R., Reeves, S.A., et al. (1995). Huntingtin is a cytoplasmic protein associated with vesicles in human and rat brain neurons. Neuron *14*, 1075-1081.

DiFiglia, M., Sapp, E., Chase, K.O., Davies, S.W., Bates, G.P., Vonsattel, J.P., and Aronin, N. (1997). Aggregation of huntingtin in neuronal intranuclear inclusions and dystrophic neurites in brain. Science (New York, N.Y.) *277*, 1990-1993.

Dong, X.-x., Wang, Y., and Qin, Z.-h. (2009). Molecular mechanisms of excitotoxicity and their relevance to pathogenesis of neurodegenerative diseases. Acta Pharmacologica Sinica *30*, 379-387.

Duff, K., Paulsen, J.S., Beglinger, L.J., Langbehn, D.R., Wang, C., Stout, J.C., Ross, C.A., Aylward, E., Carlozzi, N.E., Queller, S., et al. (2010). "Frontal" behaviors before the diagnosis of Huntington's disease and their relationship to markers of disease progression: evidence of early lack of awareness. The Journal of neuropsychiatry and clinical neurosciences *22*, 196-207.

Dunah, A.W., Jeong, H., Griffin, A., Kim, Y.M., Standaert, D.G., Hersch, S.M., Mouradian, M.M., Young, A.B., Tanese, N., and Krainc, D. (2002). Sp1 and TAFII130 transcriptional activity disrupted in early Huntington's disease. Science (New York, N.Y.) *296*, 2238-2243.

Duyao, M., Ambrose, C., Myers, R., Novelletto, A., Persichetti, F., Frontali, M., Folstein, S., Ross, C., Franz, M., Abbott, M., et al. (1993). Trinucleotide repeat length instability and age of onset in Huntington's disease. Nature genetics *4*, 387-392.

Eckert, G.P., Vardanian, L., Rebeck, G.W., and Burns, M.P. (2007). Regulation of central nervous system cholesterol homeostasis by the liver X receptor agonist TO-901317. Neuroscience letters *423*, 47-52.

El-Daher, M.T., Hangen, E., Bruyere, J., Poizat, G., Al-Ramahi, I., Pardo, R., Bourg, N., Souquere, S., Mayet, C., Pierron, G., et al. (2015). Huntingtin proteolysis releases non-polyQ fragments that cause toxicity through dynamin 1 dysregulation. Embo j *34*, 2255-2271.

Engqvist-Goldstein, A.E., Warren, R.A., Kessels, M.M., Keen, J.H., Heuser, J., and Drubin, D.G. (2001). The actin-binding protein Hip1R associates with clathrin during early stages of endocytosis and promotes clathrin assembly in vitro. The Journal of cell biology *154*, 1209-1223.

Espenshade, P.J. (2006). SREBPs: sterol-regulated transcription factors. Journal of cell science *119*, 973-976.

Espenshade, P.J., and Hughes, A.L. (2007). Regulation of sterol synthesis in eukaryotes. Annual review of genetics *41*, 401-427.

Estrada-Sanchez, A.M., and Rebec, G.V. (2012). Corticostriatal dysfunction and glutamate transporter 1 (GLT1) in Huntington's disease: interactions between neurons and astrocytes. Basal ganglia *2*, 57-66.

Evans, S.J., Douglas, I., Rawlins, M.D., Wexler, N.S., Tabrizi, S.J., and Smeeth, L. (2013). Prevalence of adult Huntington's disease in the UK based on diagnoses recorded

in general practice records. Journal of neurology, neurosurgery, and psychiatry *84*, 1156-1160.

Evers, M.M., Tran, H.D., Zalachoras, I., Meijer, O.C., den Dunnen, J.T., van Ommen, G.J., Aartsma-Rus, A., and van Roon-Mom, W.M. (2014). Preventing formation of toxic N-terminal huntingtin fragments through antisense oligonucleotide-mediated protein modification. Nucleic acid therapeutics *24*, 4-12.

Faideau, M., Kim, J., Cormier, K., Gilmore, R., Welch, M., Auregan, G., Dufour, N., Guillermier, M., Brouillet, E., Hantraye, P., et al. (2010). In vivo expression of polyglutamine-expanded huntingtin by mouse striatal astrocytes impairs glutamate transport: a correlation with Huntington's disease subjects. Human molecular genetics *19*, 3053-3067.

Fan, M.M., and Raymond, L.A. (2007). N-methyl-D-aspartate (NMDA) receptor function and excitotoxicity in Huntington's disease. Progress in neurobiology *81*, 272-293.

Feldman, H.H., Doody, R.S., Kivipelto, M., Sparks, D.L., Waters, D.D., Jones, R.W., Schwam, E., Schindler, R., Hey-Hadavi, J., DeMicco, D.A., et al. (2010). Randomized controlled trial of atorvastatin in mild to moderate Alzheimer disease: LEADe. Neurology *74*, 956-964.

Fernandes, H.B., and Raymond, L.A. (2009). Frontiers in Neuroscience
NMDA Receptors and Huntington's Disease. In Biology of the NMDA Receptor. A.M. Van Dongen, ed. (Boca Raton (FL): CRC Press/Taylor & Francis
Taylor & Francis Group, LLC.).

Ferrante, R.J., Gutekunst, C.A., Persichetti, F., McNeil, S.M., Kowall, N.W., Gusella, J.F., MacDonald, M.E., Beal, M.F., and Hersch, S.M. (1997). Heterogeneous topographic and cellular distribution of huntingtin expression in the normal human neostriatum. The Journal of neuroscience : the official journal of the Society for Neuroscience *17*, 3052-3063.

Fradejas, N., Pastor, M.D., Burgos, M., Beyaert, R., Tranque, P., and Calvo, S. (2010). Caspase-11 mediates ischemia-induced astrocyte death: involvement of endoplasmic reticulum stress and C/EBP homologous protein. Journal of neuroscience research *88*, 1094-1105.

Fusco, F.R., Chen, Q., Lamoreaux, W.J., Figueredo-Cardenas, G., Jiao, Y., Coffman, J.A., Surmeier, D.J., Honig, M.G., Carlock, L.R., and Reiner, A. (1999). Cellular localization of huntingtin in striatal and cortical neurons in rats: lack of correlation with neuronal vulnerability in Huntington's disease. The Journal of neuroscience : the official journal of the Society for Neuroscience *19*, 1189-1202.

Gagnon, J.F., Petit, D., Latreille, V., and Montplaisir, J. (2008). Neurobiology of sleep disturbances in neurodegenerative disorders. Current pharmaceutical design *14*, 3430-3445.

Galehdar, Z., Swan, P., Fuerth, B., Callaghan, S.M., Park, D.S., and Cregan, S.P. (2010). Neuronal apoptosis induced by endoplasmic reticulum stress is regulated by ATF4-CHOP-mediated induction of the Bcl-2 homology 3-only member PUMA. The Journal of neuroscience : the official journal of the Society for Neuroscience *30*, 16938-16948.

Gamba, P., Testa, G., Gargiulo, S., Staurenghi, E., Poli, G., and Leonarduzzi, G. (2015). Oxidized cholesterol as the driving force behind the development of Alzheimer's disease. Frontiers in aging neuroscience *7*, 119.

Gambazzi, L., Gokce, O., Seredenina, T., Katsyuba, E., Runne, H., Markram, H., Giugliano, M., and Luthi-Carter, R. (2010). Diminished activity-dependent brain-derived neurotrophic factor expression underlies cortical neuron microcircuit hypoconnectivity resulting from exposure to mutant huntingtin fragments. The Journal of pharmacology and experimental therapeutics *335*, 13-22.

Gao, X., Campbell, W.A.t., Chaibva, M., Jain, P., Leslie, A.E., Frey, S.L., and Legleiter, J. (2016). Cholesterol Modifies Huntingtin Binding to, Disruption of, and Aggregation on Lipid Membranes. Biochemistry *55*, 92-102.

Gauthier, L.R., Charrin, B.C., Borrell-Pages, M., Dompierre, J.P., Rangone, H., Cordelieres, F.P., De Mey, J., MacDonald, M.E., Lessmann, V., Humbert, S., et al. (2004). Huntingtin controls neurotrophic support and survival of neurons by enhancing BDNF vesicular transport along microtubules. Cell *118*, 127-138.

Gill, S., Chow, R., and Brown, A.J. (2008). Sterol regulators of cholesterol homeostasis and beyond: the oxysterol hypothesis revisited and revised. Progress in lipid research *47*, 391-404.

Goldberg, Y.P., Nicholson, D.W., Rasper, D.M., Kalchman, M.A., Koide, H.B., Graham, R.K., Bromm, M., Kazemi-Esfarjani, P., Thornberry, N.A., Vaillancourt, J.P., et al. (1996). Cleavage of huntingtin by apopain, a proapoptotic cysteine protease, is modulated by the polyglutamine tract. Nature genetics *13*, 442-449.

Goldstein, J.L., DeBose-Boyd, R.A., and Brown, M.S. (2006). Protein Sensors for Membrane Sterols. Cell *124*, 35-46.

Gottlieb, D., Carter, H.E., Sloneker, J.H., and Ammann, A. (1958). Protection of fungi against polyene antibiotics by sterols. Science (New York, N.Y.) *128*, 361.

Graham, R.K., Deng, Y., Slow, E.J., Haigh, B., Bissada, N., Lu, G., Pearson, J., Shehadeh, J., Bertram, L., Murphy, Z., et al. (2006). Cleavage at the caspase-6 site is required for neuronal dysfunction and degeneration due to mutant huntingtin. Cell *125*, 1179-1191.

Gutekunst, C.A., Li, S.H., Yi, H., Ferrante, R.J., Li, X.J., and Hersch, S.M. (1998). The cellular and subcellular localization of huntingtin-associated protein 1 (HAP1): comparison with huntingtin in rat and human. The Journal of neuroscience : the official journal of the Society for Neuroscience *18*, 7674-7686.

Gutekunst, C.A., Li, S.H., Yi, H., Mulroy, J.S., Kuemmerle, S., Jones, R., Rye, D., Ferrante, R.J., Hersch, S.M., and Li, X.J. (1999). Nuclear and neuropil aggregates in Huntington's disease: relationship to neuropathology. The Journal of neuroscience : the official journal of the Society for Neuroscience *19*, 2522-2534.

Haines, T.H. (2001). Do sterols reduce proton and sodium leaks through lipid bilayers? Progress in lipid research *40*, 299-324.

Hallett, P.J., Spoelgen, R., Hyman, B.T., Standaert, D.G., and Dunah, A.W. (2006). Dopamine D1 activation potentiates striatal NMDA receptors by tyrosine phosphorylation-dependent subunit trafficking. The Journal of neuroscience : the official journal of the Society for Neuroscience *26*, 4690-4700.

Hanaka, S., Abe, T., Itakura, H., and Matsumoto, A. (2000). Gene expression related to cholesterol metabolism in mouse brain during development. Brain & development *22*, 321-326.

Hands, S.L., and Wyttenbach, A. (2010). Neurotoxic protein oligomerisation associated with polyglutamine diseases. Acta neuropathologica *120*, 419-437.

Harjes, P., and Wanker, E.E. (2003). The hunt for huntingtin function: interaction partners tell many different stories. Trends in biochemical sciences *28*, 425-433.

Harzer, K., and Kustermann-Kuhn, B. (2001). Quantified increases of cholesterol, total lipid and globotriaosylceramide in filipin-positive Niemann-Pick type C fibroblasts. Clinica chimica acta; international journal of clinical chemistry *305*, 65-73.

Her, L.S., and Goldstein, L.S. (2008). Enhanced sensitivity of striatal neurons to axonal transport defects induced by mutant huntingtin. The Journal of neuroscience : the official journal of the Society for Neuroscience *28*, 13662-13672.

Ho, L.W., Brown, R., Maxwell, M., Wyttenbach, A., and Rubinsztein, D.C. (2001). Wild type Huntingtin reduces the cellular toxicity of mutant Huntingtin in mammalian cell models of Huntington's disease. Journal of medical genetics *38*, 450-452.

Holbert, S., Dedeoglu, A., Humbert, S., Saudou, F., Ferrante, R.J., and Neri, C. (2003). Cdc42-interacting protein 4 binds to huntingtin: neuropathologic and biological evidence for a role in Huntington's disease. Proceedings of the National Academy of Sciences of the United States of America *100*, 2712-2717.

Holmberg, C.I., Staniszewski, K.E., Mensah, K.N., Matouschek, A., and Morimoto, R.I. (2004). Inefficient degradation of truncated polyglutamine proteins by the proteasome. The EMBO journal *23*, 4307-4318.

Hooghwinkel, G.J., Borri, P.F., and Bruyn, G.W. (1966). Biochemical studies in Huntington's chorea. II. Composition of blood lipids. Acta neurologica Scandinavica *42*, 213-220.

Horton, J.D., Goldstein, J.L., and Brown, M.S. (2002). SREBPs: activators of the complete program of cholesterol and fatty acid synthesis in the liver. Journal of Clinical Investigation *109*, 1125-1131.

Huang, K., Yanai, A., Kang, R., Arstikaitis, P., Singaraja, R.R., Metzler, M., Mullard, A., Haigh, B., Gauthier-Campbell, C., Gutekunst, C.A., et al. (2004). Huntingtin-interacting protein HIP14 is a palmitoyl transferase involved in palmitoylation and trafficking of multiple neuronal proteins. Neuron *44*, 977-986.

Iguchi, Y., Yamaguchi, M., Sato, H., Kihira, K., Nishimaki-Mogami, T., and Une, M. (2010). Bile alcohols function as the ligands of membrane-type bile acid-activated G protein-coupled receptor. J Lipid Res *51*, 1432-1441.

Imarisio, S., Carmichael, J., Korolchuk, V., Chen, C.W., Saiki, S., Rose, C., Krishna, G., Davies, J.E., Ttofi, E., Underwood, B.R., et al. (2008). Huntington's disease: from pathology and genetics to potential therapies. The Biochemical journal *412*, 191-209.

Irons, M.B., and Tint, G.S. (1998). Prenatal diagnosis of Smith-Lemli-Opitz syndrome. Prenatal diagnosis *18*, 369-372.

Iwabuchi, S., Koh, J.Y., Wang, K., Ho, K.W., and Harata, N.C. (2013). Minimal Change in the cytoplasmic calcium dynamics in striatal GABAergic neurons of a DYT1 dystonia knock-in mouse model. PloS one *8*, e80793.

Jana, N.R., Dikshit, P., Goswami, A., Kotliarova, S., Murata, S., Tanaka, K., and Nukina, N. (2005). Co-chaperone CHIP associates with expanded polyglutamine protein and promotes their degradation by proteasomes. The Journal of biological chemistry *280*, 11635-11640.

Jankovic, J. (2008). Parkinson's disease: clinical features and diagnosis. Journal of neurology, neurosurgery, and psychiatry *79*, 368-376.

Janowski, B.A., Grogan, M.J., Jones, S.A., Wisely, G.B., Kliewer, S.A., Corey, E.J., and Mangelsdorf, D.J. (1999). Structural requirements of ligands for the oxysterol liver X receptors LXRalpha and LXRbeta. Proceedings of the National Academy of Sciences of the United States of America *96*, 266-271.

Jasinska, M., Owczarek, J., and Orszulak-Michalak, D. (2007). Statins: a new insight into their mechanisms of action and consequent pleiotropic effects. Pharmacological reports : PR *59*, 483-499.

Javitt, N.B. (2002). 25R,26-Hydroxycholesterol revisited: synthesis, metabolism, and biologic roles. J Lipid Res *43*, 665-670.

Jeong, H., Then, F., Melia, T.J., Jr., Mazzulli, J.R., Cui, L., Savas, J.N., Voisine, C., Paganetti, P., Tanese, N., Hart, A.C., et al. (2009). Acetylation targets mutant huntingtin to autophagosomes for degradation. Cell *137*, 60-72.

Jia, K., Hart, A.C., and Levine, B. (2007). Autophagy genes protect against disease caused by polyglutamine expansion proteins in Caenorhabditis elegans. Autophagy *3*, 21-25.

Jick, H., Zornberg, G.L., Jick, S.S., Seshadri, S., and Drachman, D.A. (2000). Statins and the risk of dementia. Lancet *356*, 1627-1631.

Joseph, S.B., McKilligin, E., Pei, L., Watson, M.A., Collins, A.R., Laffitte, B.A., Chen, M., Noh, G., Goodman, J., Hagger, G.N., et al. (2002). Synthetic LXR ligand inhibits the development of atherosclerosis in mice. Proceedings of the National Academy of Sciences of the United States of America *99*, 7604-7609.

Joseph, S.B., and Tontonoz, P. (2003). LXRs: new therapeutic targets in atherosclerosis? Current opinion in pharmacology *3*, 192-197.

Kalchman, M.A., Graham, R.K., Xia, G., Koide, H.B., Hodgson, J.G., Graham, K.C., Goldberg, Y.P., Gietz, R.D., Pickart, C.M., and Hayden, M.R. (1996). Huntingtin is ubiquitinated and interacts with a specific ubiquitin-conjugating enzyme. The Journal of biological chemistry *271*, 19385-19394.

Kaltenbach, L.S., Romero, E., Becklin, R.R., Chettier, R., Bell, R., Phansalkar, A., Strand, A., Torcassi, C., Savage, J., Hurlburt, A., et al. (2007). Huntingtin interacting proteins are genetic modifiers of neurodegeneration. PLoS genetics *3*, e82.

Katja, N., Hubert, S., and Frank, W.P. (2009). Marked differences in cholesterol synthesis between neurons and glial cells from postnatal rats. Journal of neurochemistry *109*, 125-134.

Kegel, K.B., Kim, M., Sapp, E., McIntyre, C., Castano, J.G., Aronin, N., and DiFiglia, M. (2000). Huntingtin expression stimulates endosomal-lysosomal activity, endosome tubulation, and autophagy. The Journal of neuroscience : the official journal of the Society for Neuroscience *20*, 7268-7278.

Kegel, K.B., Meloni, A.R., Yi, Y., Kim, Y.J., Doyle, E., Cuiffo, B.G., Sapp, E., Wang, Y., Qin, Z.H., Chen, J.D., et al. (2002). Huntingtin is present in the nucleus, interacts with the transcriptional corepressor C-terminal binding protein, and represses transcription. The Journal of biological chemistry *277*, 7466-7476.

Kegel, K.B., Sapp, E., Yoder, J., Cuiffo, B., Sobin, L., Kim, Y.J., Qin, Z.H., Hayden, M.R., Aronin, N., Scott, D.L., et al. (2005). Huntingtin associates with acidic phospholipids at the plasma membrane. The Journal of biological chemistry *280*, 36464-36473.

Kim, K.K., Adelstein, R.S., and Kawamoto, S. (2009). Identification of neuronal nuclei (NeuN) as Fox-3, a new member of the Fox-1 gene family of splicing factors. The Journal of biological chemistry *284*, 31052-31061.

Kim, W.S., Rahmanto, A.S., Kamili, A., Rye, K.A., Guillemin, G.J., Gelissen, I.C., Jessup, W., Hill, A.F., and Garner, B. (2007). Role of ABCG1 and ABCA1 in

regulation of neuronal cholesterol efflux to apolipoprotein E discs and suppression of amyloid-beta peptide generation. The Journal of biological chemistry *282*, 2851-2861.

Kirkland, R.A., Saavedra, G.M., and Franklin, J.L. (2007). Rapid activation of antioxidant defenses by nerve growth factor suppresses reactive oxygen species during neuronal apoptosis: evidence for a role in cytochrome c redistribution. The Journal of neuroscience : the official journal of the Society for Neuroscience *27*, 11315-11326.

Kolsch, H., Ludwig, M., Lutjohann, D., and Rao, M.L. (2001). Neurotoxicity of 24-hydroxycholesterol, an important cholesterol elimination product of the brain, may be prevented by vitamin E and estradiol-17beta. Journal of neural transmission (Vienna, Austria : 1996) *108*, 475-488.

Kotzka, J., Knebel, B., Haas, J., Kremer, L., Jacob, S., Hartwig, S., Nitzgen, U., and Muller-Wieland, D. (2012). Preventing phosphorylation of sterol regulatory element-binding protein 1a by MAP-kinases protects mice from fatty liver and visceral obesity. PloS one *7*, e32609.

Koudinov, A.R., and Koudinova, N.V. (2001). Essential role for cholesterol in synaptic plasticity and neuronal degeneration. FASEB J *15*, 1858-1860.

Kumar, U., Asotra, K., Patel, S.C., and Patel, Y.C. (1997). Expression of NMDA receptor-1 (NR1) and huntingtin in striatal neurons which colocalize somatostatin, neuropeptide Y, and NADPH diaphorase: a double-label histochemical and immunohistochemical study. Exp Neurol *145*, 412-424.

Landles, C., and Bates, G.P. (2004). Huntingtin and the molecular pathogenesis of Huntington's disease. Fourth in molecular medicine review series. EMBO reports *5*, 958.

Lavezzi, A.M., Corna, M.F., and Matturri, L. (2013). Neuronal nuclear antigen (NeuN): a useful marker of neuronal immaturity in sudden unexplained perinatal death. Journal of the neurological sciences *329*, 45-50.

Leavitt, B.R., van Raamsdonk, J.M., Shehadeh, J., Fernandes, H., Murphy, Z., Graham, R.K., Wellington, C.L., Raymond, L.A., and Hayden, M.R. (2006). Wild-type huntingtin protects neurons from excitotoxicity. Journal of neurochemistry *96*, 1121-1129.

Leegwater-Kim, J., and Cha, J.-H.J. (2004). The paradigm of Huntington's disease: Therapeutic opportunities in neurodegeneration. Neurotherapeutics *1*, 128-138.

Legendre-Guillemin, V., Metzler, M., Charbonneau, M., Gan, L., Chopra, V., Philie, J., Hayden, M.R., and McPherson, P.S. (2002). HIP1 and HIP12 display differential binding to F-actin, AP2, and clathrin. Identification of a novel interaction with clathrin light chain. The Journal of biological chemistry *277*, 19897-19904.

Leoni, V., and Caccia, C. (2015). The impairment of cholesterol metabolism in Huntington disease. Biochimica et biophysica acta *1851*, 1095-1105.

Li, W., Zhang, B., Tang, J., Cao, Q., Wu, Y., Wu, C., Guo, J., Ling, E.A., and Liang, F. (2007). Sirtuin 2, a mammalian homolog of yeast silent information regulator-2 longevity regulator, is an oligodendroglial protein that decelerates cell differentiation through deacetylating alpha-tubulin. The Journal of neuroscience : the official journal of the Society for Neuroscience *27*, 2606-2616.

Liang, Y., Lin, S., Beyer, T.P., Zhang, Y., Wu, X., Bales, K.R., DeMattos, R.B., May, P.C., Li, S.D., Jiang, X.C., et al. (2004). A liver X receptor and retinoid X receptor heterodimer mediates apolipoprotein E expression, secretion and cholesterol homeostasis in astrocytes. Journal of neurochemistry *88*, 623-634.

Lim, D., Fedrizzi, L., Tartari, M., Zuccato, C., Cattaneo, E., Brini, M., and Carafoli, E. (2008). Calcium homeostasis and mitochondrial dysfunction in striatal neurons of Huntington disease. The Journal of biological chemistry *283*, 5780-5789.

Linsenbardt, A.J., Taylor, A., Emnett, C.M., Doherty, J.J., Krishnan, K., Covey, D.F., Paul, S.M., Zorumski, C.F., and Mennerick, S. (2014). Different oxysterols have opposing actions at N-methyl-D-aspartate receptors. Neuropharmacology *85*, 232-242.

Liot, G., Bossy, B., Lubitz, S., Kushnareva, Y., Sejbuk, N., and Bossy-Wetzel, E. (2009). Complex II inhibition by 3-NP causes mitochondrial fragmentation and neuronal cell death via an NMDA- and ROS-dependent pathway. Cell Death Differ *16*, 899-909.

Liot, G., Zala, D., Pla, P., Mottet, G., Piel, M., and Saudou, F. (2013). Mutant Huntingtin alters retrograde transport of TrkB receptors in striatal dendrites. The Journal of neuroscience : the official journal of the Society for Neuroscience *33*, 6298-6309.

Liscum, L., and Faust, J.R. (1989). The intracellular transport of low density lipoprotein-derived cholesterol is inhibited in Chinese hamster ovary cells cultured with 3-beta-[2-(diethylamino)ethoxy]androst-5-en-17-one. The Journal of biological chemistry *264*, 11796-11806.

Liu, B., Turley, S.D., Burns, D.K., Miller, A.M., Repa, J.J., and Dietschy, J.M. (2009). Reversal of defective lysosomal transport in NPC disease ameliorates liver dysfunction and neurodegeneration in the npc1-/- mouse. Proceedings of the National Academy of Sciences of the United States of America *106*, 2377-2382.

Liu, Y., Peterson, D.A., Kimura, H., and Schubert, D. (1997). Mechanism of cellular 3-(4,5-dimethylthiazol-2-yl)-2,5-diphenyltetrazolium bromide (MTT) reduction. Journal of neurochemistry *69*, 581-593.

Liu, Y., Wong, T.P., Aarts, M., Rooyakkers, A., Liu, L., Lai, T.W., Wu, D.C., Lu, J., Tymianski, M., Craig, A.M., et al. (2007). NMDA receptor subunits have differential roles in mediating excitotoxic neuronal death both in vitro and in vivo. The Journal of neuroscience : the official journal of the Society for Neuroscience *27*, 2846-2857.

Lund, E.G., Guileyardo, J.M., and Russell, D.W. (1999). cDNA cloning of cholesterol 24-hydroxylase, a mediator of cholesterol homeostasis in the brain. Proceedings of the National Academy of Sciences of the United States of America *96*, 7238-7243.

Lund, E.G., Xie, C., Kotti, T., Turley, S.D., Dietschy, J.M., and Russell, D.W. (2003). Knockout of the cholesterol 24-hydroxylase gene in mice reveals a brain-specific mechanism of cholesterol turnover. The Journal of biological chemistry *278*, 22980-22988.

Luthi-Carter, R., Taylor, D.M., Pallos, J., Lambert, E., Amore, A., Parker, A., Moffitt, H., Smith, D.L., Runne, H., Gokce, O., et al. (2010). SIRT2 inhibition achieves neuroprotection by decreasing sterol biosynthesis. Proceedings of the National Academy of Sciences of the United States of America *107*, 7927-7932.

Lutjohann, D., Breuer, O., Ahlborg, G., Nennesmo, I., Siden, A., Diczfalusy, U., and Bjorkhem, I. (1996). Cholesterol homeostasis in human brain: evidence for an age-dependent flux of 24S-hydroxycholesterol from the brain into the circulation. Proceedings of the National Academy of Sciences of the United States of America *93*, 9799-9804.

Mailman, T., Hariharan, M., and Karten, B. (2011). Inhibition of neuronal cholesterol biosynthesis with lovastatin leads to impaired synaptic vesicle release even in the presence of lipoproteins or geranylgeraniol. Journal of neurochemistry *119*, 1002-1015.

Martin, M.G., Pfrieger, F., and Dotti, C.G. (2014). Cholesterol in brain disease: sometimes determinant and frequently implicated. EMBO Rep *15*, 1036-1052.

Marullo, M., Valenza, M., Leoni, V., Caccia, C., Scarlatti, C., De Mario, A., Zuccato, C., Di Donato, S., Carafoli, E., and Cattaneo, E. (2012). Pitfalls in the detection of cholesterol in Huntington's disease models. PLoS currents *4*, e505886e505889a501968.

Matsuda, A., Nagao, K., Matsuo, M., Kioka, N., and Ueda, K. (2013). 24(S)-hydroxycholesterol is actively eliminated from neuronal cells by ABCA1. Journal of neurochemistry *126*, 93-101.

Mauch, D.H., Nagler, K., Schumacher, S., Goritz, C., Muller, E.C., Otto, A., and Pfrieger, F.W. (2001). CNS synaptogenesis promoted by glia-derived cholesterol. Science (New York, N.Y.) *294*, 1354-1357.

Maxfield, F.R., and Tabas, I. (2005). Role of cholesterol and lipid organization in disease. Nature *438*, 612-621.

Maxfield, F.R., and van Meer, G. (2010). Cholesterol, the central lipid of mammalian cells. Current opinion in cell biology *22*, 422-429.

Miao, L., Nielsen, M., Thewalt, J., Ipsen, J.H., Bloom, M., Zuckermann, M.J., and Mouritsen, O.G. (2002). From lanosterol to cholesterol: structural evolution and differential effects on lipid bilayers. Biophysical journal *82*, 1429-1444.

Miller, B.R., Dorner, J.L., Bunner, K.D., Gaither, T.W., Klein, E.L., Barton, S.J., and Rebec, G.V. (2012). Up-regulation of GLT1 reverses the deficit in cortically evoked striatal ascorbate efflux in the R6/2 mouse model of Huntington's disease. Journal of neurochemistry *121*, 629-638.

Mishra, R., Hoop, C.L., Kodali, R., Sahoo, B., van der Wel, P.C.A., and Wetzel, R. (2012). Serine phosphorylation suppresses huntingtin amyloid accumulation by altering protein aggregation properties. Journal of molecular biology *424*, 1-14.

Mitchell, I.J., Cooper, A.J., and Griffiths, M.R. (1999). The selective vulnerability of striatopallidal neurons. Progress in neurobiology *59*, 691-719.

Miyoshi, N., Iuliano, L., Tomono, S., and Ohshima, H. (2014). Implications of cholesterol autoxidation products in the pathogenesis of inflammatory diseases. Biochem Biophys Res Commun *446*, 702-708.

Mohammadi, A., Perry, R.J., Storey, M.K., Cook, H.W., Byers, D.M., and Ridgway, N.D. (2001). Golgi localization and phosphorylation of oxysterol binding protein in Niemann-Pick C and U18666A-treated cells. J Lipid Res *42*, 1062-1071.

Moreira Sousa, C., McGuire, J.R., Thion, M.S., Gentien, D., de la Grange, P., Tezenas du Montcel, S., Vincent-Salomon, A., Durr, A., and Humbert, S. (2013). The Huntington disease protein accelerates breast tumour development and metastasis through ErbB2/HER2 signalling. EMBO molecular medicine *5*, 309-325.

Murphy, R.C., and Johnson, K.M. (2008). Cholesterol, reactive oxygen species, and the formation of biologically active mediators. The Journal of biological chemistry *283*, 15521-15525.

Muse, E.D., Jurevics, H., Toews, A.D., Matsushima, G.K., and Morell, P. (2001). Parameters related to lipid metabolism as markers of myelination in mouse brain. Journal of neurochemistry *76*, 77-86.

Nasir, J., Floresco, S.B., O'Kusky, J.R., Diewert, V.M., Richman, J.M., Zeisler, J., Borowski, A., Marth, J.D., Phillips, A.G., and Hayden, M.R. (1995). Targeted disruption of the Huntington's disease gene results in embryonic lethality and behavioral and morphological changes in heterozygotes. Cell *81*, 811-823.

Neuwald, A.F., and Hirano, T. (2000). HEAT repeats associated with condensins, cohesins, and other complexes involved in chromosome-related functions. Genome research *10*, 1445-1452.

Nieweg, K., Schaller, H., and Pfrieger, F.W. (2009). Marked differences in cholesterol synthesis between neurons and glial cells from postnatal rats. Journal of neurochemistry *109*, 125-134.

Noguchi, N., Urano, Y., Takabe, W., and Saito, Y. (2015). New aspects of 24(S)-hydroxycholesterol in modulating neuronal cell death. Free radical biology & medicine *87*, 366-372.

North, B.J., and Verdin, E. (2007). Interphase nucleo-cytoplasmic shuttling and localization of SIRT2 during mitosis. PloS one *2*, e784.

Nowaczyk, M.J.M., and Irons, M.B. (2012). Smith-Lemli-Opitz syndrome: phenotype, natural history, and epidemiology. American journal of medical genetics. Part C, Seminars in medical genetics *160C*, 250-262.

Numa, S., and Tanable, T. (1984). Acetyl-coenzyme A carboxylase and its regulation. Fatty acid metabolism and its regulation: new comprehensive biochemistry *7*, 1-27.

Ohyama, Y., Meaney, S., Heverin, M., Ekstrom, L., Brafman, A., Shafir, M., Andersson, U., Olin, M., Eggertsen, G., Diczfalusy, U., et al. (2006). Studies on the transcriptional regulation of cholesterol 24-hydroxylase (CYP46A1): marked insensitivity toward different regulatory axes. The Journal of biological chemistry *281*, 3810-3820.

Okabe, A., Urano, Y., Itoh, S., Suda, N., Kotani, R., Nishimura, Y., Saito, Y., and Noguchi, N. (2013). Adaptive responses induced by 24S-hydroxycholesterol through liver X receptor pathway reduce 7-ketocholesterol-caused neuronal cell death. Redox biology *2*, 28-35.

Orr, A.L., Li, S., Wang, C.E., Li, H., Wang, J., Rong, J., Xu, X., Mastroberardino, P.G., Greenamyre, J.T., and Li, X.J. (2008). N-terminal mutant huntingtin associates with mitochondria and impairs mitochondrial trafficking. The Journal of neuroscience : the official journal of the Society for Neuroscience *28*, 2783-2792.

Oslowski, C.M., and Urano, F. (2011). Measuring ER stress and the unfolded protein response using mammalian tissue culture system. Methods in enzymology *490*, 71-92.

Ostlund, J.R.E., Bosner, M.S., and Stenson, W.F. (1999). Cholesterol absorption efficiency declines at moderate dietary doses in normal human subjects. J Lipid Res *40*, 1453.

Outeiro, T.F., Kontopoulos, E., Altmann, S.M., Kufareva, I., Strathearn, K.E., Amore, A.M., Volk, C.B., Maxwell, M.M., Rochet, J.C., McLean, P.J., et al. (2007). Sirtuin 2 inhibitors rescue alpha-synuclein-mediated toxicity in models of Parkinson's disease. Science (New York, N.Y.) *317*, 516-519.

Panov, A.V., Gutekunst, C.A., Leavitt, B.R., Hayden, M.R., Burke, J.R., Strittmatter, W.J., and Greenamyre, J.T. (2002). Early mitochondrial calcium defects in Huntington's disease are a direct effect of polyglutamines. Nature neuroscience *5*, 731-736.

Paoletti, P., Bellone, C., and Zhou, Q. (2013). NMDA receptor subunit diversity: impact on receptor properties, synaptic plasticity and disease. Nat Rev Neurosci *14*, 383-400.

Patterson, M.C., Hendriksz, C.J., Walterfang, M., Sedel, F., Vanier, M.T., and Wijburg, F. (2012). Recommendations for the diagnosis and management of Niemann-Pick disease type C: an update. Molecular genetics and metabolism *106*, 330-344.

Paul, R., Choudhury, A., and Borah, A. (2015). Cholesterol - A putative endogenous contributor towards Parkinson's disease. Neurochemistry international *90*, 125-133.

Paul, S.M., Doherty, J.J., Robichaud, A.J., Belfort, G.M., Chow, B.Y., Hammond, R.S., Crawford, D.C., Linsenbardt, A.J., Shu, H.J., Izumi, Y., et al. (2013). The major brain cholesterol metabolite 24(S)-hydroxycholesterol is a potent allosteric modulator of N-methyl-D-aspartate receptors. The Journal of neuroscience : the official journal of the Society for Neuroscience *33*, 17290-17300.

Peavy, G.M., Jacobson, M.W., Goldstein, J.L., Hamilton, J.M., Kane, A., Gamst, A.C., Lessig, S.L., Lee, J.C., and Corey-Bloom, J. (2010). Cognitive and functional decline in Huntington's disease: Dementia criteria revisited. Movement Disorders *25*, 1163-1169.

Peng, Y., Schwarz, E.J., Lazar, M.A., Genin, A., Spinner, N.B., and Taub, R. (1997). Cloning, human chromosomal assignment, and adipose and hepatic expression of the CL-6/INSIG1 gene. Genomics *43*, 278-284.

Perez-Severiano, F., Rios, C., and Segovia, J. (2000). Striatal oxidative damage parallels the expression of a neurological phenotype in mice transgenic for the mutation of Huntington's disease. Brain research *862*, 234-237.

Pfrieger, F.W. (2003 a). Cholesterol homeostasis and function in neurons of the central nervous system. Cellular and molecular life sciences : CMLS *60*, 1158-1171.

Pfrieger, F.W. (2003 b). Outsourcing in the brain: do neurons depend on cholesterol delivery by astrocytes? BioEssays : news and reviews in molecular, cellular and developmental biology *25*, 72-78.

Pfrieger, F.W., and Ungerer, N. (2011). Cholesterol metabolism in neurons and astrocytes. Progress in lipid research *50*, 357-371.

Phillipi, C.A., Remmington, T., and Steiner, R.D. (2008). Bisphosphonate therapy for osteogenesis imperfecta. Cochrane database of systematic reviews (Online), CD005088.
Pipalia, N.H., Hao, M., Mukherjee, S., and Maxfield, F.R. (2007). Sterol, protein and lipid trafficking in Chinese hamster ovary cells with Niemann-Pick type C1 defect. Traffic (Copenhagen, Denmark) *8*, 130-141.

Polidori, M.C., Mecocci, P., Browne, S.E., Senin, U., and Beal, M.F. (1999). Oxidative damage to mitochondrial DNA in Huntington's disease parietal cortex. Neuroscience letters *272*, 53-56.

Politis, M., Pavese, N., Tai, Y.F., Tabrizi, S.J., Barker, R.A., and Piccini, P. (2008). Hypothalamic involvement in Huntington's disease: an in vivo PET study. Brain : a journal of neurology *131*, 2860-2869.

Ponugoti, B., Kim, D.H., Xiao, Z., Smith, Z., Miao, J., Zang, M., Wu, S.Y., Chiang, C.M., Veenstra, T.D., and Kemper, J.K. (2010). SIRT1 deacetylates and inhibits SREBP-1C activity in regulation of hepatic lipid metabolism. The Journal of biological chemistry *285*, 33959-33970.

Porter, F.D., and Herman, G.E. (2011). Malformation syndromes caused by disorders of cholesterol synthesis. J Lipid Res *52*, 6-34.

Qi, L., and Zhang, X.D. (2014). Role of chaperone-mediated autophagy in degrading Huntington's disease-associated huntingtin protein. Acta biochimica et biophysica Sinica *46*, 83-91.

Quan, G., Xie, C., Dietschy, J.M., and Turley, S.D. (2003). Ontogenesis and regulation of cholesterol metabolism in the central nervous system of the mouse. Developmental Brain Research *146*, 87-98.

Radhakrishnan, A., Ikeda, Y., Kwon, H.J., Brown, M.S., and Goldstein, J.L. (2007). Sterol-regulated transport of SREBPs from endoplasmic reticulum to Golgi: Oxysterols block transport by binding to Insig. Proceedings of the National Academy of Sciences *104*, 6511-6518.

Rajan, R.S., Illing, M.E., Bence, N.F., and Kopito, R.R. (2001). Specificity in intracellular protein aggregation and inclusion body formation. Proceedings of the National Academy of Sciences of the United States of America *98*, 13060-13065.

Ravikumar, B., and Rubinsztein, D.C. (2004). Can autophagy protect against neurodegeneration caused by aggregate-prone proteins? Neuroreport *15*, 2443-2445.

Ravikumar, B., Vacher, C., Berger, Z., Davies, J.E., Luo, S., Oroz, L.G., Scaravilli, F., Easton, D.F., Duden, R., O'Kane, C.J., et al. (2004). Inhibition of mTOR induces autophagy and reduces toxicity of polyglutamine expansions in fly and mouse models of Huntington disease. Nature genetics *36*, 585-595.

Rawson, R.B. (2003). The SREBP pathway--insights from Insigs and insects. Nature reviews. Molecular cell biology *4*, 631-640.

Raymond, L.A., Andre, V.M., Cepeda, C., Gladding, C.M., Milnerwood, A.J., and Levine, M.S. (2011). Pathophysiology of Huntington's disease: time-dependent alterations in synaptic and receptor function. Neuroscience *198*, 252-273.

Regulier, E., Pereira de Almeida, L., Sommer, B., Aebischer, P., and Deglon, N. (2002). Dose-dependent neuroprotective effect of ciliary neurotrophic factor delivered via tetracycline-regulated lentiviral vectors in the quinolinic acid rat model of Huntington's disease. Human gene therapy *13*, 1981-1990.

Regulier, E., Trottier, Y., Perrin, V., Aebischer, P., and Deglon, N. (2003). Early and reversible neuropathology induced by tetracycline-regulated lentiviral overexpression of mutant huntingtin in rat striatum. Human molecular genetics *12*, 2827-2836.

Reiner, A., Albin, R.L., Anderson, K.D., D'Amato, C.J., Penney, J.B., and Young, A.B. (1988). Differential loss of striatal projection neurons in Huntington disease. Proceedings of the National Academy of Sciences of the United States of America *85*, 5733-5737.

Rigamonti, D., Bauer, J.H., De-Fraja, C., Conti, L., Sipione, S., Sciorati, C., Clementi, E., Hackam, A., Hayden, M.R., Li, Y., et al. (2000). Wild-type huntingtin protects from apoptosis upstream of caspase-3. The Journal of neuroscience : the official journal of the Society for Neuroscience *20*, 3705-3713.

Rikani, A.A., Choudhry, Z., Choudhry, A.M., Rizvi, N., Ikram, H., Mobassarah, N.J., and Tulli, S. (2014). The mechanism of degeneration of striatal neuronal subtypes in Huntington disease. Annals of neurosciences *21*, 112-114.

Rohn, T.T. (2013). Proteolytic cleavage of apolipoprotein E4 as the keystone for the heightened risk associated with Alzheimer's disease. International journal of molecular sciences *14*, 14908-14922.

Rohrl, C., Eigner, K., Winter, K., Korbelius, M., Obrowsky, S., Kratky, D., Kovacs, W.J., and Stangl, H. (2014). Endoplasmic reticulum stress impairs cholesterol efflux and synthesis in hepatic cells. Journal of lipid research *55*, 94-103.

Ron, D., and Habener, J.F. (1992). CHOP, a novel developmentally regulated nuclear protein that dimerizes with transcription factors C/EBP and LAP and functions as a dominant-negative inhibitor of gene transcription. Genes & development *6*, 439-453.

Ross, C.A. (2004). Huntington's disease: new paths to pathogenesis. Cell *118*, 4-7.

Ross, C.A., and Tabrizi, S.J. (2011). Huntington's disease: from molecular pathogenesis to clinical treatment. Lancet neurology *10*, 83-98.

Rothe, T., and Muller, H.W. (1991). Uptake of endoneurial lipoprotein into Schwann cells and sensory neurons is mediated by low density lipoprotein receptors and stimulated after axonal injury. Journal of neurochemistry *57*, 2016-2025.

Rubinsztein, D.C., and Carmichael, J. (2003). Huntington's disease: molecular basis of neurodegeneration. Expert reviews in molecular medicine *5*, 1-21.

Rudinskiy, N., Kaneko, Y.A., Beesen, A.A., Gokce, O., Regulier, E., Deglon, N., and Luthi-Carter, R. (2009). Diminished hippocalcin expression in Huntington's disease brain does not account for increased striatal neuron vulnerability as assessed in primary neurons. Journal of neurochemistry *111*, 460-472.

Rui, Y.N., Xu, Z., Patel, B., Chen, Z., Chen, D., Tito, A., David, G., Sun, Y., Stimming, E.F., Bellen, H.J., et al. (2015). Huntingtin functions as a scaffold for selective macroautophagy. Nature cell biology *17*, 262-275.

Runne, H., Regulier, E., Kuhn, A., Zala, D., Gokce, O., Perrin, V., Sick, B., Aebischer, P., Deglon, N., and Luthi-Carter, R. (2008). Dysregulation of gene expression in primary neuron models of Huntington's disease shows that polyglutamine-related effects on the striatal transcriptome may not be dependent on brain circuitry. The Journal of neuroscience : the official journal of the Society for Neuroscience *28*, 9723-9731.

Russell, D.W. (2003). The enzymes, regulation, and genetics of bile acid synthesis. Annual review of biochemistry *72*, 137-174.

Saher, G., Quintes, S., and Nave, K.A. (2011). Cholesterol: a novel regulatory role in myelin formation. The Neuroscientist : a review journal bringing neurobiology, neurology and psychiatry *17*, 79-93.

Saito, M., Benson, E.P., and Rosenberg, A. (1987). Metabolism of cholesterol and triacylglycerol in cultured chick neuronal cells, glial cells, and fibroblasts: accumulation of esterified cholesterol in serum-free culture. Journal of neuroscience research *18*, 319-325.

Sarkar, S., and Rubinsztein, D.C. (2008). Huntington's disease: degradation of mutant huntingtin by autophagy. The FEBS journal *275*, 4263-4270.

Sathasivam, K., Neueder, A., Gipson, T.A., Landles, C., Benjamin, A.C., Bondulich, M.K., Smith, D.L., Faull, R.L., Roos, R.A., Howland, D., et al. (2013). Aberrant splicing of HTT generates the pathogenic exon 1 protein in Huntington disease. Proceedings of the National Academy of Sciences of the United States of America *110*, 2366-2370.

Sato, R., Goldstein, J.L., and Brown, M.S. (1993). Replacement of serine-871 of hamster 3-hydroxy-3-methylglutaryl-CoA reductase prevents phosphorylation by AMP-activated kinase and blocks inhibition of sterol synthesis induced by ATP depletion. Proceedings of the National Academy of Sciences of the United States of America *90*, 9261-9265.

Saudou, F., and Humbert, S. (2016). The Biology of Huntingtin. Neuron *89*, 910-926.
Schilling, G., Becher, M.W., Sharp, A.H., Jinnah, H.A., Duan, K., Kotzuk, J.A., Slunt, H.H., Ratovitski, T., Cooper, J.K., Jenkins, N.A., et al. (1999). Intranuclear inclusions and neuritic aggregates in transgenic mice expressing a mutant N-terminal fragment of huntingtin. Human molecular genetics *8*, 397-407.

Schroeder, F., Holland, J.F., and Bieber, L.L. (1971). Fluorometric evidence for the binding of cholesterol to the filipin complex. The Journal of antibiotics *24*, 846-849.

Sepers, M.D., and Raymond, L.A. (2014). Mechanisms of synaptic dysfunction and excitotoxicity in Huntington's disease. Drug discovery today *19*, 990-996.

Sexton, R.C., Panini, S.R., Azran, F., and Rudney, H. (1983). Effects of 3 beta-[2-(diethylamino)ethoxy]androst-5-en-17-one on the synthesis of cholesterol and ubiquinone in rat intestinal epithelial cell cultures. Biochemistry *22*, 5687-5692.

Shafaati, M., Olin, M., Bavner, A., Pettersson, H., Rozell, B., Meaney, S., Parini, P., and Bjorkhem, I. (2011). Enhanced production of 24S-hydroxycholesterol is not sufficient to drive liver X receptor target genes in vivo. J Intern Med *270*, 377-387.

Sharp, A.H., Loev, S.J., Schilling, G., Li, S.H., Li, X.J., Bao, J., Wagster, M.V., Kotzuk, J.A., Steiner, J.P., Lo, A., et al. (1995). Widespread expression of Huntington's disease gene (IT15) protein product. Neuron *14*, 1065-1074.

Shen, J., Chen, X., Hendershot, L., and Prywes, R. (2002). ER stress regulation of ATF6 localization by dissociation of BiP/GRP78 binding and unmasking of Golgi localization signals. Dev Cell *3*, 99-111.

Simons, K., and Ikonen, E. (2000). How cells handle cholesterol. Science (New York, N.Y.) *290*, 1721-1726.

Singh, N.K., Banerjee, B.D., Bala, K., Mitrabasu, Dung Dung, A.A., and Chhillar, N. (2014). APOE and LRPAP1 gene polymorphism and risk of Parkinson's disease. Neurological sciences : official journal of the Italian Neurological Society and of the Italian Society of Clinical Neurophysiology *35*, 1075-1081.

Sipione, S., Rigamonti, D., Valenza, M., Zuccato, C., Conti, L., Pritchard, J., Kooperberg, C., Olson, J.M., and Cattaneo, E. (2002). Early transcriptional profiles in huntingtin-inducible striatal cells by microarray analyses. Human molecular genetics *11*, 1953-1965.

Sittler, A., Walter, S., Wedemeyer, N., Hasenbank, R., Scherzinger, E., Eickhoff, H., Bates, G.P., Lehrach, H., and Wanker, E.E. (1998). SH3GL3 associates with the Huntingtin exon 1 protein and promotes the formation of polygln-containing protein aggregates. Molecular cell *2*, 427-436.

Smith, D.W., Lemli, L., and Opitz, J.M. (1964). A NEWLY RECOGNIZED SYNDROME OF MULTIPLE CONGENITAL ANOMALIES. The Journal of pediatrics *64*, 210-217.

Sofroniew, M.V., and Vinters, H.V. (2010). Astrocytes: biology and pathology. Acta neuropathologica *119*, 7-35.

Song, B.L., Javitt, N.B., and DeBose-Boyd, R.A. (2005). Insig-mediated degradation of HMG CoA reductase stimulated by lanosterol, an intermediate in the synthesis of cholesterol. Cell metabolism *1*, 179-189.

Steffan, J.S., Agrawal, N., Pallos, J., Rockabrand, E., Trotman, L.C., Slepko, N., Illes, K., Lukacsovich, T., Zhu, Y.Z., Cattaneo, E., et al. (2004). SUMO modification of Huntingtin and Huntington's disease pathology. Science (New York, N.Y.) *304*, 100-104.

Steffan, J.S., Kazantsev, A., Spasic-Boskovic, O., Greenwald, M., Zhu, Y.Z., Gohler, H., Wanker, E.E., Bates, G.P., Housman, D.E., and Thompson, L.M. (2000). The Huntington's disease protein interacts with p53 and CREB-binding protein and represses transcription. Proceedings of the National Academy of Sciences of the United States of America *97*, 6763-6768.

Strober, W. (2001). Trypan blue exclusion test of cell viability. Curr Protoc Immunol *Appendix 3*, Appendix 3B.

Sun, Y., Savanenin, A., Reddy, P.H., and Liu, Y.F. (2001). Polyglutamine-expanded huntingtin promotes sensitization of N-methyl-D-aspartate receptors via post-synaptic density 95. The Journal of biological chemistry *276*, 24713-24718.

Suopanki, J., Gotz, C., Lutsch, G., Schiller, J., Harjes, P., Herrmann, A., and Wanker, E.E. (2006). Interaction of huntingtin fragments with brain membranes--clues to early dysfunction in Huntington's disease. Journal of neurochemistry *96*, 870-884.

Tabernero, A., Bolanos, J.P., and Medina, J.M. (1993). Lipogenesis from lactate in rat neurons and astrocytes in primary culture. The Biochemical journal *294 (Pt 3)*, 635-638.

Takano, H., and Gusella, J.F. (2002). The predominantly HEAT-like motif structure of huntingtin and its association and coincident nuclear entry with dorsal, an NF-kB/Rel/dorsal family transcription factor. BMC neuroscience *3*, 15.

Tao, T., and Tartakoff, A.M. (2001). Nuclear relocation of normal huntingtin. Traffic (Copenhagen, Denmark) *2*, 385-394.

Taylor, D.M., Balabadra, U., Xiang, Z., Woodman, B., Meade, S., Amore, A., Maxwell, M.M., Reeves, S., Bates, G.P., Luthi-Carter, R., et al. (2011). A brain-permeable small molecule reduces neuronal cholesterol by inhibiting activity of sirtuin 2 deacetylase. ACS chemical biology *6*, 540-546.

te Vruchte, D., Lloyd-Evans, E., Veldman, R.J., Neville, D.C., Dwek, R.A., Platt, F.M., van Blitterswijk, W.J., and Sillence, D.J. (2004). Accumulation of glycosphingolipids in Niemann-Pick C disease disrupts endosomal transport. The Journal of biological chemistry *279*, 26167-26175.

Thompson, L.M., Aiken, C.T., Kaltenbach, L.S., Agrawal, N., Illes, K., Khoshnan, A., Martinez-Vincente, M., Arrasate, M., O'Rourke, J.G., Khashwji, H., et al. (2009). IKK phosphorylates Huntingtin and targets it for degradation by the proteasome and lysosome. The Journal of cell biology *187*, 1083-1099.

Traynelis, S.F., Wollmuth, L.P., McBain, C.J., Menniti, F.S., Vance, K.M., Ogden, K.K., Hansen, K.B., Yuan, H., Myers, S.J., and Dingledine, R. (2010). Glutamate receptor ion channels: structure, regulation, and function. Pharmacological reviews *62*, 405-496.

Trottier, Y., Lutz, Y., Stevanin, G., Imbert, G., Devys, D., Cancel, G., Saudou, F., Weber, C., David, G., Tora, L., et al. (1995). Polyglutamine expansion as a pathological epitope in Huntington's disease and four dominant cerebellar ataxias. Nature *378*, 403-406.

Trushina, E., Rana, S., McMurray, C., and Hua, D. (2009). Tricyclic pyrone compounds prevent aggregation and reverse cellular phenotypes caused by expression of mutant huntingtin protein in striatal neurons. BMC neuroscience *10*, 73.

Trushina, E., Singh, R., Dyer, R., Cao, S., Shah, V., Parton, R., Pagano, R., and McMurray, C. (2006). Mutant huntingtin inhibits clathrin-independent endocytosis and causes accumulation of cholesterol in vitro and in vivo. Human molecular genetics *15*, 3578.

Turley, S.D., Burns, D.K., Rosenfeld, C.R., and Dietschy, J.M. (1996). Brain does not utilize low density lipoprotein-cholesterol during fetal and neonatal development in the sheep. J Lipid Res *37*, 1953-1961.

Twelvetrees, A.E., Yuen, E.Y., Arancibia-Carcamo, I.L., MacAskill, A.F., Rostaing, P., Lumb, M.J., Humbert, S., Triller, A., Saudou, F., Yan, Z., et al. (2010). Delivery of GABAARs to synapses is mediated by HAP1-KIF5 and disrupted by mutant huntingtin. Neuron *65*, 53-65.

Urano, Y., Ochiai, S., and Noguchi, N. (2013). Suppression of amyloid-beta production by 24S-hydroxycholesterol via inhibition of intracellular amyloid precursor protein trafficking. FASEB journal : official publication of the Federation of American Societies for Experimental Biology *27*, 4305-4315.

Valdez, C.M., Smith, M.A., Perry, G., Phelix, C.F., and Santamaria, F. (2010). Cholesterol homeostasis markers are localized to mouse hippocampal pyramidal and granule layers. Hippocampus *20*, 902-905.

Valenza, M., Carroll, J.B., Leoni, V., Bertram, L.N., Bjorkhem, I., Singaraja, R.R., Di Donato, S., Lutjohann, D., Hayden, M.R., and Cattaneo, E. (2007). Cholesterol biosynthesis pathway is disturbed in YAC128 mice and is modulated by huntingtin mutation. Human molecular genetics *16*, 2187-2198.

Valenza, M., Leoni, V., Karasinska, J.M., Petricca, L., Fan, J., Carroll, J., Pouladi, M.A., Fossale, E., Nguyen, H.P., Riess, O., et al. (2010). Cholesterol defect is marked across multiple rodent models of Huntington's disease and is manifest in astrocytes. The Journal of neuroscience : the official journal of the Society for Neuroscience *30*, 10844-10850.

Valenza, M., Leoni, V., Tarditi, A., Mariotti, C., Bjorkhem, I., Di Donato, S., and Cattaneo, E. (2007). Progressive dysfunction of the cholesterol biosynthesis pathway in the R6/2 mouse model of Huntington's disease. Neurobiology of disease *28*, 133-142.

Valenza, M., Marullo, M., Di Paolo, E., Cesana, E., Zuccato, C., Biella, G., and Cattaneo, E. (2015). Disruption of astrocyte-neuron cholesterol cross talk affects neuronal function in Huntington's disease. Cell death and differentiation *22*, 690-702.

Valenza, M., Rigamonti, D., Goffredo, D., Zuccato, C., Fenu, S., Jamot, L., Strand, A., Tarditi, A., Woodman, B., Racchi, M., et al. (2005). Dysfunction of the cholesterol biosynthetic pathway in Huntington's disease. The Journal of neuroscience : the official journal of the Society for Neuroscience *25*, 9932-9939.

van der Burg, J.M., Bjorkqvist, M., and Brundin, P. (2009). Beyond the brain: widespread pathology in Huntington's disease. Lancet neurology *8*, 765-774.

van der Wulp, M.Y.M., Verkade, H.J., and Groen, A.K. (2013). Regulation of cholesterol homeostasis. Molecular and cellular endocrinology U6 - ctx_ver=Z39.88-2004&ctx_enc=info%3Aofi%2Fenc%3AUTF-8&rfr_id=info:sid/summon.serialssolutions.com&rft_val_fmt=info:ofi/fmt:kev:mtx:journal&rft.genre=article&rft.atitle=Regulation+of+cholesterol+homeostasis&rft.jtitle=Mol

ecular+and+cellular+endocrinology&rft.au=van+der+Wulp%2C+Mari%C3%ABtte+Y+M&rft.au=Verkade%2C+Henkjan+J&rft.au=Groen%2C+Albert+K&rft.date=2013-04-10&rft.eissn=1872-8057&rft.volume=368&rft.issue=1-2&rft.spage=1&rft_id=info:pmid/22721653&rft.externalDocID=22721653 U7 - Journal Article U8 - FETCH-pubmed_primary_227216531 *368*, 1.

van Meerloo, J., Kaspers, G.J., and Cloos, J. (2011). Cell sensitivity assays: the MTT assay. Methods in molecular biology (Clifton, N.J.) *731*, 237-245.

van Pelt, J., Wolters, P.S., Corner, M.A., Rutten, W.L., and Ramakers, G.J. (2004). Long-term characterization of firing dynamics of spontaneous bursts in cultured neural networks. IEEE transactions on bio-medical engineering *51*, 2051-2062.

Vance, J.E. (2012). Dysregulation of cholesterol balance in the brain: contribution to neurodegenerative diseases. Disease models & mechanisms *5*, 746-755.

Vance, J.E., Hayashi, H., and Karten, B. (2005). Cholesterol homeostasis in neurons and glial cells. Seminars in Cell and Developmental Biology *16*, 193-212.

Vanier, M.T. (2015). Complex lipid trafficking in Niemann-Pick disease type C. Journal of inherited metabolic disease *38*, 187-199.

Verkhratsky, A. (2005). Physiology and pathophysiology of the calcium store in the endoplasmic reticulum of neurons. Physiological reviews *85*, 201-279.

Verkhratsky, A.J., and Petersen, O.H. (1998). Neuronal calcium stores. Cell calcium *24*, 333-343.

Vonsattel, J.P. (2008). Huntington disease models and human neuropathology: similarities and differences. Acta neuropathologica *115*, 55-69.

Vonsattel, J.P., and DiFiglia, M. (1998). Huntington disease. J Neuropathol Exp Neurol *57*, 369-384.

Waelter, S., Scherzinger, E., Hasenbank, R., Nordhoff, E., Lurz, R., Goehler, H., Gauss, C., Sathasivam, K., Bates, G.P., Lehrach, H., et al. (2001). The huntingtin interacting protein HIP1 is a clathrin and alpha-adaptin-binding protein involved in receptor-mediated endocytosis. Human molecular genetics *10*, 1807-1817.

Wahrle, S.E., Jiang, H., Parsadanian, M., Legleiter, J., Han, X., Fryer, J.D., Kowalewski, T., and Holtzman, D.M. (2004). ABCA1 is required for normal central nervous system ApoE levels and for lipidation of astrocyte-secreted apoE. The Journal of biological chemistry *279*, 40987-40993.

Walker, A.K., Yang, F., Jiang, K., Ji, J.Y., Watts, J.L., Purushotham, A., Boss, O., Hirsch, M.L., Ribich, S., Smith, J.J., et al. (2010). Conserved role of SIRT1 orthologs in fasting-dependent inhibition of the lipid/cholesterol regulator SREBP. Genes & development *24*, 1403-1417.

Walker, F.O. (2007). Huntington's disease. Lancet *369*, 218-228.

Wang, Y., Muneton, S., Sjovall, J., Jovanovic, J.N., and Griffiths, W.J. (2008). The effect of 24S-hydroxycholesterol on cholesterol homeostasis in neurons: quantitative changes to the cortical neuron proteome. Journal of proteome research *7*, 1606-1614.

Wellington, C.L., Ellerby, L.M., Gutekunst, C.A., Rogers, D., Warby, S., Graham, R.K., Loubser, O., van Raamsdonk, J., Singaraja, R., Yang, Y.Z., et al. (2002). Caspase cleavage of mutant huntingtin precedes neurodegeneration in Huntington's disease. The Journal of neuroscience : the official journal of the Society for Neuroscience *22*, 7862-7872.

Werner, H.B., Kuhlmann, K., Shen, S., Uecker, M., Schardt, A., Dimova, K., Orfaniotou, F., Dhaunchak, A., Brinkmann, B.G., Mobius, W., et al. (2007). Proteolipid protein is required for transport of sirtuin 2 into CNS myelin. The Journal of neuroscience : the official journal of the Society for Neuroscience *27*, 7717-7730.

Wexler, N.S., Collett, L., Wexler, A.R., Rawlins, M.D., Tabrizi, S.J., Douglas, I., Smeeth, L., and Evans, S.J. (2016). Incidence of adult Huntington's disease in the UK: a UK-based primary care study and a systematic review. BMJ open *6*, e009070.

Wexler, N.S., Lorimer, J., Porter, J., Gomez, F., Moskowitz, C., Shackell, E., Marder, K., Penchaszadeh, G., Roberts, S.A., Gayan, J., et al. (2004). Venezuelan kindreds reveal that genetic and environmental factors modulate Huntington's disease age of onset. Proceedings of the National Academy of Sciences of the United States of America *101*, 3498-3503.

Wheeler, V.C., White, J.K., Gutekunst, C.A., Vrbanac, V., Weaver, M., Li, X.J., Li, S.H., Yi, H., Vonsattel, J.P., Gusella, J.F., et al. (2000). Long glutamine tracts cause nuclear localization of a novel form of huntingtin in medium spiny striatal neurons in HdhQ92 and HdhQ111 knock-in mice. Human molecular genetics *9*, 503-513.

Whitney, K.D., Watson, M.A., Collins, J.L., Benson, W.G., Stone, T.M., Numerick, M.J., Tippin, T.K., Wilson, J.G., Winegar, D.A., and Kliewer, S.A. (2002). Regulation of cholesterol homeostasis by the liver X receptors in the central nervous system. Molecular endocrinology (Baltimore, Md.) *16*, 1378-1385.

Williams, K. (1993). Ifenprodil discriminates subtypes of the N-methyl-D-aspartate receptor: selectivity and mechanisms at recombinant heteromeric receptors. Mol Pharmacol *44*, 851-859.

Wong, Y.C., and Holzbaur, E.L. (2014). The regulation of autophagosome dynamics by huntingtin and HAP1 is disrupted by expression of mutant huntingtin, leading to defective cargo degradation. The Journal of neuroscience : the official journal of the Society for Neuroscience *34*, 1293-1305.
Xia, J., Lee, D.H., Taylor, J., Vandelft, M., and Truant, R. (2003). Huntingtin contains a highly conserved nuclear export signal. Human molecular genetics *12*, 1393-1403.

Xiang, Z., Valenza, M., Cui, L., Leoni, V., Jeong, H.K., Brilli, E., Zhang, J., Peng, Q., Duan, W., Reeves, S.A., et al. (2011). Peroxisome-proliferator-activated receptor gamma coactivator 1 alpha contributes to dysmyelination in experimental models of

Huntington's disease. The Journal of neuroscience : the official journal of the Society for Neuroscience *31*, 9544-9553.

Xifro, X., Garcia-Martinez, J.M., Del Toro, D., Alberch, J., and Perez-Navarro, E. (2008). Calcineurin is involved in the early activation of NMDA-mediated cell death in mutant huntingtin knock-in striatal cells. Journal of neurochemistry *105*, 1596-1612.

Xu, Q., Bernardo, A., Walker, D., Kanegawa, T., Mahley, R.W., and Huang, Y. (2006). Profile and regulation of apolipoprotein E (ApoE) expression in the CNS in mice with targeting of green fluorescent protein gene to the ApoE locus. The Journal of neuroscience : the official journal of the Society for Neuroscience *26*, 4985-4994.

Yamanaka, K., Saito, Y., Yamamori, T., Urano, Y., and Noguchi, N. (2011). 24(S)-hydroxycholesterol induces neuronal cell death through necroptosis, a form of programmed necrosis. The Journal of biological chemistry *286*, 24666-24673.

Yamanaka, K., Urano, Y., Takabe, W., Saito, Y., and Noguchi, N. (2014). Induction of apoptosis and necroptosis by 24(S)-hydroxycholesterol is dependent on activity of acyl-CoA:cholesterol acyltransferase 1. Cell Death Dis *5*, e990.

Zala, D., Benchoua, A., Brouillet, E., Perrin, V., Gaillard, M.C., Zurn, A.D., Aebischer, P., and Deglon, N. (2005). Progressive and selective striatal degeneration in primary neuronal cultures using lentiviral vector coding for a mutant huntingtin fragment. Neurobiology of disease *20*, 785-798.

Zala, D., Bensadoun, J.C., Pereira de Almeida, L., Leavitt, B.R., Gutekunst, C.A., Aebischer, P., Hayden, M.R., and Deglon, N. (2004). Long-term lentiviral-mediated expression of ciliary neurotrophic factor in the striatum of Huntington's disease transgenic mice. Experimental neurology *185*, 26-35.

Zala, D., Hinckelmann, M.V., and Saudou, F. (2013). Huntingtin's function in axonal transport is conserved in Drosophila melanogaster. PloS one *8*, e60162.

Zarrouk, A., Nury, T., Samadi, M., O'Callaghan, Y., Hammami, M., O'Brien, N.M., Lizard, G., and Mackrill, J.J. (2015). Effects of cholesterol oxides on cell death induction and calcium increase in human neuronal cells (SK-N-BE) and evaluation of the protective effects of docosahexaenoic acid (DHA; C22:6 n-3). Steroids *99*, 238-247.

Zeron, M.M., Chen, N., Moshaver, A., Lee, A.T., Wellington, C.L., Hayden, M.R., and Raymond, L.A. (2001). Mutant huntingtin enhances excitotoxic cell death. Molecular and cellular neurosciences *17*, 41-53.

Zhang, F.L., and Casey, P.J. (1996). Protein prenylation: molecular mechanisms and functional consequences. Annual review of biochemistry *65*, 241-269.

Zhang, X., Abels, E.R., Redzic, J.S., Margulis, J., Finkbeiner, S., and Breakefield, X.O. (2016). Potential Transfer of Polyglutamine and CAG-Repeat RNA in Extracellular Vesicles in Huntington's Disease: Background and Evaluation in Cell Culture. Cellular and molecular neurobiology *36*, 459-470.

Zhang, Y., Li, M., Drozda, M., Chen, M., Ren, S., Mejia Sanchez, R.O., Leavitt, B.R., Cattaneo, E., Ferrante, R.J., Hayden, M.R., et al. (2003). Depletion of wild-type huntingtin in mouse models of neurologic diseases. Journal of neurochemistry *87*, 101-106.

Zhao, L., and Brinton, R.D. (2003). Vasopressin-induced cytoplasmic and nuclear calcium signaling in embryonic cortical astrocytes: dynamics of calcium and calcium-dependent kinase translocation. The Journal of neuroscience : the official journal of the Society for Neuroscience *23*, 4228-4239.

Zheng, Z., and Diamond, M.I. (2012). Huntington disease and the huntingtin protein. Progress in molecular biology and translational science *107*, 189-214.

Zhou, M., Diwu, Z., Panchuk-Voloshina, N., and Haugland, R.P. (1997). A stable nonfluorescent derivative of resorufin for the fluorometric determination of trace hydrogen peroxide: applications in detecting the activity of phagocyte NADPH oxidase and other oxidases. Analytical biochemistry *253*, 162-168.

Zuccato, C., Ciammola, A., Rigamonti, D., Leavitt, B.R., Goffredo, D., Conti, L., MacDonald, M.E., Friedlander, R.M., Silani, V., Hayden, M.R., et al. (2001). Loss of huntingtin-mediated BDNF gene transcription in Huntington's disease. Science (New York, N.Y.) *293*, 493-498.

6. Publications during PhD

1. Taylor DM, Moser R, Régulier E, Breuillaud L, Dixon M, Beesen AA, Elliston L, **Silva Santos Mde F**, Kim J, Jones L, Goldstein DR, Ferrante RJ, Luthi-Carter R. MAP kinase phosphatase 1 (MKP-1/DUSP1) is neuroprotective in Huntington's disease via additive effects of JNK and p38 inhibition. ***J Neurosci***. 2013 Feb 6;33(6):2313-25. doi: 10.1523/JNEUROSCI.4965-11.2013 **(IF 7.12)**.

2. Jovicic A, Zaldivar Jolissaint JF, Moser R, **Silva Santos Mde F**, Luthi-Carter R., MicroRNA-22 (miR-22) overexpression is neuroprotective via general anti-apoptotic effects and may also target specific Huntington's disease-related mechanisms. ***PLoS One***. 2013;8(1):e54222. doi: 10.1371/journal.pone.0054222. Epub 2013 Jan 17 **(IF 3.7)**.